Impact of Open Fires on Atmospheric Chemistry over the North-West Indo-Gangetic Plain Quantified Using Multi-Year OH Reactivity and Trace Gas Measurements

A thesis

submitted by

Vinod Kumar

for the fulfilment of the degree of

Doctor of Philosophy

Indian Institute of Science Education and Research Mohali

Knowledge City, Sector 81, SAS Nagar, Manauli PO 140306

Mohali, India

December 2017

Declaration

I hearby declare that this thesis submitted in fulfilment of the requirements for the award of the degree of Doctor of Philosophy is without any unauthorised external assistance and used only sources acknowledged in the work. All textual passages which are appropriated verbatim or paraphrased from published and unpublished texts as well as all information obtained from oral sources are duly indicated and listed in accordance with bibliographical rules. In carrying out this research, I complied with the rules of standard scientific practice as formulated in the statutes of the Indian Institute of Science Education and Research, Mohali. This document has not been submitted for qualifications at any other institution.

Date:
Place: Mohali

Vinod Kumar

In my capacity as the supervisor of the candidate's thesis work, I certify that the above statements by the candidate are true to the best of my knowledge.

Dr. Vinayak Sinha
(Supervisor)

Acknowledgements

I dedicate this work to lord "Shiva", the god of mountains, whose blessing enabled me to achieve this milestone.
I express my deepest regards to my Ph.D advisor Dr. Vinayak Sinha, who has been a constant source of inspiration to me. I enrolled into the Ph.D program following the footsteps of my Ph.D advisor, with a motivation of enabling myself to attain the expertise of his level. His encouragement and faith in me throughout has been extremely helpful. I find paucity of words to thank my Ph.D co-advisor Dr. Bärbel Sinha for her continuous support through out the duration of my work and showing me the perfect temperament for pursuing research as a career. I am thankful to Prof N. Sathyamurthy, founder director of IISER Mohali for showing research as the career path and providing his enormous support for establishment and running of the atmospheric chemistry facility where I worked during Ph.D. I owe my sincere gratitude and thankfulness to Dr. Samrat Ghosh for monitoring my progress during Ph.D and for his helpful and valuable advice. I extend my sincere thanks to Prof. Thomas Wagner for providing me an opportunity to participate in several field campaigns and sharing his expertise of satellite remote sensing. I thank the three reviewers for for evaluation of my thesis and their helpful comments. Special thanks for Prof. E. Arunan for coming all the way to Mohali for conducting my viva voce examination. I acknowledge Dr. Glenn Wolfe for making his box model freely available for use and his valuable inputs regarding use of the model. I acknowledge INSPIRE fellowship program of the Department of Science and Technology (DST), India for providing the financial support of my Ph.D.
Special thanks to Ms. Mehak Bansal, Mr. Gaurav Sharma, Mr. Abhishek Kumar Mishra and Mr. Hareram Yadav for extending their unstinted support, timely motivation, sympathetic attitude and unfailing backing at the most crucial hours. I would like to thank my senior Mr. Chinmoy Sarkar for his valuable guidance, constructive criticism and helpful advice throughout. I thank my colleagues Saryu Garg, Praphulla Chandra, Haseeb Hakkim, Ashish Kumar Sharma, Savita Datta, Harshita Pawar, Pallavi and Yash Maurya for all their help and co-operation. Mr. Abhishek Kumar Mishra and Mr. Praphulla Chandra also provided their valuable feedback and inputs while writing this thesis.

Words are not enough to express my heartfelt thanks and gratitude to my parents and my sisters for their unconditional support, motivation and prayers that made this thesis possible. Their innumerable sacrifices have brought me to the position where I stand today. Last but not the least, I thank the administrative staffs of IISER Mohali, whose continuous work in the background ensured smooth functioning in the foreground.

Vinod Kumar

List of Publications

Publications from this thesis:

1. **Kumar, V.**, and Sinha, V., 'VOC–OHM : A new technique for rapid measurements of ambient total OH reactivity and volatile organic compounds using a single proton transfer reaction mass spectrometer': ***International Journal of Mass Spectrometry***, *374*, 55–63, doi: 10.1016/j.ijms.2014.10.012, **2014. (Cited 15 times)** (**Awarded the best student paper award by International journal of Mass spectrometry and Elsevier for the year 2014**)

2. **Kumar, V.**, Sarkar, C. and Sinha. V., 'Influence of post-harvest crop residue fires on surface ozone mixing ratios in the N.W. IGP analyzed using 2 years of continuous in situ trace gas measurements': ***Journal of Geophysical Research: Atmospheres***, *121*, 2015JD024308,**2016. (Cited 6 times)** doi: 10.1002/2015JD024308, 2016.

3. **Kumar, V.**, Chandra, B. P. and Sinha. V., 'Large unexplained suite of chemically reactive compounds present in ambient air due to biomass fires': under review in ***Scientific Reports***.

4. **Kumar, V.**, Sarkar, C. and Sinha. V., 'Isoprene and acetaldehyde dominate VOC OH reactivities and Ozone formation potentials in the N.W. IGP': ***in preparation***.

Co-authored publications:

5. Sarkar, C., **Kumar, V.**, and Sinha, V. , 'Massive emissions of carcinogenic benzenoids from paddy residue burning in North India': **Current Science**, *104(12)*, 1703–1706, url: http://www.currentscience.ac.in/Volumes/104/12/1703.pdf, **2013. (Cited 16 times)**

6. Sinha, V., **Kumar, V.**, and Sarkar, C., 'Chemical composition of pre-monsoon air in the Indo–Gangetic Plain measured using a new air quality facility and PTR-MS: high surface ozone and strong influence of biomass burning': ***Atmos. Chem.***

Phys., *14 (12)*, 5921 - 5941, doi: 10.5194/acp-14-5921-2014, **2014. (Cited 40 times)**

7. Pawar, H., Sachan, H., Garg, S., Arya, R., **Kumar, V.**, Sarkar, C., Chandra, B. P. and Sinha, B., 'Quantifying the contribution of long–range transport to Particulate Matter (PM) loading at a suburban site in the north–western Indo Gangetic Basin': ***Atmos. Chem. Phys.***, *15 (16)*, 9501-9520, doi: 10.5194/acp-15-9555-2015, **2015. (Cited 11 times)**

8. Sinha, B., Sangwan, K. S., Maurya, Y., **Kumar, V.**, Sarkar, C., Chandra, B. P. and Sinha. V., 'Assessment of crop yield losses in Punjab and Haryana using 2 years of continuous in situ ozone measurements': ***Atmos. Chem. Phys.***, *15 (16)*, 2355–2404, doi: 10.5194/acp-15-9555-2015, **2015. (Cited 7 times)**

9. Sarkar, C., Sinha, V., **Kumar, V.**, Rupakheti, M., Panday, A., Mahata, K. S., Rupakheti, D., Kathayat, B., and Lawrence, M. G.: 'Overview of VOC emissions and chemistry from PTR-TOF-MS measurements during the SusKat-ABC campaign: high acetaldehyde, isoprene and isocyanic acid in wintertime air of the Kathmandu Valley': ***Atmos. Chem. Phys.***, *16 (6)*, 3979 - 4003, doi: 10.5194/acp-16-3979-2016,**2016. (Cited 18 times)**

Synopsis

Human beings utilize fire in different ways e.g. in industries, for cooking and heating, clearing fields for agriculture and getting rid of waste. Geological records suggest the appearance of fire soon after the appearance of plants (420 million years ago), whereas evidence of controlled human induced fires for protection from wild animals and cooking food are found from 1 million to 1.5 million years ago. Despite providing mankind with economic and ecological support, fire emissions have become a matter of growing concern post-industrialisation. Large open fires perturb atmospheric chemistry through direct emissions and photochemical transformation of the direct emissions to secondary gases and aerosol particles resulting in strong air quality and climate feedbacks. Further they can serve as both sources and sinks of ambient hydroxyl (OH) radicals, which control the oxidizing efficiency of the atmosphere and are responsible for removal of major climate active gases and pollutants. The Indo-Gangetic Plain (IGP) which provides habitat, food and other resources to more than one-seventh of the world population is vulnerable to severe air pollution. Similar to several regions of the world, the Indo-Gangetic Plain (IGP) is impacted by large scale open burning as a result of post harvest fires, periodic clearing of landfills through controlled burning and small diffused open fires lit for waste disposal and domestic heating in winter. Research on this topic in this demographically important region of the world has however been limited to bulk analyses of aerosols, measurement of long-lived greenhouse gases including ozone and few light hydrocarbons (C2 – C4 compounds), without adequate knowledge about all relevant volatile organic compounds (VOCs) and a process based mechanistic understanding of the total ambient chemical reactivity introduced due to such fires and formation of secondary pollutants. Hydroxyl (OH) radicals control removal rates of gaseous pollutants. Measurement of total OH reactivity of air thus provides a robust quantitative measure of the total reactive pollutant loading of air masses. Lack of direct OH reactivity measurements, as well as absence of multi-year measurements of major reactive VOCs, carbon monoxide and nitrogen oxides simultaneously with ozone have prevented quantitative assessments of ozone production chemistry and the budget of reactive VOCs. In particular we still do not understand the enhanced chemical reactivity in ambient atmospheric environments

due to biomass fires. This thesis work addresses some of these key knowledge gaps through in situ measurements made possible by development and deployment of a new analytical technique (VOC-OHM) for quantification of total OH reactivity and measurements of a suite of reactive volatile organic compounds and ozone from a strategic site in the IGP made continuously for more than a year.

Chapter 1: Introduction

The first chapter of this thesis provides an introduction to atmospheric chemistry and describes the importance of volatile organic compounds (VOCs) and OH reactivity measurements. An overview of the role of VOCs as precursors of tropospheric ozone, review of ozone and VOC measurements from the IGP and the need for multi-year in situ measurements characterizing inter-annual and intra-annual seasonal variability and meteorological drivers is discussed. The novelty and need for direct measurements of OH reactivity to constrain VOC emissions budgets is accompanied by a summary of the growing dataset of OH reactivity studies that have been carried out worldwide. After summarizing these aspects, I present the motivation for my thesis work. The main scientific questions which I have addressed in this thesis are:

1. How do the concentrations of ozone, carbon monoxide and NO_x change in response to changes in meteorological conditions and anthropogenic perturbations (e.g. agricultural residue fires) in different seasons in the north-west Indo-Gangetic Plain? Are the temporal patterns and seasonal behavior reproducible for more than one year?

2. Which VOCs are the major drivers for peak daytime production of tropospheric ozone in different seasons? Is the peak daytime ozone production limited by availability of NO_x or by availability of VOCs in the N.W. IGP?

3. How do the ambient concentrations of VOCs, OH reactivity due to measured VOCs and ozone production potential vary over different seasons of the year in the north-west IGP? Which periods of year are expected to have highest total OH reactivity?

4. How to enable rapid online measurements of VOCs and total OH reactivity using a single proton transfer reaction mass spectrometer without compromising on the sensitivity, accuracy and detection limit of both OH reactivity and VOC measurements?

5. How much extra reactivity do the emissions from summertime agricultural residue fires in the N.W. IGP introduce directly and indirectly (through secondary pro-

cesses) into the ambient atmospheric environment? Are all the important chemical constituents involved in this process measured and incorporated in detailed atmospheric chemistry models?

Chapter 2: Influence of post-harvest crop residue fires on surface ozone mixing ratios in the N.W. IGP analyzed using two years of continuous in situ trace gas measurements

In this chapter, I report the first simultaneous two-year-long in situ dataset of ozone, CO and NO_x acquired from August 2011 - September 2013 at a representative site in the N.W. IGP (30.667 °N, 76.729 °E ; 310 m above mean sea level). These criteria air pollutants affect air quality and tropospheric chemistry but factors that control them in the densely populated N.W. Indo-Gangetic Plain (IGP) are poorly understood. Hence, the impact of emissions and meteorology on the diel and seasonal variability of O_3, CO and NO_x were investigated in this chapter. Regional post-harvest wheat residue fires were found to contribute majorly to high hourly averaged ozone concentrations ($\sim$ 80 ppb). In the absence of the wheat residue fires, ozone was much lower (by 19 ppb). Paddy residue fires also enhanced the peak ozone concentrations by $\sim$ 7 ppb, despite lower radiation and temperature relative to the "clean" post monsoon period ozone concentrations. d[O_3]/dt (from sunrise till daytime O_3 maxima), was highest during periods influenced by post-harvest fires in post monsoon season (9.2 ppb h^{-1}) and lowest during monsoon season (4.1 ppb h^{-1}). Analysis of air mass clusters revealed that enhanced chemical formation of O_3 and not transport was the driver of the summertime and post monsoon ambient O_3 maxima. Despite having high daytime NO_x (> 12 ppb) and CO (> 440 ppb) in winter, average daytime O_3 was less than 40 ppb due to reduced photochemistry and fog. Average daytime O_3 during the monsoon was less than 45 ppb due to washout of precursors and suppressed photochemistry due to cloud cover. The 8 h national ambient air quality standard (NAAQS) for O_3 was violated on 451 days (62 % of the total) in the period August 2011 - September 2013. The results revealed the periods/seasons with highest ozone pollution during the year and highlighted that substantial mitigation efforts are required to reduce regional O_3 pollution in the N.W. IGP due to agricultural fires.

Chapter 3: Isoprene and acetaldehyde dominate VOC OH reactivities and ozone formation potentials in the N.W. IGP

In this chapter, I report the first year-long high temporal resolution dataset of 23 VOCs from the north-west IGP including several that are reported for the first time

over the Indian region. High surface ozone is a critical environmental issue in the Indo-Gangetic Plain (IGP) due to frequent exceedance events (> 60 % annually) in the 8 h average national ambient air quality standard. The reactive VOC precursors of ozone are regionally poorly understood due to lack of measurements quantifying their diel and seasonality variability. These VOCs were measured with a PTR-MS at a regionally representative suburban site in the N.W. IGP (30.667 °N, 76.729 °E; 310 m above mean sea level). Detailed analyses of the diel and seasonal variability of VOCs, OH reactivity and ozone formation potential were performed. The highest ranking VOCs (based on annual average measured concentrations ± 1 σ ambient variability) included methanol (32.2 ± 19.7 ppb), acetaldehyde (5.9 ± 3.9 ppb), acetone (5.6 ± 5.1 ppb), formamide (4.0 ± 1.6 ppb), toluene (2.3 ± 2.8), formaldehyde (2.1 ± 0.9 ppb), C-8 aromatics (1.7 ± 2.2 ppb), benzene (1.6 ± 1.7 ppb) and isoprene (1.5 ± 1.0 ppb). In addition significantly high concentrations were observed at mass to charge ratios where multiple species may contribute using the PTR-QMS technique e.g. m/z = 61 (6.9 ± 6.3 ppb) and m/z 47 (6.1 ± 3.5 ppb). Surprisingly high mixing ratios of isoprene were observed throughout the year with the maximum during clean post monsoon (2.3 ppb) and minimum during winter (1.1 ppb). The maximum calculated OH concentrations ranged from 2.7×10^6 molecule cm^{-3} (winter) to 6.6×10^6 molecule cm^{-3} (summer) and were employed for calculation of ozone formation potentials. The average of peak daytime (11:00 - 14:00 L.T.) ozone formation potential for different seasons ranged between 10.2 ppb h^{-1} in winter to 31.3 ppb h^{-1} in the clean post monsoon. Crop residue fires caused an enhancement of 7.5 ppb h^{-1} in the summertime ozone formation potential. These fires are found to be a strong source of acetaldehyde, C-9 aromatics and isoprene which have a strong ozone formation potential. Isoprene and acetaldehyde contributed majorly towards the daytime VOC OH reactivity and ozone formation potential, accounting for greater than 38 % of the total calculated using all the measured compounds. Remarkably, the ozone production regime varied seasonally in response to emissions and meteorology and was not always limited by availability of NO_x as has been reported till date. Isoprene and acetaldehyde measurements are extremely rare over the Indian region and their measurements need to be made a priority for understanding and mitigating ozone formation over the IGP.

Chapter 4: VOC-OHM: A new technique for rapid measurements of ambient total OH reactivity and volatile organic compounds using a single proton transfer reaction mass spectrometer

In this chapter I present a novel hyphenated technique called VOC-OHM (for Volatile Organic Compounds – OH reactivity Measurement) that enables rapid ambient measure-

ments of both VOCs and total OH reactivity using a single PTR-MS. Ambient measurements of total hydroxyl radical (OH) reactivity and volatile organic compounds (VOC) are critical for investigating reactive emissions, atmospheric oxidation and formation of secondary pollutants such as ozone and organic aerosol, all of which have consequences for atmospheric chemistry, air quality, and health risk assessment studies. Both the ambient VOCs and the total ambient OH reactivity can be measured using proton transfer reaction mass spectrometers (PTR-MS). However, this has always required deployment of two separate instruments (either two PTR-MS or a GC-PID and PTR-MS), wherein one instrument measures ambient VOCs and the other instrument measures the total OH reactivity using the comparative reactivity method (CRM). Due to material (e.g. power, space) or financial constraints, deploying two PTR-MS instruments is not always possible and yet it is desirable to quantify both VOCs and OH reactivity. VOC-OHM successfully couples the typical VOC and CRM experimental set ups without compromising on the PTR-MS's ability to measure either parameter. The design of the VOC-OHM system, its validation, optimization and results of field tests are described in detail. The VOC-OHM system measures the ambient VOCs and OH reactivity every hour for $\sim$ 20 minutes duration, with an ambient data gap of $\sim$ 13 minutes between VOC and OH reactivity measurements. Thus rapid temporal changes in the ambient chemical composition and reactivity are easily quantified. The technique also demonstrates a new safer and portable substitute for pressurized zero air bottles that have been required thus far in CRM OH reactivity deployments. VOC-OHM also demonstrates a new approach to achieve additional specificity at ppt level in mass spectrometers with a mass resolution less than or equal to 1 by constraining the rate constant for reaction with hydroxyl radicals, of the major reactive isobaric contributor to a particular m/z. This is useful for example to distinguish isoprene from furan at m/z 69. The sampling periods and VOC speciation achieved using VOC-OHM can be customized depending on user preferences, providing more options for the majority of users possessing only a single PTR-MS.

Chapter 5: Large missing OH reactivity fueled by agricultural fires

Agricultural burning is a widespread practice globally, which impacts atmospheric chemistry, air quality and climate. A fundamental question that is still poorly understood concerns the extra reactivity that emissions from fires introduce directly and indirectly (through secondary processes) into ambient atmospheric environments, and whether all important chemical constituents involved in this process have been identified and incorporated in models. In this chapter, by carrying out a novel field study, I investigated the

impact of summertime agricultural fires by measuring the total ambient OH reactivity of air and a suite of all major known OH reactants at the IISER Mohali atmospheric chemistry facility (30.667 °N, 76.729 °E; 310 m a.s.l.), a regionally representative suburban site located downwind of agricultural fields in the north-west IGP from March – May 2013 during pre-harvest and the post-harvest periods which were influenced by agricultural fires. It was found that the missing OH reactivity fraction increased from 5 % in pre-harvest (non-fire influenced) summertime air to a massive 40 % in post-harvest summertime air influenced by large scale agricultural burning, while accounting for the same set of OH reactants and oxidation products. The increase in the missing OH reactivity was also accompanied by greater than two-fold increase in absolute total OH reactivity from 28 s^{-1} to 64 s^{-1} between the two periods. Thus, some very reactive compounds resulting from the agricultural burning remain unknown. Increased missing OH reactivity between the two summertime periods was associated with increased concentrations of compounds with strong photochemical source such as acetaldehyde, acetone, hydroxyacetone, nitromethane, amides, isocyanic acid and primary emissions of acetonitrile and aromatic compounds. Currently even the most detailed state-of-the-art atmospheric chemistry models exclude formamide, acetamide, nitromethane and isocyanic acid and their highly reactive precursor alkylamines (e.g. methylamine, ethylamine, dimethylamine, trimethylamine). As OH chemistry governs the removal rate of climate active gases and formation of ozone and aerosol, these findings have major implications for understanding and predicting tropospheric chemistry and air-quality-climate feedbacks in fire-impacted atmospheric environments.

Thus, overall my thesis work and its findings represent major advancements in acquisition of new strategic knowledge necessary for detailed quantitative understanding of the impact of open fires on atmospheric composition and chemistry over the north-west Indo-Gangetic Plain and the chemical speciation and reactivity perturbations that can be caused by large scale biomass fires, an emission activity that impacts the global atmosphere and occurs on varied temporal and spatial scales worldwide.

Contents

Chapter 1

Introduction

The ancient Hindu mythology believes that the creation, sustenance and survival of humans, animals and plants on earth are dependent on the "panchtatva" which are "kshiti (land or soil)", "jal (water)", "pawak (fire)", "gagan (sky)" and "sameer (air)", without which there is no possibility of life (Prasad, 2016).

" क्षिति, जल, पावक, गगन, समीरा।
पंच् तत्व रचित अधम शरीरा ॥ "

While these "tatvas" interact among themselves, human beings and the other living beings (e.g. plants and animals) also dynamically interact with these "panchtatva" during their life span. During the course of evolution, the human beings started taking control over these "tatvas", and utilized them for various kinds of constructive activities.
Over the course of past one and half century, the excessive use, intervention and manipulation with natural resources have led to contamination of the essentials, be it water, land or air. Fire, once thought to be the ultimate destroyer, was controlled (Harari, 2015) and used for various purpose like bio-fuel burning for heating and cooking (Brain and Sillent, 1988), industrial heating or biomass/garbage burning. Although fires serve humans, yet it adds up various pollutants in the air which are clearly sensed by either vision, smell and other means of physical interaction with human body. Pollution unambiguously affects living organisms be it plants, animals or human beings. A severe implication of such a pollution event was faced in the 1950s and 1960s when entire Los Angeles was engulfed with a thick blanket of smog (Haagen-Smit, 1952).

A physical observation of a pollution event can be in form of visibility deterioration, bad odour, skin irritation or medical condition, but at the same time it is important to understand the chemical composition and its sources to find a proper cure and mitigation step. For example, Figure 1.1 shows the photograph of my hostel residence area taken in the afternoon time (between 2:00 pm and 3:00 pm) on two days in the month of October.

Figure 1.1: Top: Visual observation of my resident institute (in north India) on a normal day in the afternoon in the month of October and Bottom: Photograph of the same place taken after 17 days in same month in afternoon time.

The top panel represents the clear sky condition on a clean day whereas the bottom panel shows the same area on a polluted day. The smog conditions were associated with deteriorated visibility, burning smell and eye irritation. Similar (or even worse) conditions can be observed quite frequently over north India. There have been previous works and news articles which attribute the cause of such conditions to prevalent crop residue fires, industrial emissions, vehicular emissions and other types of biomass combustion, e.g. garbage burning and biofuel combustion. The motivation of this work is to quantitatively understand the effect of these emissions in the atmosphere (the "air" and "sky" components of the "panchtatva") from an atmospheric chemistry perspective.

1.1 Gas phase atmospheric chemistry

The atmosphere is a mixture of gases and suspended solids and liquids, which surround the earth from the ground to $\sim$ 110 km. Based on the broad vertical variation of temperature, the atmosphere is divided into four layers, namely Troposphere, Stratosphere, Mesosphere and Thermosphere. The layer of the atmosphere closest to the Earth's surface is called the troposphere which ranges upto 18 km over the equator and upto 8 km over the poles. Though troposphere is the thinnest layer of atmosphere, yet due to higher pressure near the surface it contains more than 90 % of the mass of the atmosphere. It is this layer which directly interacts with humans, animals and plants and where rainfall occurs.

In terms of composition, Nitrogen(N_2) and Oxygen (O_2) account for 78 % and 21 % respectively of the atmosphere. The water vapour content of the atmosphere is highly variable. All gases present in the atmosphere apart from N_2 and O_2 are collectively called traces gases. Among the trace gases, Argon (Ar) comprises 0.9 %, whereas gases like Carbon dioxide (CO_2), Neon, Helium, Methane (CH_4), Nitrous oxide (N_2O), Ozone (O_3) and Volatile Organic Compounds (VOCs) collectively comprise 0.1 % of atmosphere, out of which more than 93 % is only CO_2. VOCs are defined as class of organic compounds having high vapour pressure (greater than 0.01 kPa at 25 °C) and low boiling point (50 °C to 260 °C) at 1 atmosphere (1.013×10^5 Pa) (Koppmann, 2007).

While the major components of the atmosphere are important in terms of the composition, the reactive trace gases are the ones whose concentrations have changed drastically since industrialization and these are more important in terms of air quality, health effect and climate effect. According to fourth and fifth IPCC assessment report CO_2, CH_4 and tropospheric Ozone (O_3) are the three most important gases in terms of their global warming potential (IPCC, 2007, 2013). Radiative forcing of an atmospheric constituent X is the parameter for assessing the global warming potential, which is defined as re-

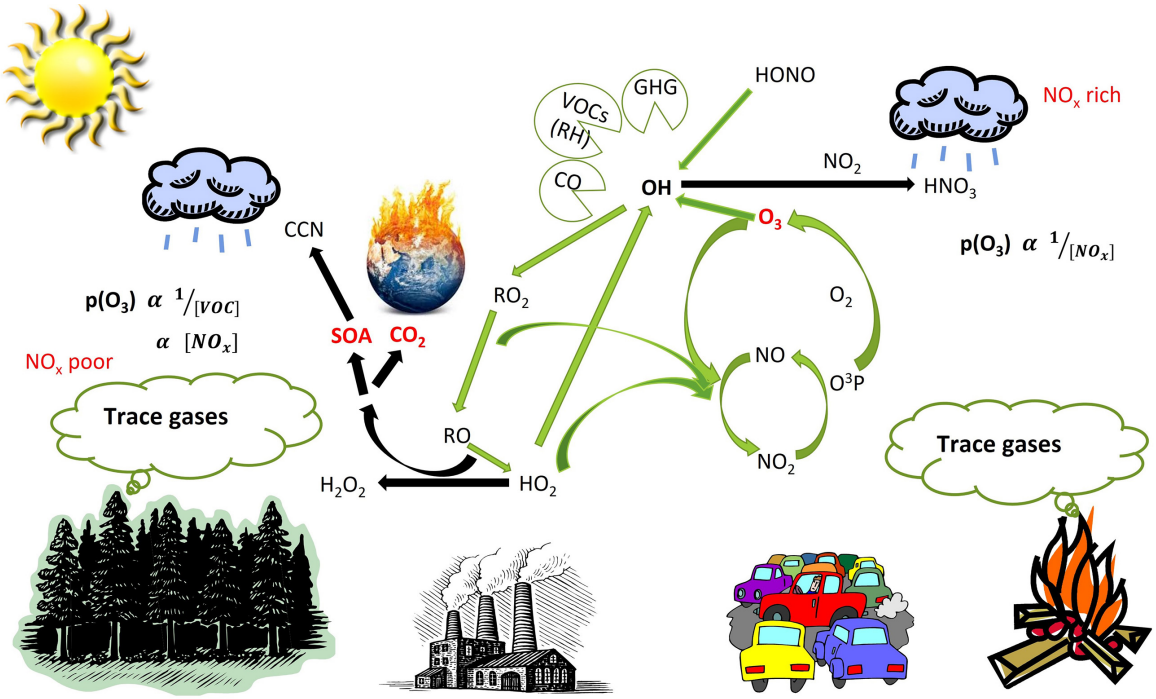

Figure 1.2: Illustrative cartoon of atmospheric chemistry of the troposphere highlighting the effects of biogenic and anthropogenic emissions and chemical transformations.

sulting flux imbalance in the radiative budget for the earth system caused by total extra amount added to the atmosphere since 1750 (pre-industrial time). On a per molecule basis, one of the constituents may have a higher global warming potential than the other, but for assessing the radiative forcing, both the extra amount in the atmosphere relative to pre-industrial time and individual global warming potential per unit mass should be considered. The radiative forcing of reactive trace gases e.g. CO, NO_x (sum of NO and NO_2) and non-methane VOCs (NMVOCs) were not included in the fourth IPCC assessment report (year 2007), but their important contributions were realized in terms of their indirect radiative forcing and are included in the fifth IPCC assessment report (year 2013). These compound are the precursors of tropospheric O_3, CO_2 and secondary organic aerosols (SOA) which have a direct impact on global warming. Moreover these gases directly affect air quality, public health and crop yields at concentrations above certain threshold levels. An illustrative cartoon from emission of VOCs and NO_x to conversion in greenhouse gases and aerosols has been shown in Figure 1.2.

While NO_x is emitted mostly from anthropogenic sources e.g. traffic and various types of burning, VOCs are emitted from both biogenic and anthropogenic sources. During the daytime, there is always a fast interconversion among NO - NO_2 - O_3 at a time scale of

few minutes. This interconversion can be represented by reactions [R1] to [R3].

$$NO_2 + h\nu \xrightarrow{J(NO_2)} NO + O\,(^3P) \qquad (\lambda < 420nm) \qquad \text{[R1]}$$

$$O\,(^3P) + O_2 + M \xrightarrow[cm^6\,molecule^{-2}\,s^{-1}]{k_{(T)}=6.0\times10^{-34}(\frac{T}{300})^{-2.3}} O_3 + M \qquad \text{[R2]}$$

$$NO + O_3 \xrightarrow[cm^3\,molecule^{-1}\,s^{-1}]{k_{(298)}=1.9\times10^{-14}} NO_2 + O_2 \qquad \text{[R3]}$$

Here M is a molecule present in air (usually N_2 and O_2) that absorbs the excess vibrational energy and hence stabilizes the O_3 molecule formed. If the role of VOCs is not taken into account and only these three compounds are considered, reactions [R1] to [R3] lead to a null cycle and a photostationary state (PSS) between NO_x and O_3 is attained. Since reaction [R2] is much faster than reaction [R3], reactions [R1] and [R3] control the rate of production and loss of ozone. The attainment of photostationary state (PSS) is characterized by Leighton ratio, "Φ" (Leighton, 1961), which is defined as

$$\Phi = \frac{J(NO_2) \times [NO_2]}{k_{[R3]} \times [O_3] \times [NO]} \qquad (1.1)$$

where $J(NO_2)$ is the photolysis frequency of NO_2 and $k_{[R3]}$ is the rate constant of reaction [R3]. $J(NO_2)$ is a function of the NO_2 absorption cross section (σ_{NO_2}), the quantum yield of reaction [R1] (q_{NO_2}) and the actinic flux (I_λ) in the UV-A range (320 – 420 nm).

$$J(NO_2) = \int_\lambda q_{NO_2}(\lambda)\sigma_{NO_2} I_\lambda d\lambda \qquad (1.2)$$

The *actinic flux* is defined as the total radiative energy flux incident on a sphere having unity cross sectional area, irrespective of the beam direction. In the absence of any competing reaction, that is when ozone is the sole NO to NO_2 conversion oxidant, Φ becomes *1* and a dynamic equilibrium is maintained between NO, O_3 and NO_2 and the above mentioned reactions result in no net production of O_3 i.e. a null cycle.

In the troposphere, ozone is formed mostly outside the photostationary state between NO, NO_2 and O_3 which is fuelled by the VOCs. The VOCs (represented as R_iH) emitted from various sources are oxidized by OH radicals ($^\bullet$OH) in the daytime through reactions [R4] and [R5] forming peroxy radicals (XO_2= RO_2 + HO_2) (Finlayson-Pitts and Jr., 2000).

$$R_iH + OH \xrightarrow{O_2} R_iO_2 + H_2O \qquad \text{[R4]}$$

$$CO + OH \xrightarrow{O_2} HO_2 + CO_2 \qquad [R5]$$

The rate of production of peroxy radicals depends both on VOCs and OH radical concentrations.

$$P_{R_iO_2} = k_{(R_iH+OH)}[R_iH][OH] \qquad (1.3)$$

The peroxy radicals serve as extra oxidant to convert NO to NO_2, perturbing the PSS of NO_x and O_3 and contributing to enhanced O_3 production through reactions [R6] to [R8]:

$$R_iO_2 + NO \longrightarrow R_iO + NO_2 \qquad [R6]$$

The R_iO radical can react with O_2, or can isomerize or thermally decompose. Typically a carbonyl compound and hydroperoxy (HO_2) radical is produced.

$$R_iO + O_2 \longrightarrow R_i^{'}CHO + HO_2 \qquad [R7]$$

$R_i^{'}CHO$ can either photolyze to produce HO_x (OH and HO_2) and result in chain branching or can react with OH to continue the chain propagation. HO_2 oxidizes NO to NO_2 which in turn can produce O_3.

$$HO_2 + NO \xrightarrow[cm^3\,molecule^{-1}\,s^{-1}]{k_{(298)}=8.1\times10^{-12}} NO_2 + OH \qquad [R8]$$

Here R and $R^{'}$ can be alkyl/alkenyl/alkynyl groups.

In a high VOC (or NO_x poor) environment, the O_3 production reaction chain can be terminated by loss of HO_x radicals from the system by the radicals radical reaction [R9]

$$HO_2 + HO_2 \xrightarrow[cm^3\,molecule^{-1}\,s^{-1}]{k_{(298)}=1.7\times10^{-12}} H_2O_2 + O_2 \qquad [R9]$$

Under such an environment, ozone production rate (P_{O_3}) is linearly dependent on NO_x concentrations.

$$P_{O_3} = 2k_{[R8]}(\frac{P_{HO_x}}{k_{[R9]}})^{\frac{1}{2}} n_{NO} \qquad (1.4)$$

Here (P_{HO_x}) represents HO_x productions rate and n_{NO} represents NO number density.

However in a polluted environment where NO_x concentrations are high, OH radicals get scavenged by NO_2 by reaction [R10] producing HNO_3 which is removed from air by wet deposition. This also leads to competition between VOCs and NO_2 to react with OH

leading to suppressed XO_2 (RO_2 + HO_2) production.

$$OH + NO_2 + M \xrightarrow[\mathrm{cm^6\,molecule^{-2}\,s^{-1}}]{\mathrm{k_{(T)}}=2.0\times10^{-30}(\frac{T}{300})^{-3.0}} HNO_3 + M \qquad \text{[R10]}$$

Under such conditions O_3 production is limited by supply of hydrocarbons and is inversely proportional to the NO_x concentrations.

$$P_{O_3} = \frac{2k_{[R4]}P_{HOx}n_{RH}}{k_{[R10]}n_{NO_2}n_M} \qquad (1.5)$$

In this generic reaction scheme, two molecules of ozone are produced by oxidation of one molecule of VOCs. Even in this simplified reaction scheme, O_3 production can either be linearly or inversely dependent on NO_x concentrations depending on the kind of regime. The number of molecules of ozone produced per molecule of a VOC oxidized can be higher for hydrocarbon with higher number of carbon atoms. This will also lead to further intricacy in dependency of O_3 production on VOCs or NO_x. After several steps of oxidation, the VOCs can either get converted to CO_2 or become more polar and of high molecular weight, leading to production of secondary organic aerosols (SOA). Both O_3 and CO_2 provide positive feedback to radiative forcing, affecting the global warming. SOA can influence the cloud condensation nuclei (CCN) and affect the quantity and pattern of rain (Rosenfeld et al., 2008). SOA also leads to deterioration in visibility and poor air quality. Various atmospheric models utilize the accurate measurement of concentration of trace gases and radical species, chemical mechanisms including the rate constants and the meteorological conditions for understanding atmospheric chemistry.

1.1.1 Importance of OH radicals and OH reactivity measurements

OH radicals govern the oxidative capacity of the atmosphere in the daytime and hence play a central role in the atmospheric chemistry (Levy, 1971). These are named detergent of the atmosphere (Lelieveld et al., 2008) as they initiate the chain reaction with practically all the reactive VOCs and trace gases in the atmosphere, make them more polar by oxidation in order to facilitate easy removal from the atmosphere. The atmospheric lifetime of OH radicals is less than one second and can even be few milliseconds in polluted environments. Given the large amount of CO and CH_4 added to the atmosphere (2.5 billion and 0.6 billion tonnes per year, respectively (Wennberg, 2006), in the absence of OH radicals, their concentrations would be 10 times higher than the present atmospheric

levels. During the course of this oxidation process, O_3 and secondary organic aerosols (SOA) are produced which in-turn affect the climate and air quality (Gligorovski et al., 2015; Berndt et al., 2016).

In the lower troposphere, the primary pathway for production of OH radicals involves photolysis of ozone molecules to produce excited oxygen atom (reaction [R11]) (Ravishankara et al., 1998)

$$O_3 + h\nu \xrightarrow{J(O^1D)} O\,(^1D) + O_2 \qquad (\lambda < 330nm) \qquad \text{[R11]}$$

O (^{1}D) reacts with water vapour to produce two OH radicals :

$$O\,(^1D) + H_2O \xrightarrow[cm^3\,molecule^{-1}\,s^{-1}]{k_{(298)}=5.97\times10^{-24}} 2\,OH \qquad \text{[R12]}$$

Apart from the primary pathway, three important pathways as source of OH radicals in the troposphere include conversion from HO_2 radicals by reaction with NO according to reaction [R8] or by reaction with O_3 according to reaction [R13] (Lelieveld et al., 2004), photolysis of nitrous oxide (HONO) in urban polluted environments with high NO_x levels and photolysis of H_2O_2 (Zhou et al., 2002).

$$HO_2 + O_3 \xrightarrow[cm^3\,molecule^{-1}\,s^{-1}]{k_{(298)}=2.01\times10^{-15}} 2\,O_2 + OH \qquad \text{[R13]}$$

$$HONO + h\nu \longrightarrow OH + NO \qquad (\lambda < 390nm) \qquad \text{[R14]}$$

$$H_2O_2 + h\nu \longrightarrow 2\,OH \qquad (\lambda < 360nm) \qquad \text{[R15]}$$

There are other sources for production of OH radicals in the troposphere like ozonolysis of alkenes and some other biogenic VOCs (Hens et al., 2014) or photolysis of organic peroxides. Hence the source of OH radicals in the troposphere is generally well understood (Gligorovski et al., 2015). For the accuracy of the atmospheric models, it is quite important to accurately constrain the total OH sink.

The major sink of OH radicals is via its reaction with VOCs and inorganic trace gases like NO_x, O_3 and SO_2. The most recent and updated global models classify the OH sinks among inorganics (NO_x, O_3, SO_2 etc.), CO, CH_4, C1 VOCs and C2*(having ≥ 2 carbon atoms) VOCs lumped as a single entity without providing details of their speciation (Lelieveld et al., 2016). The global budget of OH radicals in terms of production pathways

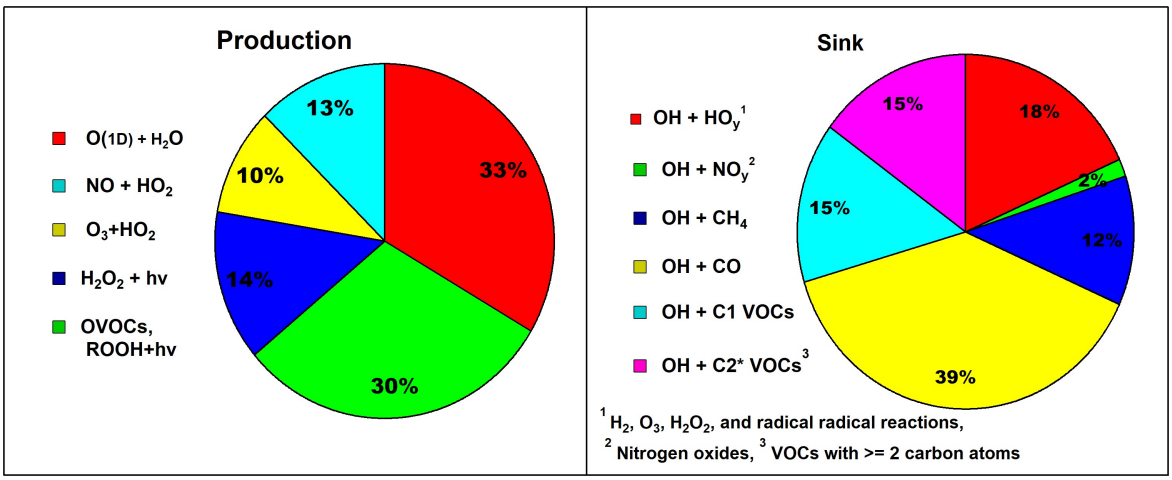

Figure 1.3: Annual global mean of tropospheric sources and sinks of OH radicals (Lelieveld et al., 2016).

and sink reactions are shown in Figure 1.3.

The OH reactivity of an OH reactant is defined as the product of its concentration $[X_i]$ (e.g. X_i = CO, O_3, VOCs, NO_x etc.) and its rate coefficient for reaction with the hydroxyl radical (k_{OH+X_i}), expressed mathematically as:

$$\text{OH Reactivity} = k_{OH+X_i}[X_i] \tag{1.6}$$

Given the large number of different classes of VOCs, it is practically impossible to measure all the OH sinks separately. Hundreds of thousands of VOCs (Goldstein and Galbally, 2007) having various functional groups (Lewis et al., 2000) have been detected in the atmosphere which are present in concentration ranging from few parts per trillion (ppt) to parts per million (ppm) and many more remain unidentified. Due to their chemical diversity, low concentrations and small lifetimes, the accurate quantification of ambient VOCs continue to pose analytical challenges. Even with the simultaneous deployment of various state of the art analytical techniques (Heard, 2008), it is usually impossible to detect and quantify all the VOCs present in the atmosphere.

The total OH reactivity (represented as the first order chemical loss rate of OH radicals in the air) is defined mathematically as the sum of individual OH reactivities of all the reactants present in air.

$$\text{Total OH Reactivity} = \sum_i k_{OH+X_i}[X_i] \tag{1.7}$$

Direct measurement of total OH reactivity was first made possible by Kovacs and

Brune (2001) in the year 1999 by monitoring the decay rate of synthetically generated OH radicals in a flow tube, using laser induced fluorescence (LIF). Four years later, in 2003, Sadanaga et al. (2004a) developed another instrument which measured total OH reactivity of ambient air by monitoring the decay rate of OH in flow tube using a laser-induced pump-probe technique. Both of these instruments are based on in situ detection of OH which required high power lasers and are typically difficult to deploy on field or on moving platforms. Sinha et al. (2008) developed a new technique called the comparative reactivity method (CRM), based on chemical ionization mass spectrometry for direct measurement of total OH reactivity by utilizing the competitive kinetics of reaction of air and a reagent molecule with synthetically generated OH radicals in a glass reactor. It did not require in situ measurement of OH, and rather the concentration of a reagent molecule at concentration of few tens of ppb is monitored at various stages. Being less power demanding, more stable and relatively easier to deploy on field, CRM revolutionized the direct total OH reactivity measurements (Williams and Brune, 2015). Intercomparison studies of the two LIF based OH reactivity measurement systems and the CRM technique have been performed in atmospheric simulation chamber (Fuchs et al., 2017) and in ambient condition (Hansen et al., 2015). These studies have provided important information regarding possible artefacts and the corresponding corrections required for the data processing for various instruments which depend on the operating conditions for the measurements (e.g. alignment of photolysis laser beam and determination of instrumental zero for the LIF instruments, photolysis of VOCs and correction of artefact due to high NO concentration in the CRM technique). Table 1.1 compiles the list of the direct measurements of total OH reactivity reported till date at various places in the world.

Table 1.1: Measured total OH reactivity and the missing fraction reported at different location in the world.

Location	Year	Measured OH reactivity (s^{-1})	Missing fraction (%)	Reference
Nashville	Summer 1999	11.3	∼30	(Kovacs et al., 2003)
New York	Summer 2001	15 - 25	< 10	(Ren et al., 2003)
New York	Winter 2004	18 - 35	–	(Ren et al., 2006)
Mexico	Spring 2003	10 - 120	30	(Shirley et al., 2006)
Houston	Summer 2000	7 - 12	–	(Mao et al., 2010)
Houston	Summer 2006	9 - 22	–	(Mao et al., 2010)
Tokyo	2003-2004	10 - 100	< 30	(Sadanaga et al., 2004a,b)

continued ...

... continued

Location	Year	Measured OH reactivity (s^{-1})	Missing fraction (%)	Reference
Tokyo	Spring 2009	10 - 35	< 22	(Kato et al., 2011)
Mainz	Summer 2005	10.4	–	(Sinha et al., 2008)
Paris	Winter 2010	10 - 130	10 - 54	(Dolgorouky et al., 2012)
Lille	Autumn 2012	∼ 70	–	(Hansen et al., 2015)
Beijing	Summer 2013	20	25	(Williams et al., 2016)
Dunkirk	Summer 2014	10 - 130	–	(Michoud et al., 2015)
Pensylvania	Spring 2002	6.1	–	(Ren et al., 2005)
Weybourne	Spring 2004	4.85	∼ 38	(Lee et al., 2009)
Pearl river delta	Summer 2006	10 - 120	<50	(Lou et al., 2010)
Yufa, China	Summer 2006	10 - 30	–	(Lu et al., 2013)
Spain	Winter 2008	6.3 - 85	–	(Sinha et al., 2012)
Jülich	Summer 2005	6 - 20	∼ 40	(Elshorbany et al., 2012)
Whiteface mountain	Summer 2002	5.6	< 10	(Ren et al., 2006)
Michigan	Summer 2000	1 - 12	∼ 50	(Di Carlo et al., 2004)
Suriname	Spring 2005	53	–	(Sinha et al., 2008)
Hyytiälä	Summer 2008	3.5 - 60	25 - 75	(Sinha et al., 2010)
Rocky mountain	Summer 2008	6.7	29.5	(Nakashima et al., 2014)
Hyytiälä	Summer 2010	3 - 76	58 - 89	(Nölscher et al., 2012b)
Borneo	Summer 2008	5 - 80	∼ 67	(Edwards et al., 2013)
Michigan	Summer 2009	1 - 42	∼ 55	(Hansen et al., 2014)
California forests	Summer 2009	1.25	∼ 33	(Mao et al., 2012)
Manaus	2012-2013	9.9 - 62.4	49 - 79	(Nölscher et al., 2016)
Haute, France	Summer 2014	3 - 70	–	(Zannoni et al., 2016)
Brent, Alabama	Summer 2013	4 - 60	5 - 32	(Kaiser et al., 2016)

Measured total OH reactivity is shown as averaged values or as ranges of diel variations

continued ...

... continued

Location	Year	Measured OH reactivity (s^{-1})	Missing fraction (%)	Reference
or as ranges of the entire campaign)				

Simultaneous measurement of OH reactivity and concentrations of OH reactants enables constraining of VOC budget in an atmosphere. A difference between directly measured total OH reactivity and OH reactivity due to all the measured species (calculated OH reactivity) is regarded as the missing OH reactivity and provides valuable information about completeness of the measurement suite. Analyses of missing OH reactivity in various kinds of environments have yielded important information about new emission processes and chemical transformation previously overlooked or not detected by direct measurements (Di Carlo et al., 2004; Ren et al., 2006; Nölscher et al., 2012b). Simultaneous measurement of OH reactivity and VOCs concentration within a chamber enables validation of chemical mechanisms and product speciation for a targeted species e.g. isoprene (Nölscher et al., 2014).

OH reactivity studies are also helpful for constraining the OH radical budget, for understanding the ozone production regime and SOA production chemistry (Kubistin et al., 2010; Sinha et al., 2012; Zhao et al., 2015). Since OH radicals are very reactive and are present in very low concentration in the atmosphere ($<$ 1 ppt), a steady state assumption for OH and knowledge of total loss rate of OH (L_{OH}) would also enable identification of OH production rate (P_{OH}) according to following equation:

$$\frac{d[OH]}{dt} = P_{OH} - L_{OH} = 0 \tag{1.8}$$

Since VOCs are primarily oxidized by OH radicals, eventually producing tropospheric ozone in several reaction steps, the tendency of these VOCs to react with OH radicals (OH reactivity) has been widely used for assessing the ozone formation potential (Stroud et al., 2008; Sarkar et al., 2016). Higher ambient concentration of a VOC as compared to another does not directly translate into its environmental impact in terms of ozone formation potential. For example, ozone formation potential of isoprene (C_5H_8) is $>$ 150 times higher than that of CO (Carter, 1994), whereas the ambient concentration of isoprene is generally 2-3 orders of magnitude lower than that of CO. There are other scales for assessing the ozone production potential of different VOCs e.g. Maximum incremental reactivity (MIR)(Carter, 1994) and Photochemical ozone creation potential (POCP)(Derwent et al., 1996). These provide information of increment in ozone mass due to addition of a given mass of particular VOC ($\frac{d[O_3]}{d[VOC]}$) under high NO_x condition,

but again are able to do a good job only for measured compounds.

1.2 Present status of ozone and VOC measurements in the Indo-Gangetic Plain

There are very few long-term in situ measurement studies of ozone and its precursors performed in the IGP. Surface ozone in the IGP was first reported for the period 1989 - 1990 from Delhi (Varshney and Aggarwal, 1992) and Varanasi (Pandey and Agrawal, 1992). The first continuous online measurements of O_3 from IGP was performed during winter 1993 which reported daytime 30 min average O_3 mixing ratios between 34 ppb and 126 ppb at various locations in Delhi (Singh et al., 1997). Short term measurements cannot explain the effect of changing meteorological conditions and emission over a full year. The two previous long term in situ datasets reported from the IGP are from Agra (27.18 °N, 78.02 °E, 169 m a.s.l.) (Singla et al., 2011) and more recently from Kanpur (26.46 °N, 80.33 °E, 125 m a.s.l) (Gaur et al., 2014) in the central IGP. While Singla et al. (2011) reported monthly average O_3 mixing ratios ranging between 9 ppb and 45 ppb and NO_2 mixing ratios ranging between 15 ppb and 35 ppb, Gaur et al. (2014) reported monthly average O_3 mixing ratios ranging between 9 ppb and 41 ppb and NO_x mixing ratios ranging between 3 ppb and 9 ppb respectively. Singla et al. (2011) observed the maximum and minimum daytime eight-hour average mixing ratio of ozone to be 89 ppb in summers and 7 ppb in winters respectively. Similarly summertime (pre-monsoon) maximum mixing ratio of ozone was observed by Gaur et al. (2014) with an hourly average value of up to 107 ppb, but in contrast the minimum hourly average of 1.1 ppb was observed in monsoon season. Based on the satellite data between 1979 to 1992, the rate of increase in tropospheric ozone was reported to be twice as high over the IGP as compared to South India (Lal et al., 2012).

The reported measurements of the precursors of ozone from the IGP are even more scarce. Whereas Mallik and Lal (2014) reported satellite retrieved monthly average CO mixing ratios over Delhi between 100 ppb and 300 ppb during the years 2005 - 2010, Gaur et al. (2014) reported the monthly average CO mixing ratios at Kanpur during years 2009 - 2013 ranging between 520 ppb and 1020 ppb. However, both the studies reported maximum CO mixing ratio during winter and minimum in monsoon seasons. All these previous studies from the IGP have emphasized the need of long term measurements of ozone and its precursors from more sites.

While there are handful of continuous online measurements of O_3, NO_x and CO from the IGP, there are no reported online measurements of reactive VOCs from this region

until 2013. One year long offline measurement of less reactive VOCs (C2 - C5 non methane hydrocarbons (NMHC)) have been reported by a few measurements over India (Rao et al., 1997; Mallik et al., 2014; Sahu and Lal, 2006a,b; Swamy et al., 2012). Various other studies have measured the mixing ratios of aromatic VOCs (benzene, toluene, ethylbenzene and xylene) or total lumped VOC concentration in three metro cities in India (Delhi, Mumbai and Kolkata) using offline techniques and reported only seasonal or monthly average concentrations (Hoque et al., 2008; Khillare et al., 2008; Srivastava et al., 2006; Dutta et al., 2009; Srivastava et al., 2005). It can be noted that these measurements exclude reactive VOCs e.g. isoprene, oxygenated VOCs e.g. acetaldehyde and methanol and acetonitrile which is a chemical tracer of biomass burning. The first online measurement of VOCs was reported from our research group by Sarkar et al. (2013) where two days of 1-minute time resolution data of acetonitrile and aromatic VOCs e.g. benzene, toluene, sum of C-8 aromatics and sum of C-9 aromatics was reported. This study was followed by the work of Sinha et al. (2014) where one month long high temporal resolution data of nine VOCs including isoprene, aromatics, oxygenated VOCs (methanol, acetaldehyde, acetone) and acetonitrile in the summer season at a suburban site in the N.W. IGP. High concentrations of reactive VOCs e.g. methanol, isoprene and acetaldehyde and biomass burning tracer e.g. acetonitrile was reported by Sinha et al. (2014) in the summertime air of IGP, which was generally higher than the ambient levels reported anywhere in the world. More recently, Chandra and Sinha (2016) have reported three years' online measurements of aromatic VOCs (benzene, toluene, sum of C-8 aromatics and sum of C-9 aromatics), acetonitrile and isocyanic acid from post monsoon season of the north-west Indo-Gangetic Plain and documented their enhancement due to paddy residue fires. Few short term measurements of up to one month have highlighted the important role of VOCs from other urban locations of western India (Sahu and Saxena, 2015; Sahu et al., 2016)

1.3 Research motivation

The Indo-Gangetic Plain (IGP) is the agricultural nerve of South Asia as it produces a variety of food crops for the sustenance of the vast human population of 1.67 bn people (source: The world bank *http : //data.worldbank.org/region/SAS*)). Large urban, agricultural, forest fire and industrial emission from this region add several teragrams of reactive gaseous pollutants into the atmosphere (Venkataraman et al., 2006; Zhang et al., 2009). On the other hand, due to longer period of intense solar radiation, high ambient temperature and high humidity, large oxidant concentrations are also expected in this region which tend to transform and remove these gaseous pollutants via several chemical reactions.

Biomass burning is known to emit a large suite of reactive pollutants in the atmosphere (Crutzen and Andreae, 1990; Andreae and Merlet, 2001). Out of the fourteen specific radiative forcing components, the emissions from biomass fires affect eight e.g. ozone, long-lived greenhouse gases, aerosols (direct), aerosols (indirect), surface albedo, stratospheric water vapour, solar irradiance and linear contrail (Bowman et al., 2009). Controlled combustion of crop residue under laboratory conditions has revealed emissions of a complex suite of more than 200 identified VOCs (Stockwell et al., 2015; Gilman et al., 2015). In the north-west Indo-Gangetic Plain (N.W. IGP) almost 12 Mha area of land is being used for growing the major cereal crops (e.g. rice and wheat) (Aggarwal et al., 2004) in a rotation system. After harvesting the wheat crop, there is a narrow time window to clear the field for sowing the next crop. Due to lack of proper processing units, it is a usual practice to burn the crop residue to prepare the field for the next crops. The satellite observation in the year 2005 have estimated > 12000 km^2 of paddy and > 5500 km^2 of wheat field burnt in the N.W. IGP itself (Badarinath et al., 2006).

Previous studies on crop residue fires from India have mostly focussed on aerosols and primarily emitted long lived trace gases e.g. carbon dioxide, nitrous oxide, methane and carbon monoxide (Sahai et al., 2007; Venkataraman et al., 2006). Proton transfer reaction mass spectrometer (PTR-MS) enables real-time measurements of VOCs at time resolution of few seconds as it does not require any sample treatment and ambient air is continuously monitored . Chandra and Sinha (2016) have used PTR-MS to report three years' dataset from post monsoon season of the N.W. IGP to document the enhancement and health effects of several benzenoids and isocyanic acid due to paddy residue fire emissions. This study only focuses on the post monsoon periods to show the effect of crop residue fires on few VOCs (mostly benzenoids, acetonitrile and isocyanic acid).

Hence it is very important that long term measurement ozone and aerosols are accompanied with the measurement of its precursors including speciated VOCs and meteorological parameters. Except for the recent measurements from our group (Sinha et al., 2014; Chandra and Sinha, 2016; Sarkar et al., 2013) there is hardly any information about the long-term concentrations and variability of VOCs, specific sources and processes governing their concentrations and their role towards ozone production in the South Asia. Non availability of year-long measured dataset of VOCs limits the understanding of impact of various emission sources (e.g. wood and bio-fuel burning in winter, crop residue burning in summertime and post-monsoon, biomass and garbage burning active throughout the year, enhanced biogenic emission during and after the monsoon rain, traffic emissions and industrial emissions), sink processes (e.g. monsoon rain and winter fog) active during different seasons of a year, varying meteorology and chemical transformations and fetch region.

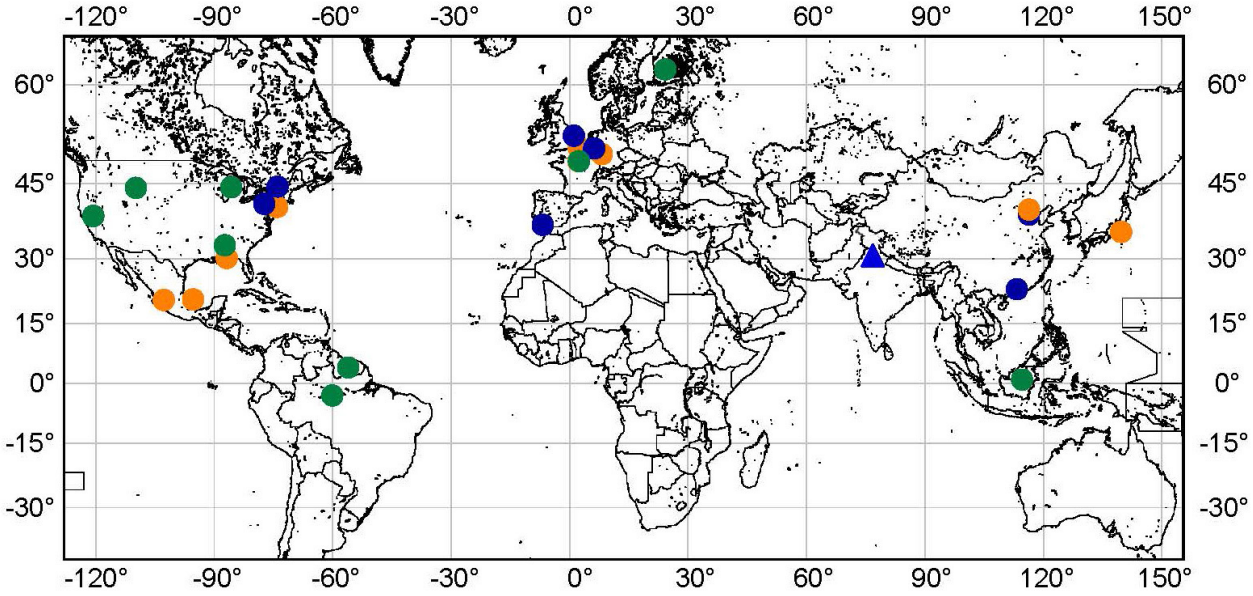

Figure 1.4: Map of the world showing the location of Mohali and locations where direct measurements of Total OH reactivity have been reported. The yellow, blue and green circles show the urban, suburban and forested environments. The blue triangle represents Mohali.

This also emphasizes the need of direct measurement of total OH reactivity to accurately constrain the total reactive pollutant loading and ozone production regimes. It is also equally important to obtain simultaneous in situ measurements of VOCs concentration along with the total OH reactivity for more appropriate scientific outcome in terms of targeted ozone mitigation strategy. Simultaneous measurements of VOCs, total OH reactivity and reactive inorganic trace gases e.g. NO_x, sulphur dioxide (SO_2) and ozone allows evaluation of instantaneous ozone production regime, identification of major components among various VOCs and inorganic trace gases which limit the ozone production in the daytime and also an estimation of reactive pollutants present in the ambient air which are not measured. The constraints with the analytical techniques till date allowed a PTR-MS to perform either VOCs concentration measurements or total OH reactivity measurements using CRM technique (Sinha et al., 2008). In our laboratory where only one PTR-MS was deployed, it was desirable to find a way to perform both VOCs and OH reactivity measurement with the same PTR-MS.

These measurements in this region of the world in periods influenced by large scale open crop residue fires would also facilitate first assessment of OH reactivity perturbation of ambient air due to active fires. Analysis of missing OH reactivity would also be helpful for assessment of unmeasured primary emissions and their oxidation products.

1.4 Thesis outline

With the work presented in this thesis I would like to address the knowledge gaps highlighted in the preceding discussion by addressing following scientific problems:

1. How do the concentrations of ozone, carbon monoxide and NO_x change in response to changes in meteorological conditions and anthropogenic perturbations (e.g. agricultural residue fires) in different seasons in the north-west Indo-Gangetic Plain? Are the temporal patterns and seasonal behavior reproducible for more than one year?

2. Which VOCs are the major drivers for peak daytime production of tropospheric ozone in different seasons? Is the peak daytime ozone production limited by availability of NO_x or by availability of VOCs in the N.W. IGP?

3. How do the ambient concentrations of VOCs, OH reactivity due to measured VOCs and ozone production potential vary over different seasons of the year in the north-west IGP? Which periods of year are expected to have highest total OH reactivity?

4. How to enable rapid online measurements of VOCs and total OH reactivity using a single proton transfer reaction mass spectrometer without compromising on the sensitivity, accuracy and detection limit of both OH reactivity and VOC measurements?

5. How much extra reactivity do the emissions from summertime agricultural residue fires in the N.W. IGP introduce directly and indirectly (through secondary processes) into the ambient atmospheric environment? Are all the important chemical constituents involved in this process measured and incorporated in detailed atmospheric chemistry models?

The first question is discussed in chapter 2, wherein I have presented two year-long measurement of O_3, NO_x and CO along with acetonitrile which is a biomass burning tracer and meteorological parameters from a site in the N.W. IGP. Airmass clusters arriving at the receptor site were classified into different clusters to pin point the specific impact of crop residue fires in the summertime and post monsoon on the ambient concentration of these species. The second and third questions are addressed in 3, wherein I have presented one year long online measurements of 23 different VOCs whose primary source in the atmosphere include different classes e.g. biogenic, urban, industrial, biomass burning and photo-oxidation. The VOC OH reactivity and ozone production is calculated for different seasons using the measured VOC concentration. The sensitivity of peak daytime ozone

production is evaluated by comparing the VOCs OH reactivity and NO_x OH reactivity. The fourth question is addressed in chapter 4, wherein I have discussed the development of a new analytical tool which enables rapid sequential measurements of ambient VOC concentration and total OH reactivity using a single PTR-MS. It also adds specificity to a PTR-MS equipped with a quadrupole mass analyzer to differentiate between isobars by evaluating the kinetics of reaction of a VOC with OH radicals. The field deployment of this technique provided the first measurement of total OH reactivity from the South Asia. The final question is addressed in chapter 5 where I have presented the results of measurement of total OH reactivity together with VOCs and other trace gases from the NW IGP during normal summertime condition and summertime influenced by wheat residue fires. A 0-D box model constrained with the measured VOCs and utilizing the Master Chemical Mechanism (MCM version 3.3.1) was used to evaluate the fraction of total OH reactivity which could not be explained by the measured set of gases and their secondary oxidation products during both the periods. Substantial evidence of emission of several reactive nitrogen containing VOCs from the crop residue fires were obtained from these measurements.

Chapter 2

Influence of post harvest crop residue fires on surface ozone mixing ratios in the N.W. IGP analyzed using two years of continuous in situ trace gas measurements

Abstract

Ozone, CO and NO_x are criteria air pollutants affecting air quality and tropospheric chemistry but factors that control them in the densely populated north-west Indo-Gangetic Plain (N.W. IGP) are poorly understood. In this chapter, I report the first simultaneous two-year-long in situ dataset of ozone, CO and NO_x acquired from August 2011 - September 2013 at a representative site in the N.W. IGP (30.667 °N, 76.729 °E ; 310 m above mean sea level). Drivers of the diel and seasonal variability of O_3, CO and NO_x in terms of season specific processes (e.g. suppressed transport and efficient wet scavenging of primary emissions and suppressed photochemistry due to cloud cover during the summer monsoon, intense photochemistry during summer) and emissions (e.g. crop residue fires and wintertime open biomass combustion for domestic heating) were clearly elucidated. In particular the impact of post harvest crop residue fires was found to profoundly impact the in situ chemistry of ozone formation. Regional post-harvest wheat residue fires were found to contribute majorly to high hourly averaged ozone concentrations ($\sim$ 80 ppb). In the absence of the wheat residue fires, ozone was much lower (by 19 ppb). Paddy residue fires also enhanced the peak ozone concentrations by $\sim$ 7 ppb, despite lower radiation and

temperature relative to the "clean" post monsoon period ozone concentrations. d[O_3]/dt (from sunrise till daytime O_3 maxima), was highest during periods influenced by post-harvest fires in post monsoon season (9.2 ppb h^{-1}) and lowest during monsoon season (4.1 ppb h^{-1}). Analysis of air mass clusters revealed that enhanced chemical formation of O_3 and not transport was the driver of the summertime and post monsoon ambient O_3 maxima. Despite having high daytime NO_x (> 12 ppb) and CO (> 440 ppb) in winter, average daytime O_3 was less than 40 ppb due to reduced photochemistry and fog. Average daytime O_3 concentration during the monsoon was less than 45 ppb due to washout of precursors and suppressed photochemistry due to cloud cover. The 8 h national ambient air quality standard (NAAQS) for O_3 was violated on 451 days (62% of the total) in the period August 2011 - September 2013. The results revealed the periods/seasons with highest ozone pollution during the year and highlighted that substantial mitigation efforts are required to reduce regional O_3 pollution in the N.W. IGP due to agricultural fires.

2.1 Introduction

Tropospheric ozone (O_3), carbon monoxide (CO) and nitrogen oxides (NO_x) are criteria air pollutants that affect ambient air quality, human health and climate (U.S.EPA, 1990). In particular, tropospheric O_3 is a short-lived climate pollutant (SLCP) (Schmale et al., 2014). Exposure to high concentration of tropospheric O_3 causes significant crop yield losses (Ashworth et al., 2015; Giles, 2005; Sinha et al., 2015) and pulmonary diseases (Haagen-Smit, 1952; Jerrett et al., 2009). In the troposphere, O_3 is the primary precursor of hydroxyl radicals (Heard and Pilling, 2003). It is also an important atmospheric oxidant that forms secondary organic aerosol by oxidizing reactive terpenes through ozonolysis reactions (Carlton et al., 2009).

CO and NO_x pose health risks at elevated concentrations. CO exposure affects the oxygen carrying capacity of blood and can cause cardiovascular diseases and even death (Hexter and Goldsmith, 1971; Prockop and Chichkova, 2007). Short-term exposure of NO_2 even below 20 ppb can cause respiratory problems in infants whereas elevated concentration > 100 ppb of NO_2 is considered toxic (U.S.EPA, 2008; WHO, 2005). Both CO and NO_x contribute to the formation of tropospheric O_3 through non-linear radical chemistry (Sinha et al., 2012)and are mainly emitted from anthropogenic sources (Bergamaschi et al., 2000; Miyazaki et al., 2012). Rapid urbanization and economic growth have caused an increase in their sources which is detrimental to air quality, crop productivity and climate (Giles, 2005).

The N.W. Indo-Gangetic Plain (IGP) is the agricultural "bread basket" of South Asia as it produces a variety of food crops that feed 1.67 billion people (FAO, 2013). Satellite

data acquired over the years 1979 -1992 indicate that the rate of increase in tropospheric O_3 of 3 - 5.6 % per decade is more than twice as high as that in the sites in southern India, which showed an increase of 1.2 - 2 % per decade in the same period (Lal et al., 2012). In contrast to the sites in western and southern India, where annual maxima of O_3 have been reported in winter (Ahammed et al., 2006; Lal et al., 2000), the annual O_3 maxima in the IGP is typically observed during the early summer or late spring season (Gaur et al., 2014; Ghude et al., 2008; Ojha et al., 2012). While satellite data are inherently attractive and useful due to their widespread availability and spatial coverage, they have limitations in terms of accuracy over regions where they have not been validated using in situ data and ground truthing. Further, the resolution of satellites (including temporal resolution and coverage) is too coarse to capture the heterogeneity of short lived pollutants such as NO_x and O_3. This is the case over much of the IGP and other understudied regions of the world. Satellite data for tropospheric O_3 retrieval require corrections for stratospheric O_3, which in turn depends on the accurate resolution of temporal- spatial changes in the height of the tropopause. Despite the obvious importance and need for quality-assured long duration in situ data from the N.W. IGP region on O_3, carbon monoxide and nitrogen oxides, to the best of our knowledge no previous long term dataset reporting simultaneous in situ measurements of these gases from the N.W. IGP has been presented in the peer-reviewed literature. The only studies reporting more than a year's data for the aforementioned trace gases are from Kanpur and Agra, which are located in the central IGP (Gaur et al., 2014; Singla et al., 2011). High temporal resolution in situ measurements performed over the duration of more than one year help elucidate the effects of seasonality and diel activity on atmospheric composition and chemistry and such datasets afford the opportunity to test whether seasonal variability and extreme events are captured by satellite retrievals and model simulations.

The spread of mechanized combine harvester technology since 1986 has led to the intensification of post harvest crop residue burning in the N.W. IGP (> 12000 km^2 and > 5500 km^2 was burnt to rid fields of paddy and wheat straw, respectively in 2005 (Badarinath et al., 2006). This activity occurs in April - May (primarily for wheat straw) and October - November (primarily for paddy straw) (Irwine, 2014). Though several previous studies have highlighted the detrimental impact of agricultural crop residue fires (e.g., Sahai et al., 2007), no previous work has quantified the influence of agricultural crop residue fires in the N.W. IGP on surface O_3, CO and NO_x concentrations using in situ data. The objective of the present study is to investigate the impact of emissions and meteorology on the diel and seasonal variability of O_3, CO and NO_x with a focus on regional agricultural crop residue fires. A quality controlled two-year-long high temporal resolution in situ dataset of ozone, nitrogen oxides and carbon monoxide acquired

from August 2011 to December 2013 at a regionally representative suburban site in the N.W. IGP was employed for this purpose. Daily MODIS (Moderate Resolution Imaging Spectroradiometer) satellite-derived fire count data and ancillary in situ acetonitrile data (a chemical tracer for emissions from biomass fires (Chandra and Sinha, 2016; Holzinger et al., 1999) were also used for periods affected by the regional crop residue fires. The two-year-long dataset provided the confidence in characterizing the effect of meteorology and emissions in different seasons by ruling out effects of anomalous years as this study analyzes data from August 2011 - September 2013. Analysis of air mass clusters was undertaken to determine whether regional chemical O_3 production or transported O_3 was the major contributor to the high O_3 concentrations observed during periods influenced by the agricultural crop residue fires. An assessment of compliance with the 8 hours averaged national ambient air quality O_3 standard of India for the two-year-long dataset was also undertaken.

2.2 Materials and methods

2.2.1 Site description and measurements

The data presented in this work pertaining to O_3, CO and NO_x were measured at the Indian Institute of Science Education and Research (IISER) Mohali atmospheric chemistry measurement facility (30.667 °N, 76.729 °E ; 310 m above mean sea level) from 16 August 2011 to 5 September 2013 at a temporal resolution of 1 minute. Measurement of acetonitrile (CH_3CN), a chemical tracer for biomass fire emissions, was available from 24 August 2011 onwards whereas measurement of co-located meteorological parameters e.g. wind speed, wind direction, solar radiation, ambient temperature and relative humidity were available from 25 November 2011 onwards at similar temporal resolution (Chandra and Sinha, 2016).

The site is a regionally representative suburban location in the N.W. Indo-Gangetic Plain. A complete description of the site and comprehensive technical details pertaining to sampling, data quality assurance and calibration protocols have been previously described in Sinha et al. (2014). Briefly, the nearest neighbouring cities are Mohali, Chandigarh and Panchkula, which lie in the wind sector north to east of the site. This sector is classified as the urban sector due to the dominance of urban emission sources. The wind sector spanning south to north-west is dominated by agricultural and rural land use and is the most frequent fetch region upwind of the site during the year. To the south and south-east, the land use is mixed-rural and industrial in nature. The Himalayan mountain range lies $\sim$ 30 km in the N.W. to S.E. direction. We note further that Sinha et al.

(2015) conducted a review of multi-year O_3 data reported previously from several sites in north India (see Table 4 of Sinha et al., 2015) which showed that the seasonality and O_3 concentrations measured at our site are regionally representative. In August 2015, a new highway (Aerocity road) and international airport were commissioned in the urban fetch region (north east – south), increasing the traffic density near the site for this fetch region. Under calm wind conditions and when the wind blows from this sector (note it is not the most frequent direction), the site is now better classified as "urban". However, this has no bearing on the data presented in this work which is from 2011 – 2013, when the site was sub-urban even for this fetch region.

Ambient ozone measurement was performed by UV photometry technique (Huntzicker and Johnson, 1979) using Thermo Fischer Scientific 49i analyzer. O_3 absorbs UV radiation ($\lambda < 320$ nm) with an absorption maxima at 253.84 nm. Mercury (Hg) lamp is used as UV source. The instrument is designed to operate in the Beer Lambert regime where the absorbance due to ozone molecules is proportional to the number of ozone molecules in the air sample. The sample drawn through the inlet line passes through a solenoid valve which divides and alternates the flow between two streams, one of which passes through MnO_2 based ozone scrubber and serves as reference. Both the cells containing sample and reference are illuminated by single lamp and the intensity of the UV light is measured by photo diode detectors at the end of the cells. With ageing the efficiency of both the UV light source and the detector can decrease and to account for this and characterize the instrument's accuracy, the O_3 analyzer was calibrated using a NIST traceable O_3 primary standard generator (Model 49i PS; Thermo Fischer Scientific, Franklin, USA). Between 16 August 2011 and 06 September 2013, a total of 21 span calibrations experiments (in the range of 25 ppb – 125 ppb) were performed for O_3. The average ($\pm$ 1σ) of slopes of linear fits ($r^2 > 0.99$) between measured and introduced O_3 concentrations in these calibration experiments was 0.99 $\pm$ 0.06 (range 0.83 and 1.08). The major gaps in the two-year O_3 dataset were a two week period from 6 to 21 July 2012 and a three day period from 19 August 2013 to 21 August 2013 owing to maintenance issues.

NO_x (NO and NO_2) measurements were performed by chemiluminescence technique using a Thermo Fischer Scientific 42i trace level analyzer. The detection principle is based on the reaction of NO with O_3 inside a reaction chamber and subsequent production of luminescence in the wavelength range of 600 - 3000 nm. Ozone is generated inside the instrument using an ozonator to provide excess ozone for the chemiluminescence reaction. The ozone is also required for a dynamic zero during the measurement through a pre-reactor, where NO reacts with ozone prior to the reaction chamber. A three way solenoid valve inside the instrument continuously alternates the sample flow to directly reach the reaction chamber or via pre-reactor unit. The size of pre-reactor is constrained so that

greater than 99 % of a 200 ppb NO sample reacts before entering the reaction chamber, and yet is small enough to avoid potential interferents to pass to the reaction chamber. For measurement of NO_2, all the NO_2 in the sample stream is converted to NO prior to reaction with O_3. This is accomplished by a NO_2 to NO molybdenum converter heated at 325 °C. This converter is known to convert other reactive nitrogen species (e.g. nitric acid (HNO_3), nitrous acid (HONO), nitrate radical (NO_3), dinitrogen pentoxide(N_2O_5), peroxynitric acid (HNO_4), alkyl nitrates ($RONO_2$), peroxyalkyl nitrates ($ROONO_2$) and peroxyacyl nitrates (PAN) ($R(O)O_2NO_2$)) into NO as well (Sinha et al., 2014; Wang et al., 2002). Hence the nitrogen dioxide (NO_2) measurements reported in this work should be regarded as upper limits of the actual ambient NO_2 (hereafter referred to as NO_2*). Between 16 August 2011 and 06 September 2013, a total of 18 span calibration experiments (in the range of 10 ppb – 50 ppb) were performed using a custom ordered NO gas standard (Chemtron Science Laboratories Pvt. Ltd., Mumbai, 6 ppm in nitrogen, stated uncertainty 5 %). The average ($\pm$ 1σ) of the slopes of linear fits ($r^2 > 0.96$) between measured and introduced NO was 1.04 $\pm$ 0.10 (range 0.88 and 1.28) in these calibration experiments. The major gap in the timeline of NO_x data was from 23 to 27 March 2013 due to flow problems.

Carbon monoxide (CO) was measured by gas filter correlation (GFC) non dispersive infra-red (NDIR) technique using Thermo Fischer Scientific 48i trace level enhanced analyzer. GFC-NDIR technique for monitoring of trace level CO was developed by the US-EPA project and has been used extensively in other scientific studies (de Gouw et al., 2009; Andreae et al., 2012). Water vapour and CO_2 are known to cause interferences at ambient CO levels using NDIR technique, but gas filter correlation provides selectivity for CO (Chaney and McClenny, 1977). Between 16 August 2011 and 06 September 2013, a total of 17 span calibration experiments (in the range of 100 ppb – 1500 ppb) were performed using a custom ordered CO gas standard (Chemtron Science Laboratories Pvt. Ltd., Mumbai, 22 ppm in nitrogen, stated uncertainty 5 %). The average ($\pm$ 1σ) of slopes of linear fits ($r^2 > 0.99$) between measured and introduced CO was 1.04 $\pm$ 0.10 (range 0.82 and 1.22) for these calibration experiments. There were no breaks from the regular protocol for daily zero drift checks. The major gaps in the timeline of CO data were from 06 to 20 April 2012 and from 19 August 2013 to 21 August 2013 due to problems with the internal heater and pressure sensor and maintenance issues and from 11 to 29 September 2012 due to the failure of an internal pump.

Acetonitrile was measured using a high sensitivity proton transfer reaction – quadrupole mass spectrometer (PTR-QMS) (Model 11-07HS-088; Ionicon Analytik Gesellschaft, Austria)(Sinha et al., 2014). Between 16 August 2011 and 06 September 2013, 9 calibration experiments were performed to check the sensitivity of PTR-QMS for detection of ace-

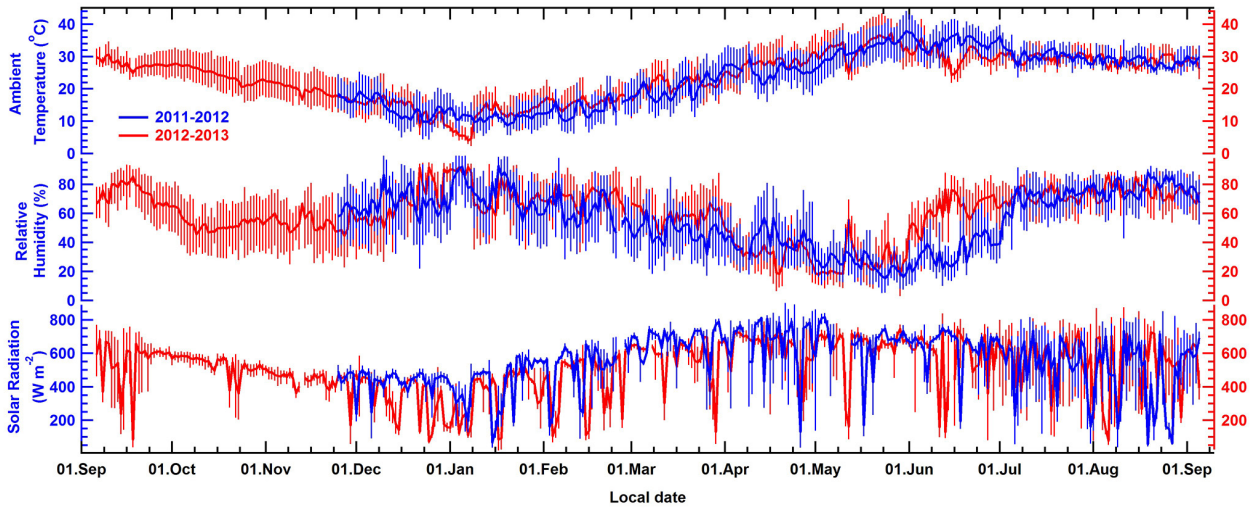

Figure 2.1: Daily average trend of relative humidity, ambient temperature and peak daytime (12:00 - 14:00 local time (L.T.)) solar radiation for the measurement period. Blue lines show data for the period from November 2011 to August 2012 (meteorological station was installed on Nov 25, 2011) on the left axes and red lines show data for the period from September 2012 to September 2013 on the right axes. Vertical bars represent the daily variability as 90^{th} and 10^{th} percentiles of the measured monthly data.

tonitrile (in the range 1 ppb – 20 ppb). The average ($\pm$ 1σ) of the slopes of linear fits ($r^2 > 0.99$) between detected normalized counts per second (ncps) and introduced acetonitrile (ppb) was 17.90 $\pm$ 2.28 ncps ppb^{-1} (range 14.29 and 21.10) in these calibration experiments (Chandra and Sinha, 2016).

Meteorological sensors (Met One Instruments Inc., Oregon, USA) were co-located with the trace gas sampling inlets as shown in Figure 5 of Sinha et al. (2014).

2.2.2 Meteorology and classification of seasons

According to the Indian Meteorological Department (IMD), an year is classified into four seasons: winter, summer (or pre-monsoon), monsoon (rainy) and post monsoon (autumn) (*http : //www.imd.gov.in/section/nhac/dynamic/FAQ_monsoon.htm*). Based on this classification, January and February comprise winter, March - May comprise summer, June - September comprise monsoon and October – December, the post monsoon seasons. The basis for this classification is the "All-India" ambient temperature and rainfall, although regional onset and end of seasons can vary significantly. For meaningful analysis of the chemical data presented in this work and delineation of seasons, the measured in situ meteorological datasets and satellite-derived fire counts data were collectively employed (e.g., Chandra and Sinha, 2016).

Figure 2.1 shows the daily average of relative humidity (top panel), ambient tem-

perature (middle panel) and peak daytime (12:00 h - 14:00 h local time) solar radiation (bottom panel) measurements made at the site from November 2011 to September 2012 in blue and from September 2012 to September 2013 (in red). As the meteorological sensors were installed only on 25 November, 2011 meteorological data is not available prior to November, 2011. The vertical bars reflect the daily variability (as 10^{th} and 90^{th} percentiles). Table 2.1 lists the dates and durations of seasons at the measurement site in 2011, 2012 and 2013 (06 September 2011 – 05 September 2013). The onset of wintertime is defined to be when the daily temperature minima and the daily solar radiation maxima fell below 10 °C and 500 W m $^{-2}$, respectively. The wintertime months of December and January were characterized by dense fog as can be inferred from the high relative humidity (> 80 % RH) and low solar radiation (Figure 2.1). This dense fog in the winter months with visibility < 1 km can spread over an area of $\sim$ 1500 km $\times$ 400 km as a blanket over the entire IGP (Gautam, 2014). The end of winter and beginning of summer was defined to be when the daily ambient temperature minima and solar radiation maxima exceeded 10 °C and 500 W m $^{-2}$, respectively. Thus in 2011-12, winter was from 10 December 2011 – 29 February 2012 and in 2012-13 it was from 10 December 2012 – 28 February 2013. Summer is characterized by high daytime temperatures (> 40 °C), intense solar radiation and dry conditions (< 40 % RH) which are favourable for photochemical formation of O_3. Thus in 2012, summer was from 01 March 2012 – 01 July 2012 and in 2013 it was from 01 March 2013 – 12 June 2013. The monsoon season followed after summer, and its start was determined on the basis of the first rain event after the prevailing wind direction switches from predominantly north-westerly flow to south-easterly flow. In the monsoon season, the air has high relative humidity (> 60 % RH most of the time), heavy rainfall, thunderstorms and diffused solar radiation due to cloud cover, despite temperatures above 30 °C on most days. Figure 2.1 shows that the variability in peak solar radiation is highest during the winter and monsoon seasons, which is due to fog and dynamic cloud cover changes, respectively. In 2012, monsoon was from 02 July 2012 – 18 September 2012 and in 2013 it was from 13 June 2013 – 05 September 2013. The post monsoon season marks the transition period between the monsoon and winter seasons. Clear sky and less polluted conditions were observed at the start of the post monsoon season. Due to anthropogenic perturbations in the form of large scale post harvest agricultural crop residue burning in April - May (mainly wheat) and October - November (mainly paddy), the summer and post monsoon seasons were further sub-divided into two periods (classified as clean and periods influenced by wheat and paddy residue fires).

Figure 2.2 shows the daily MODIS fire counts data in 2011 - 2012 (blue bars) and 2012 - 2013 (red bars) for the relevant study periods (September 2011 to September 2012 and September 2012 to September 2013). The daily fire counts data (at > 50 % confidence

Table 2.1: Classification of seasons and number of measured data points and overall ambient data coverage for each trace gas from September 2011 - September 2013.

Season	**Time Period**	**NO_x**	**CO**	**O_3**
		Number of data points (n)		
Post Monsoon (clean)	06 September 2011 – 10 October 2011	34560	26382	33310
Post monsoon (paddy residue fire influenced)	11 October 2011 – 09 December 2011	86400	83179	83678
Winter	10 December 2011 – 29 February 2012	118081	116941	113638
Summer (clean)	01 March 2012 – 30 April 2012 and 22 June 2012 – 01 July 2012	102241	97978	85290
Summer (wheat residue fire influenced)	01 May 2012 – 21 June 2012	74879	72783	70092
Monsoon	02 July 2012 – 18 September 2012	113759	100810	84700
Post Monsoon (clean)	19 September 2012 – 10 October 2012	31680	31527	31297
Post monsoon (paddy residue fire influenced)	11 October 2012 – 09 December 2012	86400	79182	83156
Winter	10 December 2012 – 28 February 2013	116639	113820	111060
Summer (clean)	01 March 2012 – – 30 April 2013	87841	73349	82410
Summer (wheat residue fire influenced)	01 May 2013 – 12 June 2013	61919	60431	58754
Monsoon	13 June 2013 – 18 September 2012	123840	114702	114764
Overall ambient data coverage (%)		94	92	94

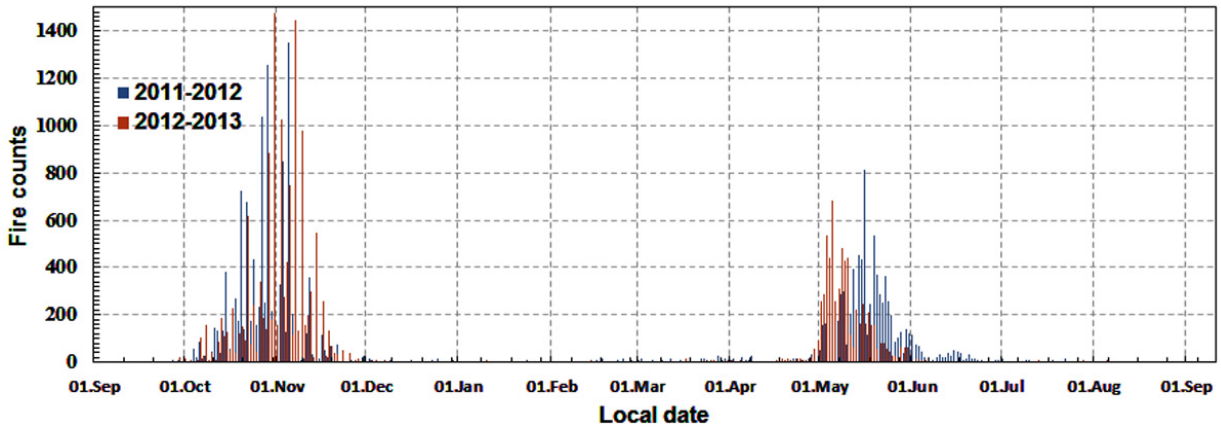

Figure 2.2: Daily fire counts observed by MODIS at greater than 50 % confidence interval over the region of North West Indo-Gangetic Plain between 28 °N to 33 °N and 72 °E to 79 °E from September 2011 to September 2012 in blue bars and from September 2012 to September 2013 in red bars.

interval) were obtained using MODIS onboard Terra and Aqua satellites at a spatial resolution of 1 km × 1 km for the region spanning 28 °N - 33 °N latitude and 72 °E - 79 °E longitude. Intense fire activities were observed during the post monsoon season from the second week of October until the end of November in both 2011 and 2012 and in summer from the first week of May in both 2012 and 2013. Summertime crop residue burning (mainly wheat) ends with the arrival of monsoon rains which occurred on 21 June in 2012 and 12 June in 2013. Consequently, the summertime crop residue burning occurred on fewer days in 2013 relative to 2012. For the present analysis, we considered the start of the period in summer influenced by wheat residue fires (termed "polluted summer") to be from 01 May in both 2012 and 2013. The start of the period influenced by paddy residue fires during the post monsoon season (termed "polluted post monsoon") was considered to be 11 October, as explained and justified in Chandra and Sinha (2016) using objective set of criteria. We note that while the exact dates for the respective periods can be debated by 1 - 2 days for the wheat/paddy fire influenced periods in individual years, we chose 01 May/11 October to be the start date for each year and 09 December as the end date for polluted post monsoon. Note also, that our sensitivity tests carried out by including or excluding few days does not change any of the scientific conclusions derived from subsequent analyses presented in this work.

Figure 2.3(a-f) provides an overview of season-specific wind roses at the site using wind speed and wind direction data acquired from 25 November 2011 to 06 September 2013. The data pertaining to each specific season in 2011, 2012 or 2013 was consolidated season-wise to simplify the visualization in Figure 2.3 and get an overview picture of the period investigated in this study. Note, there, there was hardly any inter annual

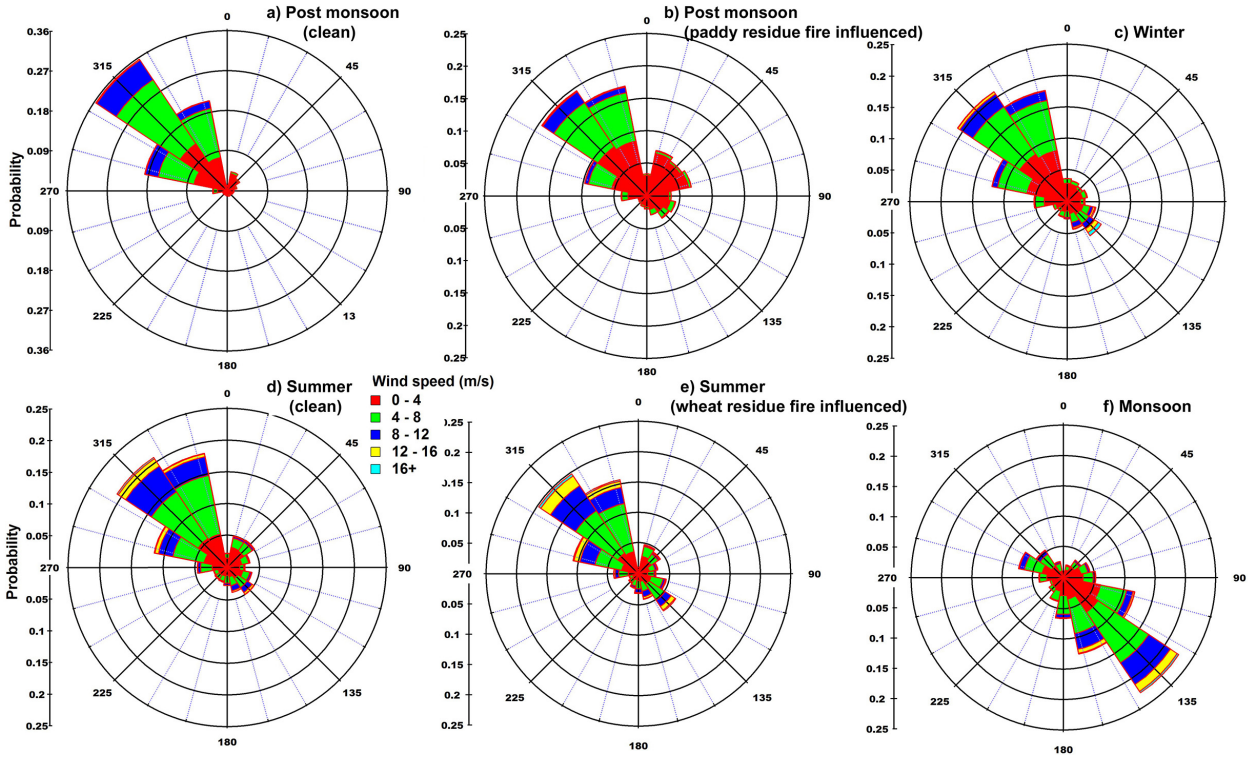

Figure 2.3: Wind rose plot from measured in situ data of wind speed and wind direction for a) post monsoon (clean), b) post monsoon (paddy residue fire influenced), c) winter, d) summer (clean), e) summer (wheat residue fire influenced) and f) monsoon seasons for the entire measurement period. The radius axes represent the probability of an airmass arriving from the particular wind speed and wind direction bin.

variability in the season specific wind flow pattern at the site. It can be seen that the most prevalent wind direction at the site is from the north-west (e.g. winter, summer and post monsoon), where the land use is primarily agricultural and rural in nature (Sinha et al., 2014). About 40 % of the time, the sector spanning from north to west acted as the fetch region at high wind speeds (between 4 $\mathrm{m\,s^{-1}}$ - 16 $\mathrm{m\,s^{-1}}$). This renders the site appropriate for investigating long range transport processes from regions west of the measurement site (Pawar et al., 2015). In the monsoon season, the wind blows from the sector spanning south to east. Stagnant conditions are observed more frequently in the winter and polluted post monsoon, whereas summer, monsoon and clean post monsoon are characterized by high wind speeds.

Variations in meteorological conditions, such as ambient temperature, solar radiation, rainfall, wind pattern and relative humidity, which occur over the course of several months, have impacts on physical and chemical processes and influence the ambient concentrations of chemical species. The delineation of seasons in the manner described above permitted meaningful analysis of the O_3, NO_x, CO and acetonitrile data for assessing the impact of

agricultural crop residue fires as discussed in the subsequent sections.

2.3 Results and discussion

2.3.1 Variability of nighttime and daytime O_3, NO, NO_2^*, CO and acetonitrile from September 2011 - September 2013

Figure 2.4 a and 2.4 b show the time series of the daily average daytime and nighttime mixing ratios respectively, for O_3 (top panel), NO_2^* (second panel), NO (third panel), acetonitrile (a chemical marker for emissions from biomass fires; fourth panel) and CO (bottom panel) during different seasons from September 2011 – September 2013. The solid lines represent the daytime (night time) average for 2011 - 2012 in blue and 2012 - 2013 in red, whereas the vertical bars capture the daily variability as 10^{th} and 90^{th} percentiles. Shaded regions of the graph indicate the periods affected by the crop residue fires. Since the measured dataset does not belong to a normal distribution, we have carried out the "non parametric Kruskal-Wallis test", for the measured datasets of CO, NO, NO_2^*, O_3 and acetonitrile (one minute temporal resolution), to quantify statistical differences in trace gas concentrations measured during the pre-harvest and post harvest (influenced by crop residue fires) periods in the summer and post monsoon seasons of 2012 and 2013. For both the years, a Chi-squared approximated p-value of less than 0.0001 at a significance interval $>$ 99.999 % was obtained for CO, NO, NO_2, O_3 and acetonitrile (a chemical tracer for emissions from the biomass fires) for each pair of clean and crop residue fire affected period. This revealed that the datasets measured in the pre and post-harvest periods belong to statistically different distributions. Table 2.1 summarizes the number of available 1-minute temporal resolution ambient measurements for different seasons and overall ambient data coverage from which the present datasets have been derived (n $>$ 26000 measurements for each season and n $>$ 952100 measurements for the full measurement period, for each trace gas).

Each season is characterized by distinct meteorological and/or emission activities as discussed in Section 2.2.2. Daytime was defined as the period when solar radiation exceeded 50 W m $^{-2}$ (Gerosa et al., 2007). For the post monsoon period of 2011 when the measured solar radiation data was not available, daytime was considered between 07:00 to 17:00 Local Time (L.T.) which is consistent with the observed daytime hours during post monsoon season of 2012. Owing to absence of photolysis and photochemical oxidation at night, the daytime and nighttime periods had distinct chemical sinks. The primary emission sources active throughout the year were traffic, garbage fires and biofuel burning for cooking purpose (Garg et al., 2015). Additional emissions in the polluted summer and

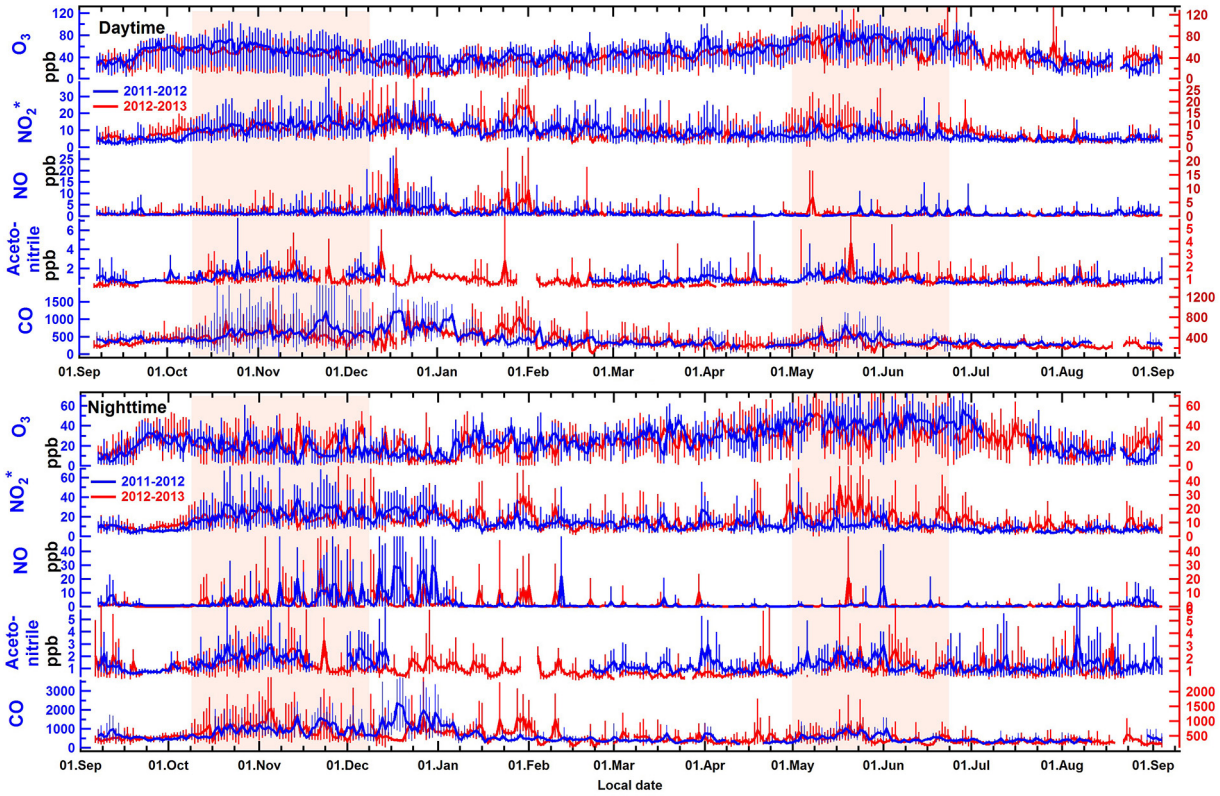

Figure 2.4: a) Daytime and b) Nighttime daily average mixing ratios of O_3, $NO_2{}^*$, NO, Acetonitrile and CO for the period 06 September 2011 – 05 September 2012 in blue (left axes) and for the period 06 September 2012 – 05 September 2013 in red (right axes). The vertical bars above and below the solid lines show the daily variability as 90^{th} and 10^{th} percentile. Shaded regions highlight periods influenced by the post harvest crop residue fires.

polluted post monsoon seasons occurred due to crop residue fires and in winter due to open burning of combustible material for domestic heating (Garg et al., 2015).

Table 2.2: Average ± 1σ (ambient variability) daytime and nighttime mixing ratios (in ppb) of CO, NO, $NO_2{}^*$ and O_3 for individual seasons from September 2011 to September 2013.

	CO		NO		$NO_2{}^*$		O_3	
	Day	Night	Day	Night	Day	Night	Day	Night
Post monsoon 2011 (clean)	417.0±173.8	503.9±174.8	0.9±1.6	0.6±1.1	5.6±3.3	7.8±4.8	53.6±20.6	25.7±11.7
Post monsoon 2011 (paddy residue fire influenced)	620.2±279.8	969.5±598.1	1.6±2.9	4.7±10.9	12.5±7.9	23.7±15.4	54.9±25.6	18.0±12.5
Winter 2011-2012	547.3±334.3	793.8±660.1	2.2±3.7	5.2±12.6	12.0±5.9	16.7±10.1	40.2±18.1	21.0±13.1
Summer 2012 (clean)	302.6±132.1	392.2±167.9	0.9±3.4	0.4±1.9	7.4±5.2	11.5±7.8	55.9±19.4	32.9±15.4
Summer 2012 (wheat residue fire influenced)	424.0±223.0	580.9±282.3	0.8±2.8	0.8±4.6	8.3±5.5	12.0±7.9	69.9±23.3	43.6±17.7
Monsoon 2012	291.5±77.7	388.0±157.8	1.0±2.0	1.5±3.3	4.6±2.4	6.7±3.6	32.9±14.7	15.7±12.6
Post monsoon 2012 (clean)	371.2±101.5	466.8±141.7	0.9±1.8	0.3±1.2	5.8±3.4	7.6±4.4	53.4±21.8	27.9±14.2
Post monsoon 2012 (paddy residue fire influenced)	448.3±183.5	737.0±477.6	1.6±3.0	4.2±11.3	8.6±4.5	15.0±8.7	51.2±23.3	20.9±15.9
Winter 2012-2013	445.7±226.0	568.7±363.3	2.5±4.7	2.8±8.9	9.4±5.9	12.7±8.2	32.1±17.9	16.7±13.1
Summer 2013 (clean)	282.6±124.0	388.2±208.6	0.8±2.2	0.7±3.2	5.7±4.3	9.6±7.6	51.7±18.4	30.1±13.9
Summer 2013 (wheat residue fire influenced)	308.6±131.3	467.7±265.8	0.8±2.7	1.1±5.9	8.4±5.4	16.0±11.7	67.9±24.3	38.6±18.2
Monsoon 2013	244.8±75.6	309.4±140.7	0.5±1.4	0.6±2.3	4.7±3.3	7.9±6.2	44.6±24.2	25.8±21.0

Table 2.2 summarizes the seasonally averaged daytime and nighttime mixing ratios of these chemical species. As observed from Figure 2.4 a and 2.4 b, Figure 2.5 and Table 2.2, the time series of O_3 mixing ratios show a similar trend over the course of two different years. In general, the minimum mixing ratios of daytime O_3 ($<$ 45 ppb) are observed in winter or monsoon seasons followed by post monsoon season and normal summertime conditions ($\sim$ 51 - 56 ppb). The maximum average daytime O_3 mixing ratios are observed during periods influenced by the wheat residue fires in summer ($\sim$ 68 - 70 ppb). During winter season, O_3 concentrations in the daytime generally reached 40 ppb whereas nighttime concentrations were usually below 10 ppb in January and below 20 ppb in February 2012. Figure 2.1 shows that winter months have the lowest temperatures and lowest solar radiation. These conditions are unfavourable for photochemical formation of O_3, despite significant emissions of precursors such as CO and NO_x in the daytime (comparable to the polluted summer and post monsoon). During the cold winter nights, open burning of combustible material (leaves, wood, plastic, garbage) for heating purposes (Garg et al., 2015) in combination with a shallow and stagnant nocturnal boundary layer results in high concentrations of NO (daytime $>$ 2.2 ppb ; nighttime $>$ 2.8 ppb), $NO_2{}^*$ (daytime $>$ 9.4 ppb ; nighttime $>$ 12.7 ppb) and CO (daytime $>$ 445.7 ppb ; nighttime $>$ 568.7 ppb). This results in fairly efficient nighttime titration of NO with O_3 (see Table 2.2 and Figure 2.4 (a-b)). Average acetonitrile concentrations measured during the winter season were 1.1 $\pm$ 0.7 (1 σ ambient variability) ppb. During winter 2012 - 2013 rain events were also observed on 14 December 2012, 17 January 2013, 18 January 2013, 05 February 2013, 16 February 2013, 23 February 2013, 26 February 2013 and 27 February 2013 whereas winter 2011 - 2012 was drier. Winter rains deter the open burning and hence comparatively lower concentrations of CO and NO_x were observed during winter 2012 - 2013. Although the wintertime mixing ratios of CO and NO_x are lower in 2011 - 2012 as compared to 2012 - 2013, the observed seasonal trends for these species are similar in both the years (see Table 2.2 and Figure 2.5).

The winter season is followed by the clean summer season in which the air is drier ($\sim$ 40 % RH). The need for nighttime fires for warmth reduces when the winter fog lifts and both daytime and nighttime O_3 concentrations increase. The clean summer is followed by the polluted summer season, which is characterized by large-scale wheat residue burning in the agricultural fields. In 2012, the polluted summer occurred primarily in May. Sinha et al. (2014) reported speciated volatile organic compounds (VOCs), CO and NO_x during May 2012 and more recently Kumar and Sinha (2014) measured high average OH reactivities of 53 s^{-1} (range 20 s^{-1} - 108 s^{-1}) in May 2013. OH reactivity which is the product of the rate constant of a pollutant with the hydroxyl radical and the pollutant's concentration is a robust measure of the total reactive pollutant loading of ambient air (Sinha et al.,

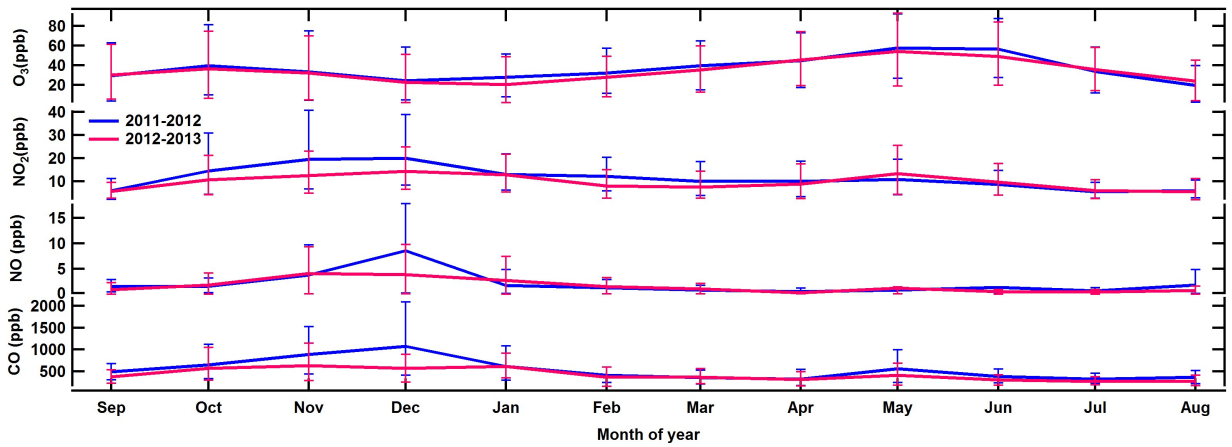

Figure 2.5: Average monthly trend of O_3, NO_2*, NO and CO for the period 06 September 2011 – 05 September 2012 in blue and for the period 06 September 2012 – 05 September 2013 in red. Vertical bars represent the monthly variability as 10^{th} and 90^{th} percentiles of the measured monthly data.

2012). During May 2013, the high average OH reactivities of 53 s^{-1} measured at the site are consistent with high reactive pollutant loading in summer due to emissions from the wheat residue fires. In addition to the high fire counts observed during this period (see Figure 2.2), an enhancement of 0.45 ppb was observed in the average concentration of acetonitrile from the baseline values of 0.8 ppb in the clean summer season which also indicates enhanced loading of other reactive VOCs co-emitted from the wheat residue fires. The average concentration of acetonitrile observed during the polluted summer season is significantly higher than those reported elsewhere in the world during summertime (see Table 3 of Sinha et al., 2014). May month was characterized by the highest number of O_3 exceedance days in the 8 h national ambient air quality standard (29 days out of 31 in 2012 and 30 days out of 31 in 2013) for any single calendar month during the year. Peak O_3 production is either VOC and NO_x limited or NO_x limited in summer in the agricultural regions of the IGP (Sinha et al., 2014) and hence, an increase in O_3 precursors relative to the clean summer (Sinha et al., 2014) would contribute to enhancement in the ambient average O_3 during the daytime. The high daytime regional O_3 ($\sim$ 80 ppb) also contributes to high nighttime O_3 concentrations ($\sim$ 40 ppb).

The monsoon season is characterized by moist air ($\sim$ RH $>$ 60 %), cloudy skies and removal of water soluble precursors of O_3 (Gaur et al., 2014). These factors collectively contribute to the cleanest air of the year with daytime O_3 rarely exceeding 45 ppb and nighttime O_3 close to 20 ppb. CO and NO_x are also characterized by their lowest daytime and nighttime concentrations of the year. The wet conditions likely reduce open burning for waste disposal (Sinha et al., 2014) so that biomass burning emissions are much lower compared to other seasons. Since CO, NO and NO_2 have low solubilities (Henry law's

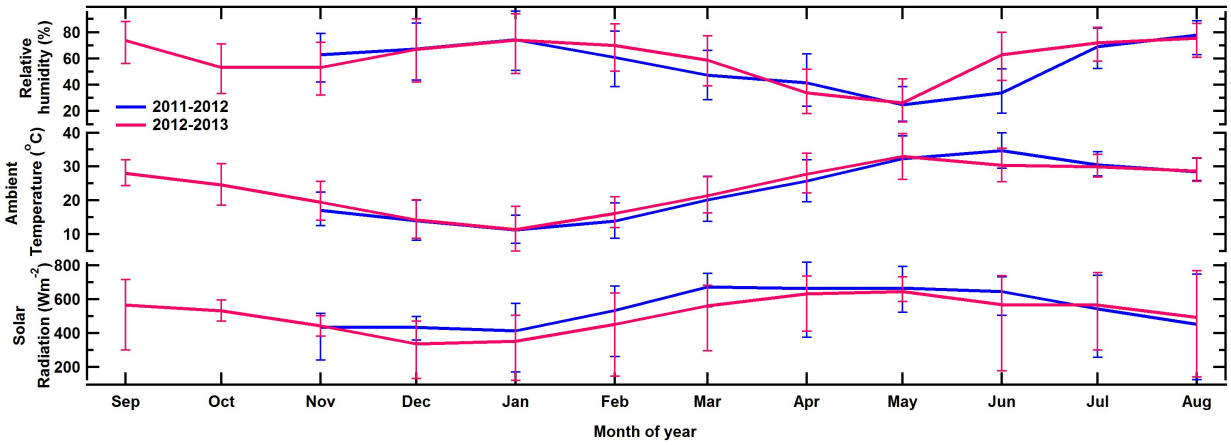

Figure 2.6: Average monthly trend of relative humidity, ambient temperature and peak daytime (12:00 h - 14:00 h local time) solar radiation for the period 06 September 2011 – 05 September 2012 in blue and for the period 06 September 2012 – 05 September 2013 in red. Vertical bars represent the monthly variability as 10^{th} and 90^{th} percentiles of the measured monthly data.

coefficient 9.7×10^{-6}, 1.9×10^{-5} and 1.2×10^{-4} mol m^{-1} Pa^{-1} for CO, NO, NO_2, respectively (Sander, 2015)), wet scavenging is not expected to be of major direct consequence for these species, except close to point sources where their concentrations are high.

The post monsoon season that follows is characterized by drier conditions relative to the monsoon (mean monthly RH decreases to 60 % RH; see Figure 2.6). Figure 2.2 shows the daily peak daytime (12:00 - 14:00 local time) solar radiation data for both monsoon and clean post monsoon periods during 2013. It can be clearly seen that the variability is much lower during the clean post monsoon and also there are more instances of low radiation days during the monsoon season supporting our contention. As the vegetation is no longer water limited, clear sky conditions favour biogenic emissions of species such as isoprene from vegetation which have high O_3 formation potential. Thus, conditions favour enhanced photochemical production of O_3. This is also seen in high d[O_3]/dt in the morning hours as discussed later in section 2.3.2.1. The daytime O_3 rises significantly to concentrations similar to the clean summer ($\sim$ 53 ppb). Mixing ratios of CO and NO_x also increase relative to those in monsoon.

The occurrence of paddy residue fires from mid-October until the first week of December marks the polluted post monsoon season (Chandra and Sinha, 2016). O_3 concentrations do not decrease despite reductions in radiation and temperature as the emission of reactive VOCs (see Sarkar et al., 2013; Chandra and Sinha, 2016), NO_x and CO under stagnant meteorological conditions (see Figure 2.3 e and Figure 2.3 f) increase the reactivity and O_3 production efficiency (see discussion in Section 2.3.2.1). Average acetonitrile mixing ratios observed during this period were 1.6 $\pm$ 1.1 ppb as compared to 0.9 $\pm$ 0.8

ppb in the clean post monsoon. Nighttime O_3 concentrations in polluted post monsoon season are lower relative to the clean post monsoon, due to fairly effective titration of O_3 with NO emissions from the paddy fires. This is analyzed further in Section 2.3.3.

Primary pollutants have high daytime and nighttime concentrations in winter and periods affected by paddy residue fires and wheat residue fires due to biomass burning. The minimum concentration of primary pollutants is observed in monsoon season due to reduction in biomass combustion (wet conditions) followed by clean summer and clean post monsoon seasons.

2.3.1.1 Comparison with National Ambient Air Quality Standards of India (NAAQS)

In order to provide a legal framework to curb air pollution, the Ministry of Environment and Forests (MOEF), India implemented the revised national ambient air quality standards (NAAQS) for several air pollutants in the year 2009. The 8 hour average NAAQS limit for ozone is 100 $\mu g\,m^{-3}$ ($\sim$ 50 ppb at Normal Temperature and Pressure (NTP)). For calculations, the measured 1-minute data was averaged to yield hourly averaged temporal resolution data. A running 8-hour average was then calculated using the hourly data. Only those days were considered for comparison, for which the measurement coverage comprised at least 75 % of the day (18 hours). The maximum average O_3 mixing ratio for any continuous 8-hour interval (e.g. between 00:00 - 08:00 local time; 01:00 - 09:00 local time and so on) in a day (U.S.EPA, 1998) was compared with the 8 h NAAQS for O_3, to obtain the number of O_3 exceedance days. During the entire measurement period, out of 726 such days, the 8 h average O_3 mixing ratio exceeded the standard on 451 days (or 62 % of the year). Figure 2.7 shows a calendar of the measurement period colour coded by the daily 8 h maximum average O_3 concentration (Carslaw and Ropkins, 2012). In addition, we found that 307 O_3 exceedance events occurred in the 1 h O_3 NAAQS of 180 $\mu g\,m^{-3}$ ($\sim$ 91 ppb at NTP), out of which 110 and 98 events (68 % of the total number of such events) occurred during the polluted summer season of 2012 and 2013 respectively. The higher number of exceedance events in the 1 hour NAAQS suggests that crop residue fires further enhance the peak daytime O_3 concentration and worsen an already alarming situation. This is examined in more detail in the subsequent sections.

At the site, the $NO_2{}^*$ levels never exceeded the 24 h average NAAQS limit ($\sim$ 42 ppb at NTP) during August 2011 - September 2013. For the entire measurement period, CO concentrations also never exceeded the 8 h average CO NAAQS limit of $\sim$ 1742 ppb.

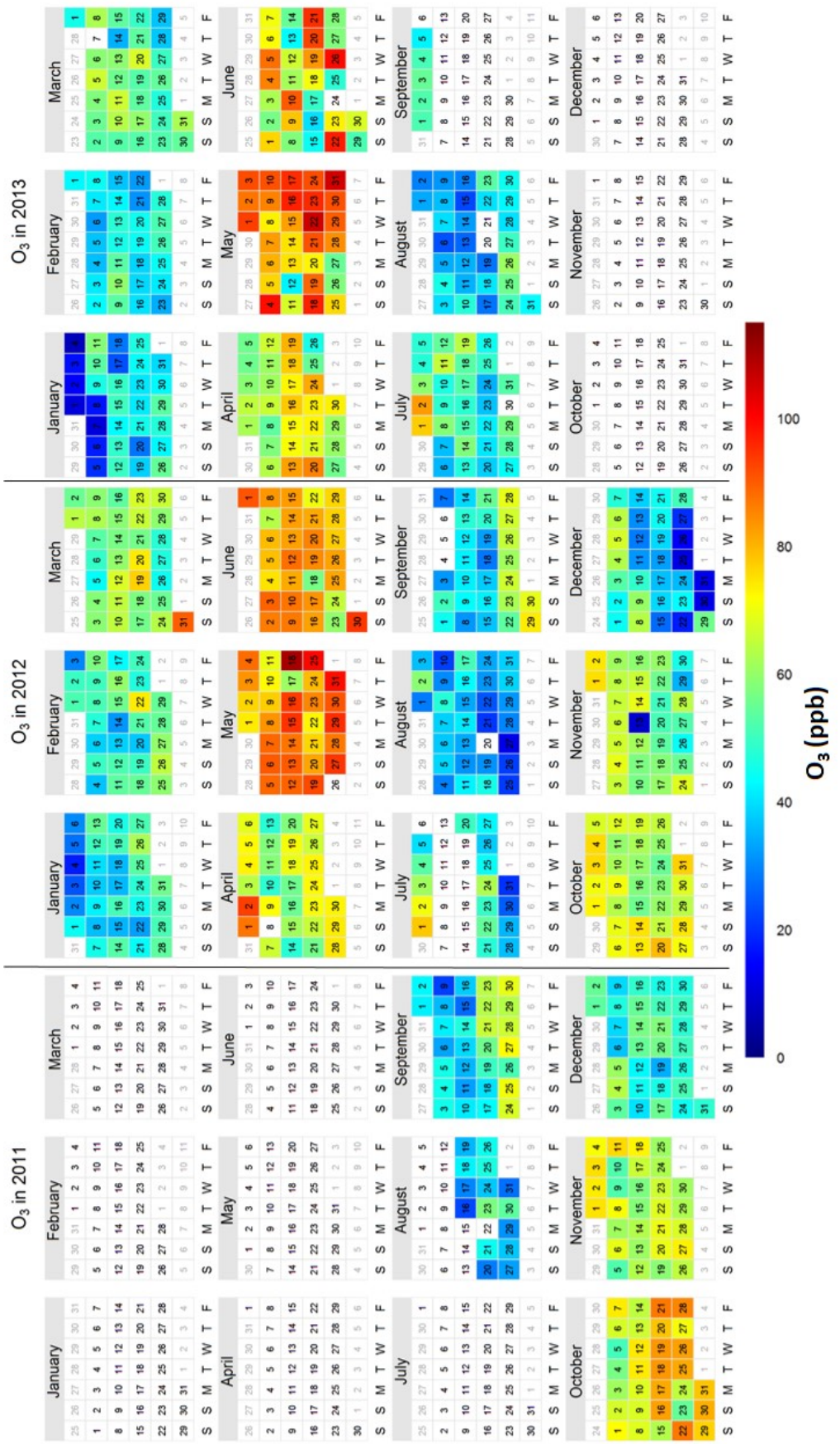

Figure 2.7: Calendar dates from 16 August 2011 to 05 September 2013, colour coded according to values of the daily maximum 8 h running average of ozone mixing ratios.

2.3.2 Season-specific diel variability of O_3, NO, NO_2^* and CO

Figure 2.8 (a-d) summarize the diel variation in average mixing ratios of CO, O_3, NO and NO_2^* in winter (grey), clean summer (red), polluted summer (brown), monsoon (blue), clean post monsoon (green) and polluted post monsoon (light brown), respectively combined for the two-year period from September 2011 - September 2013. Diel profiles help elucidate time dependent emission activity. Irrespective of season, under normal meteorological conditions at a surface site in the plains, the daytime boundary layer height is always higher compared to the nocturnal boundary layer (NBL) height (Stull, 1988). A bimodal profile was observed for CO throughout the year. The sources contributing to CO in morning hours were 1) early morning flush due to breaking of NBL (Koppmann, 2007) and 2) biofuel combustion. Vertical mixing is suppressed in the shallow nocturnal boundary layer (NBL) as the increase in potential temperature with height within the NBL makes it stable. An air parcel lifted up in the NBL will return to its initial position as it is colder than its surrounding. Dilution in an elevated daytime boundary layer drives the daytime minima of CO, as its reaction with hydroxyl radicals is too slow on hourly time scales to account for a significant chemical loss. Sources of the nighttime CO were inefficient biofuel burning (wood, charcoal and cow-dung cakes) for cooking purpose and traffic emissions as also discussed by Sinha et al. (2014). Very high peaks between 19:00 - 22:00 L.T. were observed for CO ($>$ 1000 ppb) and NO_x ($>$ 30 ppb) during winter and the polluted post monsoon season, due to widespread biomass combustion for domestic heating in the former and crop residue burning in the latter (in addition to the normal sources) and stagnant meteorological conditions. The diel maxima in other seasons also occurred generally between 19:00 - 22:00 L.T. for CO and NO_x. In all seasons, the morning peaks ($<$ 800 ppb for CO and $<$ 20 ppb NO_x) occur between 07:00 - 09:00 L.T. and are less pronounced than the evening peaks. Sources of CO and NO_x are traffic and biofuel combustion for cooking. The evening peaks are more prominent due to lower boundary layer in the evening and traffic rush being higher in the evening. Winter and polluted post monsoon were characterized by the highest concentrations. Traffic emissions contributed to the observed concentration increases in the evening as well. Bimodal peaks in CO and NO_x have been reported previously from other sites in India e.g. Mumbai (Lal and Patil, 2001) and are typical of urban and suburban surface sites influenced by urban emissions around the world (Koppmann, 2007).

The daytime O_3 maxima was attained by 11:00 L.T. in all seasons (except winter where it occurred at 15:00 L.T.) and concentrations declined typically after 17:00 L.T. The monsoon season had the lowest average daytime O_3 concentration ($<$ 45 ppb for peak daytime hours) and difference between daytime and nighttime ($<$ 28 ppb) due to unfavourable conditions for photochemical formation of O_3. Note that during winter

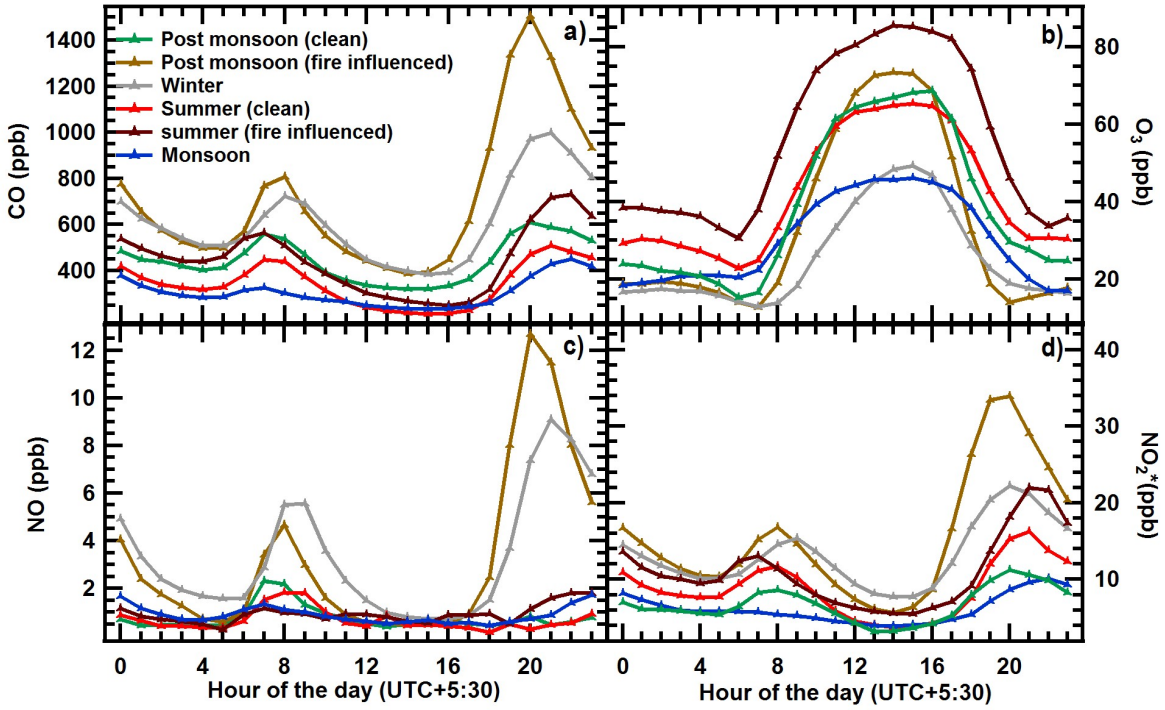

Figure 2.8: Season specific average diel profiles in the measured concentrations of a) CO, b) O_3, c) NO and d) NO_2^* calculated using the composite dataset from September 2011 - September 2013 wherein each season occurred twice and in different years. The colour code in the legend indicates the season.

months despite similar radiation as in the month of August and lower temperatures; the peak daytime average O_3 concentrations still reached 50 ppb, and the peak daytime concentration was $\sim$ 35 ppb higher than the nighttime values.

The diel profiles of O_3 also suggest that accumulation of nocturnal NO_x reservoirs (e.g. HONO) occurs in all seasons. When these species photo-dissociate at sunrise, they produce NO, which titrates O_3 resulting in a minimum of the daytime O_3 concentration just after sunrise (at $\sim$ 06:00 L.T. except for winter and polluted post monsoon when it is observed at $\sim$ 07:00 L.T.). During the winter and the polluted post monsoon seasons, the average evening time (19:00 - 21:00 L.T.) NO concentrations of circa 10 ppb efficiently titrate O_3, resulting in nighttime concentrations of O_3 at the site of less than 20 ppb during these seasons. Except the clean summer, polluted summer and clean post monsoon seasons, where the average nighttime concentrations were rather high (circa 30 - 44 ppb), the nighttime O_3 concentrations were less than 50 % of the daytime concentrations (see Table 2.2). The difference between average peak daytime and minimum O_3 was $>$ 55 ppb during the fires affected summer and post monsoon periods.

Using diel box and whiskers profiles of CO, acetonitrile and aromatic VOCs, Chandra

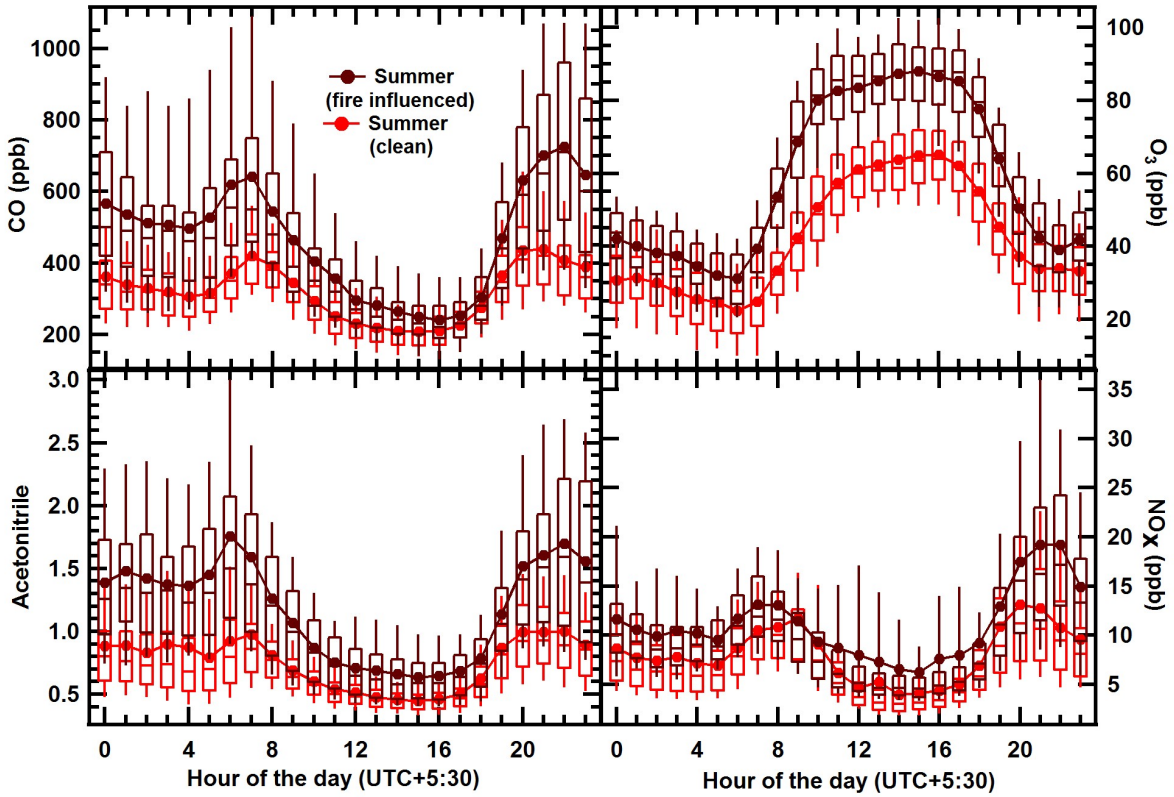

Figure 2.9: Diel box and whiskers plot of measured concentrations of CO, O_3, Acetonitrile and NO_x (NO + NO_2) for airmasses filtered for the rural/agricultural fetch region (wind sector south to north-west) and wind speed bin of 1 - 5 m s^{-1} for summer periods influenced by the wheat residue fires (in brown) and the clean summer (in red) using the composite data measured in 2012 and 2013.

and Sinha (2016) have shown the contribution of crop residue fires towards enhanced emissions in the post monsoon season. In the summer season too, the diel profile of acetonitrile concentration in the airmass arriving from rural/agricultural sector at wind speeds less than 5 m s^{-1} and greater than 1 m s^{-1} (which filters off both long range transport and stagnant conditions) for the wheat residue fire affected periods show enhancement > 0.500 ppb in the evening and night hours (see Figure 2.9).

2.3.2.1 Analysis of season specific d[O_3]/dt between sunrise and peak daytime hourly average O_3

The rate of change of surface ozone at any site is dependent on its net chemical production (production-loss), surface deposition and advection (Cazorla and Brune, 2010). Shortly after sunrise until attainment of the peak daytime O_3 mixing ratios, the chemical production term tends to be the largest at a typical surface site. Using the O_3 diel concentration profiles in Figure 2.8, the rate of change in ambient O_3 (d[O_3]/dt) during

Table 2.3: Start and end time of O_3 build-up hours and the net rate of change of ozone during the O_3 build-up hours representative for different seasons estimated using two years of measurement.

Season	O_3 build-up start hour (L.T.)	start hour of O_3 peak daytime plateau (L.T.)	$d[O_3]/dt$ (ppb h^{-1})
Winter	08:00	15:00	4.9
Summer (clean)	06:00	12:00	6.1
Summer (wheat residue fire influenced)	06:00	12:00	8
Monsoon	07:00	12:00	4.1
Post monsoon (clean)	07:00	13:00	8
Post monsoon (paddy residue fire influenced)	07:00	13:00	9.2

the O_3 build-up hours (from sunrise till the start of peak daytime plateau region; see Table 2.3 for the seasonally relevant hours) was calculated for each season. The observed summertime $d[O_3]/dt$ is higher by 1.9 ppb h^{-1} in the periods affected by the wheat residue fires (8.0 ppb h^{-1}) as compared to normal conditions. Similarly, for post monsoon season, periods affected by paddy residue fires, $d[O_3]/dt$ exceed the unperturbed values of the clean post monsoon periods (8.0 ppb h^{-1}) by 1.2 ppb h^{-1}. Wintertime $d[O_3]/dt$ for the build-up hours is 4.9 ppb h^{-1} whereas in the monsoon season it is at 4.1 ppb h^{-1}. High $d[O_3]/dt$ for build-up hours observed for the polluted summer and polluted post monsoon seasons suggest that crop residue fires strongly influence the in situ O_3 formation chemistry due to addition of reactive precursors of O_3 (NO_x, CO and VOCs) during both polluted summer (Sinha et al., 2014) and polluted post monsoon season (Sarkar et al., 2013). High $d[O_3]/dt$ of 8.0 ppb h^{-1} in the clean post monsoon is likely to be due to enhanced biogenic emissions during these seasons as mentioned in Section 2.1. But the influence of paddy residue fires emission is even stronger as observed by $d[O_3]/dt$ value of 9.2 ppb h^{-1} in the late post monsoon. Naja and Lal (2002) have shown the hourly $d[O_3]/dt$ values at different cities of India e.g. Delhi, Pune, Ahmedabad and Gadanki. The maximum $d[O_3]/dt$ at any hour from sunrise till attainment of peak daytime hourly average O_3 was ~ 6 ppb h^{-1} at Ahmedabad and Gadanki. Thus, values observed at this site during all the seasons except winter and monsoon (> 6 ppb h^{-1}) are higher. Cloudy and cleaner conditions in the monsoon and less availability of solar radiation in the wintertime contribute to the lower $d[O_3]/dt$ values in these seasons.

2.3.3 Impact of regional post harvest wheat and paddy residue fires on ozone

Large scale regional crop residue fires in the post harvest periods of summer and post monsoon cause emissions of a suite of gases (Murali et al., 2010; Sahai et al., 2007; Stockwell et al., 2015; Yokelson et al., 2013) and aerosol particles (Kaskaoutis et al., 2014), affecting the chemical and radiative properties of the atmosphere.

I note from Figure 2.3 (b,c,e & f), that due to similar fetch regions during the clean and polluted summer and post monsoon seasons the clean periods can be regarded as "baseline periods" for assessing the impact of crop residue fires on ambient O_3 concentrations. As O_3 is formed by photochemical reactions which depend on radiation and temperature, we analyze the average diel profiles of solar radiation, ambient temperature and O_3 for clean and crop residue fire influenced periods of the summer and post monsoon seasons. Figure 2.10 (a) shows the average diel profile of ambient O_3 (blue line and markers), acetonitrile (brown lines and markers), ambient temperature (black line and markers) and solar radiation (red line and markers) during the clean (broken line) and polluted (solid line) summer seasons derived from composite measurements of two years. Figure 2.10 (b) shows similar information pertaining to the clean and polluted post monsoon seasons. Note that in the polluted summer, the peak daytime O_3 concentrations ($\sim$ 85 ppb) are about 19 ppb higher than those observed during the clean summer season (circa 66 ppb), even though the intensity and available hours of solar radiation are very similar during both seasons. The noteworthy differences are therefore in terms of the ambient temperature and enhanced emissions from the biomass fires during the polluted summer. The ambient temperature difference of 9 °C between the clean summer and polluted summer is in part due to lower temperatures in March, which cause a temperature difference of 3.3 °C. The remaining temperature difference is likely as a result of the fires which could cause warming of the lower troposphere due to emission of absorbing aerosols and the energy release from the pyrogenic activity (Bowman et al., 2009). An enhancement > 0.44 ppb can also be seen in acetonitrile mixing ratios during night hours which indicates co-emission of other VOCs from wheat residue burning activity.

Sinha et al. (2014) have previously shown that during May 2012, plumes from wheat residue fires also caused a three-fold enhancement in the concentrations of CO, NO_x and reactive volatile organic compounds such as acetaldehyde, isoprene and benzenoids. Thus, it is plausible that the increase in peak hourly O_3 from 66 ppb to 85 ppb is driven by the changed reactivity and O_3 production efficiency of air as a result of chemical composition changes due to the wheat residue fire emissions. As the site experiences long range transport frequently in summer (Pawar et al., 2015), in the next section we

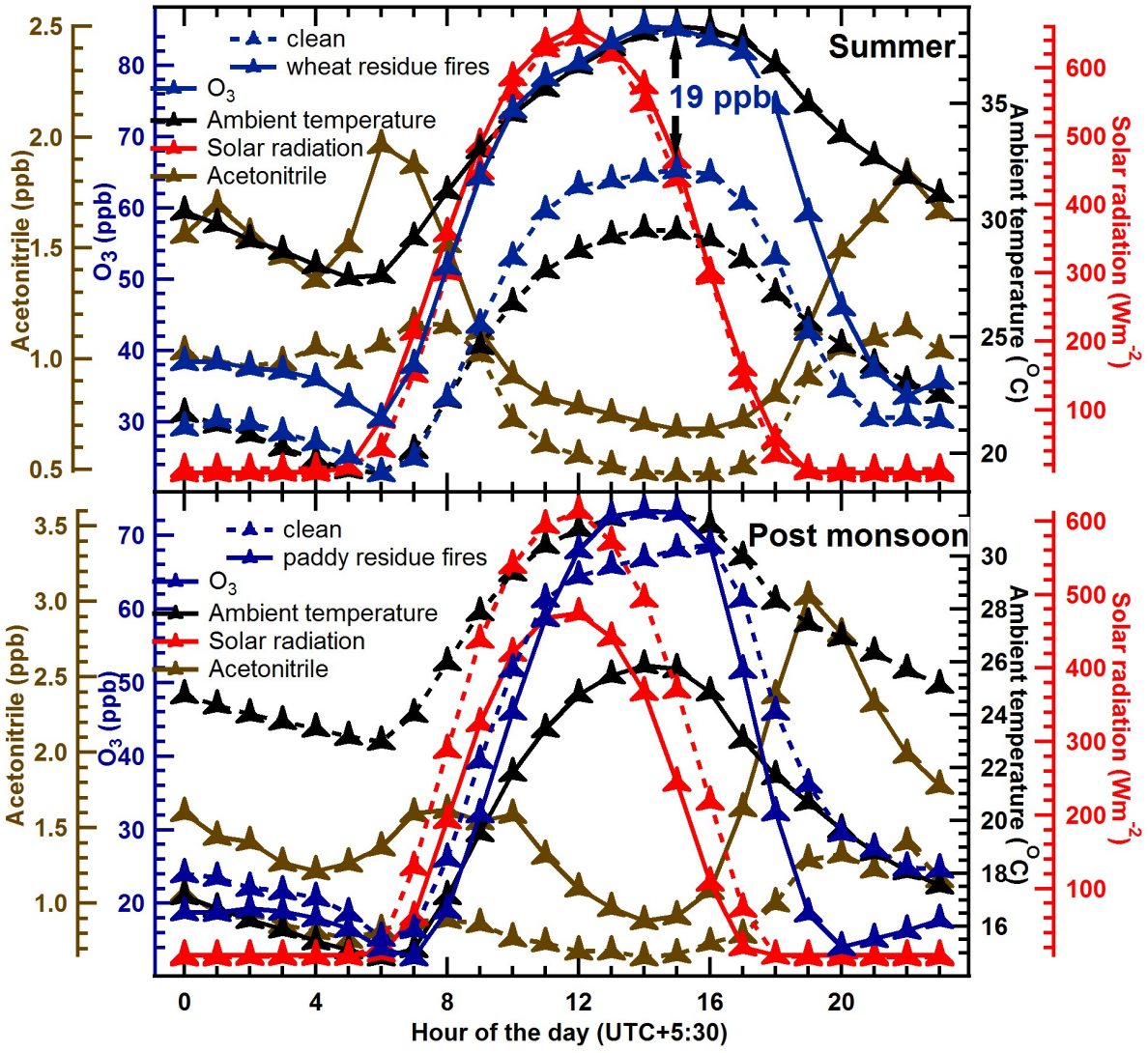

Figure 2.10: Average diel profile of ambient ozone, ambient temperature solar radiation and acetonitrile during the clean (dotted lines) and crop residue fire influenced (solid lines) periods in a) summer and b) post monsoon season calculated using the composite dataset from September 2011 - September 2013.

determine whether regional chemical O_3 production or transported O_3 was the major contributor to the high O_3 concentrations observed during the polluted summer season. The measured dataset for summer season was also filtered for rural/agricultural fetch region (wind sector: south to north-west) and wind speed bin of 1 - 5 $m\,s^{-1}$. It should be noted that effect of local emissions would be significantly reduced by excluding airmass with wind speed < 1 $m\,s^{-1}$ from the analysis. Due to maximum contact time of in the air masses over the burning wheat fields, an enhancement of ~ 22 ppb in the peak daytime O_3 concentrations was observed during the period influenced by wheat residue fires relative to the "clean" pre-harvest periods for these airmasses. This enhancement is much higher (by 3 ppb) compared to the case where the dataset is not filtered and similar stronger enhancement occurs in acetonitrile at night when most fires are lit (see Figure 2.9 and Figure 2.10). The enhancement in the evening and night time acetonitrile is also ~ 0.05 ppb (~ 11 %) higher if the dataset is similarly filtered only for the rural/agricultural sector. Figure 2.10 (b) shows that the peak hourly daytime O_3 mixing ratios during periods influenced by the paddy residue fires in the post monsoon season were ~ 73 ppb. Lower solar radiation (~ 140 $W\,m^{-2}$ differences in peak values), provide less favourable conditions for biogenic emissions in the polluted post monsoon. However, the effects of these factors are compensated by the combination of increased ambient reactivity due to emissions of CO, NO_x and VOCs co-emitted with acetonitrile from the paddy residue fires (Chandra and Sinha, 2016; Sarkar et al., 2013), leading to enhancement of ~ 7 ppb in peak daytime O_3 concentrations as compared to 66 ppb during the clean periods. The lower O_3 concentration observed at night during the polluted post monsoon is due to increased titration of O_3 by NO at night and is consistent with higher NO_x emissions during the polluted post monsoon season as a result of the paddy residue fires (Sarkar et al., 2013).

2.3.3.1 Constraining relative importance of transport and ozone chemical formation by air mass cluster analysis

To determine whether regional chemical O_3 production or transported O_3 was the major reason for the high O_3 concentrations in summer and post monsoon seasons, we examined the difference in daytime O_3 concentrations between the clean and crop residue fire influenced periods, for airmass clusters that were least affected by long-range transport. In a study that examined the climatology of air masses at the measurement site over a two-year period. Pawar et al. (2015) showed that airmasses arriving at the IISER Mohali atmospheric chemistry facility could be classified into six different clusters. Out of these six, two, namely the slow westerly and local clusters, were not influenced significantly by long-range transport in the 72 hours preceding their arrival and spent considerable

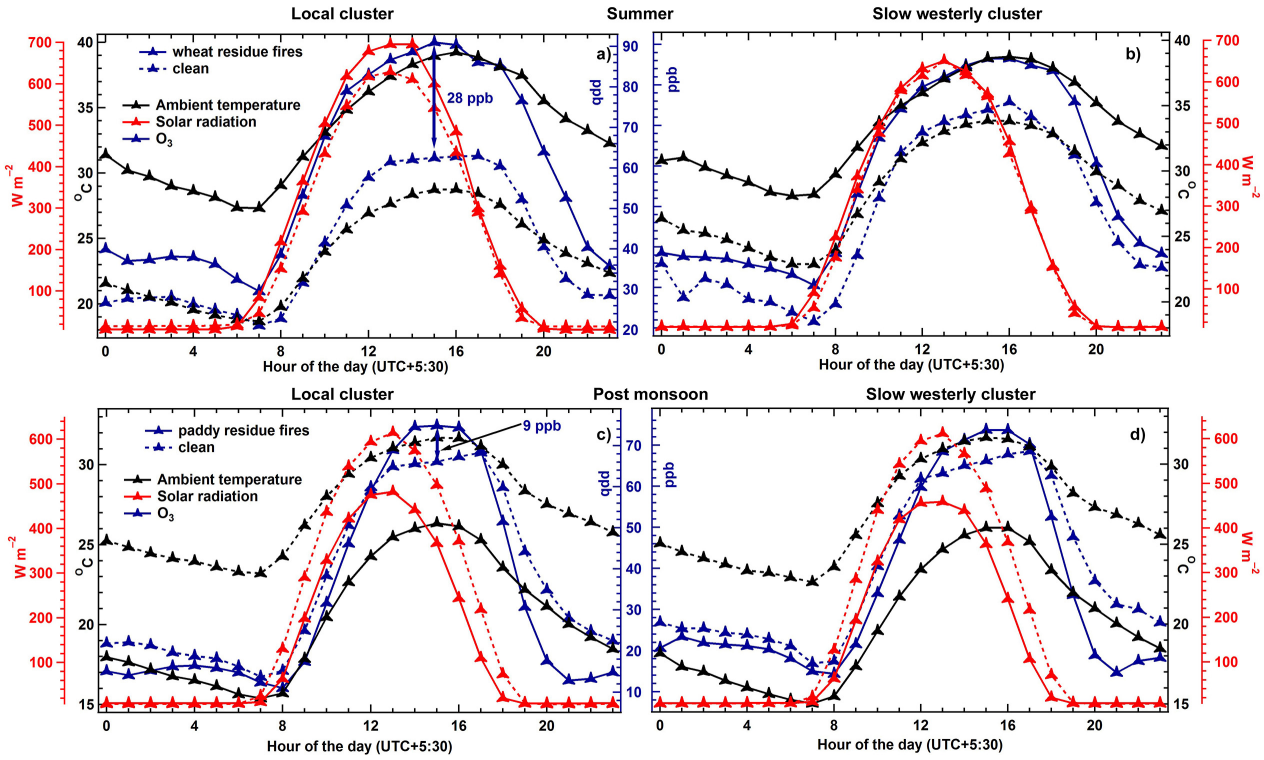

Figure 2.11: (a-d). Average diel profile of ambient ozone, ambient temperature and solar radiation during the clean (dotted lines) and crop residue fire influenced (solid lines) periods in summer (top panel) and post monsoon (bottom panel) calculated using the composite dataset from September 2011 - September 2013 for the airmass belonging to local cluster (left) and slow westerly cluster (right).

contact time over the agricultural fetch regions of the N.W. IGP.

As the post harvest crop residue fires are widespread over this fetch region (N.W. of site) during the polluted summer and polluted post monsoon periods, the influence of the crop residue fires on regional chemical formation of O_3 could be elucidated by examining the "slow westerly" and "local" clusters for the respective clean and polluted periods. The total number of clear sunny days having airmasses belonging to the slow westerly cluster for clean summer, polluted summer, clean post monsoon and polluted post monsoon were 29, 31, 20 and 37 respectively, whereas the total number of sunny days for airmasses belonging to the local cluster were 53, 31, 27 and 61, respectively. Hence, analyses of the average diel O_3 profiles using data associated with airmasses belonging to these two clusters, for different periods is statistically reasonable. Clear sunny days were defined as days for which the standard deviation in solar radiation was less than 10 % of the 30-minute average for at least 2 hours between 11:00 LT and 15:00 LT.

Figure 2.11 shows the average diel profile of solar radiation, ambient temperature and surface O_3 in a manner similar to Figure 2.10 for (a) the local cluster and (b) the slow

westerly cluster air masses during summer. The available hours and intensity of solar radiation were similar for the polluted and clean periods of summer. The local cluster in the polluted summer season showed peak daytime O_3 concentrations of $\sim$ 91 ppb which are about 28 ppb higher than concentrations observed during the clean summer season ($\sim$ 63 ppb). Note that without cluster specific analysis, this enhancement was much lower ($\sim$ 19 ppb), when all airmass clusters including those affected by long-range transport (Figure 2.10 a) were considered, suggesting that the non-local airmasses tend to lower O_3 concentrations during this period, rather than enhance them. This suggests that the enhanced O_3 concentrations in the polluted summertime are not driven by long-range transport of O_3. We note that the higher temperatures in the polluted period would contribute to the high daytime O_3 by affecting the sinks and photochemical production of O_3 for a given mix of O_3 precursor concentrations. However, considering the large difference in magnitude of 28 ppb observed between the clean and polluted periods for the local cluster, the contribution of the wheat emissions in enhancing concentrations of O_3 precursors (for both VOCs and NO_x; Sinha et al., 2014) and altering the chemical O_3 production potential is likely to be as significant. This is also supported by the fact that during the polluted post monsoon season, despite decreases in temperature and radiation relative to the clean post monsoon period, an enhancement of $\sim$ 7 ppb was observed in daytime O_3 concentrations. For the slow westerly cluster, the enhancement during the polluted summer is much lower ($\sim$ 12.5 ppb) leading to a peak O_3 mixing ratio of 86.5 ppb. This is likely due to the fact that air masses belonging to the slow westerly cluster descend from the free troposphere less than 30 hours prior to their arrival at the receptor site (Pawar et al., 2015), and have less contact time with the surface air into which emissions from the burning activity are released.

The bottom panel of Figure 2.11 shows the average diel profile of surface O_3, solar radiation, and ambient temperature for the local cluster (c) and slow westerly cluster air masses (d) during the post monsoon season. Paddy residue fires in the post monsoon season caused enhancement of $\sim$ 9 ppb (as compared to clean post monsoon) in the peak daytime O_3 concentration of 66 ppb in the airmass arriving from the local cluster, despite having lower radiation and temperature. The lower absolute increase in O_3 concentration in post monsoon periods as compared to the summertime condition suggest that the emission of O_3 precursors due to the paddy fires are able to compensate for lower radiation and temperature, leading to the peak O_3 mixing ratio of $\sim$ 75 ppb. A corresponding enhancement of $\sim$ 7 ppb was observed for the slow westerly cluster during the post monsoon season. The higher contact time of the local cluster airmasses with regions affected by the paddy residue fires can be discerned from up to 15 ppb lower nighttime O_3 mixing ratios in these air masses when compared to the slow westerly cluster airmasses.

2.4 Conclusion

This study has examined the impact of season specific emissions (e.g. wheat residue fires in summer, paddy residue fires in post monsoon) and meteorological conditions (e.g. availability of solar radiation, ambient temperature) on ambient concentrations of O_3, CO and NO_x at a regionally representative suburban site in the N.W. IGP, over a two-year-long period from August 2011 - September 2013. The prevalence of agricultural crop residue fires in the summer and post monsoon seasons resulted in high d[O_3]/dt. In the summer season this caused $\sim$ 29 % enhancement in O_3, whereas, in the late post monsoon season, it caused an enhancement of $\sim$ 10 % in peak hourly O_3 concentrations despite lower radiation and temperatures compared to the early post monsoon. The enhancement in O_3 mixing ratios in the summertime was largest for air masses belonging to the local cluster, as they spent maximum contact time over the burning agricultural fields. The net rate of change of O_3 (d[O_3]/dt) from sunrise until attainment of peak daytime plateau region of diel profile was also observed to be the highest (9.2 ppb h^{-1}) during the fire influenced post monsoon seasons followed by 8.0 ppb h^{-1} during the clean post monsoon and fire influenced summer seasons. Exceedance of the 8 h average O_3 national ambient air quality standard (NAAQS) on 451 days during August 2011 - September 2013 ($\sim$ 62 %) suggests that regional surface O_3 pollution is serious and has been largely overlooked /unreported due to lack of in situ data from the region. Assessment of VOC specific O_3 production potentials using speciated VOC measurements will provide insights on VOCs responsible for high O_3 episodes and must be investigated on a priority basis. Deployment of new instruments capable of directly measuring the in situ chemical production of O_3 will improve apportionment of in situ chemical O_3 production and transported O_3 to ambient O_3 enhancements. Regulation of crop residue fires would certainly mitigate O_3 pollution and bring co-benefits for crop productivity, in particular for wheat, which is sown during winter in the N.W. IGP. The high summertime O_3 is not serious in terms of crop productivity as there are no standing crops at that time of the year, but impairs the regional air quality.

Chapter 3

Isoprene and acetaldehyde dominate VOC OH reactivities and ozone formation potentials in the N.W. IGP

Abstract

High surface ozone is a critical environmental concern in the Indo-Gangetic Plain (IGP) due to frequent exceedance events (> 60 % annually) in the 8 h average national ambient air quality standard. The reactive VOC precursors of ozone are regionally poorly understood due to lack of measurements quantifying their diel and seasonality variability. In this chapter, I report the first year-long high temporal resolution dataset of 23 VOCs from the north-west IGP including several that are reported for the first time over the Indian region. These VOCs were measured with a PTR-MS at a regionally representative suburban site in the N.W. IGP (30.667 °N, 76.729 °E; 310 m above mean sea level). Detailed analyses of the diel and seasonal variability of VOCs, OH reactivity and ozone formation potential were performed. The highest ranking VOCs (based on annual average measured concentrations ± 1 σ ambient variability) included methanol (32.2 ± 19.7 ppb), acetaldehyde (5.9 ± 3.9 ppb), acetone (5.6 ± 5.1 ppb), formamide (4.0 ± 1.6 ppb), toluene (2.3 ± 2.8), formaldehyde (2.1 ± 0.9 ppb), C-8 aromatics (1.7 ± 2.2 ppb), benzene (1.6 ± 1.7 ppb) and isoprene (1.5 ± 1.0 ppb). In addition significantly high concentrations were observed at mass to charge ratios where multiple species may contribute using the PTR-QMS technique e.g. m/z = 61 (6.9 ± 6.3 ppb) and m/z 47 (6.1 ± 3.5 ppb). Surprisingly high mixing ratios of isoprene were observed throughout the year with the maximum dur-

ing clean post monsoon (2.3 ppb) and minimum during winter (1.1 ppb). The maximum calculated OH concentrations ranged from 2.7×10^6 molecule cm^{-3} (winter) to 6.6×10^6 molecule cm^{-3} (summer) and were employed for calculation of ozone formation potentials. The average of peak daytime (11:00 - 14:00 L.T.) ozone formation potential for different seasons ranged between 10.2 ppb h^{-1} in winter to 31.3 ppb h^{-1} in the clean post monsoon. Crop residue fires caused an enhancement of 7.5 ppb h^{-1} in the summertime ozone formation potential. These fires are found to be a strong source of acetaldehyde, C-9 aromatics and isoprene which have a strong ozone formation potential. Isoprene and acetaldehyde contributed majorly towards the daytime VOC OH reactivity and ozone formation potential, accounting for greater than 38 % of the total calculated using all the measured compounds. Remarkably, the ozone production regime varied seasonally in response to emissions and meteorology and was not always limited by availability of NO_x as has been reported till date. Isoprene and acetaldehyde measurements are extremely rare over the Indian region and their measurements need to be made a priority for understanding and mitigating ozone formation over the IGP.

3.1 Introduction

Tropospheric ozone is one of the criteria air pollutants affecting public health, air quality, plant productivity and climate (Giles, 2005; Haagen-Smit, 1952; Sinha et al., 2015). High surface ozone is a serious concern over the demographically important Indo-Gangetic Plain (IGP), where the observed ozone concentrations can exceed the national ambient air quality standard limit frequently. A recent study showed exceedances as often as 62 % of the time in a year from a suburban site in the north-west IGP (Kumar et al., 2016). Moreover, a strong variability is also observed in the mixing ratio of ozone where daily daytime average ozone mixing ratios ranged from below 10 ppb to 92 ppb during the course of a year (Kumar et al., 2016). Although the only known chemical mechanism of production of ozone in the troposphere is photolysis of NO_2, volatile organic compounds (VOCs) fuel this process and make it non-linear and complicated. VOCs play an active role in the tropospheric ozone production by facilitating oxidation of NO to NO_2 in several reaction steps (Derwent et al., 1996; Kleinman et al., 2002; Jacob, 1999). The ozone formation potential of a VOC is governed by the rate with which it reacts with OH radicals. It is directly related to its OH reactivity according to the following equation:

$$\text{Ozone production potential} = k_{\text{OH}+VOC}[VOC] \times [\text{OH}] \times n \tag{3.1}$$

here "$k_{\mathrm{OH}+VOC}[VOC]$" represents the OH reactivity of the VOC, [OH] is the OH radical concentration and "n" represents the number of NO to NO_2 conversions occurred during the OH initiated oxidation of the VOC molecule (Sinha et al., 2012).

The direct and the indirect importance of VOCs towards the radiative forcing budget has also been realized and consequently, these were included as climate forcers in the fifth IPCC assessment report (IPCC, 2013). Because of their high reactivity with OH radicals, they also control the atmospheric lifetime of certain greenhouse gases e.g. methane. VOCs have both primary and secondary sources in the atmosphere. Among primary sources, emission from biogenic sources ($\sim$ 1150 TgC per year) dominate anthropogenic emissions by a factor of 10 on the global scale, but in urban atmosphere anthropogenic emissions often dominate (Piccot et al., 1992). Biogenic VOCs, e.g. isoprene, monoterpenes and their oxidation products e.g. formaldehyde, acetaldehyde, methanol, acetone, methyl vinyl ketone and methacrolein are the dominant VOCs in forested environment (Yáñez-Serrano et al., 2015; Ammann et al., 2004; Karl et al., 2009b; Eerdekens et al., 2009) whereas aromatics and oxygenates dominate the VOC budget in urban and suburban environment (Sarkar et al., 2016; Dolgorouky et al., 2012; Fortner et al., 2009; Karl et al., 2009a).

The reported long-term atmospheric trace gas measurements in the IGP are limited only to ozone and only a few of its precursors e.g. NO_x and CO (Gaur et al., 2014; Kumar et al., 2016; Singla et al., 2011). However, a paucity of long-term measurement of speciated VOC concentration poses severe limitations towards understanding of the individual precursors and processes governing high ozone concentrations and formation of other secondary pollutants over the IGP. Monitoring of VOCs across 18 rural and urban sites in Canada and examination of OH reactivity of these VOCs enabled evaluation of air-quality models apart from identification of the major VOCs towards ozone production in NO_x-rich and NO_x-poor atmospheric environments (Stroud et al., 2008). Characterizing the variation in individual VOC concentrations and their total OH reactivity in response to changes in fetch region, emission sources and meteorology are important for understanding secondary pollutant formation chemistry as well as for validation and improvement of non-methane VOC (NMVOC) emission inventories regionally which remain poorly constrained (Yoshino et al., 2012; Ren et al., 2008; Mao et al., 2010, 2009). From a region like the IGP where both emissions and meteorology change significantly during the course of a year (Kumar et al., 2016; Chandra and Sinha, 2016; Pawar et al., 2015), it is all the more important to acquire year-long or more in situ VOC data. Though various emission inventories e.g. REAS (Regional Emission inventory in ASia), MACCity (MACC CityZen), RETRO (REanalysis of the TROposhperic chemical composition), EDGAR (Emission Database for Global Atmospheric Research) and MEGAN (Model of Emissions

of Gases and Aerosols from Nature) contain information about anthropogenic and biogenic emissions from the IGP, these have limitations in terms of spatial resolution, mutual agreement and uncertainties due to assumed emission factors and parametrizations. For example, over the N.W. IGP, while the total emission of aromatic VOCs was estimated to be 0.65 Tg year^{-1} and higher than other compound classes according to MACCity 2008 (Granier et al., 2011), emissions of aromatics were estimated to be 1.28 Tg year^{-1} which is almost half of the total NMVOC (excluding hydrocarbons, aldehydes and aromatics) emission according to REAS 2008 (Kurokawa et al., 2013).

In this work I report the first long-term measurement of a suite of 23 VOCs using a PTR-MS from the Indo-Gangetic plain for a period from 01.03.2012 to 27.02.2013. The variability in the measured concentrations as a result of changing meteorology and emissions over six seasons is discussed in section 3.3.1. The VOC OH reactivity and the important VOCs contributing to the reactive pollutants are discussed in section 3.3.2. Finally, the contribution of measured VOCs towards the ozone production and the dependence of peak daytime ozone production on VOCs and NO_x has been studied in section 3.3.3.

3.2 Experimental

3.2.1 Measurement of VOCs with the PTR-MS

The measurement of ambient volatile organic compounds (VOCs) was performed at a representative suburban site at Mohali in the north-west IGP (30.667 °N, 76.729 °E ; 310 m above mean sea level) for a one year long period from 01 March 2012 – 27 February 2013 using a high sensitivity proton transfer reaction mass spectrometer (PTR-MS) equipped with a quadrupole mass analyzer (Model 11-07HS-088; Ionicon Analytik Gesellschaft, Austria). A detailed site description, the prevalent meteorological conditions during the course of a year, classification of seasons and emissions processes active during different seasons are described in Chapter 2 of this thesis. PTR-MS technique has been used extensively for ambient VOC measurements from varied platforms e.g. ground, ship, vehicle and aircraft and in laboratory studies (de Gouw and Warneke, 2007; Sinha et al., 2014; Crutzen et al., 2000; Nölscher et al., 2014). Analytical detail of the PTR-MS instrument used in this work, its operating conditions and calibration protocols are available in Sinha et al. (2014) and Chandra and Sinha (2016). PTR-MS is a soft chemical ionisation based mass spectrometric technique which employs hydronium ion (H_3O^+) as reagent ions. Volatile organic compounds with a proton affinity greater than that of water (165.2 kcal mol^{-1}) are ionised by proton transfer with the reagent H_3O^+ ions and

the products are detected using a quadrupole mass spectrometer (Lindinger et al., 1998). A pure stream (> 95 % purity) of H_3O^+ ions are produced inside the ion source by plasma discharge of water vapour. Proton transfer from H_3O^+ to analyte VOC molecules takes place within the drift tube and the protonated VOCs move in an electric field towards the detection system of the instrument. For acquiring the data reported in this work, PTR-MS was operated at a drift-tube voltage of 600 V, pressure of 2.2 mbar and temperature of 333 K which corresponds to an E/N ratio of $\sim$ 135 Townsend (Td). The impurity ion signals due to NO^+ and ${O_2}^+$ were always less than 0.6 % and 3.9 % respectively, of the primary ion signal. The quadrupole mass analyzer separates the product ions based on their m/z ratio and the secondary electron multiplier amplifies and detects the ion signal. The measured ion signals ($I(RH^+)$) in counts per second (cps) are normalized to a sum of primary ion (H_3O^+) signal ($I(H_3O^+)$) and first water cluster ($(H_2O)H_3O^+$) signal ($I(H_3O^+(H_2O))$) of 1.0×10^6 cps, drift tube pressure (P_{drift}) of 2 mbar and drift tube temperature (T_{drift}) of 25 °C using the following normalization equation previously discussed in Sinha et al. (2009); Tani et al. (2004)

$$\text{ncps} = \frac{I(RH^+) \times 10^6}{I(H_3O^+) + I(H_3O^+(H_2O))} \times \frac{2}{P_{\text{drift}}} \times \frac{T_{\text{drift}}}{298.15} \tag{3.2}$$

The normalized signals (normalized counts per second or ncps) are then converted to ppb using the sensitivity factors derived from the calibration experiments. Calibration using dynamic dilution at four different target concentrations in the range of 3 ppb – 10 ppb at different RH (0 % to 90 %) was performed on 6 May 2012 and another 5 point calibration at two different RH (0 % and 70 %) was performed on 13 December 2012 with a custom ordered VOC standard (Apel-Riemer Environmental, Inc., Colorado, USA). Several other three point calibrations were performed on 22 February 2012, 17 April 2012, 14 May 2012, 16 August 2012, 7 November 2012, 13 December 2012, 9 January 2013 and 7 February 2012. The standard calibration gas mixture containing 13 VOCs (methanol, acetonitrile, acetaldehyde, acetone, dimethylsulphide (DMS), isoprene, methyl vinyl ketone (MVK), methyl ethyl ketone (MEK), benzene, toluene, p-xylene, 1,2,4-trimethylbenzene and alpha-pinene) at a mixing ratio of $\sim$ 500 ppb was dynamically diluted by mixing with zero air (class 5, Sigma gases) passed through the heated catalytic converter of gas calibration unit (GCU 2.0). Figure 3.1 shows example of calibration plots for acetonitrile, acetaldehyde, isoprene, methyl ethyl ketone, benzene and toluene at 70 % RH, in which the measured normalized counts per second at their corresponding m/z channels (on Y-axis) is plotted against the introduced mixing ratio (X-axis).

The slope of the calibration plot (ncps ppb^{-1}) represents the sensitivity of PTR-MS instrument at m/z corresponding to the measured VOCs. The instrumental background

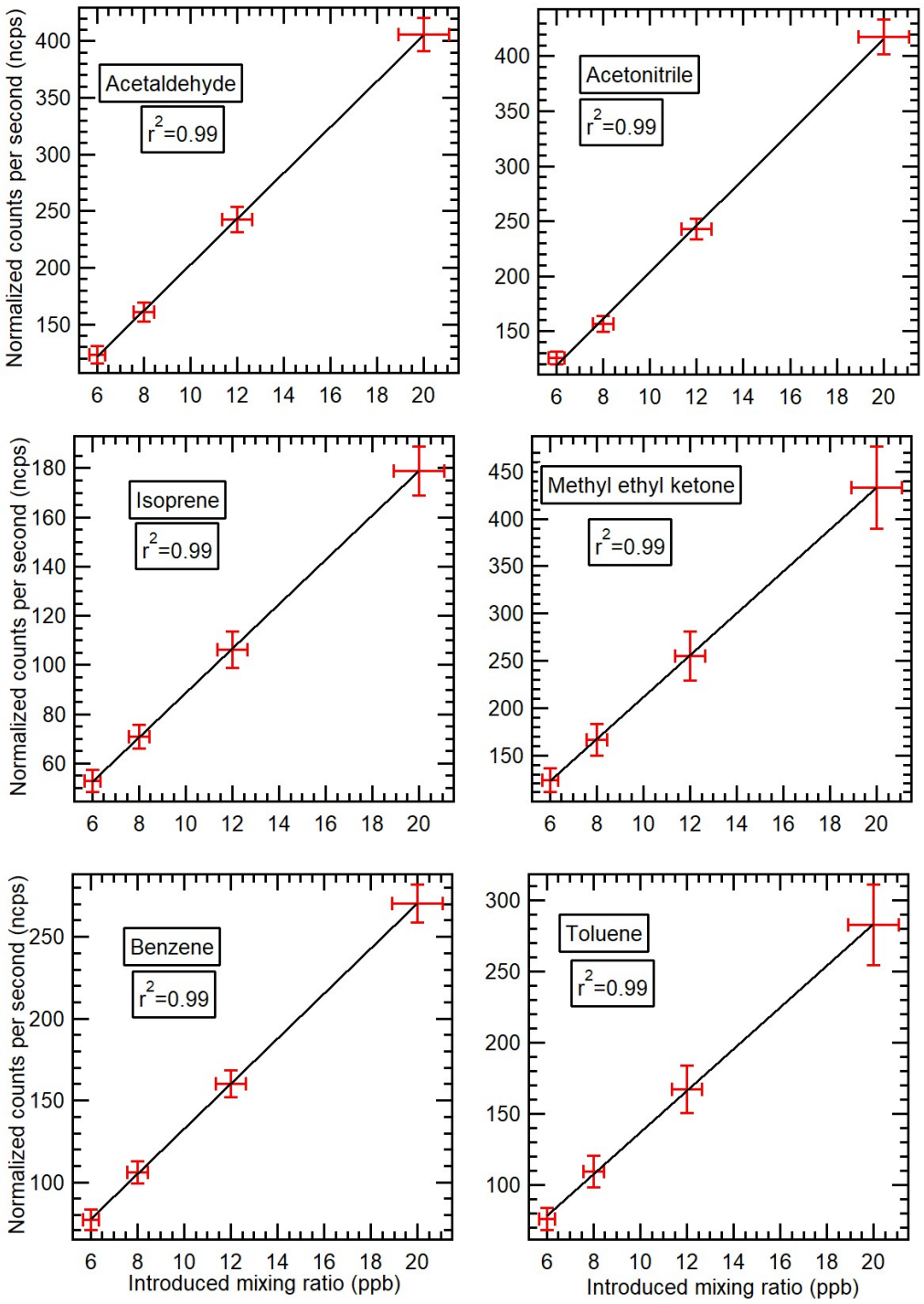

Figure 3.1: Example plot showing calibration sensitivity and linearity of acetonitrile, acetaldehyde, isoprene, methyl ethyl ketone, benzene and toluene signals in a PTR-MS calibration experiment at 70% RH. The horizontal error represent the root mean square propagation of errors due 6 % uncertainty in the VOC standard and 2 % error for each of the two mass flow controllers used for calibration. The vertical error bars represent 2 σ instrumental precision error while sampling the standard gas at each dilution mixing ratio.

at different m/z channels was also determined by sampling the zero air through the instrument at the same operating conditions. The detection limit of the PTR-MS at different m/z channels was calculated by dividing the 2 σ variability while sampling zero air (in the normalized counts per second) by the corresponding sensitivity factors. The detection limits at various m/z channels for which a corresponding VOC standard was available was less than 130 ppt except methanol for which it was 460 ppt. The total uncertainty corresponding to individual measured VOCs was calculated using root mean square propagation of individual uncertainties like the 6 % accuracy error inherent in the VOC gas standard concentration, the 2 σ instrumental precision error while sampling 6 ppb of the VOC and error in the flow reproducibility of the two mass flow controllers. The total uncertainty was less than 15 % for the measurements of VOCs for which standards are available.

The sensitivity factors obtained at 70% RH corresponding the m/z at which these VOCs are detected are listed in Table 3.1 for the two calibration experiments. Figure 3.2 shows an example of trend in sensitivities of acetonitrile, acetaldehyde, isoprene, methyl ethyl ketone and toluene during PTR-MS calibration experiments conducted over the study period. The drift in the sensitivity factors obtained in the calibration performed on 06 May 2012 and 13 December 2012 was less than 16 % for all the VOCs present in the standard apart from acetaldehyde for which it was $\sim$ 23%.

The VOC measurements were performed in selected ions monitoring mode in which 23 VOCs were monitored at a time resolution of 1 minute. The dwell time at each m/z channel corresponding to the individual VOCs in the ion-selective monitoring mode was 1 s. The sensitivity factors (normalized counts per seconds per ppb or ncps ppb^{-1}) obtained for 70% RH at various m/z channels were used to derive the mixing ratios (in ppb) of the corresponding VOCs from measured normalized counts per seconds (ncps). For compounds that were not present in VOC gas standard, the sensitivity factors were determined theoretically according to following equation which takes into account the electric field across the drift tube and transmission efficiencies of $VOCH^+$ ions and H_3O^+ ions (de Gouw and Warneke, 2007):

$$\textit{Sensitivity (}\text{ncps ppb}^{-1}\textit{)} = 10^{-3} \times \frac{k_{H_3O^+ + VOC} \cdot L}{\mu_0 N_0} \times \frac{N^2}{E} \times \frac{T_{VOCH^+}}{T_{H_3O^+}} \tag{3.3}$$

Here, $k_{H_3O^+ + VOC}$ = Rate constant of proton transfer from hydronium ion to a VOC
L = Length of drift tube (9.2 cm)
μ_0 = Reduced mobility of H_3O^+ ions (2.76 cm^2 V^{-1} s^{-1}) (Dotan et al., 1976)
N = Number density of gases in the drift tube
E = Electric field across the drift tube

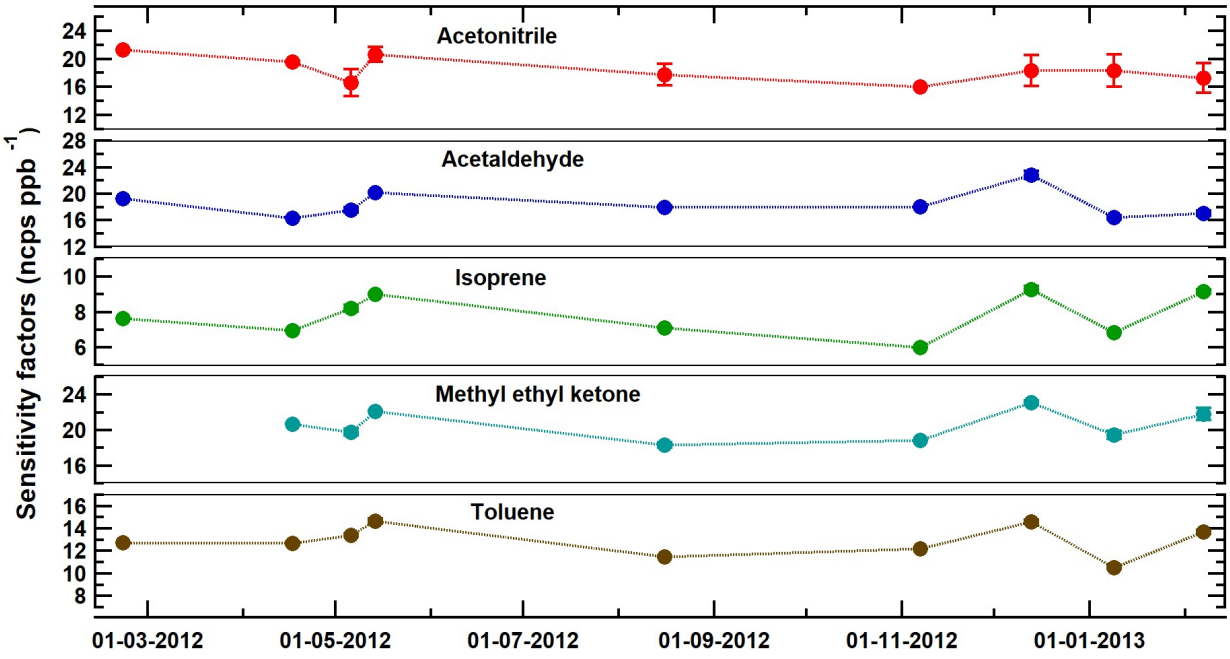

Figure 3.2: Trend in sensitivities of acetonitrile, acetaldehyde, isoprene, methyl ethyl ketone and toluene during PTR-MS calibration experiments conducted over the study period. Vertical bars at each point correspond to the 1 σ uncertainty.

$\frac{T_{\mathrm{VOCH^+}}}{T_{\mathrm{H_3O^+}}}$ = Ratio of transmission efficiencies of protonated VOC ion and hydronium ion

The values of $k_{\mathrm{H_3O^+ + VOC}}$ for different VOCs were taken from Zhao and Zhang (2004) and the transmission efficiencies at different m/z channels provided by Ionicon Analytik Gesellschaft, Austria for our instrument were used for calculation of respective sensitivity factors. For compounds that were present in the VOC gas standard, I compared the differences between the sensitivity factors derived using calibration experiments and the theoretically derived sensitivity factors. These were less than 30 % in each case (see Figure 3.3 and Table 3.1).

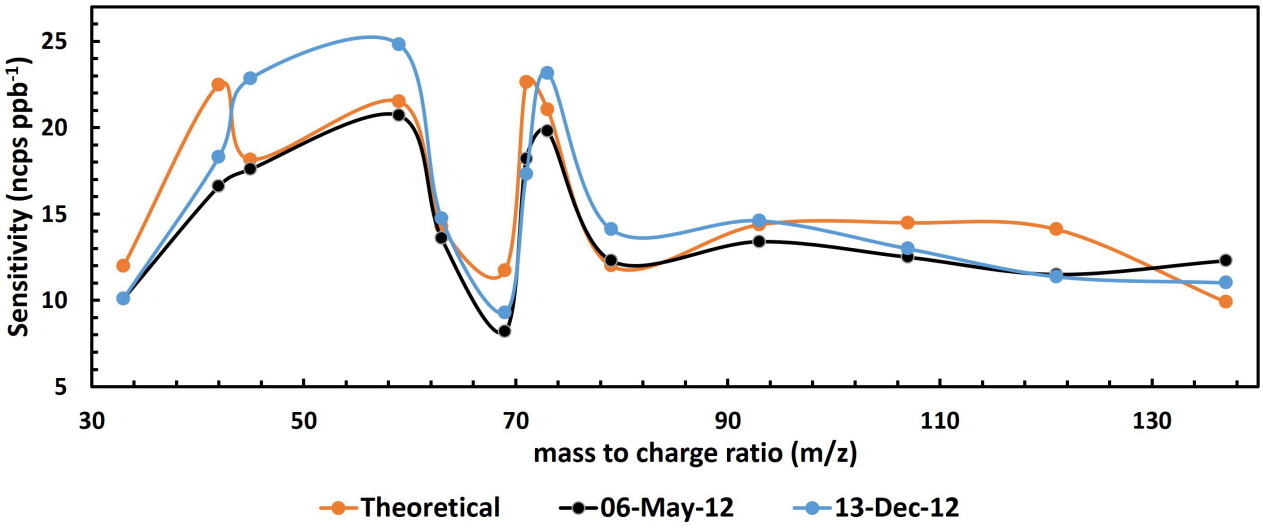

Figure 3.3: Comparison of theoretically calculated and experimentally obtained sensitivity factors from calibration experiments for VOCs detected using the PTR-MS at different m/z channels.

Table 3.1: Comparison of theoretically calculated and experimentally obtained sensitivity factors for VOCs detected at different m/z channels.

m/z	**Measured Species**	$\mathbf{k_{H_3O^+ + VOC}}$* $cm^3\,s^{-1}$	**Transmission efficiency**	**Sensitivity factor (ncps/ppb)**		
				Calculated	**06-05-2012**	**13-12-2012**
33	Methanol	2.69×10^{-9}	0.672	12.0	10.1 ± 0.1	10.1 ± 0.1
42	Acetonitrile	4.74×10^{-9}	0.715	22.5	16.6 ± 1.9	18.3 ± 2.2
45	Acetaldehyde	3.74×10^{-9}	0.732	18.1	17.6 ± 0.4	22.9 ± 0.6
59	Acetone	3.94×10^{-9}	0.824	21.5	20.7 ± 0.5	24.8 ± 1.0
63	DMS	2.53×10^{-9}	0.851	14.3	13.6 ± 0.1	14.7 ± 0.3
69	Isoprene	1.99×10^{-9}	0.889	11.7	8.2 ± 0.2	9.3 ± 0.2
71	MVK	3.79×10^{-9}	0.901	22.6	18.2 ± 0.4	17.3 ± 0.9
73	MEK	3.48×10^{-9}	0.913	21.1	19.8 ± 0.4	23.2 ± 0.2
79	Benzene	1.92×10^{-9}	0.943	12.0	12.3 ± 0.1	14.1 ± 0.0
93	Toluene	2.17×10^{-9}	1	14.4	13.4 ± 0.1	14.6 ± 0.2
107	p-xylene	2.27×10^{-9}	0.963	14.5	12.5 ± 0.1	13.0 ± 0.3
121	1,2,4-Trimethylbenzene	2.40×10^{-9}	0.887	14.1	11.5 ± 0.2	11.4 ± 0.2
137	Monoterpenes	2.00×10^{-9}	0.747	9.9	12.3 ± 0.1	11.0 ± 0.2

* Taken from Zhao and Zhang (2004)

A Proton Transfer Reaction Mass Spectrometer equipped with a quadrupole mass analyzer (PTR-QMS) cannot resolve nominal isobaric compounds (ions with the same nominal m/z) with its unity mass resolution and hence identification of compounds based only on the m/z values can in principle provide the upper limit of the true ambient concentrations of compounds. However, reviews (de Gouw and Warneke, 2007; Blake et al., 2009) of several studies and inter-comparisons between PTR-MS and other more specific analytical techniques (e.g. gas chromatography based instruments) in diverse environments and plumes have shown that for compounds such as methanol, acetonitrile, acetaldehyde, acetone, dimethylsulphide, methyl ethyl ketone, sum of C-8 aromatics, sum of C-9 aromatics and sum of methyl vinyl ketone and methacrolein, only minor contributions from other isobaric compounds have been observed in ambient atmospheric environments. Hence one can be confident of the compound assignment for these species using PTR-QMS.

3.2.2 Ancillary measurements

CO measurements were performed using an online gas filter correlation (GFC) non-dispersive infrared (NDIR) spectroscopy based analyzer. NO_x (sum of NO and NO_2) was measured online using chemiluminescence based trace level analyzer. NO_x is first converted in NO using a molybdenum converter heated at 350 °C and which further reacts with high concentration of O_3 generated within the instrument to produce a chemiluminescence. The working principle, detection limit, measurement uncertainties, calibration protocol and major interferences for these measurements are discussed in Chapter 2 of the thesis. Total solar radiation (spanning the wavelength range from 280 nm to 2800 nm) was measured continuously every minute using a pyranometer (Model 095 pyranometer, Met One Instruments Inc., Oregon, US) (Kumar et al., 2016).

3.2.3 Calculation of OH number density and ozone production potential

The calculation of ozone production potential using equation 3.1 requires the hydroxyl radical concentrations (OH number density) and "n" in addition to the VOC concentrations and the relevant rate constants of reaction of VOCs with OH radicals (Hewitt, 1999). For the calculation of ozone production potential using equation 3.1, the parameter "n" was taken to be 2 for all the VOCs apart from CO, for which it was taken to be 1 (Sinha et al., 2012). Previous studies reporting the ozone production potential e.g. by Sinha et al. (2012) and by Sarkar et al. (2016) assumed a constant OH number density equal to the global mean average OH number density of 1.0×10^6 molecules cm^{-3} for this calcu-

lation. However, for studies covering multiple seasons involving change in solar radiation (and in turn $J(O^1D)$ and OH production), the seasonal variability of the OH number density needs to be taken into account. Hence, direct measurements of global solar radiation were used to constrain the OH number density calculations. Using a five-year long measurement period, Rohrer and Berresheim (2006) previously demonstrated that OH number density can be determined using a single parameter $J(O^1D)$ as a power-law function independent of any chemical composition changes.

$$OH = a \times (\frac{J(O^1D)}{10^{-5}s^{-1}})^b + c \tag{3.4}$$

The OH number density at our site was estimated using the above equation using the coefficients for the relation taken from the Hohenpeissenberg meteorological observatory ($a = 2.4 \times 10^6$ cm^{-3}, $b = 1$ and $c = 0.13 \times 10^6$ cm^{-3}). The coefficients a, b and c depend on the environmental conditions of a site and are observed be constant for a longer period of up to 5 years (Rohrer and Berresheim, 2006). These coefficients will differ for our measurement site, but the bias caused in OH concentrations will be a systematic offset hence I do not expect these to affect the analysis for seasonal differences in the ozone production potential, which is the present objective. The calculation of OH number density can be further improved by taking into account the HONO concentrations, which can be included in future measurement. The $J(O^1D)$ values are derived from $J(NO_2)$ using an empirical relationship derived between the two using TUV model, which is discussed in subsequent paragraph. $J(NO_2)$ is calculated using directly measured global solar radiation at our site and site dependent UV-A surface albedo (0.05 at the measurement site (Feister and Grewe, 1995))(Trebs et al., 2009). It should be noted that directly measured global solar radiation (which a parameter used to the scaling of $J(NO_2)$ itself is sensitive to solar zenith angle (SZA) under varying atmospheric conditions. Model calculations for $J(O^1D)$ and $J(NO_2)$ were performed for one full month (March 2012) at one-hour time resolution using version 5.2 of the NCAR TUV model (Madronich and Flocke, 1999) for the measurement location. The model inputs of cloud optical depth, ozone column, aerosol optical depth, surface temperature and NO_2 column over the study area for the calculation of $J(O^1D)$ and $J(NO_2)$ were accessed using Giovanni 4 www interface (*http://giovanni.gsfc.nasa.gov/giovanni/*). A sensitivity study was carried out to check the dependence of the $J(O^1D)$ on the ambient range of model input parameters e.g. solar zenith angle, cloud optical depth, ozone column, aerosol optical depth, NO_2 column and surface temperature.

Figure 3.4(a-f) show the variability of $J(O^1D)$ individually on solar zenith angle (SZA), cloud optical depth, ozone column, aerosol optical depth (AOD), NO_2 column and surface

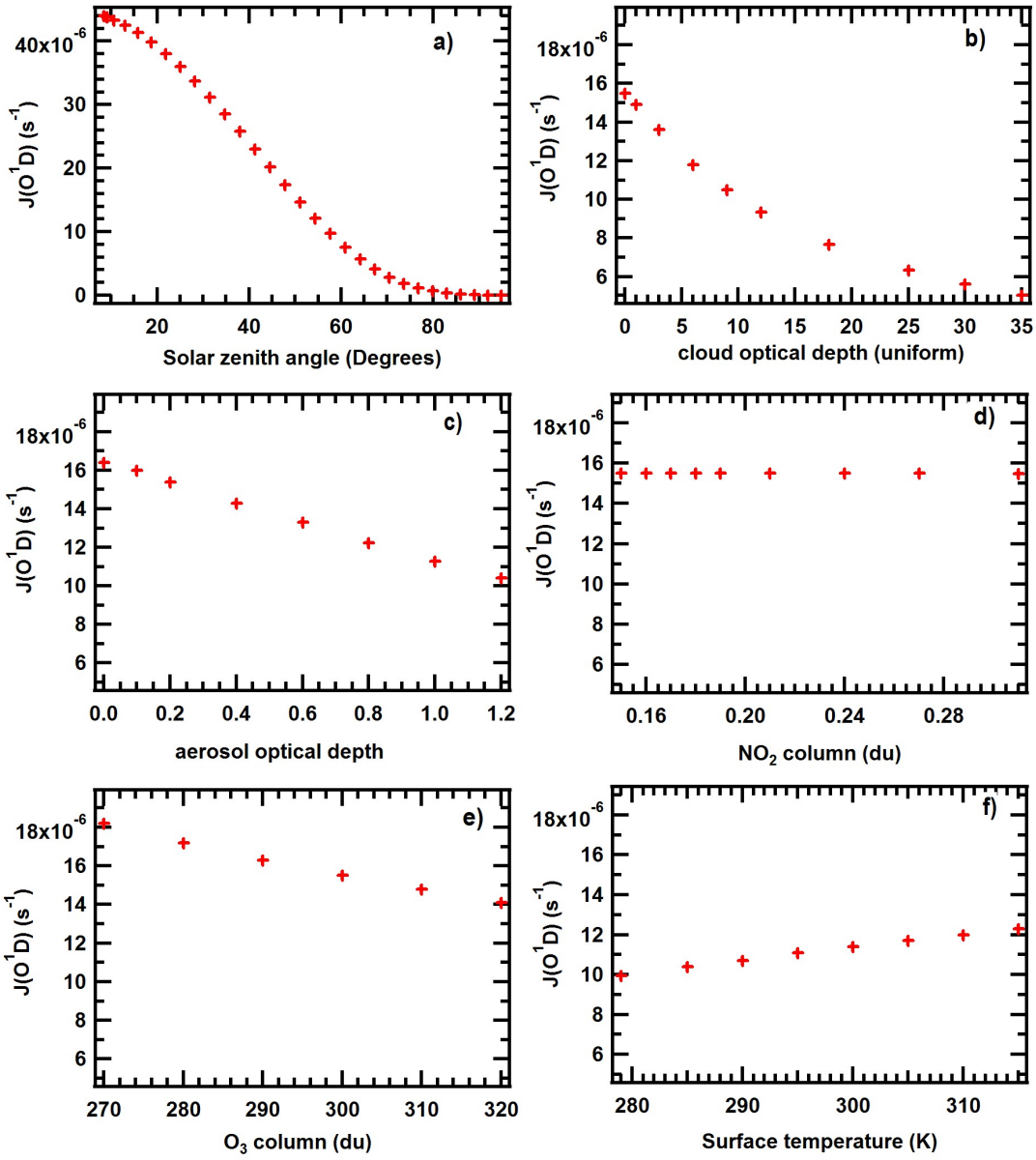

Figure 3.4: Sensitivity of $J(O^1D)$ towards a particular input parameter (a. solar zenith angle, b. uniform cloud optical depth, c. aerosol optical depth, d. NO_2 column, e. O_3 column and e. surface temperature) keeping the other parameters fixed.

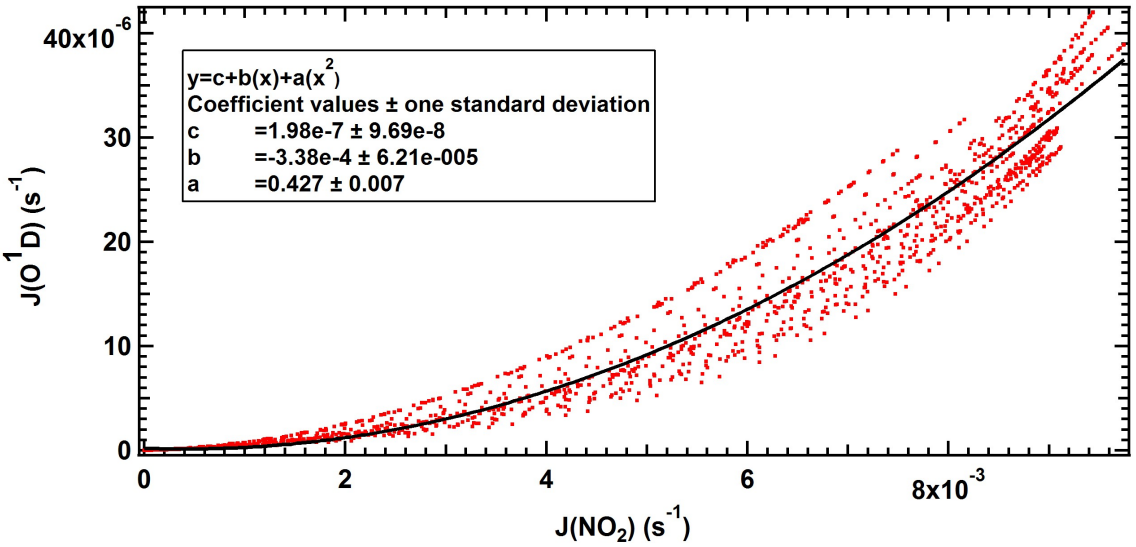

Figure 3.5: Variation of the model derived $J(O^1D)$ for different values of $J(NO_2)$ and a second order polynomial fit between $J(O^1D)$ and $J(NO_2)$.

temperature while keeping the other parameters fixed. At a smaller SZA, the incoming solar radiation has to travel a smaller path which reduces the scattering and absorption of these radiations by gases and particles in the atmosphere. Hence $J(O^1D)$ has higher values at low SZA. With the increase in cloud optical depth, less solar radiation reaches the surface resulting in lower $J(O^1D)$. Similarly, at higher AOD and higher ozone column, increase in scattering and absorption respectively of the incoming solar radiation results in smaller $J(O^1D)$ values. NO_2 column within the general atmospheric range does not have as significant effect on $J(O^1D)$ compared to other input parameters discussed previously. The quantum yield for the photo-dissociation increases with an increase in surface temperature as more number of molecules possess higher internal energy which is close to that required for photo-dissociation (Shetter et al., 1988). Hence the $J(O^1D)$ values increase with increase in surface temperature. An empirical relationship between $J(NO_2)$ and $J(O^1D)$ was estimated by fitting a second order polynomial between their calculated values at our site values which is

$$J(O^1D)) = 0.427 \times J(\mathrm{NO_2})^2 - 3.380 \times 10^{-4} \times J(\mathrm{NO_2}) + 1.988 \times 10^{-7} s^{-1} \qquad (3.5)$$

Figure 3.5 shows a scatter plot of $J(O^1D)$ vs $J(NO_2)$ and the second order polynomial fit for the data points. The constant a, b and c in the fit represent the second order coefficient, first order coefficient and the constant term respectively.

Figure 3.6 shows the diel profile of OH radical concentration estimated for different seasons for which the maximum daytime hourly average concentration ranges between

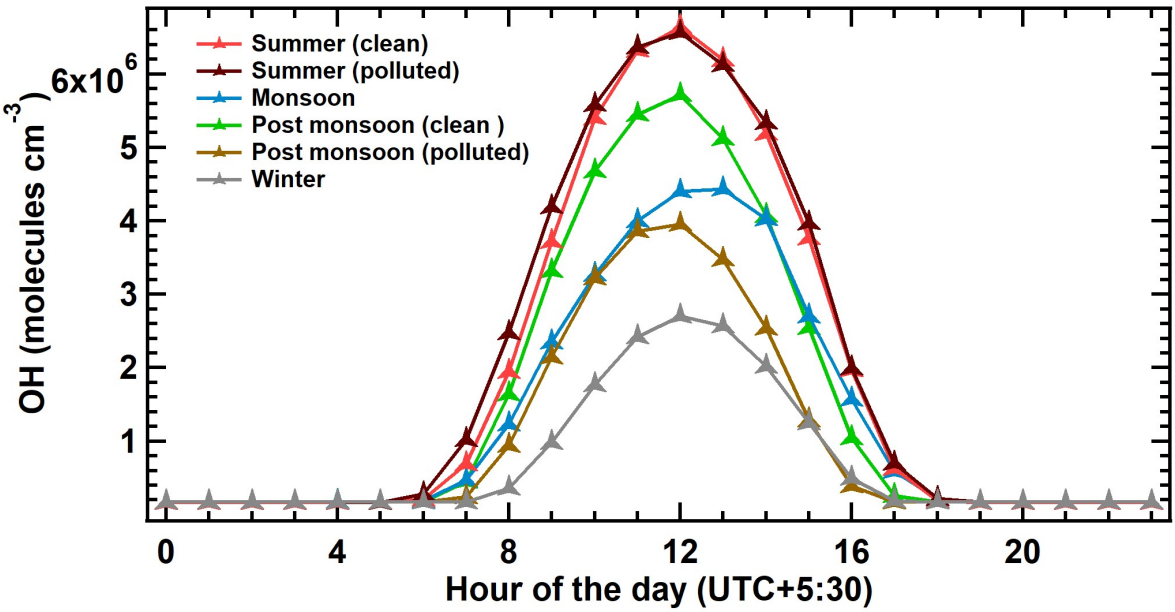

Figure 3.6: Average diel profile of calculated OH concentration at different for the different seasons during the study period.

2.7×10^6 molecule cm^{-3} and 6.6×10^6 molecule cm^{-3} for different seasons of the year. The maximum is observed in the summer seasons because of the maximum intensity and available hours of the solar radiation while the minimum is observed in the winter season because of lower solar radiation. Overcast conditions in the monsoon seasons cause smaller OH number density as compared to clean post monsoon even though there is greater availability of water vapour in the air. The shape and range of diel profile of estimated OH radicals concentration (daytime maxima of 6.6×10^6 molecule cm^{-3}) are comparable to that reported during dry summers at Bakersfield, California, which is an urban location surrounded by agricultural fields (Brune et al., 2016). The range of OH radical concentration is in agreement of those reported at various location in the world during different seasons (Stone et al., 2012).

3.3 Discussion

3.3.1 Time series and season-wise diel concentration profiles of VOCs

Figure 3.7 shows the time series of the measured data at 8 hour temporal resolution from March 2012 - March 2013 of the mixing ratios (ppb) of methanol, acetaldehyde, acetone in the top panel; sum of monoterpenes, sum of methyl vinyl ketone and methacrolein,

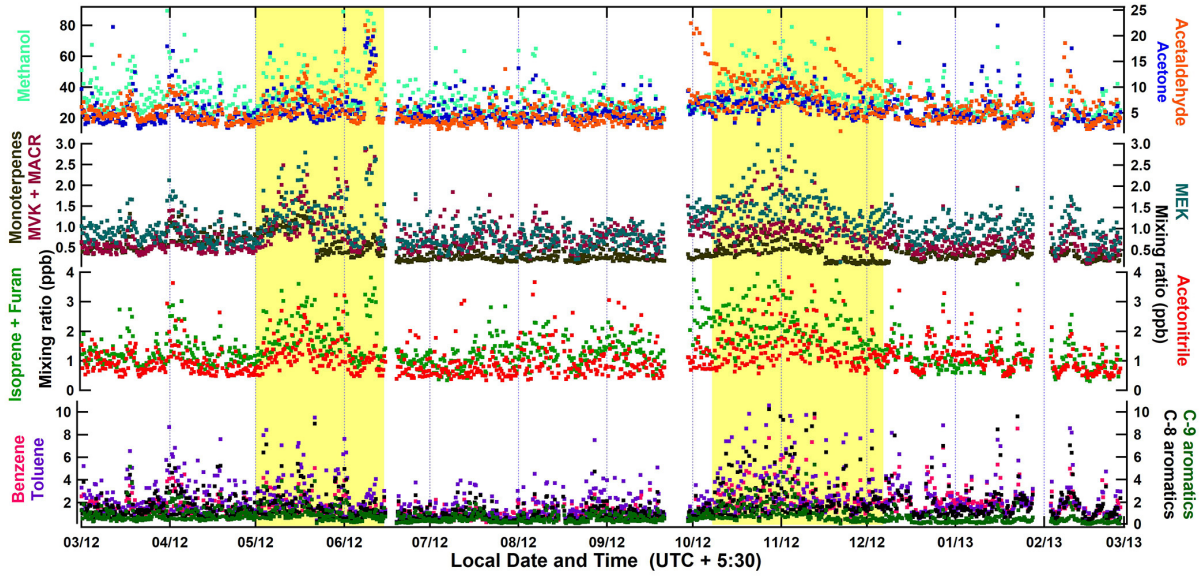

Figure 3.7: Time series of eight hours resolution measured mixing ratio of methanol, acetaldehyde, acetone (top panel), sum of monoterpenes, sum of methyl vinyl ketone and methacrolein, methyl ethyl ketone (second panel), sum of isoprene and furan, acetonitrile (third panel) and benzene, toluene, sum of C-8 aromatics, sum of C-9 aromatics (bottom panel).

methyl ethyl ketone in second panel; sum of isoprene and furan, acetonitrile in third panel and benzene, toluene, sum of C-8 aromatics, sum of C-9 aromatics VOCs in bottom panel.

The classification of year-long measurement period in seasons at Mohali has been discussed in Chapter 2 and the corresponding dates for these seasons are: clean summer (01 March 2012 – 30 April 2012 and 22 June 2012 – 01 July 2012), polluted summer (01 May 2012 – 21 June 2012), monsoon (02 July 2012 – 18 September 2012), clean post monsoon (19 September 2012 – 10 October 2012), polluted post monsoon (11 October 2012 – 09 December 2012) and winter (10 December 2012 – 28 February 2013). Highest concentrations of VOCs were observed over extended periods in the polluted periods of summer and post-monsoon (shaded in yellow in Figure 3.7) when the N.W. IGP region is influenced by the widespread crop residue fires (Chandra and Sinha, 2016; Kumar et al., 2016; Badarinath et al., 2006). The composition of the measured VOC suite is dominated by oxygenated VOCs with methanol mixing ratios (5^{th} and 95^{th} percentiles) ranging from 16.6 to 66.3 ppb, acetaldehyde from 2.2 to 13.2 ppb and acetone from 2.3 to 12.5 ppb for the entire year long period. The second most dominant class of VOCs in terms of their measured concentrations are aromatics for whom the 5th and 95th percentile of the mixing ratios range between 0.3 to 4.3 ppb for benzene, 0.4 to 6.8 ppb for toluene and 0.3 to 4.8 ppb for sum of C-8 aromatics during the entire year. Isoprene concentrations range from

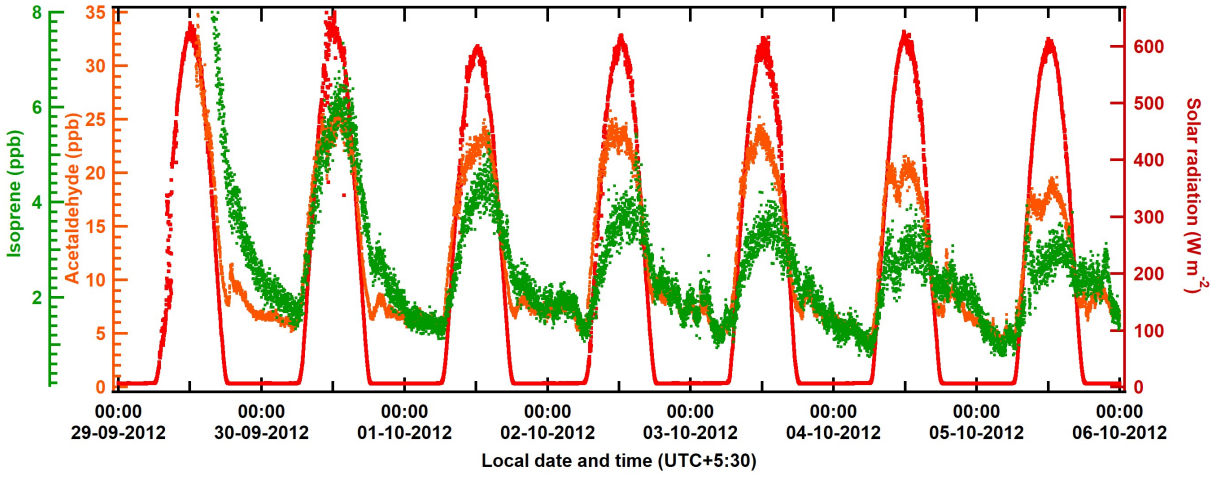

Figure 3.8: Time series of measured solar radiation (on the right axis) and mixing ratios of isoprene and acetaldehyde (left axis) for a one week period from 29 September 2012 to 06 October 2012 highlighting their strong biogenic sources.

0.5 to 3.3 ppb (5^{th} and 95^{th} percentile). High isoprene seasonal average concentration > 1.1 ppb is observed throughout the year at our measurement location. Among all seasons the maximum daytime (periods when solar radiation 50 W m $^{-2}$ (Gerosa et al., 2007)) concentration of isoprene (2.9 ppb) was observed in clean post monsoon when ample amount of soil moisture is present after monsoon rains and clear sky conditions are observed due to the absence of clouds. The major isoprene emitting tree species in the study region are poplar (Populus deltoides, a non-native species introduced in 1950), eucalyptus (Eucalyptus tereticornis) and mango (Mangifera indica) (Sinha et al., 2014). The concentrations of acetonitrile (a chemical marker compound for biomass burning) ranged from 0.5 to 3.3 ppb (5^{th} and 95^{th} percentiles). Very high concentration of acetaldehyde and isoprene concentration are observed from 29 September 2012 to 06 October 2012. The trends of the measured mixing ratio of both isoprene and acetaldehyde as shown in Figure 3.8, strongly follow that of solar radiation confirming their strong biogenic emission in this period.

Biomass burning active seasons in the N.W. IGP were polluted post monsoon (paddy residue fires), polluted summer (wheat residue fires) and winter (biofuel combustion for domestic heating), when very high acetonitrile concentrations (seasonal average concentrations of 1.5 ppb, 1.2 ppb and 1.1. ppb respectively) and high concentrations of aromatic VOCs are observed. Several other biomass burning events (e.g. garbage burning, leaf litter burning) spanning a smaller time scale of one day or less are observed in other seasons, which are evident from peaks in mixing ratios of measured VOCs (for example on 18 March 2012, 31 March 2012 and 18 April 2012 in clean summer and 13 July 2012, 06 August 2012 and 06 September 2012 in monsoon). Lower concentration of all the VOCs are observed in the monsoon season which is due to reduced emission and photochemical production

for VOCs having biogenic and photo-oxidation sources respectively. Biomass burning sources are also least active in the monsoon season, which results in smaller concentration of aromatic VOCs, acetonitrile and other VOCs (e.g. oxygenated VOCs and isoprene) which are emitted from biomass fires apart from their primary production pathway. Very low methanol and acetone concentrations are observed in the winter season when a thick blanket of fog is prevalent over the entire IGP and in monsoon season. The water droplets appear to act as a strong sink of methanol and acetone due to its high water solubility (Henry's law constant : 2.0 $\mathrm{mol\,m^{-3}\,Pa^{-1}}$ for methanol and 0.3 $\mathrm{mol\,m^{-3}\,Pa^{-1}}$ for acetone) (Sander, 2015)). Lower concentrations of the measured VOCs are also observed on the winter days when strong fog events are observed (e.g. 18 December 2012- 20 December 2012, 02 January 2013 and 18 January 2013). The range of mixing ratios and the seasonal variability of VOCs observed at Mohali is summarized in Table 3.2.

The top twelve VOCs according to their measured annual average concentrations were methanol (32.2 ± 19.7 ppb), acetic acid (6.9 ± 6.3 ppb), formic acid (6.1 ± 3.5 ppb), formamide (4.0 ± 1.6 ppb), acetaldehyde (5.9 ± 3.9 ppb), acetone (5.6 ± 5.1 ppb), acrolein (2.6 ± 2.3 ppb), toluene (2.3 ± 2.8), formaldehyde (2.1 ± 0.9 ppb), C-8 aromatics (1.7 ± 2.2 ppb), benzene (1.6 ± 1.7 ppb) and isoprene (1.5 ± 1.0 ppb).

Table 3.2: Average ± 1σ (ambient variability) mixing ratios (in ppb) of the measured VOCs in different seasons and for the measurement period spanning from March 2012 to March 2013.

	Summer		Monsoon	Post Monsoon		Winter	Overall
	Clean	Polluted		Clean	Polluted		
Methanol	33.2 ± 17.0	41.2 ± 23.6	28.4 ± 16.9	27.2 ± 9.1	37.7 ± 25.1	25.7 ± 13.5	32.2 ± 19.7
Acetonitrile	0.9 ± 0.7	1.2 ± 0.8	1.0 ± 1.1	1.0 ± 0.7	1.5 ± 1.1	1.1 ± 0.7	1.1 ± 0.9
Acetaldehyde	4.7 ± 2.2	7.0 ± 4.6	4.2 ± 2.1	9.9 ± 6.3	8.7 ± 4.2	5.3 ± 3.4	5.9 ± 3.9
Acetone$^{\alpha}$	4.9 ± 5.2	6.7 ± 5.2	4.9 ± 4.3	5.9 ± 3.2	6.7 ± 3.9	5.2 ± 7.2	5.6 ± 5.1
Isoprene$^{\beta}$	1.2 ± 0.6	1.9 ± 1.1	1.2 ± 0.6	2.3 ± 1.3	2.1 ± 1.2	1.1 ± 0.7	1.5 ± 1.0
MVK$^{\gamma}$	0.6 ± 0.3	1.3 ± 0.9	0.7 ± 0.4	1.0 ± 0.3	1.0 ± 0.6	0.6 ± 0.4	0.8 ± 0.6
MEK$^{\delta}$	0.9 ± 0.4	1.4 ± 0.9	0.8 ± 0.4	1.2 ± 0.4	1.4 ± 0.8	0.9 ± 0.4	1.1 ± 0.6
Benzene	1.5 ± 1.3	1.5 ± 1.6	1.0 ± 1.1	1.1 ± 0.6	2.4 ± 2.5	2.0 ± 1.8	1.6 ± 1.7
Toluene	2.2 ± 2.4	2.5 ± 2.9	1.6 ± 1.8	1.6 ± 1.0	3.5 ± 4.0	2.2 ± 2.5	2.3 ± 2.8
C-8 aromatics	1.6 ± 1.6	1.8 ± 2.4	0.9 ± 1.0	1.2 ± 0.8	2.6 ± 3.4	1.7 ± 2.1	1.7 ± 2.2
C-9 aromatics	0.9 ± 1.0	1.1 ± 1.2	0.6 ± 0.5	0.7 ± 0.4	1.2 ± 1.5	0.4 ± 0.5	0.8 ± 1.0
Monoterpenes	0.6 ± 0.3	0.7 ± 0.4	0.3 ± 0.2	0.3 ± 0.1	0.4 ± 0.4	0.3 ± 0.3	0.5 ± 0.3
Formaldehyde	1.6 ± 0.4	2.5 ± 1.2	1.5 ± 0.4	2.5 ± 0.6	3.1 ± 0.8	2.0 ± 0.8	2.1 ± 0.9
Formamide	3.3 ± 0.6	4.2 ± 1.8	3.1 ± 1.3	3.7 ± 1.1	5.5 ± 1.5	4.3 ± 1.5	4.0 ± 1.6
Acetamide	0.6 ± 0.3	1.0 ± 0.7	0.7 ± 0.4	0.8 ± 0.4	1.1 ± 0.3	1.1 ± 0.5	0.9 ± 0.5
Formic acid$^{\epsilon}$	3.7 ± 1.0	6.4 ± 4.9	4.6 ± 2.4	8.5 ± 3.2	9.6 ± 2.5	6.8 ± 3.0	6.1 ± 3.5
Acrolein	2.0 ± 1.7	2.8 ± 2.5	2.0 ± 1.4	2.8 ± 1.0	4.1 ± 3.0	2.5 ± 2.5	2.6 ± 2.3
Acetic acid$^{\zeta}$	5.2 ± 5.1	8.9 ± 7.2	4.5 ± 4.4	8.4 ± 5.1	10.9 ± 6.7	6.4 ± 6.4	6.9 ± 6.3
DMS	0.3 ± 0.1	0.3 ± 0.1	0.3 ± 0.1	0.2 ± 0.1	0.3 ± 0.1	0.2 ± 0.1	0.3 ± 0.1
Hydroxyacetone	0.9 ± 0.5	1.7 ± 1.2	0.8 ± 0.5	1.1 ± 0.5	1.7 ± 1.1	1.0 ± 0.8	1.2 ± 0.9
2,3-Butanedione	0.7 ± 0.3	1.2 ± 0.9	0.6 ± 0.3	1.0 ± 0.3	1.3 ± 0.6	0.7 ± 0.4	0.9 ± 0.6
Phenol	0.6 ± 1.4	0.6 ± 0.6	0.4 ± 0.3	0.4 ± 0.2	0.8 ± 1.1	0.4 ± 0.2	0.5 ± 0.8
Styrene	0.3 ± 0.4	0.4 ± 0.4	0.2 ± 0.2	0.1 ± 0.1	0.4 ± 0.5	0.2 ± 0.3	0.3 ± 0.4

PTR-QMS measurements of VOCs have minor interference from nominal isobaric contribution (de Gouw and Warneke, 2007).
$^{\alpha}$sum of acetone and propanal, $^{\beta}$sum of Isoprene and furan, $^{\gamma}$ sum of MVK and methacrolein, $^{\delta}$ sum of MEK and methylglyoxal
$^{\epsilon}$ sum of ethanol and formic acid, $^{\zeta}$ sum of acetic acid glycolaldehyde and methylformate

3.3.1.1 Season-wise diel concentration profile of measured VOCs

For the analysis of their season-wise diel concentration profiles, the measured VOCs are classified into two groups based on their major sources in the atmosphere. These are 1. VOCs with primary emission sources only (Acetonitrile, Benzene, toluene, C-8 aromatics, C-9 aromatics, styrene, isoprene, monoterpenes and dimethylsulphide (DMS)) and 2. VOCs that have equally strong primary and secondary sources through photo-oxidation of precursors (acetaldehyde, methyl vinyl ketone (MVK), hydroxyacetone, formaldehyde, phenol, 2,3-butanedione, methanol, acetone, acrolein, methyl ethyl ketone (MEK), ethanol, acetic acid, formamide and acetamide. Figure 3.9(a-i) show the average diel concentration profiles of these primary VOCs which are measured at the sub-urban site.

While acetonitrile is emitted from biomass burning (Holzinger et al., 1999), aromatic VOCs e.g. benzene, toluene, C-8 aromatics, C-9 aromatics and styrene are representative of anthropogenic emissions i.e. e.g. traffic and biomass burning. Isoprene and monoterpenes are mostly known to be emitted from biogenic sources (Guenther et al., 2006, 1991; Yáñez-Serrano et al., 2015) apart from contribution from biomass burning (Akagi et al., 2011; Sinha et al., 2014; Christian et al., 2003), whereas DMS is a marine airmass tracer and also known to be emitted from biomass fires (Sinha et al., 2007; Stockwell et al., 2015; Charlson et al., 1987). Bimodal shape of diel profile of acetonitrile, which is a chemical tracer for biomass burning is observed in all the seasons. The biomass and biofuel burning is used for cooking in all the seasons and additionally for domestic heating during winters. Open crop residue fires in the post monsoon and winter lead to the maximum evening time mixing ratio of acetonitrile. All the primary aromatic species show a clear bimodal profile in all the seasons with the evening time peaks more prominent than morning time. These peaks are due to emission of aromatic VOCs from the vehicular traffic and biomass/biofuel combustion. Rapid chemical oxidation and dilution in an elevated daytime boundary layer result in the minimum daytime concentrations of these VOCs. Massive emissions of these carcinogenic benzenoids were reported by Sarkar et al. (2013) and Chandra and Sinha (2016), which is also evident from the highest evening time peaks in the polluted post monsoon season. A unimodal shape of the diel profile of isoprene concentrations with an enhancement in the daytime is observed in all seasons except the summer seasons. Biogenic emission of isoprene is strongly dependent on leaf temperature. Guenther et al. (1991) have observed increased isoprene emission with increasing temperature up to $\sim$ 36 °C for the eucalyptus plants, and a further increase in temperature ceases the isoprene emissions. During the summer seasons in the IGP, the daytime temperature readily reaches more than 40 °C in the daytime (Kumar et al., 2016), hence a decreased emission which is readily oxidized by OH radicals in the daytime and diluted in a daytime boundary layer of $>$ 2.4 km in height (Sinha et al., 2014) results in daytime

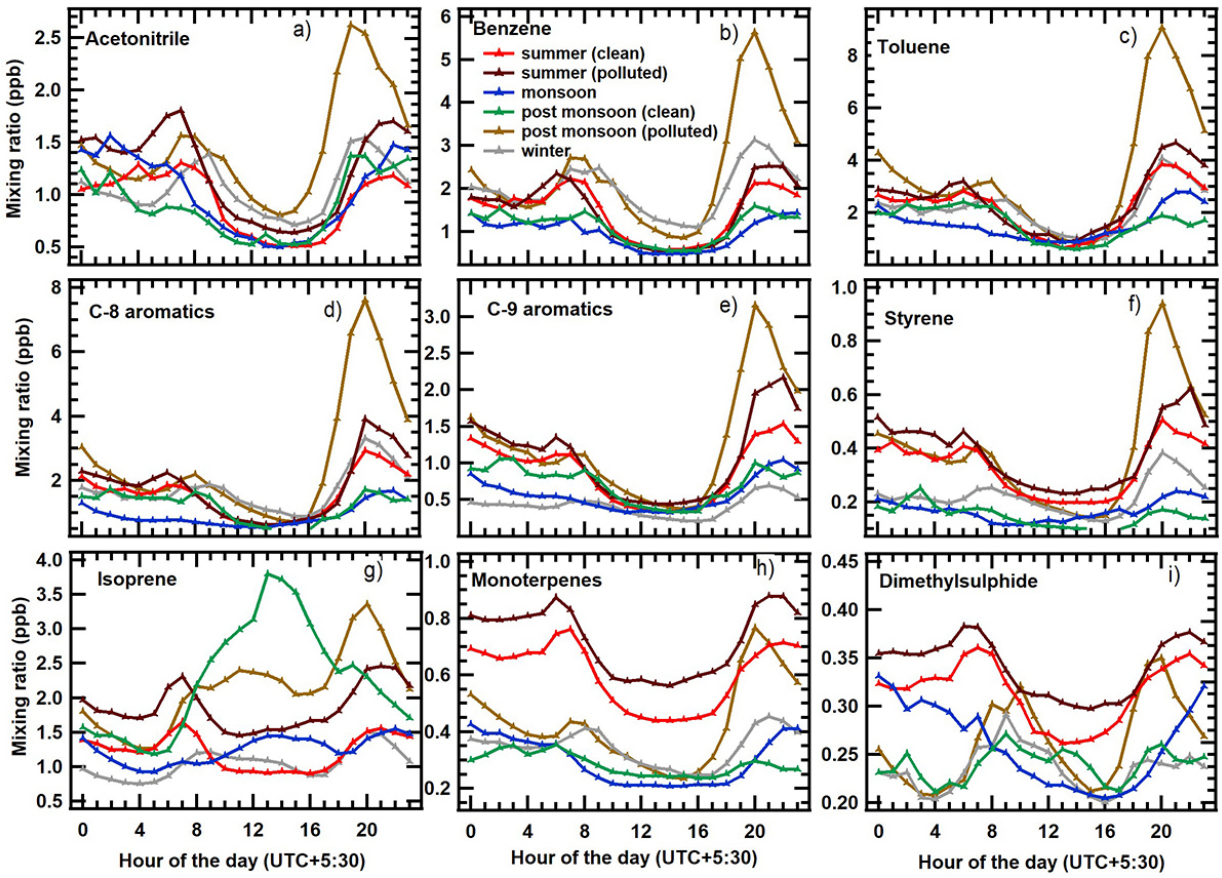

Figure 3.9: (a-i): Diel profile of average measured mixing ratio of the VOCs (Acetonitrile, Benzene, toluene, C-8 aromatics, C-9 aromatics, styrene, isoprene, monoterpenes and DMS) which have primary emission sources for the different seasons during the measurement period.

minima of isoprene concentrations. The morning time temperatures are more favourable for biogenic emissions in the summertime, which can also be inferred from early morning (06:00 - 08:00 L.T.) enhancement in the diel profile of isoprene concentration. Evening time enhancement in isoprene is most prominent in crop residue burning influenced periods of summer and post-monsoon highlighting their direct emission from these fires. Monoterpenes concentration do not show daytime enhancements in any of the seasons which is consistent with the fact that monoterpenes emission from biogenic sources occurs during both daytime and nighttime. At our site, we think that due to lack of strong monoterpenes emitting trees, emissions from direct sources such as biomass burning and dilution effects driven by boundary layer dynamics are the driver for its bimodal behaviour in all seasons (Stockwell et al., 2015). Since the measurement site is not close to marine environments, low concentration (< 400 ppt) and small diel variation is observed for DMS which is mainly due to boundary later dynamics.

Figure 3.10(a-n) show the average diel concentration profiles of the VOCs for different seasons which have strong primary and secondary emission sources. Acetaldehyde, methyl vinyl ketone (MVK), hydroxyacetone, formaldehyde, acetone and methanol are atmospheric oxidation products of isoprene and other hydrocarbons. Acetaldehyde, formaldehyde, acetone and methanol have a strong primary biogenic source also (Millet et al., 2010; Jacob et al., 2005), apart from significant contribution from anthropogenic sources also e.g. biomass fires and industrial emissions (Stockwell et al., 2015). Phenol and 2,3-Butanedione are formed as atmospheric oxidation of aromatic VOCs e.g. benzene and C-9 aromatics (Rasmussen and Khalil, 1983; Bandow and Washida, 1985). Formamide and acetamide can be directly emitted from fires apart from being formed as oxidation products of alkylamines which are in turn also emitted from biomass fires and animal husbandry (Ge et al., 2011; Nielsen et al., 2012).

High daytime mixing ratio (> 6 ppb) and a diel profile similar to that of isoprene is observed for acetaldehyde in the clean post monsoon season highlighting strong biogenic contribution towards its emissions in this season. Increased daytime concentrations of acetaldehyde, hydroxyacetone, MVK and formaldehyde are observed in all seasons except the summer seasons. The magnitude of the diel variation is minimum in the monsoon season. Similarly 2,3-butanedione, formamide and acetamide show daytime increase in all the seasons except summertime due to their photochemical production. Both formamide and acetamide show enhanced nighttime concentration in winter nights also, which could be due to direct emissions from wood burning used for domestic heating. In addition to the daytime enhancements, comparable peaks are also observed in the evening hours during the summer and post monsoon seasons influenced by crop residue fires consistent with primary emission of these VOCs from the open fires. The boundary layer height is maxi-

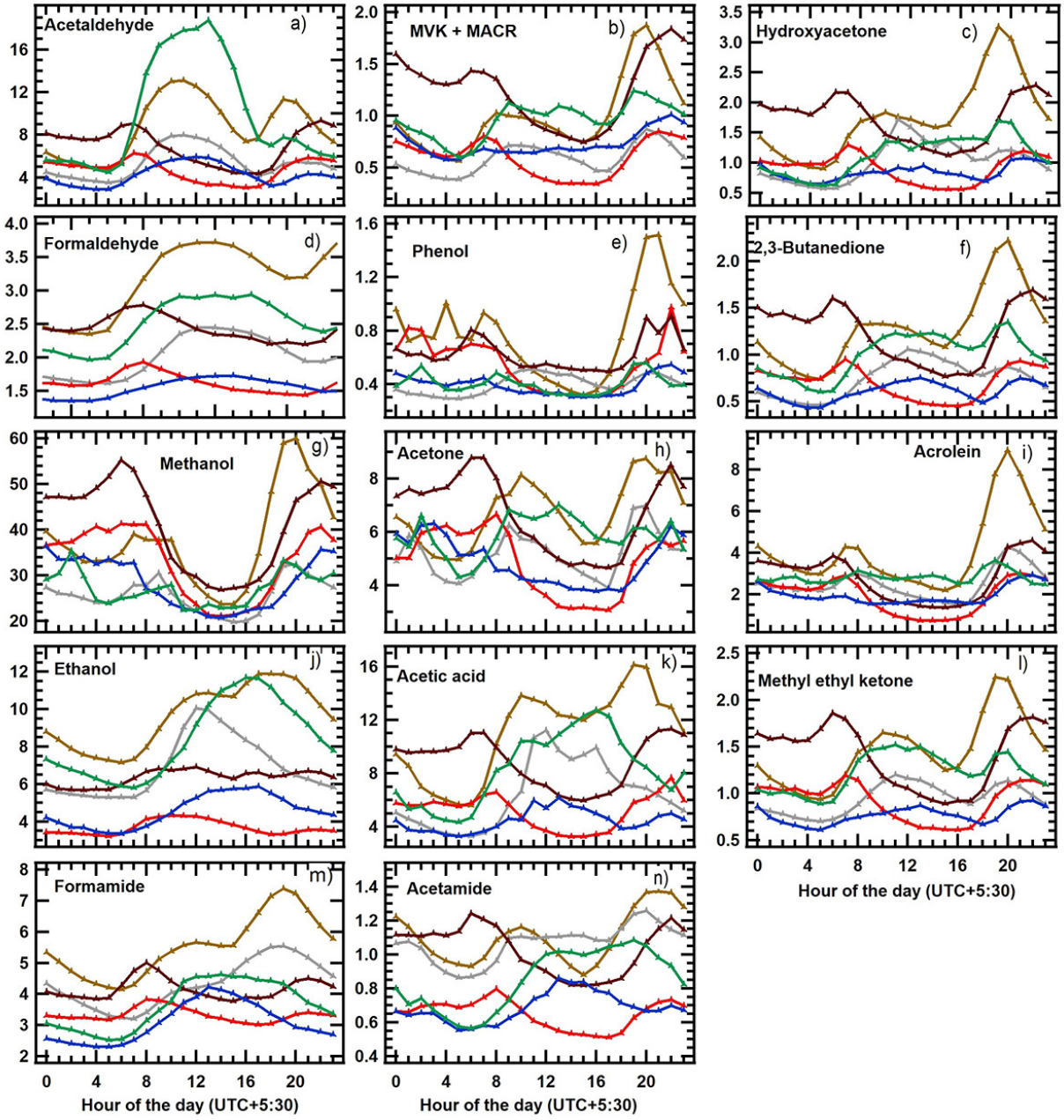

Figure 3.10: (a-n). Diel profile of average mixing ratio of 14 measured VOCs which have both primary and secondary sources in the atmosphere, for the different seasons during the study period.

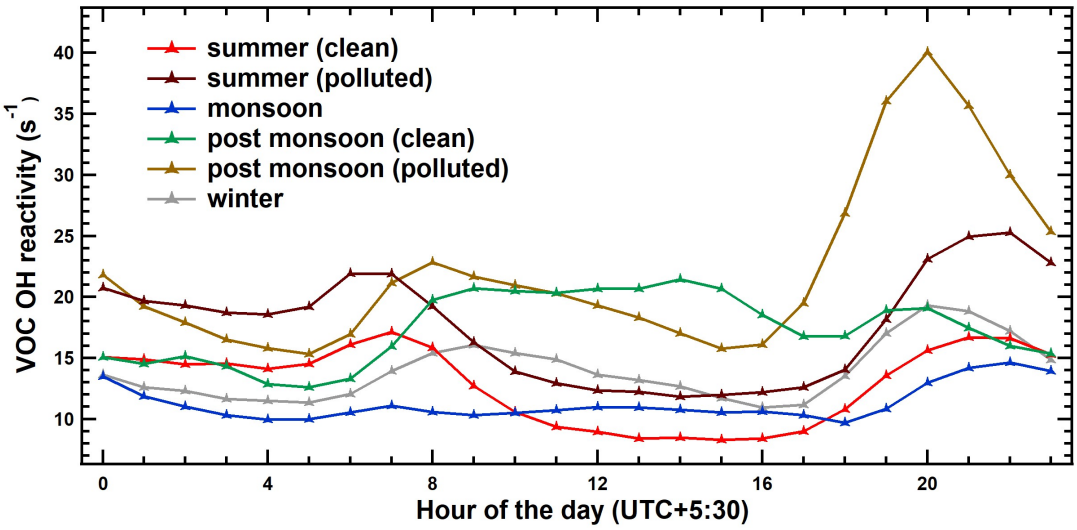

Figure 3.11: Diel profile of average calculated OH reactivity due to measured VOCs (including CO) for the different seasons during the measurement period.

mum in the summer among all the seasons of the year, and hence the enhanced dilution in the summer could be overwhelming the production due to photo-oxidation, resulting in daytime decrease in concentration of these VOCs. A bimodal shape in diel profile of measured methanol concentrations for all the seasons suggests that anthropogenic sources dominate its emission at our site. Bimodal profile is also observed for acrolein mixing ratios for all the seasons except monsoon and clean post monsoon seasons for which a relatively flatter diel profile was observed. This suggests that acrolein at the measurement site has major contribution from anthropogenic sources (e.g. biofuel/biomass burning or vehicular emissions) and not from oxidation of unsaturated hydrocarbons (e.g. 1,3-Butadiene)(Destaillats et al., 2002).

3.3.2 Seasonal and diel variability of VOC OH reactivity

The calculation of VOC OH reactivity takes into account both the concentration of VOCs and their reaction tendency with OH radicals and hence represents the reactive VOC loading of the air. The season-wise diel variability of hourly averaged VOC OH reactivity is shown in Figure 3.11. It ranged between 8.3 s^{-1} in the afternoon (clean summer season) to 40.1 s^{-1} during the night time hours of the polluted post-monsoon season.

It shows a bimodal shape with peaks in the morning and evening hours and minima during afternoon hours for all the seasons except clean post monsoon and monsoon seasons. The higher VOC reactivity is caused due to higher emissions from biofuel/biomass burning and traffic in the morning and evening time further amplified by a shallow bound-

ary layer. Stronger chemical loss due to atmospheric oxidants and dilution in an elevated daytime boundary layer leads to an overall low concentration of VOCs and hence a low VOC OH reactivity in the daytime during these seasons. Figure 10 of Sinha et al. (2014) also show bimodal characteristics in the diel profile of measured VOCs concentration with peaks in the morning and evening hours and minima in afternoon time during a representative month in summer. In the polluted post monsoon and polluted summer seasons, crop residue burning in the evening hours result in higher reactivity compared to other seasons. Kumar et al. (2016) have previously observed comparable mixing ratios of primary criteria air pollutants e.g. NO_x and CO during evening and night time (20:00 – 23:00 LT) hours of polluted post monsoon and winter, but the VOC OH reactivity during the night hours of polluted post monsoon season is $\sim$ 17 s^{-1} higher than that in the winter season (18.9 s^{-1}). This difference mainly arises due to enhanced contribution of isoprene, C-9 aromatics, acrolein and acetaldehyde towards the measured OH reactivity in the polluted post monsoon seasons (18.1 s^{-1}) as compared to the winter season (8.5 s^{-1}). The large spatial extent ($>$ 12000 km^2 area in Punjab only for paddy crop (Badarinath et al., 2006)) and the amount burnt ($>$ 48 Tg of cereals crop waste in the western IGP (Venkataraman et al., 2006)) makes crop residue fires in the polluted post monsoon a stronger source of these VOCs than wintertime biofuel burning. Both the clean and polluted period of summer follow similar characteristic in diel profile of calculated OH reactivity, but the levels were always high in polluted summer. The difference in the diel profile of hourly average values of VOC OH reactivity between the clean and polluted summer is $\sim$ 4 s^{-1} in the afternoon time which increases to up to $\sim$ 9 s^{-1} in the late evening and night hours. As mentioned previously in this section and also by Kumar et al. (2016), the crop residue fires which are more active in the evening hours increase the reactive pollutant loading of the atmosphere and in turn the total OH reactivity. Dilution of the emitted pollutants and efficient removal of reactive VOCs by oxidation in the daytime tend to cease the difference in the OH reactivity between the polluted and clean summer. The clean post monsoon season witnesses high OH reactivity in the afternoon period. The soil moisture availability, the optimum daytime temperature of $\sim$ 35 °C and cleaning of leaf surfaces after monsoon rains provide favourable conditions for biogenic emissions of isoprene, acetaldehyde and other alkenes and formation of their oxidation products e.g. formaldehyde, acetaldehyde, hydroxyacetone and methyl vinyl ketone (Kesselmeier and Staudt, 1999). Minimum values and relatively flat diel profile is observed of the calculated OH reactivity in the monsoon season apart from minor enhancement in the nighttime. This is because the diel variability for the individual VOCs was also minimum in the monsoon season. The ranking of different seasons according to their average VOC OH reactivity in descending order is polluted post monsoon (22.1 $\pm$

11.6 s^{-1}) > polluted summer (17.9 ± 9.8 s^{-1}) > clean post monsoon (17.4 ± 5.2 s^{-1}) > winter (13.9 ± 7.4 s^{-1}) > clean summer (12.0 ± 6.6 s^{-1}) > monsoon (11.3 ± 4.1 s^{-1}).

3.3.2.1 Contribution of measured VOCs towards the OH reactivity

Figure 3.12 shows the percentage contribution of different VOCs listed in Table 3.2 to the VOC OH reactivity for the morning (06:00-09:00 Local Time (L.T.)), afternoon (13:00-16:00 L.T.) and evening (20:00-23:00 L.T.) hours in different seasons of the year. The individual contributions calculated using average values over the full year is represented in the pie chart of Figure 3.12.

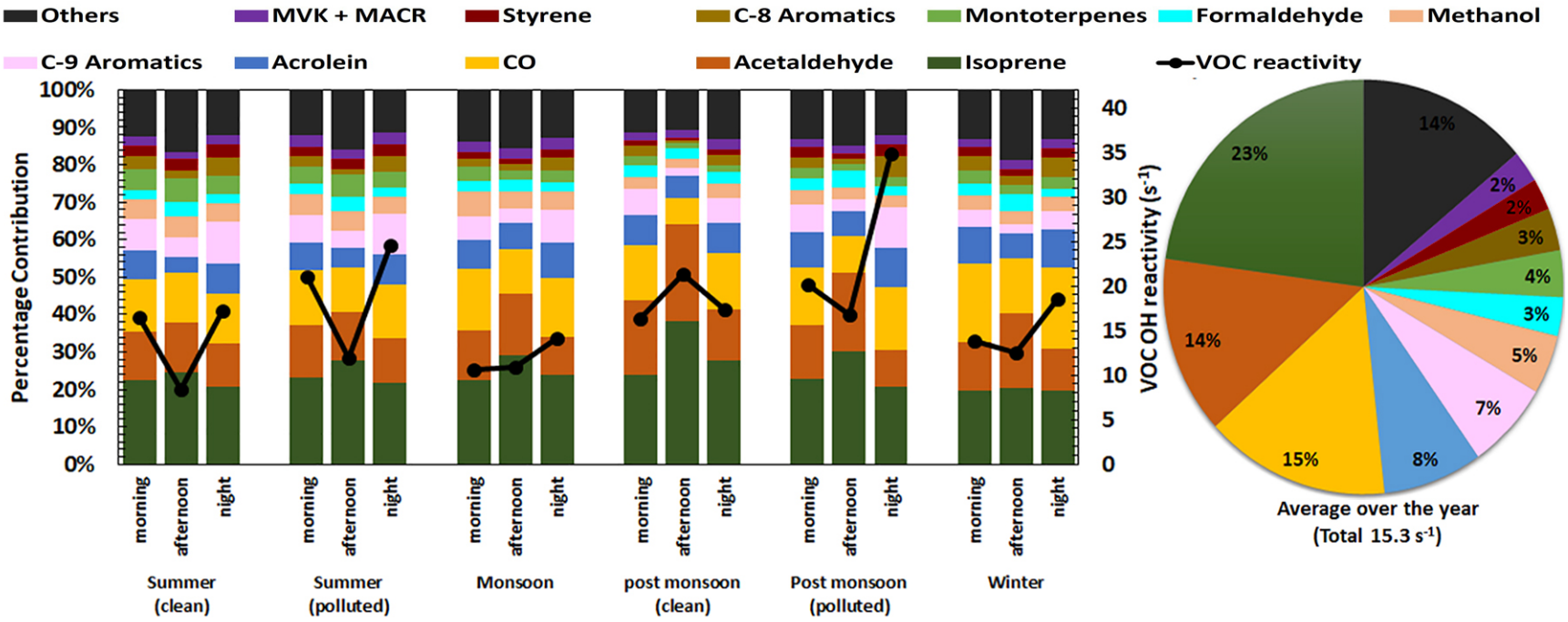

Figure 3.12: Individual percentage contribution of measured VOCs and CO to the reactive atmospheric organic pollutant loading during morning (06:00-09:00 L.T.), afternoon (13:00-16:00 L.T.) and night (20:00-23:00 L.T.) hours for different seasons. The total measured organic relative pollutant loading of the atmosphere which is represented by the OH reactivity due to measured VOCs and CO, is shown as black line and markers on the right axis. The pie chart represents the individual contributions averaged over the year-long measurement period for all the hours of the day.

The top five VOCs in terms of their relative contributions are isoprene, acetaldehyde, CO, acrolein and sum of C-9 aromatics, accounting for $\sim$ 67 % of the VOC OH reactivity. Irrespective of the season, isoprene and acetaldehyde are the dominant OH reactant contributing together to more than 38 % of the afternoon time VOC OH reactivity. The maximum contribution of these two compounds was observed in the post monsoon seasons ($\sim$ 64 % for clean and $\sim$ 60 % for polluted period). Oxygenated VOCs contribute to more than 37 % of the VOC OH reactivity in all the seasons with the maximum of 49 % in the afternoon time of post monsoon seasons (both clean and polluted). Although CO contributes to more than 70 % of the total measured reactive carbon content in all the seasons, it accounts for less than 21 % of the VOC OH reactivity in all the seasons (maximum CO contribution was observed during winter nights). Among the terpenes, the contribution of isoprene is maximum during afternoon time of clean post monsoon season (38 %), whereas the contribution of monoterpenes is maximum on summer afternoons (6-7 %).

Significantly high daytime contribution (44 %) of isoprene and acetaldehyde in the measured VOCs budget have recently been observed in the Kathmandu valley also in the subcontinent during the wintertime (Sarkar et al., 2016). Keeping the forested environments aside, most of the studies observe very low mixing ratio (and reactive contribution) of isoprene in the wintertime (Langford et al., 2010; Dolgorouky et al., 2012; Yoshino et al., 2012). It is remarkable that in the Indian subcontinent, isoprene is a significant VOCs even in the wintertime (Barletta et al., 2002; Sarkar et al., 2016).

3.3.3 Ozone production potential

Unlike the OH reactivity, the ozone production potential takes into account both the reactive VOC loading and the OH radical concentration, both of which are important factors for formation of ozone in the troposphere. Figure 3.13 shows the diel profile of calculated instantaneous ozone production potential due to measured VOCs and CO for the different seasons marked by different colored lines and markers. The diel average peak daytime (11:00 L.T. – 14:00 L.T., when the when the maxima in the diel profile of solar radiation and ozone production is observed at this site) ozone production potential was found to be maximum in the clean post monsoon seasons at 31.3 ppb h^{-1} and minimum was observed to be 10.2 ppb h^{-1} in the winter season. The calculated ozone production potential for the peak daytime hours was 15.3 ppb h^{-1} under normal summertime condition, but it increased by 7.5 ppb h^{-1} when wheat residue burning was active in the region during summer. The direct effect of enhanced ozone production potential was shown in Chapter 2 where $\sim$ 19 ppb enhancement was observed in the polluted period in summer

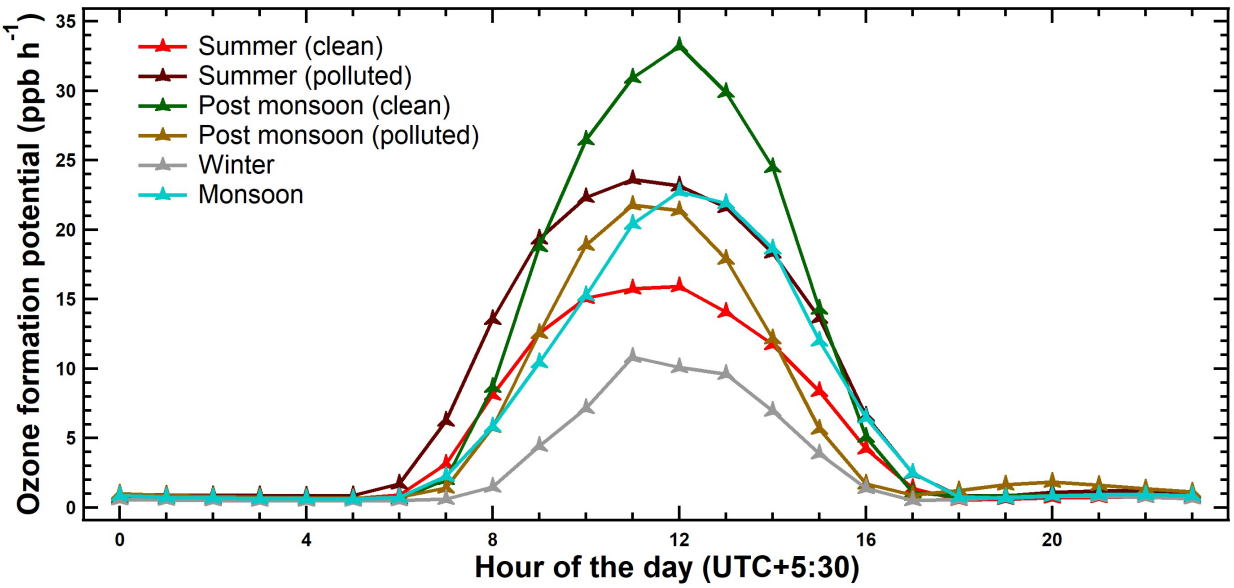

Figure 3.13: Average diel profile of VOC ozone production potential for different seasons of the study period from March 2012 to March 2013.

from the baseline ozone mixing ratio of $\sim$ 67 ppb in clean conditions.

The maximum instantaneous ozone production potential due to VOCs for the peak daytime hours did not correspond to the maximum observed ozone mixing ratio (please refer Figure 5 of Kumar et al. (2016)), and it is rather observed in crop residue fires affected periods of summer and post-monsoon. The disagreement is possible because of two reasons:

1. A large fraction of unmeasured VOCs in the crop residue fires affected period which leads to an underestimation of ozone formation potential during these seasons.

2. Different instantaneous ozone production regime (OPR) in the clean post monsoon seasons as compared to other seasons of the year.

The instantaneous ozone production regime (θ) is defined as the ratio of the lifetime of OH radicals against reaction with VOCs to that of NO_x (Kirchner et al., 2001). Since the life lime is inversely proportional to the OH reactivity, the ozone production regime is also represented as

$$\text{ozone production regime}(\theta) = \frac{NO_x\text{OH reactivity}}{\text{VOC OH reactivity}} \tag{3.6}$$

For $\theta < 0.01$ the ozone production regime (OPR) would primarily be limited by the availability of NO_x whereas for $\theta > 0.2$ ($\pm$ 0.1) the instantaneous ozone production regime would be VOC-limited. For $0.01 < \theta < 0.2$, the ozone production regime will be dependent

Table 3.3: Peak daytime (11:00-14: L.T.) ozone production regime indicator θ values for different seasons of the year.

Season	**OPR indicator (θ)**
Summer (clean)	0.22
Summer (polluted)	0.20
Monsoon	0.17
Post monsoon (clean)	0.07
Post monsoon (polluted)	0.13
winter	0.27

strongly on both VOC and NO_x concentrations. The peak daytime time (11:00-14:00 L.T., when the when the maxima in the diel profile of solar radiation and ozone production is observed at this site) values of θ for different seasons are shown in Table 3.3 and it ranges between 0.07 (clean post monsoon) and 0.27 (winter) for different seasons. The VOC OH reactivity term used to calculate θ only includes the contribution from measured VOCs listed in Table 3.2 and CO which will be significantly lower than the actual directly measured total VOC OH reactivity. Additionally, the NO_x reactivity in the numerator also slightly overestimated, as the NO_x measurements using chemiluminescence technique provides an upper estimate of the total NO_x (Sinha et al., 2014). Hence, actual θ is expected to be lower than what is reported in this study.

Hence in the clean post monsoon season, the daytime ozone production potential is expected to be limited by the availability of NO_x whereas, for all other seasons, it is strongly dependent on both VOC and NO_x mixing ratio. In a NO_x-limited regime, the ozone production potential is least affected by the availability of VOCs and hence a higher VOC ozone production potential will not translate into significantly higher mixing ratio of ozone and it will rather be dependent on NO_x concentrations, which is already low during clean post monsoon. During the polluted post monsoon season, even a lower daytime ozone production potential of 11.6 ppb h^{-1}, the dependency of ozone production on both VOC and NO_x and their high concentration, results in observed ozone mixing ratio comparable to that in the clean post-monsoon (see Figure 5 of Kumar et al. (2016)).

3.4 Conclusion

This work presents the first continuous long-term online measurement of a suite of 23 VOCs using a PTR-MS from the north-west Indo-Gangetic plain in Mohali for a period spanning from 01 March 2012 to 27 February 2013. In terms of their measured concentration, oxygenated VOCs are the most important among the measured VOCs with an annual average concentration of methanol, acetaldehyde, and acetone at 32.2, 5.9 and 5.6

ppb respectively. Despite being a suburban location, the annual average concentration of 1.6 ppb of isoprene is observed which is primarily due to biogenic emissions in the daytime and biomass burning emissions in the nighttime. Crop residue burning in the summer and post-monsoon seasons is found to cause approximately two-fold enhancements in evening and night time concentrations of acetonitrile, isoprene, aromatics and oxygenated VOCs. Very high seasonal average concentration of carcinogenic aromatic VOCs e.g. benzene and toluene at 1.5 and 2.5 ppb for the polluted summer and 2.4 and 3.5 ppb for polluted post monsoon respectively are observed. Favourable conditions for biogenic emissions e.g. soil moisture availability and uninterrupted sunlight in the clean post monsoon season results in maximum daytime observed concentrations of isoprene and acetaldehyde.

The average diel profile of OH reactivity due to measured species ranges between 8.1 s^{-1} and 40 s^{-1} in different seasons. Crop residue fires increase the night time VOC OH reactivity from 17.4 s^{-1} in the clean post monsoon to 34.8 s^{-1} and from 17.3 s^{-1} to 24.5 s^{-1} in the summertime. Isoprene and acetaldehyde are found to be the major contributor of reactive pollutant loading contributing to more than 38 % of the daytime VOC OH reactivity and ozone production potential in all the seasons. In terms of their OH reactivity contribution, among the different class of VOCs, oxygenated VOCs are the most important, contributing to more than 37 % of the total in all the seasons. The maximum VOC ozone production potential averaged for the peak daytime hours (11:00-14:00 L.T.) was observed to be 31.3 ppb h^{-1} in the clean post monsoon and the minimum was observed to be 10.2 ppb h^{-1} during winter. Crop residue fires in the summertime cause an increase of 7.5 ppb h^{-1} in the VOC ozone production potential from a baseline value of 15.3 ppb h^{-1}. The maximum calculated ozone production potential in the clean post monsoon does not correspond to the maximum observed ozone concentration. While the peak daytime ozone production is limited by the availability of NO_x in the clean post monsoon, both VOC and NO_x availability strongly control the peak daytime ozone production in all other seasons. Direct measurements of OH radical concentration will reduce the limitation induced due to use of estimated OH concentration for the calculation of ozone production potential as discussed in section 3.2.3. Future studies should include direct measurement of total OH reactivity and ozone production potential in all the seasons to accurately quantify the contribution of unmeasured VOCs towards the ozone production.

Chapter 4

VOC-OHM: A new technique for rapid measurements of ambient total OH reactivity and volatile organic compounds using a single proton transfer reaction mass spectrometer

Abstract

Measurements of total hydroxyl radical (OH) reactivity and volatile organic compounds (VOC) are necessary for improving our understanding of reactive emissions and atmospheric oxidation in air pollution and atmospheric chemistry studies. Proton transfer reaction mass spectrometers (PTR-MS) can measure ambient VOCs and the total ambient OH reactivity. However, till date this has always required deployment of two PTR- MS instruments, wherein one instrument measures ambient VOCs and the other instrument measures the total OH reactivity using the comparative reactivity method (CRM). Due to material (e.g. power, space) or financial constraints, deploying two PTR-MS instruments is not always possible and yet it is desirable to quantify both VOCs and OH reactivity. Here, I present a novel hyphenated technique christened VOC-OHM (for Volatile Organic Compounds – OH reactivity Measurement) that enables rapid ambient measurements of both VOC concentration and total OH reactivity using a single PTR-MS. The technique also demonstrates a new safer and portable substitute for pressurized zero air bottles that have been required thus far in CRM OH reactivity deployments. VOC-OHM successfully couples the typical VOC and CRM experimental set ups without

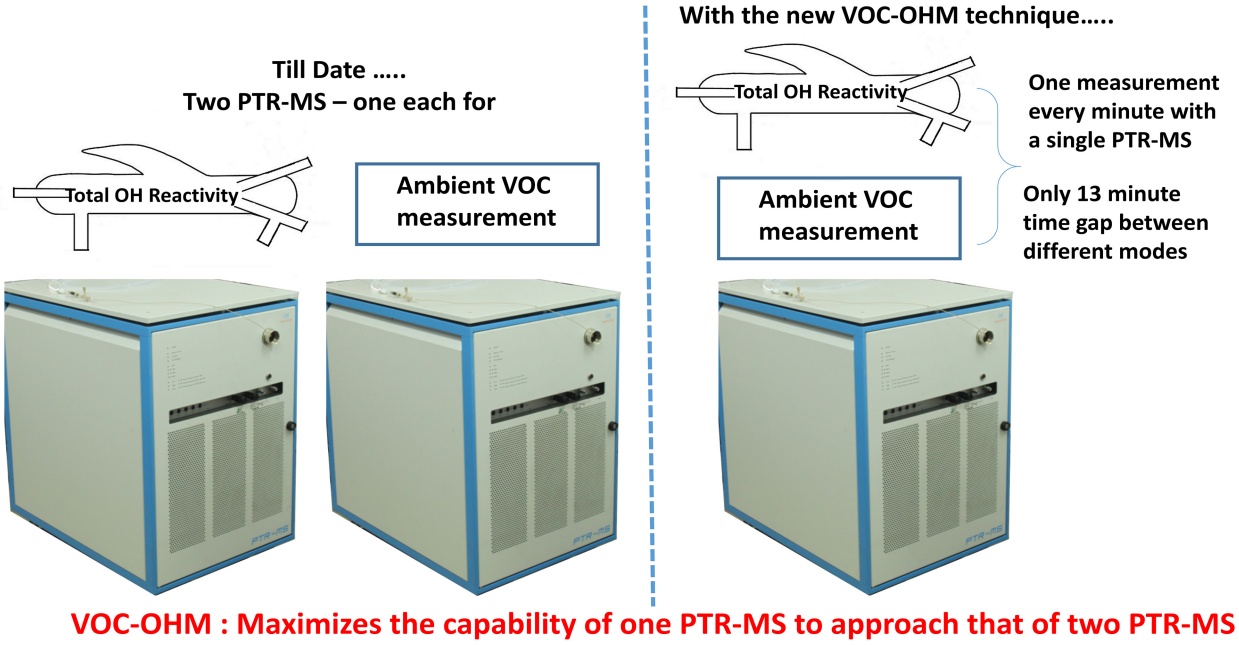

Figure 4.1: Graphical abstract showing the importance and applicability of VOC-OHM.

compromising on the PTR-MS's ability to measure either parameter. The design of the VOC-OHM system, its validation, optimization and results of field tests are described in detail. The VOC-OHM system measures the ambient VOCs and OH reactivity every hour for $\sim$ 20 minutes duration each, with an ambient data gap of $\sim$ 13 minutes in between. Thus rapid temporal changes in the ambient chemical composition and reactivity are easily quantified. This technique also demonstrates a new approach to achieve additional specificity at ppt level in mass spectrometers with a mass resolution poorer than 1 amu. This technique constrains the hydroxyl radical specific rate constants of the major reactive isobaric contributor to a particular m/z in the mass spectra, which can be used as second means for identification of the m/z mass peaks. The sampling periods and VOC speciation achieved using VOC-OHM can be customized depending on user preferences, providing more options for the majority of users possessing a single PTR-MS.

4.1 Introduction

OH radicals are the primary oxidants of the atmosphere (Heard and Pilling, 2003) . Due to their high reactivity with ambient trace gases, they act as the cleansing agents of the atmosphere. This is accomplished by oxidizing most of the primary emissions in the presence of oxygen, to products that can be more easily removed from the atmosphere (Lelieveld et al., 2004) because the products are less volatile and more water soluble. Along

with volatile organic compounds (VOCs), OH radicals drive the formation of secondary pollutants such as ozone and secondary organic aerosol (Parry et al., 2007; Levy, 1971). The total OH reactivity is defined as the summation over products of the concentration of the OH reactant $[X_i]$ (e.g. X_i = CO, VOCs, NO_2 etc.) and its rate constant with the hydroxyl radical (k_{OH+X_i}), mathematically described as equation 1.7:

Direct measurements of the total OH reactivity of ambient air in combination with measurements of major reactive volatile organic compounds permit investigation of missing reactive emissions (Sinha et al., 2010; Di Carlo et al., 2004) in atmospheric chemistry field studies. Moreover the total OH reactivity is a robust proxy for the total reactive pollutant loading of air masses and when combined with measurements of nitrogen oxides, permits derivation of instantaneous ozone production regimes (Kovacs et al., 2003; Sinha et al., 2012). The sources of hydroxyl radicals depend on only few photochemical reactions and hence are better constrained if the measurements of photolysis frequencies (e.g. J($O(^1D)$), J(HCHO), J(H_2O_2), J(HONO)) and precursors (e.g. HONO, peroxides and alkyl peroxy radicals) are available. However, the total OH reactivity which represents the collective sink term is more difficult to constrain as it depends on the multitude of reactive species present in ambient air. Thus, direct measurements of the total OH reactivity also permit an accurate assessment of the atmospheric hydroxyl radical budget (Hofzumahaus et al., 2009), which represents a key test for our understanding of atmospheric chemistry in different environments. For direct measurements of total OH reactivity, there are three well established methods, two of which (namely Total OH loss measurement (Ingham et al., 2009; Kovacs and Brune, 2001) and pump-probe method (Sadanaga et al., 2004a) are based on laser induced fluorescence (LIF) and derive the OH reactivity of ambient air by detecting the decay of artificially produced OH radicals in a flow tube injected with ambient air. The third method, namely the Comparative Reactivity Method (CRM)(Sinha et al., 2008), uses a proton transfer reaction mass spectrometer or a gas chromatograph equipped with a photo-ionization detector (GC-PID)(Nölscher et al., 2012a) for detection of pyrrole (a reagent molecule) during an in situ competitive kinetics experiment.

In terms of cost and logistical constraints (power consumption, size, weight and laser stability), which are very important considerations for instrumental deployment in field studies, laser induced fluorescence based systems are generally more difficult to deploy than proton transfer reaction mass spectrometers. However, even proton transfer reaction mass spectrometers are expensive and cost upwards of 200,000 euros each. Till date in all the field studies either two PTR-MS systems or a GC-PID and a PTR-MS have been required to perform ambient measurements of VOCs as well as the total OH reactivity. As far as the CRM method is concerned, the PTR-MS remains a better choice for the

detector as the GC-PID has many limitations for this application (Nölscher et al., 2012a). It would thus be extremely beneficial, to be able to deploy a single PTR-MS system configured for rapid measurements of both reactive VOCs and the total OH reactivity, so that meaningful information pertaining to diel VOC and OH reactivity profiles can be obtained using only one instrument.

In this work, I present a new technique, termed VOC-OHM (Volatile Organic Compound-OH reactivity Measurement), that enables a single PTR-MS instrument to be employed for direct and rapid sequential ambient measurements of total OH reactivity and reactive VOCs in a semi-automated manner. The technique was tested in the laboratory for analytical constraints specific to both CRM OH reactivity measurements and ambient PTR-MS VOC measurements, and optimized. Successful acquisition of ambient data at a site in India where the ambient chemical composition shows pronounced diel variability in response to emission activity and meteorological factors is also demonstrated. Finally, the advantages and limitations of VOC-OHM, in comparison to the traditional two PTR-MS systems' deployment is discussed.

4.2 Experimental

4.2.1 Measurement of ambient volatile organic compounds and pyrrole using a proton transfer reaction mass spectrometer (PTR-MS)

A high sensitivity quadrupole proton transfer reaction mass spectrometer (PTR-QMS) (Model 11-07HS-088; Ionicon Analytik Gesellschaft, Austria) was used to perform sequential measurements of ambient VOCs and pyrrole (the reagent molecule measured in the comparative reactivity method)(Sinha et al., 2008). Analyte molecules can be detected in the PTR-MS if their proton affinity (P.A.) exceeds that of water vapour (Lindinger et al., 1998) (P.A. = 165.2 kcal mol^{-1}). A pure flow of the hydronium reagent ions (> 95 % purity) is produced in the ion source region of the PTR-MS using a plasma discharge in a hollow cathode which are then directed towards the drift tube. A potential difference of 600 V is applied across the drift tube where a constant pressure of 2.2 mbar and temperature of 60 °C is maintained. This corresponds to an E/N ratio of 134.8 Townsend, which inhibits the formation of complex clusters inside drift tube. Within the drift tube, analyte VOCs with a proton affinity greater than that of water vapour react with reagent hydronium ions (H_3O^+) to form protonated molecular ions (with m/z = molecular ion + 1). With the exception of few classes of compounds (e.g. higher alcohols where [molecular ion – 17] peaks also occur), fragmentation of the molecular ion does not complicate the

mass spectra at the typical drift tube conditions of the PTR-MS (E/N < 140 Townsend) for several volatile organic compounds. The ions are then separated based on their m/z ratio using a quadrupole mass analyzer and detected using a secondary electron multiplier. The measured m/z ion signals in counts per second (cps) were then converted to normalized counts per second (ncps) at a drift tube pressure (P_{drift}) of 2 mbar and drift tube temperature (T_{drift}) of 25 °C using the following normalization equation previously discussed in chapter 3 (Sinha et al., 2009; Tani et al., 2004),

$$\mathrm{ncps} = \frac{I(\mathrm{RH}^+) \times 10^6}{I(\mathrm{H_3O}^+) + I(\mathrm{H_3O}^+(\mathrm{H_2O}))} \times \frac{2}{P_{\mathrm{drift}}} \times \frac{T_{\mathrm{drift}}}{298.15} \tag{4.1}$$

The normalized signals were then converted to ppb using the sensitivity factors derived from the calibration experiments. The applications of proton transfer reaction mass spectrometry for quantifying ambient VOCs and pyrrole have been discussed extensively elsewhere (de Gouw and Warneke, 2007; Sinha et al., 2009). A comprehensive description of the data quality assurance, calibration protocols for ambient VOCs and technical details of the PTR-MS and other instruments used in this work have already been provided in Sinha et al. (2014).

Table 4.1 lists the detection limits and uncertainties for the ambient VOCs measured in this work along with the m/z ratios at which they were detected. The instrument was calibrated for the measured compounds (range 0.3 ppb – 20 ppb) using a custom ordered VOC gas standard (Apel-Riemer Environmental, Inc., Colorado, USA; ∼500 ppb for each VOC, stated uncertainty = 5 %) containing compounds listed in Table 4.1. The calibrations were performed by dynamic dilution of the gas standards as described in Sinha et al. (2009, 2012). The instrumental background was determined by sampling VOC-free zero air generated using a Gas Calibration Unit (GCU-A, Ionimed Analytik). A catalytic converter inside the GCU-A oxidizes VOCs to carbon dioxide. The detection limit for the measured VOCs was defined as 2 σ of the measured normalized signal divided by the sensitivity at that m/z, while measuring zero air. The overall uncertainty was calculated using the root mean square propagation of i) 5 % accuracy error inherent in the VOC gas standard, ii) 2 σ instrumental precision error while measuring 6 ppb of VOC and iii) 2 % flow fluctuation due to each of the two mass flow controllers (MFCs) used in the calibration.

Pyrrole (C_4H_5N; M.W.: 67 g mol^{-1}) is the reagent molecule used in the comparative reactivity method for total OH reactivity measurements. It is not normally present in ambient air and can be detected accurately in the PTR-MS at m/z = 68, as most species in ambient air form protonated ions that are detected at odd m/z ratios (Sinha et al., 2008). Humidity changes from extremely dry air (∼ 0 %RH) to values above 30 % RH

Table 4.1: Nominal protonated m/z, detection limits and uncertainties of VOCs measured during the study period.

Measured Species	**Nominal protonated m/z (Th)**	**Detection limit (ppb)**	**Uncertainty (%)**
Methanol	33	0.46	10.3
Acetonitrile	42	0.03	10.1
Acetaldehyde	45	0.12	10.1
Acetone	59	0.61	10.3
Isoprene	69	0.06	15.8
Methyl vinyl ketone	71	0.02	11.6
Methyl ethyl ketone	73	0.04	10.5
Benzene	79	0.03	10.1
Toluene	93	0.05	11.5
Sum of C-8 aromatics*	107	0.04	12.4
Sum of monoterpenes†	81 (65 % fragment) and 137 (35 % fragment)	0.03	12.1
Sum of C-9 aromatics*	121	0.09	11.0

*Calibrated using p-Xylene, †Calibrated using α-Pinene, *Calibrated using 1,2,4-Trimethylbenzene

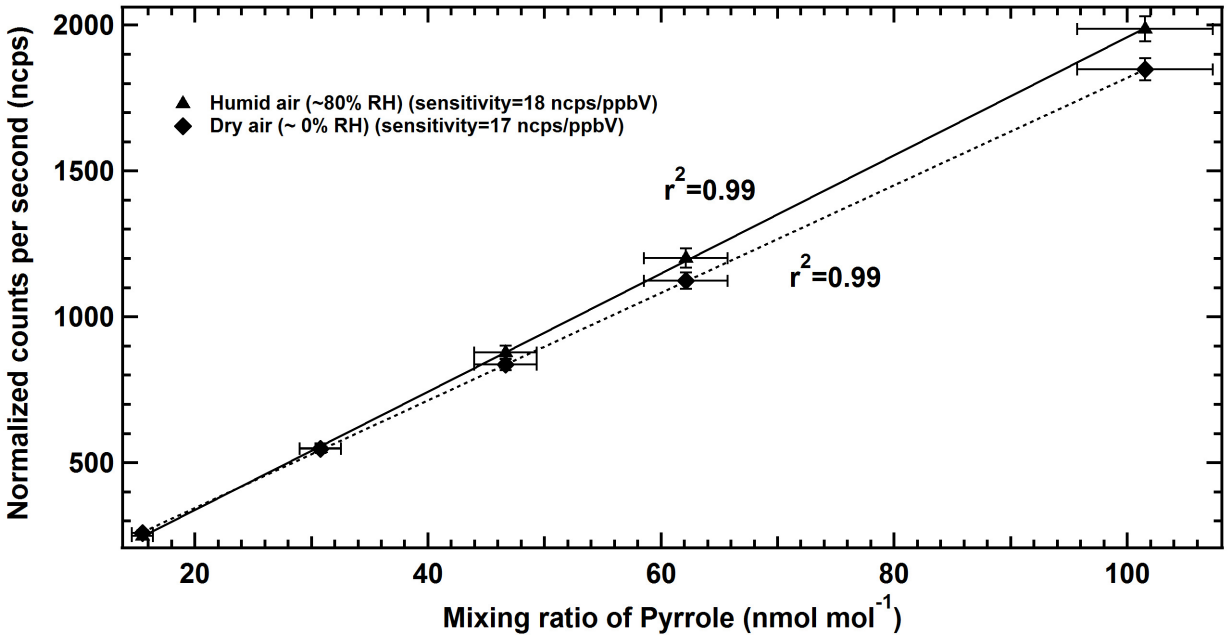

Figure 4.2: Plot showing sensitivity and linearity of pyrrole signal under both dry (∼0 % RH) and wet (∼80 % RH) conditions.

can cause differences in the detection sensitivity (Sinha et al., 2009) and were taken into account. Figure 4.2 illustrates the sensitivity and linearity of the pyrrole signal under both dry (∼ 0 % RH) and wet (80 % RH) conditions. The calibration was performed using a custom ordered pyrrole gas standard (Westfalen A.G., 9.8 ppm; stated uncertainty 10 %) dynamically diluted with zero air at 0 % RH and 80 % RH to yield five different mixing ratios in the range of 15 - 102 ppb. These concentrations represent the dynamic range and conditions under which pyrrole is measured in the comparative reactivity method. Under dry conditions, the sensitivity of the PTR-MS for pyrrole was 17 ncps ppb^{-1} while it was 18 ncps ppb^{-1} at 80 % RH. The horizontal error bars represent the accuracy error, which is the root mean square propagation of i) 10 % accuracy error inherent in the pyrrole standard used for calibration and ii) 2 % flow fluctuation due to each of the two mass flow controllers used in the calibration. The vertical error bars in Figure 4.2 represent the 2 σ instrument precision error at each dilution point.

4.2.2 Total OH reactivity measurements using the Comparative Reactivity Method (CRM)

Total OH reactivity measurements were performed using the comparative reactivity method (CRM) developed by Sinha et al. (2008). In this technique, in situ competitive kinetics is performed inside a 14 cm continuous flow glass reactor between pyrrole and

OH reactants present in ambient air, for a known concentration of synthetically generated OH radicals. OH radicals are generated by passing humidified nitrogen over the mercury vapour lamp inside the glass reactor according to following reaction :

$$H_2O \xrightarrow{184.9\,nm} OH + H \qquad [R16]$$

A proton transfer reaction mass spectrometer coupled to the glass reactor is used for fast and accurate measurements of the changing pyrrole concentrations inside the reactor. In Section 4.2.3, I describe the flow schematic and technical details of the experimental set up. Below I describe only the salient features of the three key stages involved in the CRM, and the steps involved in obtaining the OH reactivity from the pyrrole measurements during each stage. The three key stages in the CRM for OH reactivity measurements are also referred to as the C1, C2 and C3 stages of measuring pyrrole (see for e.g. Figure 1 of Sinha et al. (2009)):

1. Stage 1: In this stage, pyrrole is measured inside the reactor in a flow of dry zero air and dry nitrogen while a mercury vapour lamp (LOT-Quantum Design GmbH, P/N 90-0012-01) emits UV radiation (with emission wavelengths at 184.9 nm 253.6 nm, 312.5 nm, 365 nm and 435.8 nm). Due to the photon flux from the lamp, some of the pyrrole photolyzes (typically 10 - 25 %, more details are available in Section 4.2.1 of Sinha et al. (2008)). So, the pyrrole concentration available for chemical reactions (referred to as the C1 concentration of pyrrole) during the subsequent stages 2 and 3 is accurately known. It should be noted that during stage C1, both hydroxyl radicals and ambient air are absent. Unless flows are changed or the lamp flux output changes (which occasionally occurs over time scales of a week), the concentrations of pyrrole measured during the C1 stage do not vary and hence it is sufficient to measure the pyrrole concentration in the C1 stage once in 7 days.

2. Stage 2: In this stage, hydroxyl radicals are generated synthetically but ambient air is still absent. This stage is a chemical titration and the decrease in the measured concentration of pyrrole from C1 to the new lower concentration termed C2, yields the OH radical concentration available for competitive reactions between pyrrole and ambient air.

3. Stage 3: In this stage, pyrrole is measured in the presence of both the hydroxyl radicals and OH reactants present in ambient air. Competition between pyrrole and the OH reactants for the hydroxyl radicals (the concentration of which is known from stage 2), causes the measured signal of pyrrole to increase from C2 to a higher

concentration C3. The increase (C3 − C2), depends on the collective OH reactivity of the OH reactants present in ambient air.

The total OH reactivity of the ambient air (R_{air}) is then obtained using 4.2, a derivation of which is available in Sinha et al. (2008):

$$R_{air} = \frac{C3 - C2}{C1 - C3} \cdot k_p C1 \tag{4.2}$$

In the above discussion, It can be noted that stage 2 (C2) and stage 3 (C3) are the "active mode" and rapid switching between both stages is necessary for accurate quantification of the total ambient OH reactivity, as the C2 measurements "before and after" a C3 measurement are used to interpolate the C2 corresponding to that particular C3 stage for use in equation 4.2. From equation 4.2 it can also be seen that the total OH reactivity depends only on the pyrrole concentration in different stages (C1, C2 and C3) and the rate constants for the reaction of pyrrole with the hydroxyl radical (k_p), which is well known (Dillon et al., 2012; Atkinson et al., 1984). Corrections are applied for deviations from pseudo first order kinetics as described in Section 4.1 of Sinha et al. (2008) depending on the pyrrole /[OH] ratio given by C1/(C1-C2) (Sinha et al., 2008). The concentrations of C1 and [OH] for the measurements reported in this work were $\sim$ 68 ppb (or 1.6×10^{12} molecules cm^{-3}) and $\sim$ 26 ppb (or 6.2×10^{11} molecules cm^{-3}, respectively. Based on numerical simulations (Curtis and Sweetenham, 1988), the correction factor was:

$$R_{true} = -0.0004(R_{meas})^2 + 0.84(R_{meas}) - 0.20 \tag{4.3}$$

where R_{true} is the corrected OH reactivity and R_{meas} is the measured OH reactivity obtained by using equation 4.2. The units of R_{true} and R_{meas} are s^{-1}.

4.2.3 VOC-OHM system for rapid switching between OH reactivity and ambient VOC measurement modes using a single PTR -MS

Figure 4.3 shows the schematic of the VOC-OHM system developed and deployed in this work for rapid sequential measurements of ambient OH reactivity and VOCs. Ambient air was sampled using a Teflon inlet line (length: 15 m; inner diameter 0.31 cm) equipped with a particle filter at the inlet entrance for protection from floating debris and particles. The ambient air was then either made to flow through directly to the PTR-MS without passing through the CRM reactor (termed VOC mode) or introduced into the glass reactor (termed OH reactivity mode or OHM). In order to accomplish rapid and

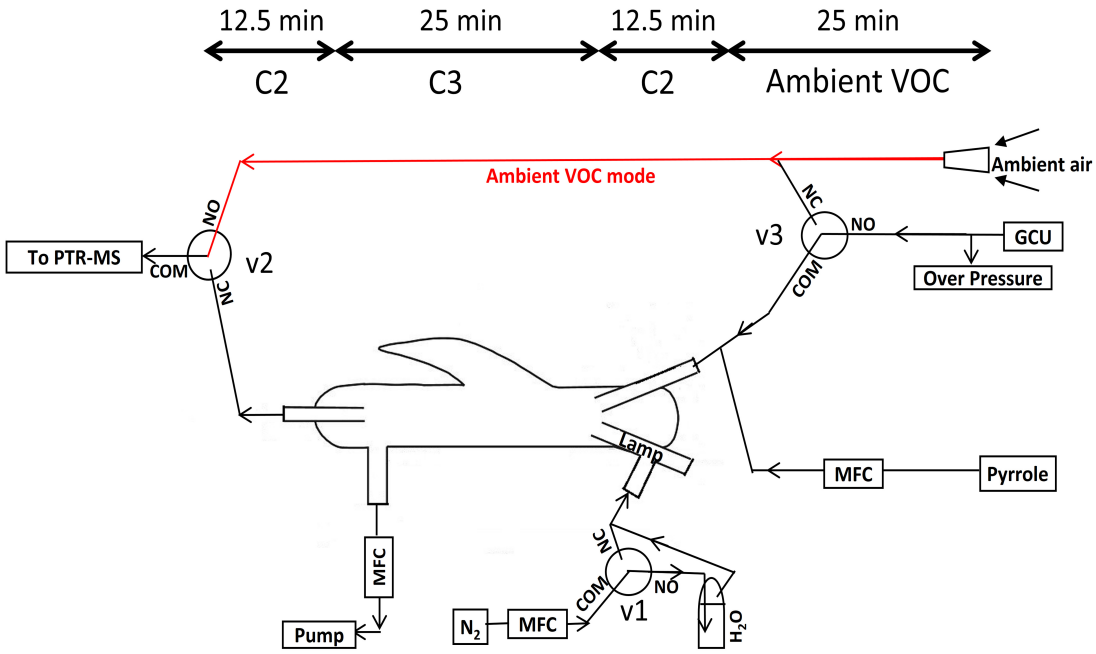

Figure 4.3: Top: Switching time between different stages of OH reactivity mode and VOC mode, below: flow schematic of VOC-OHM technique.

automatic switching between the ambient VOC and total OH reactivity measurement modes, two automatic Teflon three way valves (Parker VAC -20 PSIG), shown as v2 and v3 in Figure 4.3 were employed. Note these additional valves are also the key differences from the CRM flow schematic used in (Sinha et al., 2008) in terms of hardware.

Table 4.2 summarizes the valve configurations during different measurement stages. The additional valves were programmed using the PTR-MS Control v2.7 software which is used to operate the PTR-MS and powered using two of the six analogue output slots available on all commercial PTR-MS instruments. The valve configuration corresponding to different stages in measurement is logged with distinct "flags" in the data file, for subsequent separation and analysis of data pertaining to the ambient VOC mode and C2, C3 stages of the OH reactivity measurement mode. Other differences from previously published variants of the CRM technique (Nölscher et al., 2012b; Dolgorouky et al., 2012; Sinha et al., 2010) are that, the zero air (for the C1 and C2 steps) was generated using a Gas Calibration Unit (GCU-A, Ionimed Analytik, Innsbruck, Austria). This affords two distinct advantages. The first is that humidification of zero air to ambient air's relative humidity is readily achieved during the C2 stage, as the scrubber inside the GCU does not change the relative humidity but only removes VOCs by oxidation. Also for the C1 stage, the zero air that is generated using the GCU is dry ($\sim$ 0 % RH), as one can remove water vapour using the GCU. The GCU is equipped with a dew point mirror (DPM) that allows the gas passing through it to be set to a desired RH. The peltier cooler inside the

Table 4.2: Valve configuration in different measurement mode.

Valve V1 position	**Valve V2 position**	**Valve V2 position**	**Measurement mode**
0	0	0	Ambient VOC measurement
1	1	0	OH reactivity (C1)
0	1	0	OH Reactivity (C2)
0	0	1	Not used
0	1	1	OH Reactivity (C3)

0=normally open (NO) mode (no potential difference applied), 1=normally closed mode (NC) (24 V applied)

DPM cools the air the required dew point temperatures. The second advantage is that the GCU is safer and more convenient (especially for field deployment) as it replaces the need for pressurized zero air cylinders, which have been used in previous CRM deployments (Nölscher et al., 2012b; Dolgorouky et al., 2012; Sinha et al., 2010). The pressurized zero air cylinders are bulky to carry, difficult to stock and classified as dangerous goods.

The zero air flow from the GCU is introduced through a Teflon T-connector at over pressure so as to ensure that room air is not sucked into the reactor. The total flow in the reactor of $\sim$ 275 standard centimeter cube per minute (sccm) is maintained by the suction of the PTR-MS and exhaust pump (see Figure 4.3). The incoming flow in the reactor is due to pyrrole, nitrogen gas and zero air (while measuring C2) or ambient air (while measuring C3). Ambient air (169 sccm) is diluted inside the reactor by a factor of 1.6 as it mixes with the nitrogen flow (106.0 sccm) and pyrrole flow (2.2 sccm). A flow meter traceable/calibrated to NIST (BIOS Drycal definer 220) was used for all flow measurements. For the data reported in this work, the detection limit is $\sim$ 4.5 s^{-1} while the overall uncertainty (Sinha et al., 2008) is 18.8 % of the measured values. Various tests for the optimization of sampling time between ambient VOC mode and OH reactivity mode and to eliminate the hysteresis effect due to the stickiness of pyrrole and alternation between high (upto 100 ppb) and low concentrations ($<$ 50 ppt) in the sampling lines were necessary. These are discussed in Section 4.3.

4.2.4 Measurements of CO, NO_2, NO and SO_2

Simultaneous measurements of OH reactants other than VOCs were also performed in this study. Diel profiles and time series profiles of the OH reactants are a useful qualitative indicator for changing ambient chemical composition and reactivity. Moreover they provide a check on the data quality of the directly measured OH reactivity values as the total calculated OH reactivity due to the measured OH reactants should always be

lower than or equal to the directly measured OH reactivity, depending on the fraction of the total OH reactant suite that has been measured. Technical details of the instruments, sampling, calibration and quality assurance protocol of data for the CO, NO_2 and NO measurements are discussed in chapter 2 in greater details and also in Sinha et al. (2014). Therefore these are discussed only briefly here.

CO was measured using gas filter correlation (GFC) non dispersive infra-red (NDIR) technique (Thermo Fisher model 48i)and NO_x (NO + NO_2) was measured using the chemiluminescence technique (Thermo Fisher model 42i). Measurement of sulphur dioxide (SO_2) was carried out by pulsed UV fluorescence technique using Thermo Fischer Scientific 43i trace level enhanced analyzer. SO_2 is excited at 214 nm (absorption maxima) and the intensity of fluorescence is recorded at 350 nm (emission maxima). For the measurement of low concentration of SO_2, excitation by pulsed UV light is more efficient because of high intensity and better signal to noise ratio (Omenetto et al., 1977). The hydrocarbons (e.g toluene, *o*-xylene, *m*-xylene, *p*-xylene, *m*-ethyltoluene, ethylbenzene and 1,2,4-trimethylbenzene) present in ambient air are removed by passing the sample through a hydrocarbon kicker, as they can cause interference by also fluorescing at 350 nm (Luke, 1997). Another possible interference is due to nitric oxide (NO), which fluoresces in a range close to that of SO_2. Previous studies have shown that 500 ppb NO gives an equivalent response of 1 ppb SO_2 (Okabe et al., 1973). The maximum uncertainty in SO_2 measurements due to the presence of NO in Mohali is always < 0.3 ppb. This method has also been used previously for ambient SO_2 measurements (Wang et al., 2002). Zero drift checks and 5 point span calibration experiments were performed for SO_2, CO and NO_x analyzers on 30 April 2013, 06 May 2013 and 11 May 2013 respectively, according to the protocol described in Sinha et al. (2014). The detection limits for SO_2, CO and NO_x, measurements reported in this work were 1 ppb, 28 ppb and 114 ppt respectively.

Ambient NO concentrations above 10 ppb can cause underestimation of the measured OH reactivity in the comparative reactivity method (Sinha et al., 2008). The average NO concentration during the measurement period was 0.2 ppb, and ranged from below detection limit (<0.8 ppb) to 1.6 ppb except for two sharp peaks of circa 16 ppb at 07:50 local time and 23:30 local time on 16 May 2013. On both these occasions, the PTR-MS was not in the ambient OH reactivity mode (C3 stage), so no corrections were necessary for the OH reactivity measurements.

4.2.5 Safety Consideration

It should be noted that UV radiation (e.g. 184.9 nm) is used for generation of OH radicals inside the glass reactor. So UV protection goggles should be used during the

measurements. Apart from this, a pressure build-up in the glass reactor can cause accident. As a safety feature, the Teflon T-connector mentioned previously in the section 4.2.3 (through which zero air from GCU is introduced) prevents build-up of pressure inside the reactor, in case one or more of the other flows fail. Still it is advisable to monitor the output flow through the open end of this Teflon T-connector regularly at different stages of measurement. This also helps in checking the constancy of the total flow through the glass reactor.

4.3 Results and Discussion

4.3.1 Laboratory tests using propane standards of known OH reactivity

To assess the accuracy of the OH reactivity measurements using our system, tests were performed using a propane gas standard (Sigma gases, New Delhi., 32.0 ppm in nitrogen; stated uncertainty 5 %). The results of the tests are summarized in Figure 4.4, which shows the total measured OH reactivity (vertical axis) against the introduced OH reactivity due to the standards (horizontal axis). The method shows excellent linearity ($r^2 = 0.99$) and good accountability (slope = 0.97) over the full range of introduced OH reactivities (12 s^{-1} - 69 s^{-1}). It should be noted that a reactivity of 69 s^{-1} inside the reactor is equivalent to an ambient OH reactivity of 110 s^{-1}, considering the dilution factor of 1.6 in the CRM reactor. The propane standard was dynamically diluted with zero air to generate propane concentrations of 0.4 ppm, 0.7 ppm, 0.9 ppm, 1.4 ppm, 1.8 ppm and 2.3 ppm corresponding to introduced OH reactivities (Atkinson et al., 2006) of 12 s^{-1}, 21 s^{-1}, 27 s^{-1}, 42 s^{-1} and 69 s^{-1} respectively inside the reactor. The total uncertainty in the measured OH reactivity was $\sim$ 18 % which is represented by the vertical error bars in Figure 4.4 of the supplementary information. This was derived as the root mean square propagation of the following: i) uncertainty in the pyrrole standard (10 %); ii) uncertainty in the pyrrole + OH rate constant (13 %); iii) flow fluctuation due to five mass flow controllers (2 % each due to mass flow controllers for nitrogen, propane, pyrrole, zero air from GCU and reactor exhaust pump) and iv) 6 % due to instrumental precision error. The horizontal error bars represent the overall uncertainty in the reactivity of the introduced standard derived as the root mean square propagation of i) the uncertainty in the propane standard's concentration (5 %), ii) uncertainty in propane + OH reaction rate constant (18 %) and iii) flow fluctuations due to the mass flow controllers (2 % each due to mass flow controllers corresponding to nitrogen, propane, pyrrole, zero air from GCU and reactor exhaust pump).

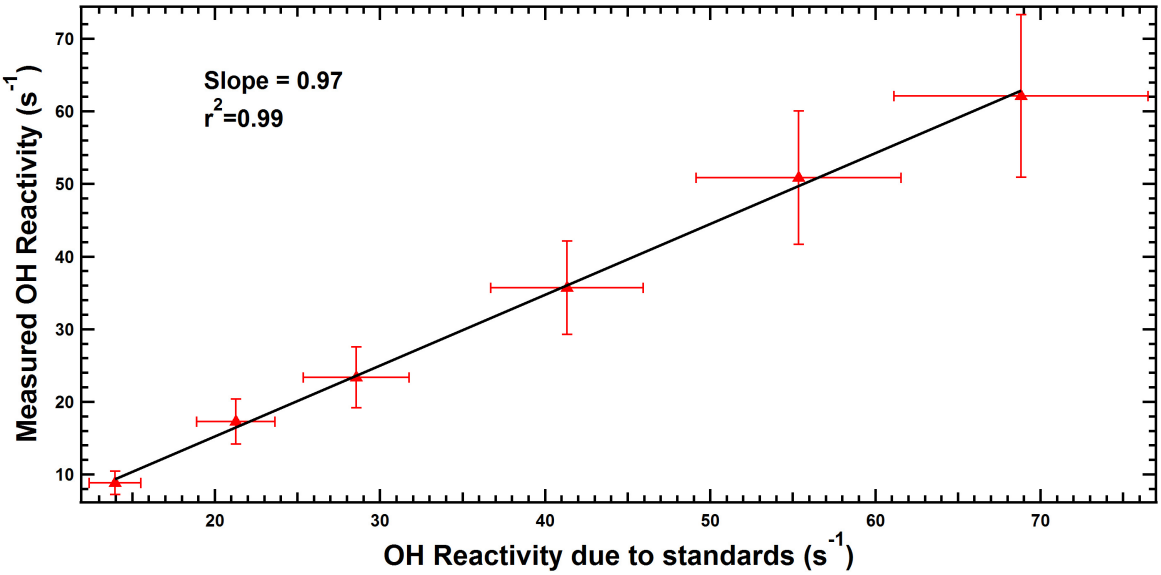

Figure 4.4: Accuracy of total OH reactivity measurements tested using propane standards of known reactivity.

4.3.2 Optimization of switching time between VOC and OHM modes using the real time data

Figure 4.5 shows the real time measured data (11 seconds time resolution) for pyrrole (red crosses and lines) on the left vertical axis and benzene (black crosses) on the right vertical axis for more than 3 hours (3 complete cycles) of measurement. I have plotted both pyrrole (tracer for OH reactivity mode) and benzene (a tracer for the ambient VOC mode) to assess how well the system worked for both modes. The regions shaded in grey in Figure 4.5 mark the periods when the system was in ambient VOC measurement mode while the regions shaded yellow and white mark the periods for C3 and C2 stages, respectively during the OHM mode. Also shown are the interpolated C2 values (as green lines in Figure 4.5 which are required for deriving the ambient OH reactivity using equation 4.2 (as discussed in Section 4.2.2). It can be seen that during the C2 stages (prior and subsequent to the C3 stage), the pyrrole concentration do not change and remain close to $\sim$ 44 ppb (1 σ < 0.9 ppb). Also note that the pyrrole concentration in the ambient VOC mode (regions shaded grey in Figure 4.5) were close to zero (below the detection limit), as pyrrole is not normally present in ambient air. The measured mixing ratios for pyrrole and benzene during the different modes and stages in Figure 4.5 confirm that the system worked well as the chemical data reflects the sampling changes. Thus, benzene mixing ratios were always highest during the ambient VOC mode, followed by the C3 stage and finally lowest (close to detection limit) in the C2 stage when zero air was sampled. On the other hand pyrrole was always highest in the C3 stage, followed by the C2 stage and

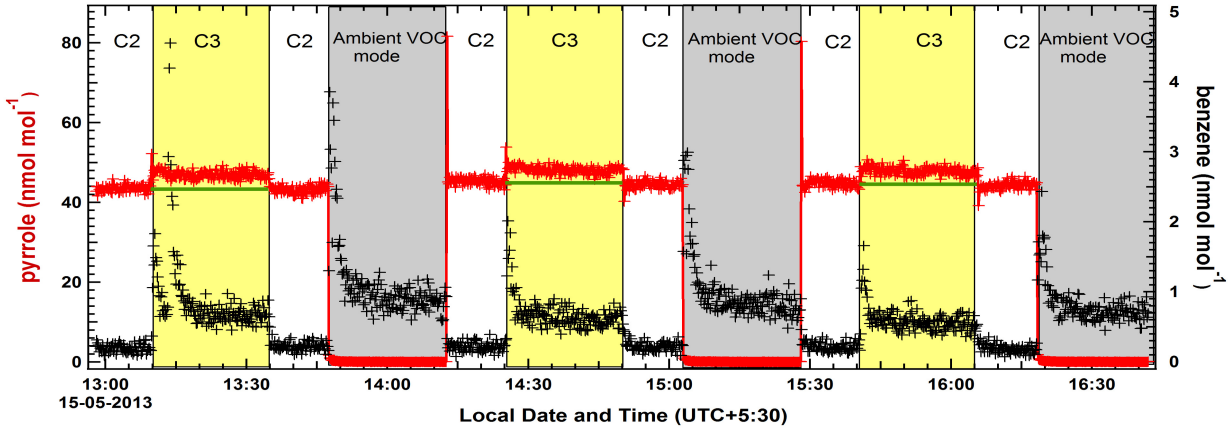

Figure 4.5: Example plot showing mixing ratio of pyrrole (red) and benzene (black) in different stages of measurement (OHM and VOC modes).

lowest (below detection limit) in the ambient VOC mode. Nonetheless while switching between the ambient VOC and OH reactivity modes as well as between different stages of the OH reactivity mode (e.g. C2 to C3 or C3 to C2), spikes occurred in the first few measurements after switching. The spikes arise from the combined effects of transient pressure changes that propagate when the valves are switched, changes in the flow paths between different modes, and due to the dead volume of air trapped in the lines, which starts moving on activation of that particular flow line giving rise to a lag effect. Wall effects in the inlets and reactor due to large concentration differences between the ambient VOC and OH reactivity modes would also contribute to the spikes. For example, while switching between the OH reactivity mode and the ambient VOC mode the signal of pyrrole (m/z=68) changes by $\sim$ 44 ppb while the concentration of benzene changes by $\sim$ 0.7 ppb in just a few seconds. In order to determine the optimal "conditioning" time between the different stages in the system, I examined the time taken for stabilization after the change in either the modes (VOC and OHM) or the stages (C2 and C3 within OHM mode).

Figure 4.6 provides a detailed zoom of one complete sequence for the switching between ambient VOC mode and the OH reactivity mode along with the C2 and C3 stages. To examine whether the humidity in the CRM reactor remained at similar concentration during both C2 and C3 stages of the OH reactivity mode, the hydrated hydronium ion signal $(H_2O)_2H_3O^+$ m/z =55) (as blue dots in Figure 4.6) was also plotted. The hydrated hydronium ion signal is a proxy for the humidity of the air (Ammann et al., 2006) sampled into the PTR-MS. A difference in absolute humidity between stage C2 and C3 of measurement can cause artefact in the OH reactivity measurement by changing the concentration of hydroxyl radicals in the reactor (Sinha et al., 2008; Nölscher et al., 2012a).

Clearly the system works well as the absolute humidity between C2 and C3 stages are almost constant. From Figure 4.6, it can also be seen that it takes $\sim$ 216 s for signals to stabilize after a switch. While switching from C2 mode of measurements to ambient VOC mode, there were spikes in the concentration of benzene followed by an exponential decay as flows and inlet conditions stabilized to the new concentration. Fitting an exponential decay function to the decaying benzene signal (Y) against time (t) yielded a lifetime (τ) of 72 seconds as shown in Figure 4.6. The exponential function had the following form:

$$Y = Y_0 + A \cdot exp(\frac{t - t_0}{\tau}) \tag{4.4}$$

In this function the constants "Y_0" and "t_0" represent the offset and the start time of the decay, whereas the fit coefficients "A" and "τ" represent the amplitude and lifetime of the decay. For an exponential decaying curve, the initial concentration reduces by 99.95 % in 3 lifetimes (that is 3×72 s = 216 s). Note that the pattern of spikes is reproducible in each cycle and other measured VOC signals (e.g. acetone, acetaldehyde, acetonitrile etc. which are not shown in Figure 4.6) also "stabilized" to the new concentration levels. On the other hand it was found that 120 seconds were sufficient for signals to stabilize between the C2 and C3 stages of the OH reactivity measurement mode. As the concentrations changes between C2 and C3 for pyrrole are not big (few ppb instead of tens of ppb between C2 and ambient VOC mode), less time is required for stabilization to the new concentration levels by the system. Thus for the settings in our system (e.g. flow rates and sampling) it was sufficient to omit the initial 4 minutes of data after switching from the C2 mode to the ambient VOC mode and 2 minutes of data after switching between C2 and C3 stages, for analysis of ambient VOCs and OH reactivity. I would like to point out however that for a similarly designed system that uses different settings for the flows and sampling, one would have to determine the relevant "stabilization" timings, as has been done in the present study.

The system described in this work is quite flexible and can be customized depending on preferences and the ambient conditions during deployment. However each new system would have to be tested and characterized suitably. Thus in principle, it is possible to vary the time periods for each measurement stage. One can also opt for measuring more masses in the selected ion monitoring VOC mode than were measured in this work or even perform mass scans. However, this will extend the time interval between ambient OH reactivity and VOC modes, affecting the robustness of the inter-comparison between the OH reactivity calculated using the measured VOCs, and the directly measured OH reactivity. Still, if the ambient air chemical composition does not vary significantly on time scales less than the interval of switching between the OH reactivity and VOC modes,

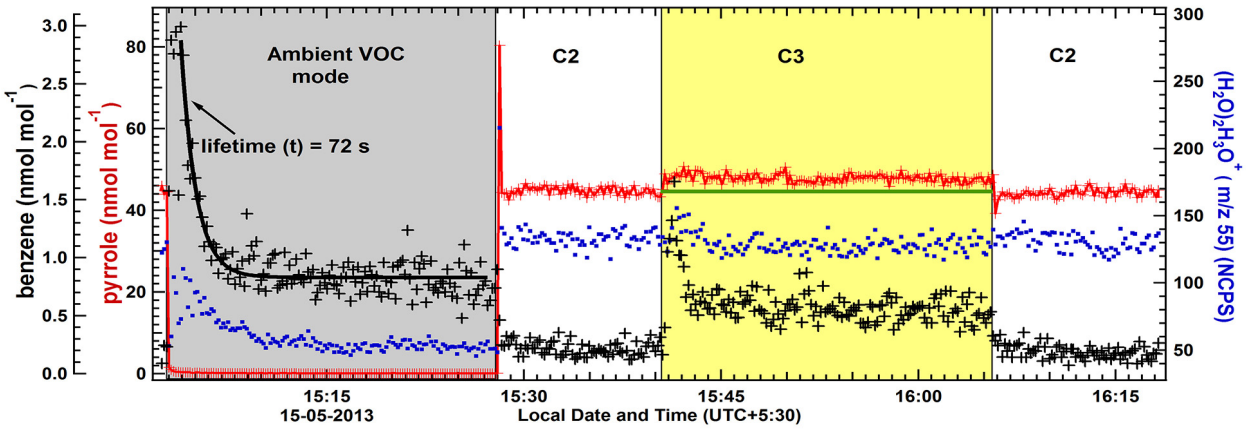

Figure 4.6: Zoom of pyrrole (red), benzene (black) and $(H_2O)_2H_3O^+$ (blue) levels during different stages of measurement for one complete cycle.

a meaningful analysis of the OH reactivity budget at the site would still be possible. Moreover if a time of flight mass analyzer is used in the PTR-MS instead of a quadrupole mass analyzer, then reduction in VOC speciation would not arise as all ions would be quantified simultaneously. A longer duration in C3 stage would imply longer time duration for ambient OH reactivity data but in case ambient humidity vary on time scales that are less than the duration of the C3 stage, the interpolation of C2 stages for the corresponding C3 stage would have reduced accuracy. The limitations of the VOC-OHM system in terms of "missing" VOC or OH reactivity mode data would be felt more acutely aboard fast moving platforms. Hence it is advisable to frame the measurement strategy depending on the primary objectives and ambient environment. Nonetheless if only a single PTR-MS can be deployed in a study, the VOC-OHM system makes it feasible to investigate the diel profiles of both VOCs and OH reactivity in a meaningful manner at the site of deployment, as the system can acquire more than 20 minutes each of ambient VOC measurements and total OH reactivity measurements every hour, at an impressive time resolution of 1 minute. This is sufficient for quantitative characterization of the diel profiles, case studies of synoptic events and establishing the impact of upwind sources on both VOC concentration and OH reactivity at the measurement site.

4.3.3 Performance of system during field deployment

In this section I present 48 hours of ambient data for both VOCs and OH reactivity acquired by deploying the VOC-OHM system at a suburban site in India influenced by both urban and agricultural emission sources. Previous measurements conducted in May 2012 at the same site yielded comprehensive information regarding diel profiles of the

reactive VOCs and major emission sources (Sinha et al., 2014). So the ambient deployment was a good test for assessing whether the VOC-OHM system could capture the typical diel and temporal trends well. Here I present the ambient measurements from 15 May 2013 - 17 May 2013. The focus here is only on the performance of the system. A full interpretation of these data together with additional data is is reported in Chapter 5.

Figure 4.7 shows the VOC data for methanol, sum of acetone and propanal, acetaldehyde (top panel), isoprene and acetonitrile (middle panel) and toluene, benzene, sum of C-8 aromatics and sum of C-9 aromatics (bottom panel) acquired using the VOC-OHM system. By plotting these compounds, the response of the system to different chemical classes (e.g. different functional groups and structure) such as oxygenated VOCs, acetonitrile, isoprene and aromatic compounds is easily ascertained. It can be seen from the data that system was able to capture the changing temporal levels of ambient VOCs through 25 minutes of measurements, in each VOC mode cycle. The measured data captured the bimodal diel profiles typical of several VOCs at the site. For example, morning and evening maxima were observed for benzene, toluene, C-8 aromatics and C-9 aromatics due to their traffic related emissions sources as well as for acetonitrile, a compound known to be emitted from biomass combustion. Mixing ratio of the measured VOCs ranged from 2.2 to 2.9 ppb for aromatic VOCs, 2.0 to 51.3 ppb for oxygenated VOCs, 1.5 ppb for acetonitrile and 2.5 ppb for isoprene. These are comparable to the range observed in the complete time series reported in May 2012 (Figure 6; Sinha et al. (2014). Peaks in methanol and isoprene both during day and night can be seen in Figure 4.7. This phenomena was already investigated and explained in Sinha et al. (2014) and attributed to industrial waste water treatment and chemical sources for methanol and both biogenic emission sources and nighttime biomass burning sources for isoprene (see Section 3.3 and 3.4 of Sinha et al. (2014)). Thus the general temporal trends in VOCs are captured well by the system which confirms that the system responds well to changing atmospheric composition.

Figure 4.8 shows the measured one minute time resolution (as grey dots) and 3 minute averaged (as black diamonds) ambient OH reactivity data on the left vertical axis. One minute (as light blue dots) and 3 minute averaged (as dark blue diamonds) total calculated OH reactivity profile due to the measured OH reactants are shown on the right vertical axis. The total calculated OH reactivity was obtained by applying equation **??** to the measured concentrations of all the VOCs listed in Table 4.1 as well as sum of that due to CO, NO_2 and SO_2. The average ($\pm$ 1 σ variability) of the total OH reactivity and the calculated OH reactivity for the period shown in this work are $\sim$ 53 ($\pm$ 17) s^{-1} and $\sim$23 ($\pm$ 8) s^{-1}, respectively. Therefore it can be noted that the 1 σ variability in both is more than 30 %. An OH reactivity level of 53 s^{-1} corresponds to an OH

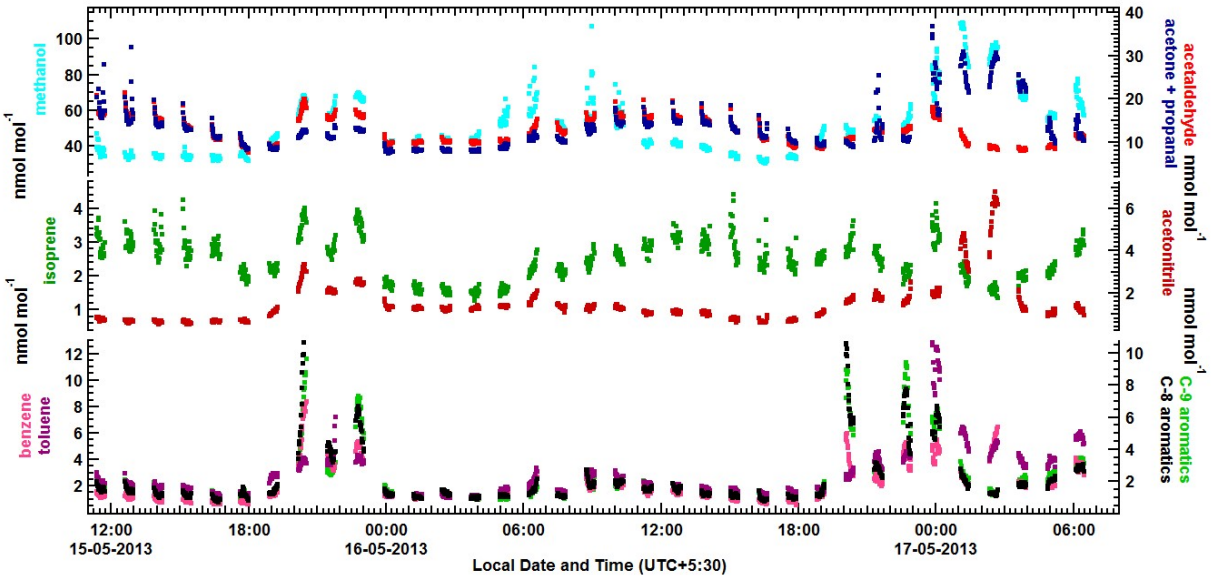

Figure 4.7: Time series of one minute data of ambient VOCs for two days measured using VOC-OHM.

life time of 19 ms. In an environment with such low OH lifetime, the OH reactivity is expected to vary significantly within time scales of few seconds. The measured total OH reactivity in Figure 4.8 clearly shows such variability in the 20 minute cycles of ambient OH reactivity measurements. Similar variability is also observed on some occasions in the 20 minute cycles of the calculated OH reactivity data (e.g. on 15 May 2013 from 20:12 - 20:33 local time and on 17 May 2013 from 05:03 - 05:15), which includes the contribution only due to the measured OH reactants. For the entire period, the measured OH reactivity is much higher than the calculated OH reactivity. This is not surprising considering that several reactive VOCs known to be present in suburban air near cities (Hewitt and Jackson, 2003) such as the reactive alkanes and 1,3 - butadiene were not measured. Also, it is reassuring that the calculated OH reactivity profile is never higher than the directly measured OH reactivity, which would have clearly signified that the direct OH reactivity measurements were inaccurate. One of the limitations of this method is that instantaneous measurements of the total and calculated OH reactivity cannot be compared, but for obtaining a diel profile, this method works quite well. The general temporal trends in the measured and calculated OH reactivities are similar confirming that the system responded well to changing ambient VOC and OH reactivity levels. To illustrate this even more clearly, I have also plotted the time series of the OH reactivity calculated using measured concentrations of CO, SO_2 and NO_2 (which did not have data gaps) in Figure 4.8 (green dots on right vertical axis). The green dots can be used as indicators of the changing chemical composition of air masses during periods when VOC

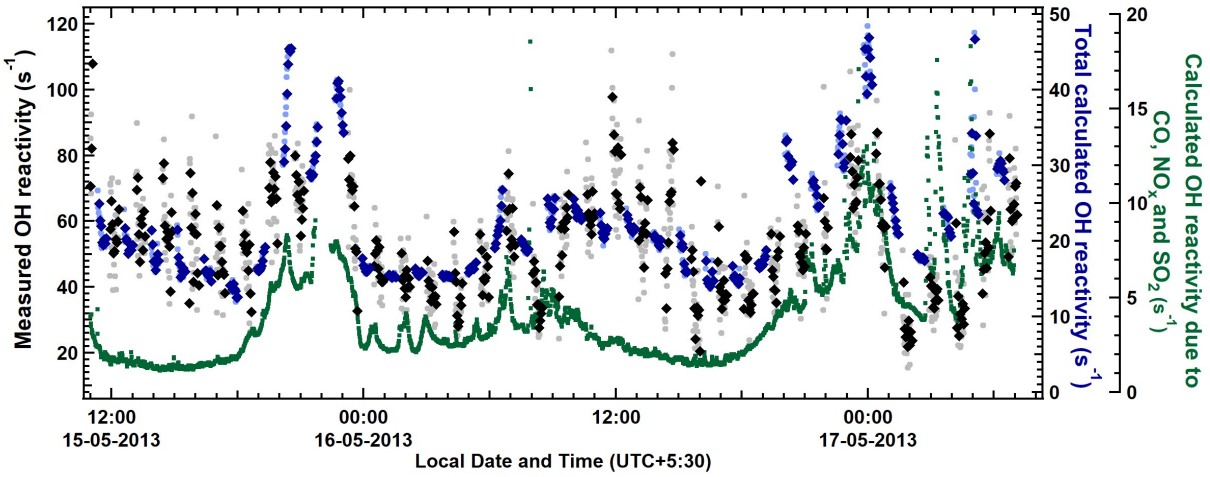

Figure 4.8: Time series of one minute data of total OH reactivity (grey dots) and calculated OH reactivity (light blue dots) for two days measured using VOC-OHM. The diamonds show 3 minute average total OH reactivity and the deep blue diamonds show 3 minute average calculated OH reactivity. The green dots show the continuous calculated OH reactivity only due to CO, NO_x and SO_2.

data was unavailable. General trends in the directly measured total OH reactivity (OHM mode) and the calculated OH reactivity due to CO, SO_2 and NO_2, are quite consistent in reflecting the changing chemical composition over the two day period. Thus, the objectives of deploying the VOC-OHM system on a single PTR-MS for yielding meaningful data on both VOCs and OH reactivity and inter comparing the trends in both have been met.

4.3.4 Novelty of the method in elucidating identity of reactive compounds contributing to the same nominal m/z channel in PTR-MS

The levels of the VOCs in the ambient VOC measurement mode and in C3 stage of measurement can be used for cross verification of identity of a VOC by estimating its rate constant of reaction with OH radical for the times when there is very little variability in levels of ambient VOCs. This is of particular significance for the nominal m/z channels where more than one compounds can be detected. For example protonated ions of both isoprene and furan have m/z 69. As at our measurement location, ambient levels of VOCs have minimum variability in the afternoon period (Sinha et al., 2014), I have estimated the rate constant of reaction of detected species at m/z 69 with OH radical using the following formula (Kato et al., 2011).

$$k_{OH+X} = \frac{ln(X_0/X_{C3})}{ln(C1/C3)} \cdot k_p \tag{4.5}$$

where $k_{(OH+X)}$ is rate constant of reaction of any species "X" with OH radicals, X_0 and X_{C3} are the ambient concentration and concentration in the stage C3 of the measurement respectively and k_p is the rate constant for the reaction of pyrrole with the hydroxyl radical. The concentration of the species measured during C2 stage (X_{C2}) provides the background and hence needs to be subtracted from both X_0 and X_{C3}. Since the ambient air entering into the reactor is diluted by a factor of 1.6 in our setup, $(X_0 - X_{C2})$ should be divided by this factor before using equation 4.5. After applying these corrections, equation 4.5 is modified as

$$k_{OH+X} = \frac{ln(X'_0/X'_{C3})}{ln(C1/C3)} \cdot k_p \tag{4.6}$$

where $X'_0 = (X_0 - X_{C2})/1.6$ and $X'_{C3} = X_{C3}$ - X_{C2}. Using the data from the time period shown in Figure 4.6 (15:05 L.T – 16:05 L.T. on 15 May 2013) the rate constant for reaction of compound detected at m/z 69 with OH radical estimated with this method is 1.18×10^{-10} $cm^3\,molecule^{-1}\,s^{-1}$. The reported values of rate constant of reaction of isoprene and furan with OH radicals are 1.01×10^{-10} $cm^3\,molecule^{-1}\,s^{-1}$ (Atkinson and Arey, 2003) and 4.01×10^{-11} $cm^3\,molecule^{-1}\,s^{-1}$ (Atkinson et al., 1983) respectively. This confirms that at our location, isoprene is the main contributor at m/z 69 and it is not furan, which was also emphasized by Sinha et al. (2014). Using this method I have also calculated the rate constant for reaction of benzene (m/z 79) and 1,2,4-trimethylbenzene (m/z 121) which were 8.46×10^{-12} $cm^3\,molecule^{-1}\,s^{-1}$ and 6.90×10^{-11} $cm^3\,molecule^{-1}\,s^{-1}$. It can be observed that, for a more reactive species more accurate rate constant can be obtained whereas for a less reactive species correct order of magnitude for the rate constant is achievable. This is because for a more reactive compound, the difference (X_{C3} - X_{C2}) can be quantified more accurately as compared to a less reactive compound. This method cannot be used verification of rate constant of oxygenated VOCs, because they can be formed inside the reactor as a result of photo-oxidation of other species.

4.4 Conclusion

A new technique called VOC-OHM that enables rapid sequential measurements of ambient VOCs and total OH reactivity has been developed, validated and tested in the field with promising results. Whereas VOC-OHM is not a complete replacement for studies in which two PTR-MS systems can be deployed, as simultaneous measurements of both VOCs and OH reactivity are not possible with the system, its ability to measure both parameters with a gap of only few minutes ($\sim$ 13 minutes in this work) does open up new possibilities. VOC-OHM adds specificity to the PTR-MS equipped with a quadrupole mass analyser to distinguish the isobaric compounds by enabling direct measurement of

their rate constants for reaction with OH radicals. There are several research groups and institutes in the world which possess only a single PTR-MS. This work provides a promising analytical technique to use the single PTR-MS for both total OH reactivity and ambient VOC measurements, and maximize the scientific outcome using available resources. This work also demonstrates a better and safer substitute for pressurized zero air bottles in the form of the gas calibration unit (GCU-A) which can be deploying for CRM OH reactivity field measurements. This system is a promising option for ground based air pollution and atmospheric chemistry studies, enabling instantaneous ozone production regimes (Sinha et al., 2012) and VOC speciation to be determined for policy makers. In addition to air pollution and atmospheric chemistry studies, the VOC-OHM system can also be applied for VOC headspace sampling studies in the food and flavour industry (Biasioli et al., 2011; Boscaini et al., 2004) and in chamber studies. Similar to ambient atmospheric chemistry field studies, by comparing the calculated OH reactivity due to the measured VOCs and the directly measured total OH reactivity in the headspace or chamber air, it would be possible to test whether the full suite of compounds present in the headspace or the chamber has been quantified or a sizeable fraction of compounds remain unmeasured.

Chapter 5

Large missing OH reactivity fueled by agricultural fires

Abstract

Biomass fires impact global atmospheric chemistry. The reactive compounds emitted and formed due to biomass fires drive ozone and organic aerosol formation, affecting both air quality and climate. A fundamental question that is still poorly understood concerns the extra reactivity that emissions from fires introduce directly and indirectly (through secondary processes) into ambient atmospheric environments, and whether all important chemical constituents involved in this process have been identified and incorporated in models. Direct hydroxyl (OH) reactivity measurements quantify total gaseous reactive pollutant loadings and comparison with measured compounds yields the fraction of unmeasured compounds. Here, I quantified the magnitude and composition of total OH reactivity in the north-west Indo-Gangetic Plain. More than 120 % increase occurred in total OH reactivity 28 s^{-1} to 64 s^{-1} and from no missing OH reactivity in the normal summertime air, the missing OH reactivity fraction increased to $\sim$ 40 % in the post-harvest summertime period influenced by large scale biomass fires highlighting presence of unmeasured compounds. Increased missing OH reactivity between the two summertime periods was associated with increased concentrations of compounds with strong photochemical source such as acetaldehyde, acetone, hydroxyacetone, nitromethane, amides, isocyanic acid and primary emissions of acetonitrile and aromatic compounds. Currently even the most detailed state-of-the-art atmospheric chemistry models exclude formamide, acetamide, nitromethane and isocyanic acid and their highly reactive precursor alkylamines (e.g. methylamine, ethylamine, dimethylamine, trimethylamine). As OH chemistry governs the removal rate of climate active gases and formation of ozone and aerosol, these findings have major implications for understanding and predicting tropospheric chemistry

and air quality-climate feedbacks in fire-impacted atmospheric environments.

5.1 Introduction

Biomass burning is a widespread practice globally (Crutzen and Andreae, 1990), which causes soil nutrient loss and impacts atmospheric chemistry, air quality and climate (Andreae et al., 2004; Yevich and Logan, 2003). Among all forms of biomass burning, agricultural waste burning is completely anthropogenic and its adverse environmental effects are exacerbated due to the short time period (few weeks) and large area, over which the activity occurs. More than 3700 Tg of agricultural residue is produced every year globally (Lal, 2005), of which 10 - 25 % is burnt over a range of spatial and temporal scales (Crutzen and Andreae, 1990) injecting several hundred teragrams of reactive pollutants into the atmosphere (Andreae et al., 2004; Yevich and Logan, 2003). Out of the 347 Tg of crop residue produced pan India in 1985, 23 % was estimated to undergo open burning in the fields adding 35 Tg of carbon in the atmosphere (Yevich and Logan, 2003). In the agriculturally productive region of north western Indo-Gangetic Plain alone, more than 67.7 Tg of crop residue is estimated to be burnt over 9593 km^2 cropland annually (Venkataraman et al., 2006). Chemical speciation studies of emissions of greenhouse gases and criteria air pollutants including carbon monoxide, nitrogen oxides, volatile organic compounds (VOCs) and aerosol particles have been investigated previously through chamber studies and in ambient plumes, revealing a large diversity of compounds in terms of their reactivity, health effects and secondary pollution potential (Stockwell et al., 2015; Andreae et al., 2004). Till date, the community tools have been limited to two types of methods for such investigations, namely, 1) controlled laboratory combustion of different types of bio-fuels for speciation of the compounds emitted from such fires and 2) ambient field studies that in addition to quantifying known major emissions from the fires also measure and model formation of known secondary pollutants such as ozone and secondary aerosol through analyses of intercepted ambient fire plumes. Obviously, the limitations of these approaches, is that they cannot reveal information on the contribution of unmeasured/unknown compounds as there is no direct measure of the total reactivity. Controlled combustion of various biomass fuels under laboratory conditions have revealed emissions of > 500 different volatile organic compounds (VOCs) (Stockwell et al., 2015; Gilman et al., 2015; Hatch et al., 2017) differing in their reactivity, health effects and secondary pollution potential (Ortega et al., 2013). Grab sampling experiments which involve collection of ambient smoke plumes directly from the fires in the agricultural fields in pressurized glass flasks/stainless steel canisters followed by subsequent analysis in the laboratory, further allow comparison of laboratory and field determined emission ratios

and emission factors for specific kind of biomass fuels (Chandra et al., 2017). Considerable uncertainty still remains concerning the identity and photochemical transformations of these emissions in ambient atmospheric environments.

The removal of pollutants from the atmosphere depends primarily on their reactivity with hydroxyl radicals (OH) (Levy, 1971; Hofzumahaus et al., 2009; Lelieveld et al., 2004). Thus, the presence of additional/unmeasured compounds that can deplete hydroxyl radicals, also has implications for the chemical lifetime of greenhouse gases such as methane, for which the main removal pathway is reaction with hydroxyl radicals (Lelieveld et al., 2004). Moreover, gas to particle conversion of reactive gases can influence the growth and properties of cloud condensation nuclei, thereby potentially affecting even the hydrological cycle1 (Rosenfeld et al., 2008). Direct measurement of the total gas phase OH reactivity (mentioned as OH reactivity henceforth) provides a measure of the total gaseous reactive pollutant burden (Sinha et al., 2009) and fraction of unmeasured reactive VOCs in an atmospheric environment by comparison with the calculated OH reactivity due to the measured OH reactants (Di Carlo et al., 2004).

This is analytically a very challenging measurement as there can be thousands of OH reactants in most atmospheric environments. A comparison of directly measured total OH reactivity with the calculated OH reactivity due to the measured OH reactants provides a measure of the fraction of unmeasured reactive VOCs in an atmospheric environment (Di Carlo et al., 2004). While previous OH reactivity measurements in forested, urban and suburban sites have improved understanding of emissions in these environments (Yang et al., 2016; Di Carlo et al., 2004; Hofzumahaus et al., 2009; Whalley et al., 2016), no such investigation of the effects of open agricultural fires using direct OH reactivity measurements in ambient environments exist. Considering the dual effect of fire emissions on production and loss of hydroxyl radicals, their impact on tropospheric oxidation chemistry is still not well understood.

Here, I investigated the impact of agricultural fires by measuring a suite of OH reactants and direct total OH reactivity at IISER Mohali atmospheric chemistry facility (30.667 °N, 76.729 °E ; 310 m a.s.l), a regionally representative suburban site located downwind of agricultural fields in the north-west IGP during the summertime pre-harvest non crop-residue fire influenced (NCFI) and post-harvest crop-residue fire influenced (CFI) periods from March – May 2013. Detailed analyses of the composition and fraction of missing OH reactivity was undertaken for both periods using a state of the art chemical box model. Further grab sampling and analyses of the chemical emissions from an agricultural biomass fire at the source were also employed for interpretation of the results.

5.2 Materials and methods

5.2.1 Site description, fetch region, meteorology and criteria for classification of Non Crop-residue Fire Influenced (NCFI) and Crop-residue Fire Influenced (CFI) periods

The ambient VOC and trace gas measurements reported here were conducted from 28 February 2013 till 31 May 2013 at the IISER Mohali atmospheric chemistry facility (30.667 °N, 76.729 °E ; 310 m a.s.l), a regionally representative suburban site located in the north-west Indo-Gangetic Plain (N.W. IGP), which has been described in detail in previous works (Sinha et al., 2014; Pawar et al., 2015). The three-month long period in 2013 captured the summertime pre-harvest and post-harvest conditions in the N.W. IGP. The year 2013 was not anomalous in terms of emissions and meteorological conditions compared to other years as demonstrated through analyses of multi-year chemical and meteorological data from the site in Chapter 2. Direct OH reactivity measurements were performed during two measurement intensives: from 10 April 2013 till 21 April 2013 to quantify the pre-harvest summertime OH reactivity and from 11 May 2013 till 17 May 2013 to quantify the post-harvest summertime OH reactivity.

The most prevalent wind direction at the site was from the north-west, where the land use is primarily agricultural and rural in nature (Sinha et al., 2014) and wheat crop is grown extensively ($\sim$ 3.5 million hectares in the state of Punjab) (Bahuguna, 2015). The black circle in Figure 5.1 shows the location of the site. The N.W. IGP is influenced by the crop residue fires in May, a practice that gained popularity with the introduction of mechanized combine harvesters in 1986. Satellite fire counts data over the region detected by the Moderate Resolution Imaging Spectroradiometer (MODIS) (Davies et al., 2009) installed on two sun-synchronous polar orbiting satellites called Aqua and Terra are shown as red dots in Figure 5.1. In the spatial extent of fires observed by the MODIS satellite, large scale fires are only observed in the states of Punjab and Haryana which majorly consist of irrigated croplands. Significant fires are not observed in the states of Jammu & Kashmir, Himachal Pradesh and Uttarakhand which comprises of forested regions (Pawar et al., 2015), so the occurrence of large scale forest fires during our study period is highly unlikely. As no major highway or industry was reported to have been commissioned in the fetch region upwind of our measurement site during the study period, it is also highly unlikely that the traffic related emission sources changed considerably between pre-harvest and post-harvest summertime periods. The start and end periods of post harvest wheat residue fires could be ascertained from the daily satellite fire counts data (shown in inset of Figure 5.1) and were found to be consistent with enhancements in chemical tracers of

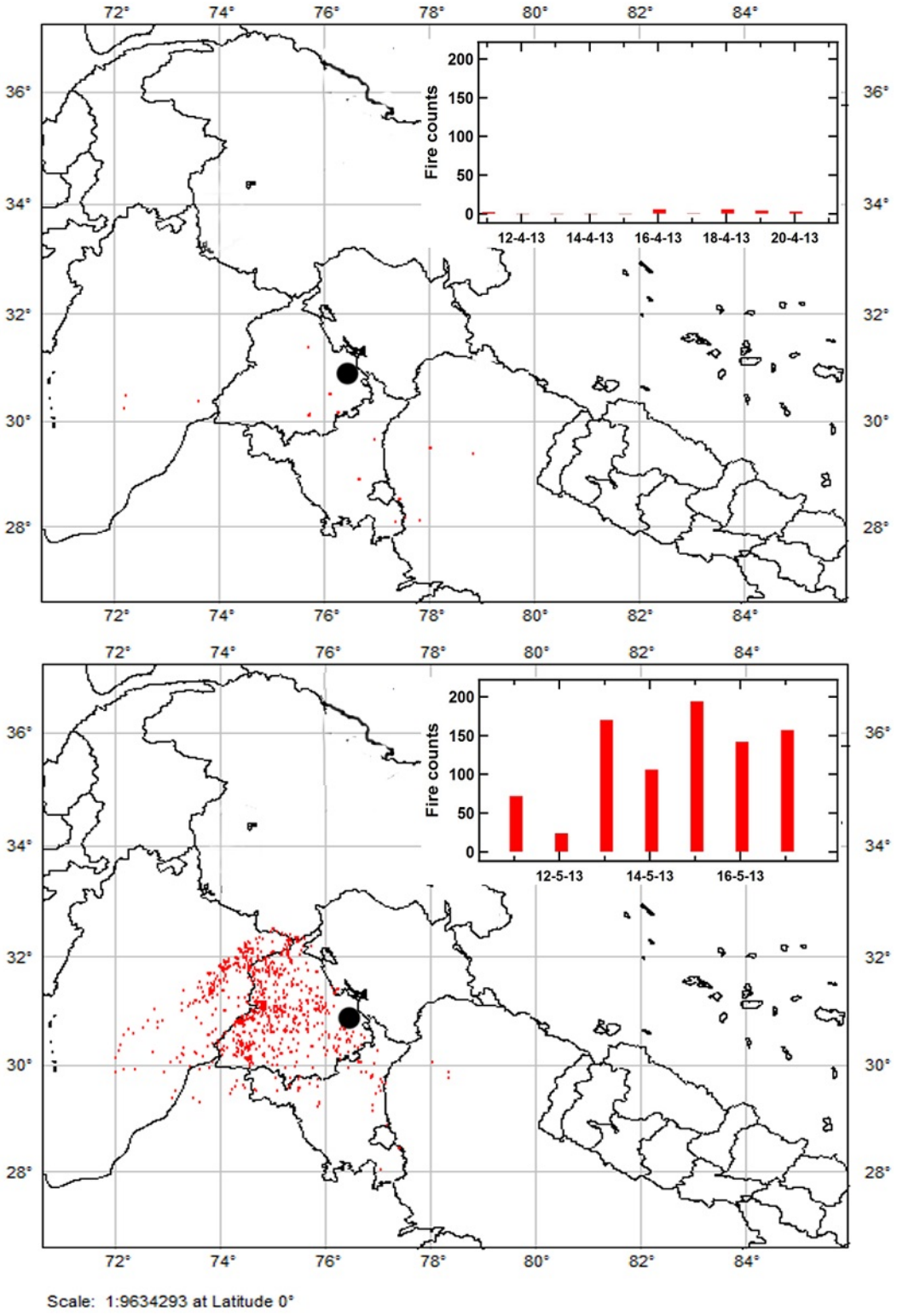

Figure 5.1: Temporal and spatial extent of fire counts detected (at $\geq$ 80 % confidence interval) during NCFI (10 April 2013 to 21 April 2013) and CFI periods (11 May 2013 to 17 May 2013) as detected using the MODIS satellite over the north-west Indo-Gangetic Plain. Black circle shows the location of the measurement site (30.667 °N, 76.729 °E ; 310 m a.s.l).

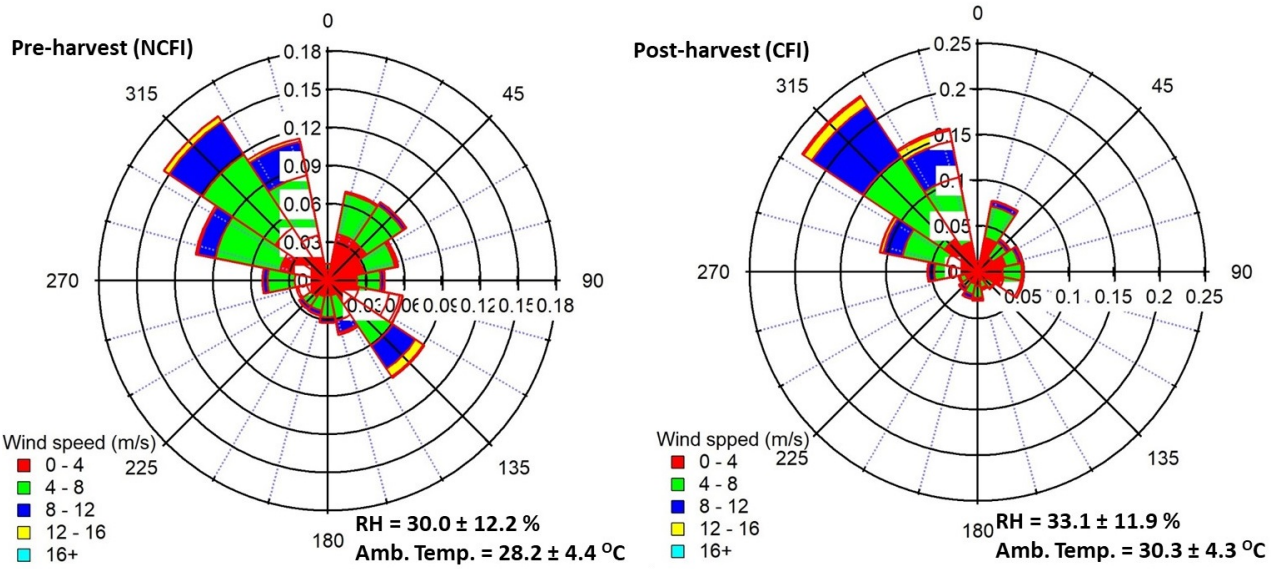

Figure 5.2: Wind rose plots showing the fractional contribution of different sectors from which airmasses arrived during the pre-harvest NCFI and post-harvest CFI periods.

biomass fires such as acetonitrile (see Table 5.2 and Figure 5.8) (Kumar et al., 2016).

Figure 5.2 shows the wind roses indicating the fetch region for the pre-harvest and post-harvest periods reported in this work along-with the temperature and relative humidity values (average ± 1 σ ambient variability). The most frequent fetch regions, temperature and relative humidity were similar for both periods. Clear sky condition was observed during both pre and post-harvest measurement periods except the period from 11 May 2013 (afternoon) till 12 May 2013 (noontime) when cloudy conditions and 16 mm of rainfall occurred. This can also be observed in the solar radiation data shown in Figure 5.5. To ensure that the only significant difference in terms of emissions is due to crop residue fires and meteorological conditions do not drive the differences between the two measurement periods, the periods with overcast condition and rainfall (shown as blue shaded region in Figure 5.5) were excluded from further analyses. Henceforth, we refer to the period from 10 April 2013 to 21 April 2013 as the pre-harvest Non Crop-residue Fire Influenced period (NCFI) and the period from 11 May 2013 to 17 May 2013 (except 11 May 2013 15:30 to 13 May 2013 11:30 local time) as the post-harvest Crop-residue Fire Influenced period (CFI). These two periods were representative of the extended pre-harvest and post-harvest summertime conditions when the crop residue fires were absent (extended NCFI period: 28 February 2013 to 30 April 2013) and when post-harvest crop residue fires occurred (extended CFI period: 01 May 2013 to 31 May 2013), respectively. This is supported by the similarity in the diel concentration profiles derived from measurements performed during the intensives (Figure 5.3) and profiles of the same

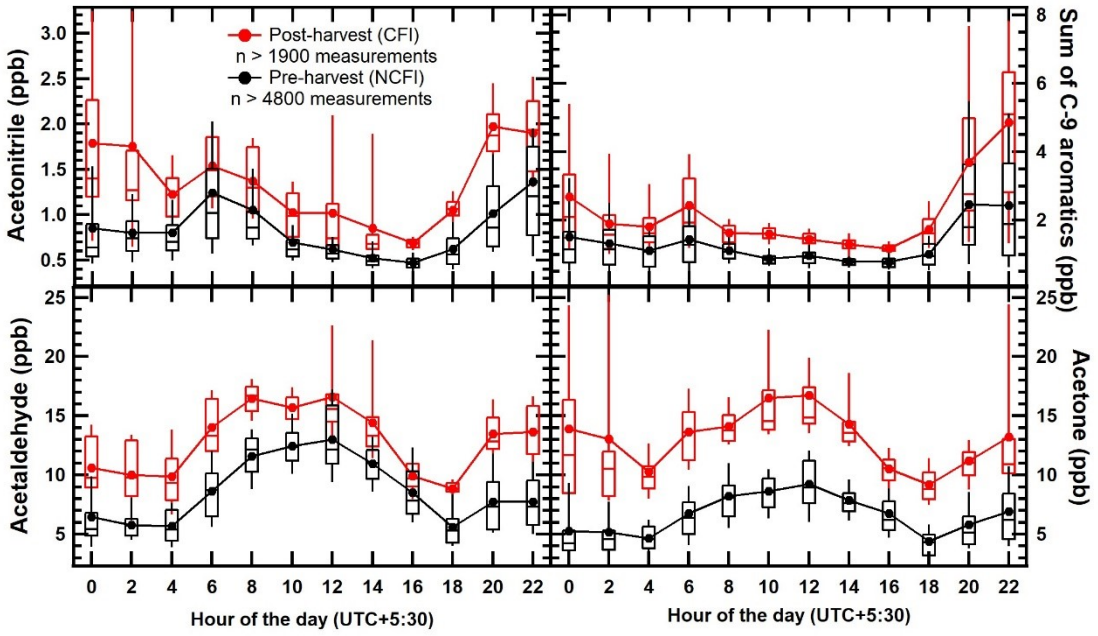

Figure 5.3: Diel box and whisker plots of measured concentrations (in ppb) of acetonitrile, sum of C-9 aromatics, acetaldehyde and acetone in the pre-harvest (NCFI) and post-harvest (CFI) period of summer 2013. The box represents inter-quartile range (25^{th} - 75^{th} percentile) whereas the whiskers represent 10^{th} and 90^{th} percentiles. Average and median are shown as solid circle and dashed line, respectively.

compounds, namely acetonitrile, sum of C-9 aromatics, acetaldehyde and acetone, for extended NCFI and extended CFI periods (Figure 5.8).

5.2.1.1 Sampling details

All the instrument inlets were co-located at $\sim$ 20 m above ground (Sinha et al., 2014). The inlets were made from Teflon tubing of inner diameter 3.18 mm and protected from dust using inline Teflon particle filters, which were changed every seven days. The facility is positioned on the rooftop and the short inlets resulted in inlet residence times $<$ 8 s. The PTR-MS instrument was housed in a separate room on the first floor and had a longer Teflon inlet line (12 m) with combined inlet residence and sampling time of $\sim$ 135 s.

5.2.2 Measurements of ambient total OH Reactivity and Volatile Organic Compounds using a Proton Transfer Reaction Mass Spectrometer

Ambient total OH reactivity and VOCs were measured using the VOC-OHM (Volatile Organic Compounds – OH reactivity Measurement) system described and characterized in detail in Chapter 4. This technique enables rapid sequential measurements of both ambient VOC concentrations and total OH reactivity at a temporal resolution of 1 minute. The VOC and OH reactivity measurement modes are alternated every $\sim$ 13 minutes using the same proton transfer reaction mass spectrometer (PTR-MS). The schematic and flow layout for sequential measurements of VOCs and OH reactivity can be found in Figure 4.3 of Chapter 4. Details pertaining to VOC measurements using the PTR-MS technique can be found in several comprehensive reviews (Hofzumahaus et al., 2009; Lindinger et al., 1998; Blake et al., 2009; de Gouw and Warneke, 2007; Chandra and Sinha, 2016; Sinha et al., 2014) and details of the OH reactivity technique can be found in previous works (Sinha et al., 2008; Hansen et al., 2015). Hence these are described briefly herein.

VOC measurements using PTR-MS are based on the principle of "soft" chemical ionization mass spectrometry in which hydronium ions H_3O^+ act as the primary reagent ions within the instrument. VOCs having a proton affinity greater than that of pure water (165.2 kcal mol^{-1}) can typically be detected at a nominal mass to charge ratio (m/z) equal to their molecular weight + 1, generally without fragmentation for small organic ions. The specific PTR-MS instrument used in this work has already been characterized in detail in previous works from our group (Sinha et al., 2014; Chandra and Sinha, 2016). The instrument was operated at a drift-tube voltage of 600 V, pressure of 2.2 mbar and temperature of 333 K corresponding to E/N ratio of $\sim$ 135 Townsend. The primary ion was greater than 7.5×10^6 (counts per second) and the impurity ions e.g. NO^+ and $O_2{}^+$ were less than 0.3 % and 3.9 % respectively of the primary ion. The dwell time at m/z channels corresponding to the individual VOCs was 1 s. The measured counts per second (cps) at each m/z channel was normalized to a total primary ion count of 1.0×10^6 cps as the sum of the primary (H_3O^+) and the first water cluster ions ($(H_2O)H_3O^+$), drift tube pressure of 2 mbar and drift tube temperature of 298 K. Dynamic dilution of VOC gas standards (Apel-Riemer Environmental, Inc., Colorado, USA) containing a mixture of 12 VOCs at $\sim$ 500 ppb was used to experimentally obtain the sensitivity in normalized cps per ppb, for methanol, acetonitrile, acetaldehyde, acetone, isoprene, methyl vinyl ketone (MVK), methyl ethyl ketone (MEK), benzene, toluene, p-xylene, 1,2,4-trimethylbenzene and alpha-pinene (Sinha et al., 2014). For other compounds reported in this work, the sensitivities were determined theoretically as discussed in Chapter 3 (equation 3.3).

I found that the differences between the sensitivity factors derived using calibration experiments and theoretically derived sensitivity factors for the compounds were within 30 % of each other. This is consistent with the predicted accuracy of PTR-MS measurements as proton transfer reactions typically occur at the collisional-limit and without specific calibration standards, the accuracy is better than 40 % (Karl et al., 2010). The detection limit of PTR-MS was typically less than 100 ppt (Kumar and Sinha, 2014). The measurement uncertainty was less than 16 % for all VOCs where experimentally determined sensitivities were obtained through calibrations. Assignment of m/z ratios (Tables 5.2 and 5.3) to specific compounds was done after careful consideration of the known fragmentation issues at certain m/z, potential isobaric interferences (discussion in section 5.2.2.1), ambient profiles, and changes in instrumental background.

OH reactivity measurements by VOC-OHM technique are based on the comparative reactivity method (Sinha et al., 2008). An initial concentration (C1) of a reagent molecule (pyrrole, C_4H_5N) is allowed to react with zero air and ambient air respectively in different steps in the presence of synthetically generated OH radicals inside the glass reactor. In the step where only pyrrole, nitrogen and zero air enter the reactor, pyrrole completely titrates OH radicals generated inside the reactor, and its concentration is C2 in this stage. The difference in pyrrole concentration between stage C1 and C2 yields the net available OH radical concentration inside the reactor. When the incoming flow of zero air inside the reactor is replaced by an equivalent flow of ambient air, there is a competition between compounds present in the ambient air and pyrrole for reaction with the net available OH radicals. The pyrrole concentration in this stage (termed C3) is higher than that in the previous stage (C2). Solving for competitive kinetics inside the glass reactor yields the total OH reactivity of the ambient air (R_{air}) which is only dependent on the measured pyrrole concentrations in different steps of the experiment and the rate constant for the reaction of pyrrole with OH radicals (k_p).

$$R_{air} = \frac{C3 - C2}{C1 - C3} \cdot k_p C1 \tag{5.1}$$

The measurement in the C3 stage is preceded and followed by C2 measurement. Hence for estimation of total OH reactivity using equation 5.1, interpolation of the C2 measurements performed before and after the C3 are necessary. In the C3 stage, $\sim$ 170 sccm of ambient air was sucked into the reactor which was diluted by the total flow through the CRM reactor ($\sim$ 275 sccm). Hence the OH reactivity obtained using equation 5.1 was multiplied by the dilution factor ($\sim$ 1.6) to quantify the total OH reactivity of ambient air. Since the total OH reactivity is determined for pseudo first order conditions, a correction factor is applied for slight deviations. This correction factor is calculated

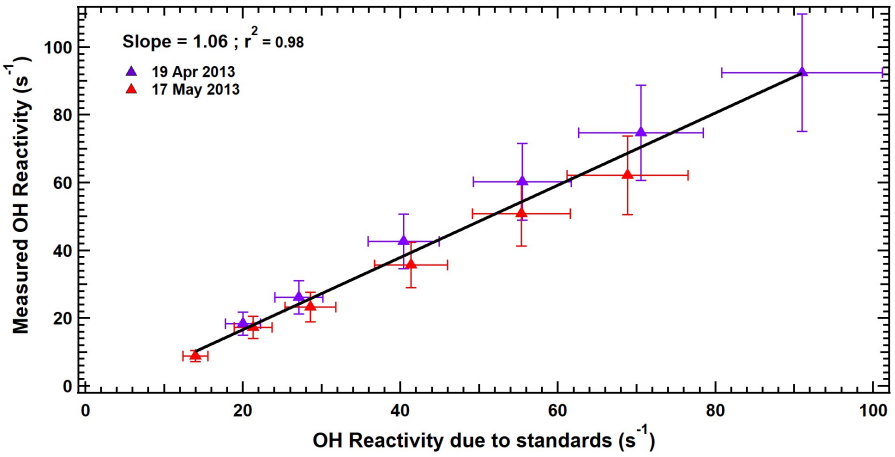

Figure 5.4: Accuracy of total OH reactivity measurements tested using propane standards of known reactivity during the NCFI and CFI measurement periods. The horizontal error bars represent the uncertainty in the OH reactivity due to the introduced standards (11.2 %) and the vertical error bars represent the total uncertainty (18.8 %) of the measured OH reactivity.

numerically (Curtis and Sweetenham, 1988) by allowing different concentrations of an OH reactant (e.g. propane) to react with OH radicals at the pyrrole/OH concentration ratio used during the experiments (Kumar and Sinha, 2014; Sinha et al., 2008). During the two measurement periods reported in this study, the pyrrole/OH ratio varied between 1.8 and 2.7. The accuracy of the method was being checked using propane standards of known reactivity during both the measurement periods. Figure 5.4 shows the results, in which the measured OH reactivity (Y axis) is plotted against the introduced OH reactivity due to standards (X axis), It can be seen that there is good reproducibility, linearity ($r^2 = 0.98$) and accountability (slope = 1.06) for the introduced reactivity over the entire dynamic range for experiments performed on 19 April 2013 during the NCFI period and on 17 May 2013 during the CFI period. Note that the maximum introduced reactivity of 91 s^{-1} during these tests actually represent 146 s^{-1} under ambient condition taking into account the dilution of ambient air inside the reactor. The detection limit for the OH reactivity measurements was 4.5 s^{-1} and the total uncertainty was 18.8 % for the setup employed herein (Kumar and Sinha, 2014).

OH reactivity measurements performed using CRM method on which our VOC-OHM system is based are known to have interferences due to following two factors:

1. Humidity difference between C2 and C3 steps of measurement which results in different amount of net available OH radicals inside the reactor for reaction with pyrrole and zero air (C2 step) and pyrrole mixed with ambient air (C3 step).

2. OH recycling due to the reaction between HO_2 and NO in an environment where

ambient NO concentrations exceed 10 ppb. Use of an advance Gas Calibration Unit (GCU-A, Ionimed Analytik) for generation of zero air directly from the ambient air, matches the humidity to that of ambient air and no significant humidity difference between C2 and C3 steps were observed during our measurements using the VOC-OHM method (Kumar and Sinha, 2014). During the measurement periods reported in this work, ambient NO concentrations were generally less than 2 ppb barring seven short peaks in which concentrations reached $\sim$ 10 ppb (20 April 2013 19:37 - 19:43, 21 April 2013 14:30 - 14:35, 13 May 2013 11:48 - 14:19, 14 May 2013 13:00 - 13:55, 14 May 2013 06:00 - 07:30, 16 May 2013 07:50 - 08:00 and 16 May 2013 23:30 - 23:40 L.T.). During most of these events, the VOC-OHM system was in C2 step when ambient air was not being sampled or in the ambient VOC measurement mode. The OH reactivity data removed due to NO peaks of 10 ppb was therefore less than $\sim$ 4.5 % of the total measured OH reactivity data.

OH reactivity due to measured OH reactants was calculated as follows (Sinha et al., 2008):

$$\text{Calculated OH Reactivity} = \sum_i k_{\text{OH}+X_i}[X_i] \tag{5.2}$$

where $[X_i]$ is the measured concentration of OH reactants listed in Table 5.2 including O_3 and SO_2, and k_{OH} is the relevant rate constant for reaction of $[X_i]$ with hydroxyl radicals which were taken from Atkinson et al. (2004, 2006).

5.2.2.1 Discussion of Potential interferences in mass identification using PTR-MS and uncertainty on the major conclusions

VOC measurements using PTR-MS are based on the principle of "soft" chemical ionization mass spectrometry in which hydronium ions (H_3O^+) act as the primary reagent ions within the instrument. VOCs having a proton affinity greater than that of pure water (165.2 kcal mol $^{-1}$) can typically be detected at a nominal mass to charge ratio (m/z) equal to their molecular weight+1, generally without fragmentation for small organic ions. A PTR-MS equipped with a quadrupole mass analyzer (PTR-QMS) cannot resolve nominal isobaric ions with its unity mass resolution and hence identification of compounds based only on the m/z values can in principle result in overestimations of the true ambient concentrations of compounds. However, reviews (de Gouw and Warneke, 2007; Yuan et al., 2017) of several studies and inter-comparisons between PTR-MS and other more specific analytical techniques (e.g. gas chromatography based instruments) in diverse environments and plumes have shown that for compounds such as methanol, acetonitrile, acetaldehyde, acetone, methyl ethyl ketone, sum of C-8 aromatics, sum of C-9 aromatics

and sum of methyl vinyl ketone and methacrolein, only minor contributions from other isobaric compounds have been observed in ambient atmospheric environments. Hence one can be confident of the compound assignment for these species using PTR-QMS. The potential interferences in the mass identification of rarely measured VOCs using PTR-QMS are discussed below

- **Butane-2,3-dione**: Methacrylic acid, crotonic acid, pentanal, pent-2-one, pent-3-one can interfere with butane-2,3-dione at m/z 87, but these compounds have been reported to cause interferences only in the forested environments (Williams et al., 2001). Previous studies reporting PTR-MS measurements from suburban locations or from biomass burning plumes have attributed m/z 87 to butane-2,3-dione only (Stockwell et al., 2015; Sarkar et al., 2016).

- **Formamide and acetamide**: The signal for acetamide was corrected for 3.4 % of acetone landing at m/z 60 due to ^{13}C isotope (Ievgeniia et al., 2008). This accounted for $\sim$ 15-20 % correction in acetamide concentration in general. Similarly, the signal for formamide was corrected for the 2.5 % contribution of acetaldehyde due to ^{13}C isotope at m/z 46.

- **Hydroxyacetone**: Butanol isomers, diethyl ether and propionic acid also contribute to m/z 75 when measured with a PTR-MS, but previous studies have found hydroxyacetone to be a main contributor (Williams et al., 2001; Sarkar et al., 2016).

- **Isoprene**: With a PTR-QMS both isoprene and furan are detected at m/z 69. However, with the deployment of VOC-OHM technique in the month of May at our measurement site, we have shown that the VOC detected at m/z is primarily isoprene (Kumar and Sinha, 2014). However, even if the contribution of furan at m/z 69 increases due to crop-residue fires, the calculated OH reactivity will decrease due to the lower rate constant of furan (4.01×10^{-11} cm^3 molecule^{-1} s^{-1}) (Atkinson et al., 1983) for reaction with hydroxyl radicals. Hence the missing OH reactivity fraction will only increase further and not affect our conclusion that crop residue fires lead to a large unexplained OH reactivity.

5.2.3 Grab sampling of fire plumes from wheat residue fires at an agricultural field

Samples of plumes from flaming (modified combustion efficiency = 0.99) and smoldering (modified combustion efficiency = 0.43) stages of wheat residue fires were collected in pressurized glass flasks wrapped with aluminium foil (Chandra et al., 2017) directly at

an agricultural field in Raipur Khurad, Mohali (30.652 °N, 76.709 °E, 305 m a.s.l.) on 2 May 2015 in the evening time (17:30 - 18:00 local time). Ambient air samples were also collected in separate glass flasks from the field before the fires were lit after ensuring there were no active nearby fires, to establish the background concentrations at the field site. All the whole air samples collected in the glass flasks were then transported and analyzed within 5 hours of sample collection at the IISER Mohali Atmospheric Chemistry Facility using the PTR-MS instrument in ion selective mode with a dwell time of 1 s. The emission factors of VOCs were calculated for flaming and smoldering stages as described in Chandra et al. (2017).

5.2.4 Ancillary measurements

Carbon monoxide (CO), sum of nitrogen dioxide and nitric oxide (NO_x), sulphur dioxide (SO_2), ozone (O_3) and meteorological parameters such as solar radiation, ambient temperature, relative humidity, wind speed and wind direction were measured continuously at a time resolution of one minute. CO, NO_x and O_3 measurements from the site have already been analyzed and reported from September 2011 to September 2013 (Kumar et al., 2016), along with a detailed description of the sampling methodology and calibration protocol (Sinha et al., 2014; Sarkar et al., 2013; Kumar et al., 2016). Briefly, CO, NO_x, SO_2 and O_3 measurements were performed using gas filter correlation non-dispersive infra-red (GFC-NDIR) technique (Model 48i), chemiluminescence technique (Model 42i), pulsed UV fluorescence technique (Model 43i) and UV absorption photometry (Model 49i; Thermo Fischer Scientific, Franklin, USA) respectively. Data for meteorological parameters were acquired from meteorological sensors (Met One Instruments Inc., Oregon, USA) installed at the measurement site and located within 2 m of horizontal distance from the instrument inlets. CO calibrations were performed on 08 April 2013 and 06 May 2013, NO_x calibrations were performed on 26 April 2013 and 22 May 2013, O_3 calibrations were performed on 28 April 2013 and 23 May 2013 and SO_2 calibrations were performed on 30 April 2013. The uncertainties in measurements of CO, NO_x, SO_2 and O_3 are less than 6 % and the detection limits of these instruments were 28 ppb, 114 ppt, 1 ppb and 1 ppb respectively. Carbon dioxide and methane concentrations in the grab samples were measured using a high precision Cavity Ring Down Spectroscopy (CRDS) analyzer (Model G2508, Picarro, Santa Clara, USA) as described in Chandra et al. (2017). These were used for calculation of emission factors

Table 5.1: Concentrations of C2-C5 alkanes and C2-C4 alkenes for the pre-harvest NCFI and post-harvest CFI periods calculated using their prescribed emission ratio to CO for crop residue fires (Andreae and Merlet, 2001) and the average measured CO concentration in the respective periods.

Hydrocarbon	Pre-harvest (NCFI)	Post-harvest (CFI)
Ethane	2.43	3.89
Propane	0.89	1.42
i-Butane	0.02	0.03
n-Butane	0.08	0.12
n-Pentane	0.03	0.04
Ethene	3.76	6.01
Propene	1.79	2.86
1-Butene	0.17	0.28
i-Butene	0.11	0.17
cis-2-Butene	0.07	0.11
trans-2-Butene	0.05	0.09
Ethyne	1.04	1.66

5.2.5 Estimation of C2 - C5 alkane and C2 - C4 alkene concentrations

For estimating the concentrations of C2 - C5 alkanes and alkenes which were not directly measured during our study (Table 5.1), I multiplied the hydrocarbon/CO emission ratios reported by Andreae and Merlet (2001) in agricultural residue fires with the average CO concentration measured during the CFI period. The hydrocarbon concentrations during the NCFI periods were then estimated by dividing the CFI period concentrations by 1.6, which was the average enhancement ratio of the directly measured VOCs between the CFI and NCFI periods.

5.2.6 OH Reactivity calculations using the Framework for 0-D Atmospheric box Modeling (F0AM) Model

A zero-dimensional atmospheric box model F0AM (Wolfe et al., 2016) was set up for calculating the OH reactivity using the measured and estimated compounds and their oxidation products. The model employs Master Chemical Mechanism (MCM) 3.3.1 chemistry (Jenkin et al., 1997; Saunders et al., 1997, 2003). The NO_2 photolysis rate constant $J(NO_2)$ was calculated using the measured solar radiation (Trebs et al., 2009). Other model prescribed photolysis frequencies (e.g. $J(O(^1D))$, J(HCHO), $J(H_2O_2)$, J(HONO)

etc.) are corrected using a factor derived using the F0AM "hybrid" method derived $J(NO_2)$(Wolfe et al., 2016). The MCM setup included a total of 1363 species and 4205 chemical reactions. The rate constants used in the model are taken from the reviewed rate constants published by Atkinson et.al. (Atkinson et al., 1983; Atkinson and Carter, 1984; Atkinson and Aschmann, 1984; Atkinson, 1986; Atkinson and Arey, 2003; Atkinson, 2003; Atkinson et al., 2006). If unavailable in the former they were taken from the NIST chemical kinetics database (Manion et al., 2015). The model was constrained with hourly averaged concentrations of all the directly measured VOCs listed in Table 5.2, VOCs measured in the extended NCFI period (Table 5.3) whose chemistry is present in MCM 3.3.1, O_3, NO_x, SO_2, $J(NO_2)$, estimated concentrations of hydrocarbons as described in previous section (Table 5.1), relative humidity and ambient temperature (Lou et al., 2010; Kaiser et al., 2016). Methane (CH_4) and hydrogen (H_2) mixing ratios are held constant at 1.8 ppm and 550 ppb respectively. The model calculated concentrations of secondary species at the end of each hour were used as the initial concentration of model run for the second hour. The simulations are performed in steady state conditions with a spin-up period of three days. A dilution in the background air with zero concentration of all the model calculated species was considered for the model setup (Wolfe et al., 2016). The dilution is parametrized according to the following first order loss equation:

$$\frac{d[X]}{dt} = K_{dil}[[X] - [X]_b] \tag{5.3}$$

Here $[X]$ is the concentration of the species and $[X]_b$ is the concentration in background air which is assumed to be zero. K_{dil} is the first order dilution constant which is chosen to be $1/86400\ s^{-1}$ corresponding to an atmospheric lifetime of 24 hours was assumed to avoid build-up of unrealistically high concentration of model calculated secondary species. Note that the following measured compounds namely isocyanic acid, formamide, acetamide, 2-furaldehyde, nitromethane and acetonitrile are not included in the MCM 3.3.1, the box model calculation do not take into account their chemistry. Also alkylamines, which are precursors of nitromethane, amides and isocyanic acid are not included in the MCM 3.3.1.

5.3 Results and Discussion

5.3.1 Time series of OH reactivity and other measured species

Figure 5.5 shows the time series of measured OH reactivity on the top panel in red and calculated OH reactivity due to in situ measured species in deep blue at a time resolution of 3 minutes for the pre-harvest NCFI (light green shaded region) and post-

harvest CFI periods (light orange shaded region). The second panel shows mixing ratio of acetaldehyde, isoprene, toluene and acetonitrile while the third panel shows the NO_x and O_3 mixing ratios. The bottom panel shows daily fire counts data over the area close to study region (28 °N – 33 °N and 72 °E – 79 °E) at a confidence interval > 80 % and in situ measured solar radiation data. The blue shaded region shows the period when rain and overcast conditions were observed.

In NCFI period, the measured three minutes time resolution data OH reactivity ranged between below detection limit (4.5 s^{-1}) to upto 94 s^{-1} except for a period in late evening of 15 April 2013, when it reached upto 180 s^{-1}. During this period, enhancements in mixing ratios of acetonitrile, acetaldehyde, toluene and NO_x were observed, which also resulted in significant enhancement in measured and the calculated OH reactivity. Ambient OH reactivity data for 19 April 2013 was not available as the response of the VOC-OHM system was being check using standards of known reactivity. In CFI period, the measured OH reactivity varied between below detection limit to 188 s^{-1}. The average measured total OH reactivity was 28.0 s^{-1} in NCFI period and 64.1 s^{-1} in CFI period corresponding to an average OH radical lifetime of 38 ms and 16 ms only. The measured values of total OH reactivity during NCFI period are comparable to those reported in the urban environment of Beijing in 2013 (Williams et al., 2016) at an average of $\sim$ 20 s^{-1} and of New York in 2001 (Ren et al., 2003) at an average of 19 s^{-1}. The high values of measured OH reactivity in CFI period are comparable to those observed during rush hours of extremely polluted Mexico City, in transported continental airmass sampled in Paris (Shirley et al., 2006; Dolgorouky et al., 2012) and during the dry conditions in the central Amazonia (Nölscher et al., 2016). Higher variability was also observed in the directly measured total OH reactivity during the CFI period, consistent with rapidly changing VOC concentrations in sampled pollution plumes (Lou et al., 2010).

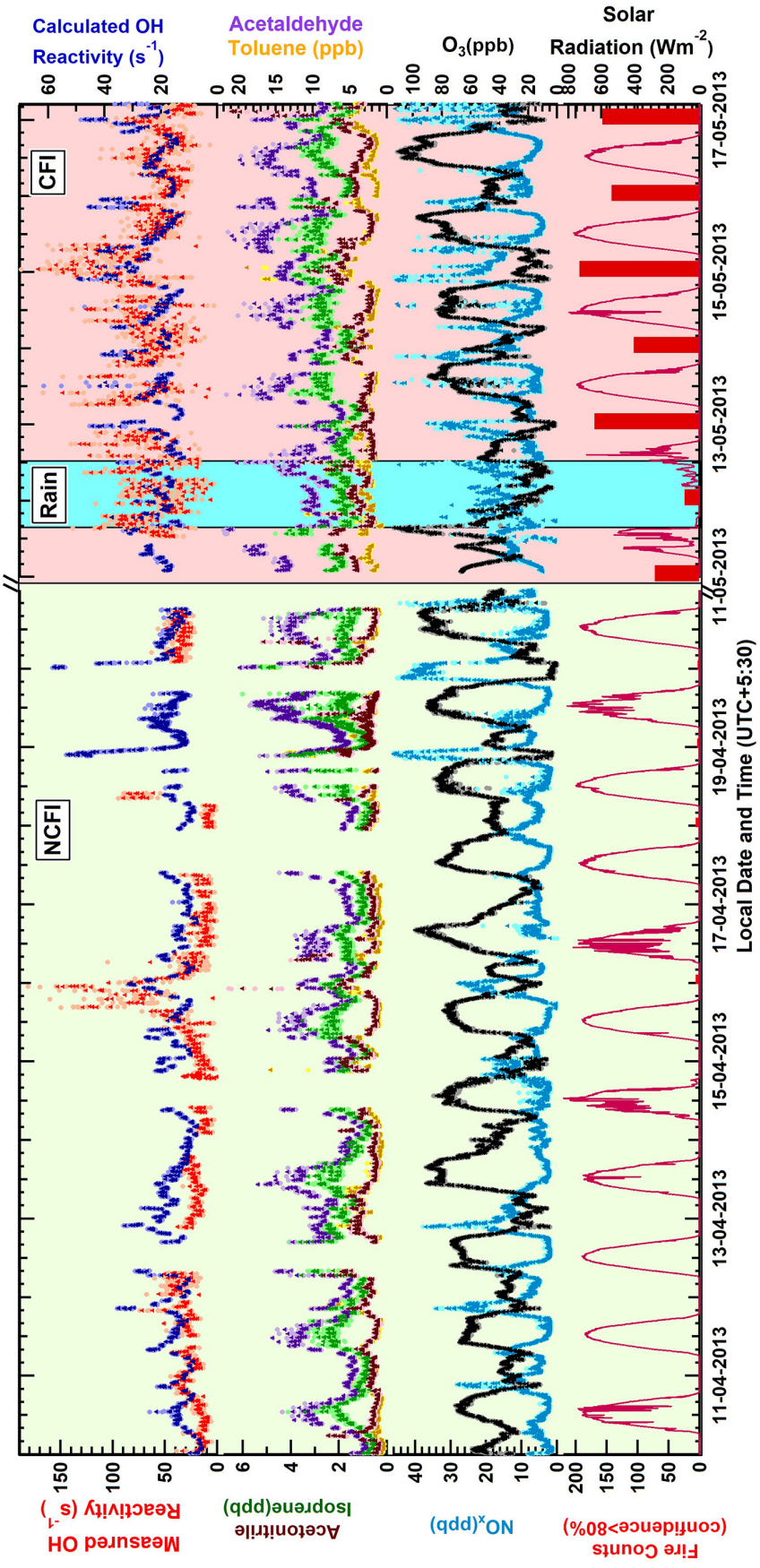

Figure 5.5: 3 min temporal resolution time series of the measured OH reactivity (left axis) and calculated OH reactivity due to measured compounds (right axis)(top panel), mixing ratios of acetonitrile, isoprene, acetaldehyde and toluene (second panel) and NO_x and O_3 (third panel). The regional (28 °N – 33 °N latitude and 72 °E – 79 °E longitude) MODIS satellite-derived daily fire counts and measured solar radiation are shown in the bottom panel. Light green shaded region shows the measurements during pre-harvest NCFI period whereas light pink shaded region shows the measurements during post-harvest CFI period. The blue shaded region shows periods when overcast conditions and rain were observed.

Table 5.2 lists the average, range of peak concentrations (75^{th} – 90^{th} percentiles) and enhancements which occurred at a confidence interval greater than 99.9 % of key measured OH reactants including acetonitrile, a chemical tracer of biomass-fires. Enhancement ratios ranging from 1.5 – 2.0 were observed for several reactive VOCs such as methyl ethyl ketone, isoprene, acetaldehyde, and sum of C-9 aromatics. Table 5.3 similarly lists the enhancement ratios of additional reactive compounds measured in the same season during the extended NCFI and CFI periods which also ranged from 1.5 – 2.2 for most compounds. A non-parametric Mann–Whitney U test was performed separately for daytime and nighttime hours to check the confidence interval at which the measurement in the two periods represent dataset with different median. The measured VOCs and NO_x pass this test at a confidence interval > 99.95 %, whereas for CO the confidence interval for distinct median is 99.9 % for daytime and 97.0 % for nighttime data.

5.3.2 Diel variability of total OH reactivity and contribution of OH reactants

Fig. 5.6 shows the magnitude and variability of the total measured OH reactivity (red) and calculated OH reactivity (black) due to measured OH reactants for both NCFI and CFI periods. The pie charts show the contribution of the individual OH reactants and the fraction that could be accounted for by the measured compounds. Both the measured and calculated OH reactivity increased significantly during CFI periods relative to NCFI periods, with greater than two-fold increase in the average measured OH reactivity (28 s^{-1} to 64 s^{-1}), accompanied by 40 % increase in average calculated OH reactivity (15 s^{-1} to 21 s^{-1}). The missing OH reactivity was the highest in the afternoon (49 %) followed by evening (30 %) and morning (27 %) hours during the NCFI period. However, during the CFI periods, surprisingly the unaccounted fraction of OH reactivity was always higher than that accounted for by the measured OH reactants ranging from as high as 69 % during morning and noon hours to 55 % in the evening hours. Typically agricultural burning of the wheat straw occurs in the evening (Chandra and Sinha, 2016) resulting in large contribution of primary emissions to pollutant loadings. The contribution of non-oxygenated VOCs (isoprene, aromatics, monoterpenes) and CO in the CFI period was less than 27 %, the maximum of which occurred during evening hours. This points to presence of many new/unmeasured VOCs during the CFI periods, with likely significant contribution from oxidation products.

The calculated OH reactivity only accounted for the directly measured OH reactants (total of seventeen gases), which does not include several reactive oxidation products such as pinonaldehyde, formaldehyde, propionaldehyde, glyoxal, methylglyoxal and acrolein

Table 5.2: Average concentration ± 1 σ ambient variability; (75^{th} – 90^{th} percentile) and enhancement ratios of the VOCs and trace gases (in ppb) directly measured along with the total OH reactivity during the pre-harvest non crop-residue fire influenced (NCFI) and post-harvest crop-residue fire influenced (CFI) periods.

Species	Pre-harvest (NCFI) Average ± 1σ (75^{th} – 90^{th} percentile)	Post-harvest (CFI) Average ± 1σ (75^{th} – 90^{th} percentile)	Enhancement ratio
Acetone$^{\surd}$	6.6 ± 1.6 (8.2 – 10.1)	13.1 ± 2.5 (14.5 – 18.2)	2.0
Methyl ethyl ketone$^{\surd}$	1.4 ± 0.4 (1.8 – 2.1)	2.7 ± 0.6 (3.1 – 3.5)	1.9
Sum of C-9 aromatics$^{\surd}$	1.3 ± 0.6 (1.5 – 2.2)	2.3 ± 1.4 (2.6 – 4.6)	1.8
Acetonitrile$^{\times}$	0.8 ± 0.6 (0.9 – 1.5)	1.4 ± 0.8 (1.7 – 2.1)	1.8
Monoterpenes$^{\surd}$	0.6 ± 0.3 (0.8 – 0.9)	1.0 ± 0.3 (1.2 – 1.4)	1.7
Isoprene$^{\surd}$	1.6 ± 0.7 (1.9 – 2.4)	2.5 ± 0.6 (2.9 – 3.3)	1.6
MVK + MACR$^{\surd}$	1.3 ± 0.4 (1.3 – 0.5)	2.0 ± 0.4 (2.4 – 2.7)	1.5
Benzene$^{\surd}$	1.4 ± 1.1 (1.7 – 2.7)	2.1 ± 1.3 (2.8 – 3.8)	1.5
Acetaldehyde$^{\surd}$	8.6 ± 3.4 (11.3 – 13.2)	12.8 ± 3.6 (15.3 – 17.0)	1.5
Sum of C-8 aromatics$^{\surd}$	2.1 ± 1.2 (2.2 – 3.3)	2.6 ± 1.6 (3.0 – 4.8)	1.2
Toluene$^{\surd}$	2.6 ± 2.1 (3.3 – 4.5)	3.2 ± 2.2 (4.1 – 5.7)	1.2
Methanol$^{\surd}$	42.6 ± 8.3 (48.8 – 62.4)	49.9 ± 10.0 (59.8 – 70.7)	1.2
$NO_x^{\surd}$	8.5 ± 7.5 (10.7 – 16.5)	14.4 ± 9.6 (18.7 – 27.1)	1.7
CO$^{\surd}$	326 ± 223 (370 – 530)	395 ± 190 (510 – 770)	1.2

$^{\surd}$Species included in the box model.

$^{\times}$Species not included in the box model.

Table 5.3: Average concentration ± 1 σ ambient variability; (75^{th} – 90^{th} percentile) and enhancement ratios of the rarely measured VOCs (in ppb) for the extended NCFI and extended CFI periods of summer 2013.

Species	Pre-harvest (NCFI) Average ± 1σ (75^{th} – 90^{th} percentile)	Post-harvest (CFI) Average ± 1σ (75^{th} – 90^{th} percentile)	Enhancement ratio
Nitromethane$^{\times}$	0.5 ± 0.1 (0.6 – 0.8)	1.1 ± 0.2 (1.3 – 1.5)	2.2
Hydroxyacetone$^{\checkmark}$	1.6 ± 0.8 (2.0 – 2.5)	3.4 ± 1.6 (4.2 – 5.8)	2.1
Acetic acid$^{\checkmark}$	13.0 ± 7.3 (16.8 – 21.2)	27.4 ± 12.3 (36.0 – 42.9)	2.1
Butane-2,3-dione$^{\checkmark}$	1.2 ± 0.6 (1.6 – 2.0)	2.3 ± 1.1 (2.9 – 3.9)	1.9
2-Furaldehyde/ 2,5-Dimethylfuran$^{\times}$	0.7 ± 0.3 (0.8 – 1.1)	1.2 ± 0.6 (1.6 – 2.2)	1.7
Acetamide/ Trimethylamine$^{\times}$	1.8 ± 0.7 (2.0 – 2.6)	3.0 ± 1.4 (2.6 – 4.0)	1.7
Ethanol/ Formic acid$^{\checkmark}$	14.5 ± 4.8 (17.1 – 20.5)	24.1 ± 9.1 (29.4 – 35.8)	1.7
Acrolein/ 1-Butene$^{\checkmark}$	3.9 ± 2.3 (4.4 – 6.2)	5.9 ± 3.1 (6.8 – 8.5)	1.5
Formamide/Ethylamine /Dimethylamine$^{\times}$	7.1 ± 2.6 (8.6 – 10.5)	10.2 ± 3.1 (11.6 – 14.8)	1.4
Styrene$^{\checkmark}$	0.3 ± 0.3 (0.3 – 0.4)	0.4 ± 0.5 (0.4 – 0.5)	1.3
Isocyanic acid$^{\times}$	1.7 ± 0.6 (2.2 – 2.6)	2.2 ± 0.7 (2.7 – 3.3)	1.3

$^{\checkmark}$Species included in the box model.

$^{\times}$Species not included in the box model.

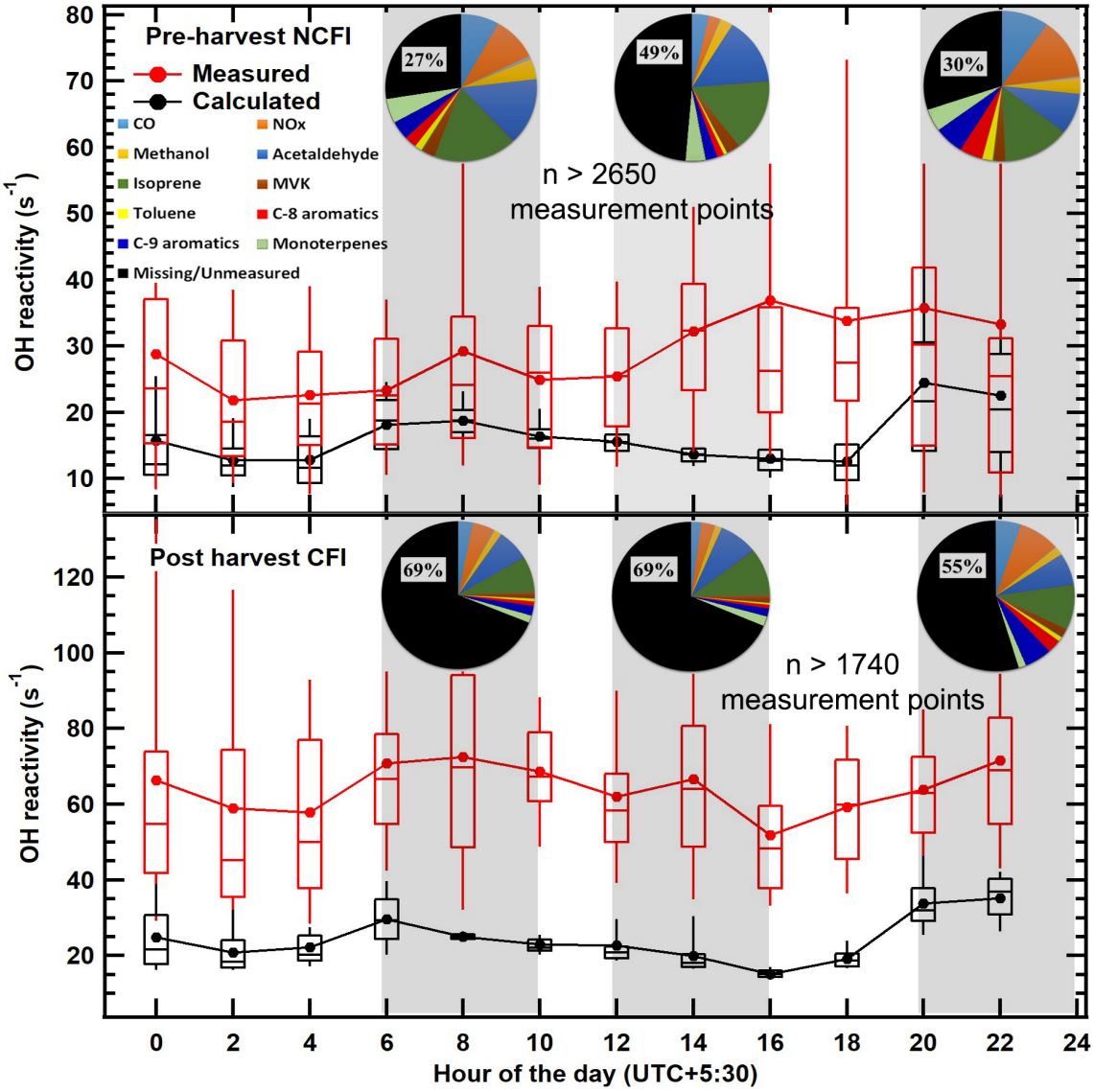

Figure 5.6: Diel box (25^{th}-75^{th} percentiles) and whiskers (10^{th}, 90^{th} percentiles) profiles of the directly measured total OH reactivity and the calculated OH reactivity due to measured species in the NCFI period (top) and CFI period (bottom). The average and various percentiles of the data in between a given 2 hour time interval are plotted against the start hour of the interval. The pie charts show partitioning of the measured OH reactivity among top ten measured OH reactants in 4-hour windows (shaded in the Figure) of the morning (06:00 – 10:00 Local Time (L.T.)), afternoon (12:00 – 16:00 L.T.) and evening time (20:00 – 24:00 L.T.).

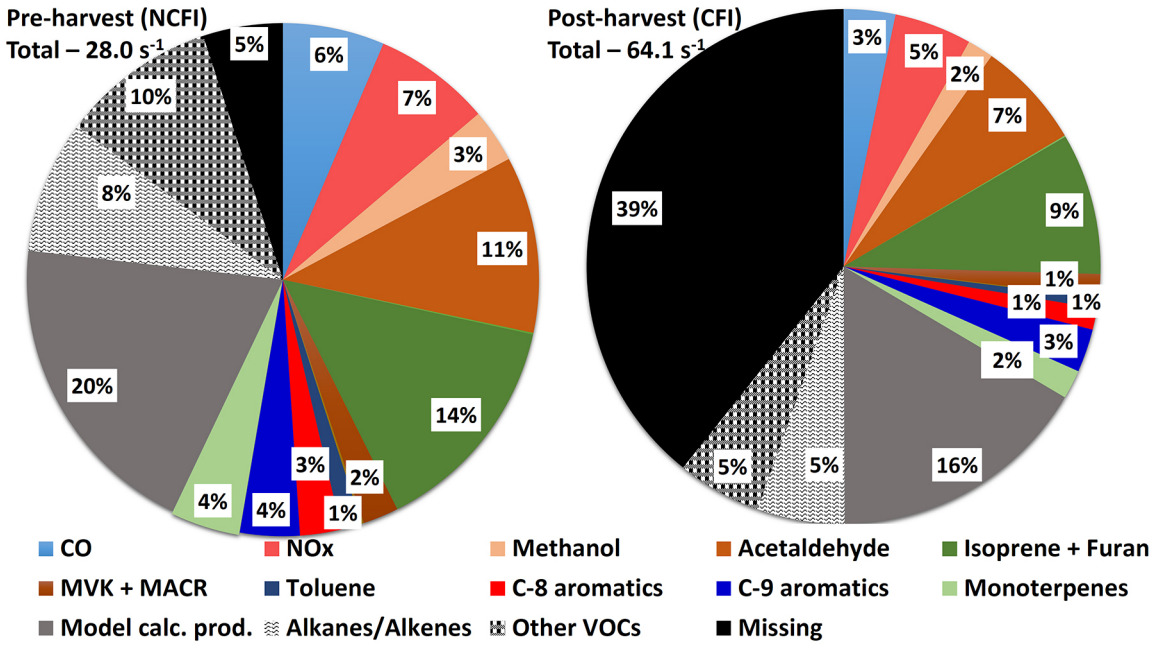

Figure 5.7: Pie charts showing the missing OH reactivities and average contribution of measured OH reactants, estimated hydrocarbons and model calculated oxidation products to the total measured OH reactivity for NCFI and CFI periods.

which are formed from the measured organic compounds. As oxygenated VOCs are known to contribute significantly towards OH reactivity of biomass burning plumes, it is important to account for them in the OH reactivity calculation (Gilman et al., 2015). Further, several compounds known to be emitted from biomass fires such as C2-C5 alkanes/alkenes and their oxidation products were missing from the set of directly measured OH reactants. To account for the contribution of all these important species that were not directly quantified, I therefore applied a 0-D steady-state box model (Wolfe et al., 2016) employing MCM 3.3.1 chemistry containing 1363 species (Jenkin et al., 2015), for analyzing the OH reactivity budget in both NCFI and CFI periods. The model was constrained with diel hourly average concentrations of seventeen measured chemical species, methane and hydrogen during respective periods, twelve approximated C2-C5 alkanes and alkenes (Tables 5.1, 5.2 and 5.3) and meteorological parameters. Figure 5.7 summarizes the results which show that the average total OH reactivity in the NCFI period can be fully explained ($\sim$ 95 %) by the species present in the model (within measurement uncertainty of $\sim$ 20 %), whereas using the same set of OH reactants and chemistry, the model is able to explain only $\sim$ 60 % of the total OH reactivity during the CFI periods. Thus a large unexplained missing OH reactivity fraction of $\sim$ 40 % persists. Overall, the contribution of oxidation products predicted by the model doubled from 5.6 s^{-1} (NCFI) to 10.2 s^{-1} (CFI), pointing to increased role of photochemically formed reactive compounds.

For many of the rarely measured VOCs (Table 5.3), a calibration gas standard was unavailable and so the total uncertainty of the measurement for these VOCs is $\sim$ 30 %. To assess how much the 30 % concentration uncertainty for rarely measured VOCs could affect the OH reactivity calculations and hence the conclusion of the large missing OH reactivity during the CFI periods, model runs were performed for the NCFI and CFI periods with 30 % higher concentrations of rarely measured VOCs compared to measured values currently used for the calculations. I found that doing so only reduces the missing reactivity fraction to 3 % (from 5 %) in NCFI period and to 37 % (from 39 %) in CFI period. Thus, my conclusion that there is a large fraction of unexplained OH reactivity in the CFI period remains unchanged. Model sensitivity runs were also performed assuming minimum and maximum rate constants for the lumped species (e.g. sum of C-8 aromatics, sum of C-9 aromatics and sum of monoterpenes) to provide upper and lower bounds (assuming the least reactive or most reactive compound contributed to the entire measured m/z) of the missing OH reactivity. The change in values of missing OH reactivity relative to present values reported in Fig. 5.7 (5 % missing in NCFI and 39 missing in CFI), still resulted in no missing OH reactivity in NCFI period (within uncertainty of measurements) and less than 6 % reduction in missing OH reactivity for the CFI period. Thus, the conclusion concerning a large fraction of unexplained OH reactivity in the CFI period remained unaffected. For estimating the concentrations of C2-C5 alkanes and alkenes which were not directly measured, I did not subtract the background CO concentrations. Generally enhancements in CO are used to estimate concentrations of hydrocarbons when multiplying by the VOC/CO emission ratios. In order to assess the magnitude of change in missing OH reactivity due to this, we undertook the following calculation. Given that the measured average CO in CFI period was 395 ppb (Table 5.2) and the 10th percentile of CO data (reasonable to consider as the background CO) in CFI period was 150 ppb, the resulting increase in missing OH reactivity due to lower approximated C2-C5 alkanes/alkenes concentrations, was found to be less than 3 % in CFI period and less than 2 % in NCFI period. Thus, no significant bias arises in the missing OH reactivity fraction during CFI and NCFI periods due to the current method of estimating the C2-C5 hydrocarbon concentrations. In addition to the C2-C5 alkanes and alkenes, larger alkanes/alkenes and furans are known to be emitted from agricultural residue fires (Andreae and Merlet, 2001). Using the emission ratio with respect to CO and the concentration enhancement in CO, we have estimated the concentration and subsequently the OH reactivity of 4-methyl-1-pentene, 1-hexene, n-hexane, isohexane, heptane, octene, 2-methylfuran, ethylfuran, dimethylfuran, tetrahydrofuran, benzofuran and furfural in the CFI period. The total OH reactivity due these species during the CFI period is 0.35 s^{-1} which is $\sim$ 0.5 % of the directly measured total OH reactivity. Again

the missing OH reactivity fraction remains virtually unchanged.

5.3.3 Enhanced emission and photochemical formation of rarely measured VOCs as a result of crop residue fires

Figure 5.8 shows the strong enhancements that occurred during the CFI period in the concentrations of acetonitrile (biomass-burning tracer), sum of C-9 aromatics (trimethylbenzenes), as well as acetaldehyde and acetone which are emitted from crop residue fires but are also formed photochemically due to oxidation of precursor compounds emitted from the fires such as C2 - C5 alkanes and alkenes (Millet et al., 2010). Surprisingly, I also observed much higher photochemical formation rates in rarely measured VOCs like hydroxyacetone and butane-2,3-dione and strong enhancements in ambient concentrations of photochemically formed nitrogenous compounds e.g. nitromethane and isocyanic acid (HNCO) during the CFI periods.

The slope of the line fit from sunrise (05:00 local time) till attainment of peak daytime concentrations for hydroxyacetone increased from 0.27 ppb h^{-1} in the NCFI period to 0.54 ppb h^{-1} in the CFI period whereas that of butane-2,3-dione increased from 0.19 ppb h^{-1} to 0.43 ppb h^{-1} between NCFI and CFI periods. The removal of HNCO from the atmosphere takes place primarily through wet and dry deposition, since the two major gas phase pathways, reaction with hydroxyl radical (OH) and photolysis are slow (Roberts et al., 2014). The solubility of HNCO and its kinetics imply lifetimes due to heterogeneous removal on the order of days to a few weeks, which would be even slower under the extremely dry conditions of the Indian pre-monsoon summer season (RH as low as 15 % in the daytime). Thus HNCO would have a high accumulation tendency under such conditions. The precursor of isocyanic acid through hydroxyl radical initiated oxidation is formamide which in turn can be formed from hydroxyl radical initiated oxidation of methylamine (Reactions [R17] to [R24]).

$$CH_3NH_2 + OH \longrightarrow CH_2NH_2 + H_2O \qquad [R17]$$

$$CH_2NH_2 + O_2 + M \longrightarrow OOCH_2NH_2 + M \qquad [R18]$$

$$OOCH_2NH_2 + NO \longrightarrow OCH_2NH_2 + NO_2 \qquad [R19]$$

$$OCH_2NH_2 + O_2 \longrightarrow HCONH_2 + HO_2 \qquad [R20]$$

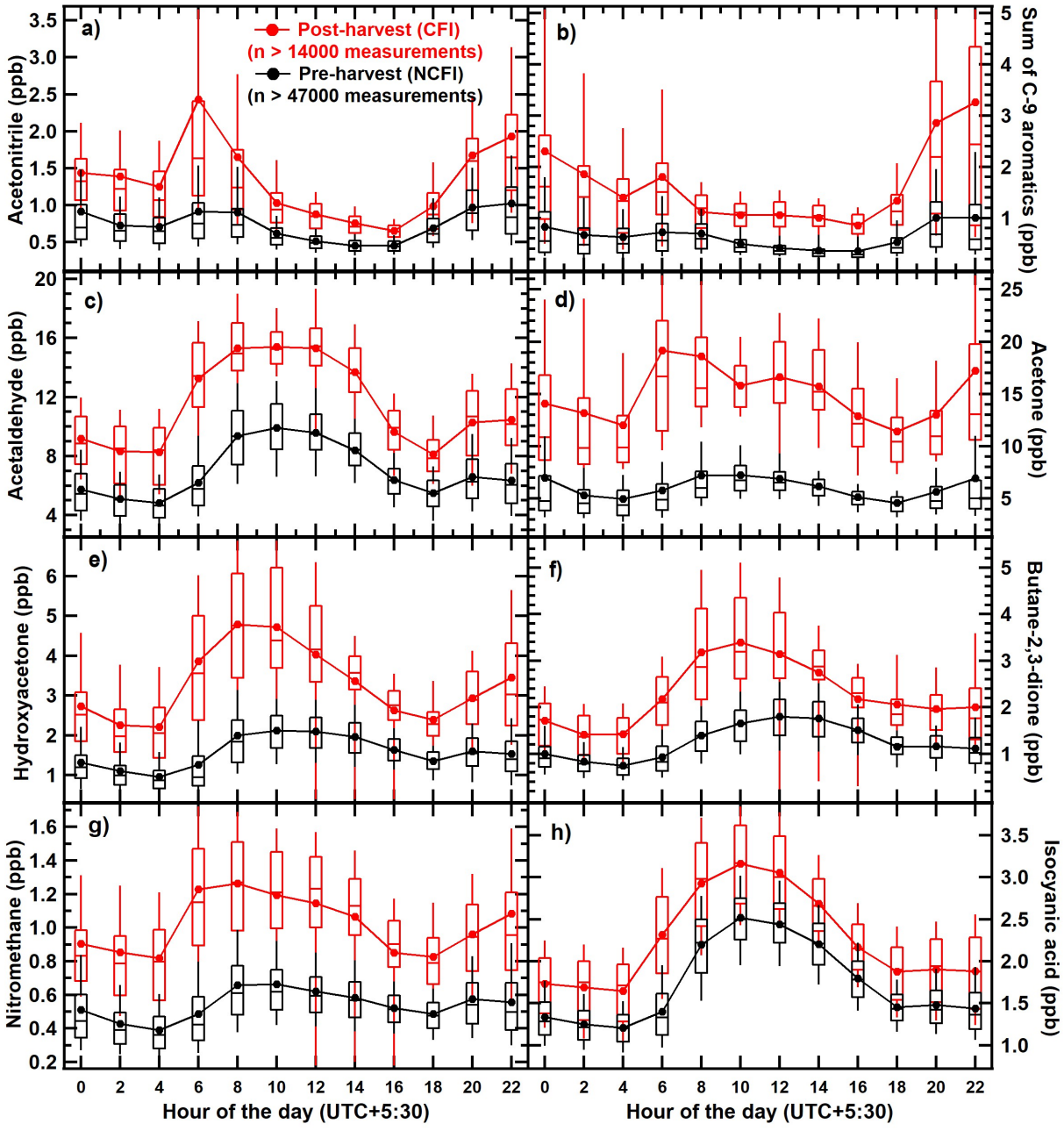

Figure 5.8: Diel box (25^{th} - 75^{th} percentiles) and whiskers (10^{th}, 90^{th} percentiles) profiles of the measured concentrations of (a-d) acetonitrile, sum of C-9 aromatics, acetaldehyde and acetone, in the CFI (red) and NCFI (black) periods and (e-h) hydroxyacetone, butane-2,3-dione, nitromethane and isocyanic acid in the extended CFI and NCFI periods of summer 2013.

$$HCONH_2 + OH \longrightarrow C(O)NH_2 + H_2O \quad [R21]$$

$$HCONH_2 + OH \longrightarrow HC(O)NH + H_2O \quad [R22]$$

$$C(O)NH_2 + O_2 \longrightarrow HNCO + HO_2 \quad [R23]$$

$$HC(O)NH + O_2 \longrightarrow HNCO + HO_2 \quad [R24]$$

Further, formation of nitromethane can occur from ozone initiated oxidation of trimethylamine, (reactions [R25] - [R27] (Nielsen et al., 2012)) which also have high OH reactivity (Table 5.4).

$$(CH_3)_3N \xrightarrow[-\ O_2]{O_3} [CH_3N^+O^-]^* \xrightarrow[-\ CH_3]{} (CH_3)_2NO \quad [R25]$$

$$(CH_3)_2NH \xrightarrow[-\ O_2]{O_3} [(CH_3)_2N(H)^+O^-]^* \longrightarrow [(CH_3)_2NOH]^* \xrightarrow[-\ O_2,\ -\ OH]{O_3} (CH_3)_2NO \quad [R26]$$

$$(CH_3)_2NO \xrightarrow[-\ O_2,\ -\ CH_3]{O_3} CH_3NO_2 \quad [R27]$$

With the PTR-MS technique dimethylamine, ethylamine and formamide can be detected at m/z 46 after protonation. Similarly trimethylamine and acetamide can be detected at m/z 60 after protonation. Since dimethylamine, ethylamine and trimethylamine cannot be formed photochemically, I attributed the signals to be majorly due to oxidation products of amine oxidation i.e. formamide at m/z 46 and acetamide at m/z 60 for the daytime data (Figure 5.9). However for the night time data, there could certainly be equally significant contribution from both the alkylamines and amides. The diel variation of m/z 46 and m/z 60 (Figure 5.9) measured with the PTR-MS clearly show strong evening time secondary peaks only during the CFI periods. These peaks would coincide very nicely with the timing of the fire activity (evening). Further it is known from laboratory studies and has been reported by Stockwell et al. (2015)(Supplement) that burning of many agricultural residues (e.g. African grass, wheat residue, paddy residue, alfalfa, hay, sugarcane and sawgrass) emits several alkylamines. It appears that higher concentrations of both amines and amides emitted at night during CFI periods tend to accumulate and just after sunrise trigger photochemical production of the oxidation products such as amides, nitromethane and isocyanic acid. As the concentrations of the precursor compounds are higher in the CFI periods, the rate of photochemical formation which depends

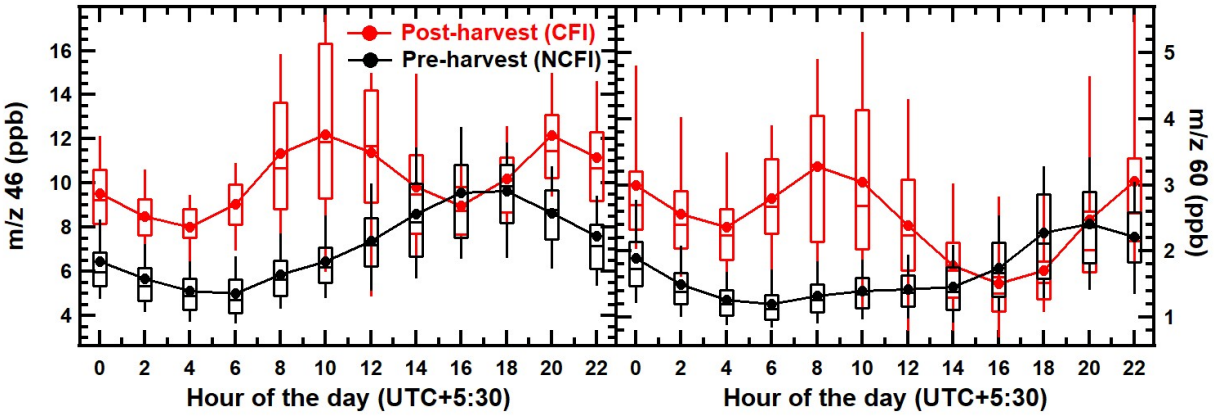

Figure 5.9: Diel box (25^{th}-75^{th} percentiles) and whisker (10^{th}, 90^{th} percentiles) plots of measured concentrations (in ppb) of m/z 46 (mainly formamide in daytime) and m/z 60 (mainly acetamide in daytime) during the extended pre-harvest NCFI (28 February 2013 to 30 April 2013) and extended post-harvest CFI period (1 May 2013 to 31 May 2013)

on the concentration of the precursor compounds is also higher in CFI period.

5.3.4 Potential contributors to the missing OH reactivity

The photochemical formation of nitromethane is likely driven by ozone initiated atmospheric oxidation of compounds such as trimethylamine which also has high OH reactivity (Table 5.4). Significant photochemical formation of formamide and acetamide was also observed in the daytime data during CFI period. The photochemical formation of several first and second generation photochemical oxidation products of amines e.g. formamide, acetamide, nitromethane and isocyanic acid strongly suggest that their precursor compounds such as alkylamines are also being emitted from crop residue fires. Both agricultural biomass fires and animal husbandry activities (Ge et al., 2011; Stockwell et al., 2015) are recognized as major atmospheric sources of alkylamines. Considering that the fetch region was similar during both the NCFI and CFI periods, and there was no evidence for substantial increase in animal husbandry activities between the two periods, I surmise that the agricultural biomass fires are a likely source for the emission of alkylamines. While the OH reactivity contribution of nitromethane, isocyanic acid, butane-2,3-dione and hydroxyacetone is collectively less than 2 s^{-1} in the CFI period, their reactive precursors such as alkylamines have very high OH reactivity (see Table 5.4) and could help explain a significant fraction of the missing OH reactivity.

Fig. 5.10 shows the correlation of the increased OH reactivity between CFI and NCFI periods with absolute concentration increases between CFI and NCFI periods of

Table 5.4: Rate constants ($cm^3\,molecule^{-1}\,s^{-1}$) of reaction with OH radicals and O_3 with the alkylamines (Atkinson and Carter, 1984; Atkinson, 1986).

Alkylamine	$k_{OH}(298)$	$k_{O_3}(298)$
Methylamine	2.20×10^{-11}	2.13×10^{-20}
Ethylamine	2.77×10^{-11}	2.76×10^{-20}
Dimethylamine	6.54×10^{-11}	2.61×10^{-18}
Trimethylamine	6.09×10^{-11}	9.73×10^{-18}

photochemically formed and nitrogen containing compounds such as hydroxyacetone, nitromethane, sum of formamide and C-2 amines, sum of acetamide and trimethylamine, acetone and acetonitrile. The individual points in the different panels were derived by calculating the differences between CFI and NCFI periods using the average diel profile data of measured OH reactivities (shown in Fig. 5.6), hydroxyacetone, nitromethane, acetone and acetonitrile (shown in Fig. 5.8) and the data for sum of formamide and C-2 amines (m/z 46), sum of acetamide and trimethylamine (m/z 60) shown in Fig. 5.9. Acetonitrile being a chemical marker for biomass burning is a proxy for primary fire emissions and its good correlation with the enhanced OH reactivity observed during CFI periods indicates that primary fire emissions which could not be measured likely contributed to the high OH reactivity in CFI period. The highest correlation ($r \geq 0.8$) was observed for sum of formamide and C-2 amines (m/z 46), sum of acetamide and trimethylamine (m/z 60), suggesting that nitrogen containing compounds may be playing a key role in driving the enhanced OH reactivity during the CFI period. Further, the good correlation ($r \geq 0.6$) of the enhanced OH reactivity in the CFI periods with hydroxyacetone, nitromethane, and acetone, all compounds which were observed to have a strong photochemical source in our measured dataset, also suggests that oxidation products of precursor compounds emitted from the fires contributed to the high measured OH reactivity in the CFI period.

Based on chamber oxidation studies of OH radical initiated oxidation of trimethylamine, 1 ppb of trimethylamine can yield 0.75 ppb of formaldehyde (HCHO) and trace amounts of less reactive nitrogen containing VOCs (amides and N-nitroamines) (Pitts et al., 1978). Using the product yields and the relevant rate constants for reaction of these oxidation products with OH radicals, the presence of an additional 14 ppb of trimethylamine like reactive compounds and the extra photo-oxidation products formed thereof, could account for the entire missing OH reactivity fraction of $\sim$ 40 % (25 s^{-1}) observed during the CFI period. While I am not suggesting that a high concentration of 14 ppb of only trimethylamine would be present in ambient air, the point is that given that dimethylamine, ethylamine and methylamine have rate constants with the hydroxyl

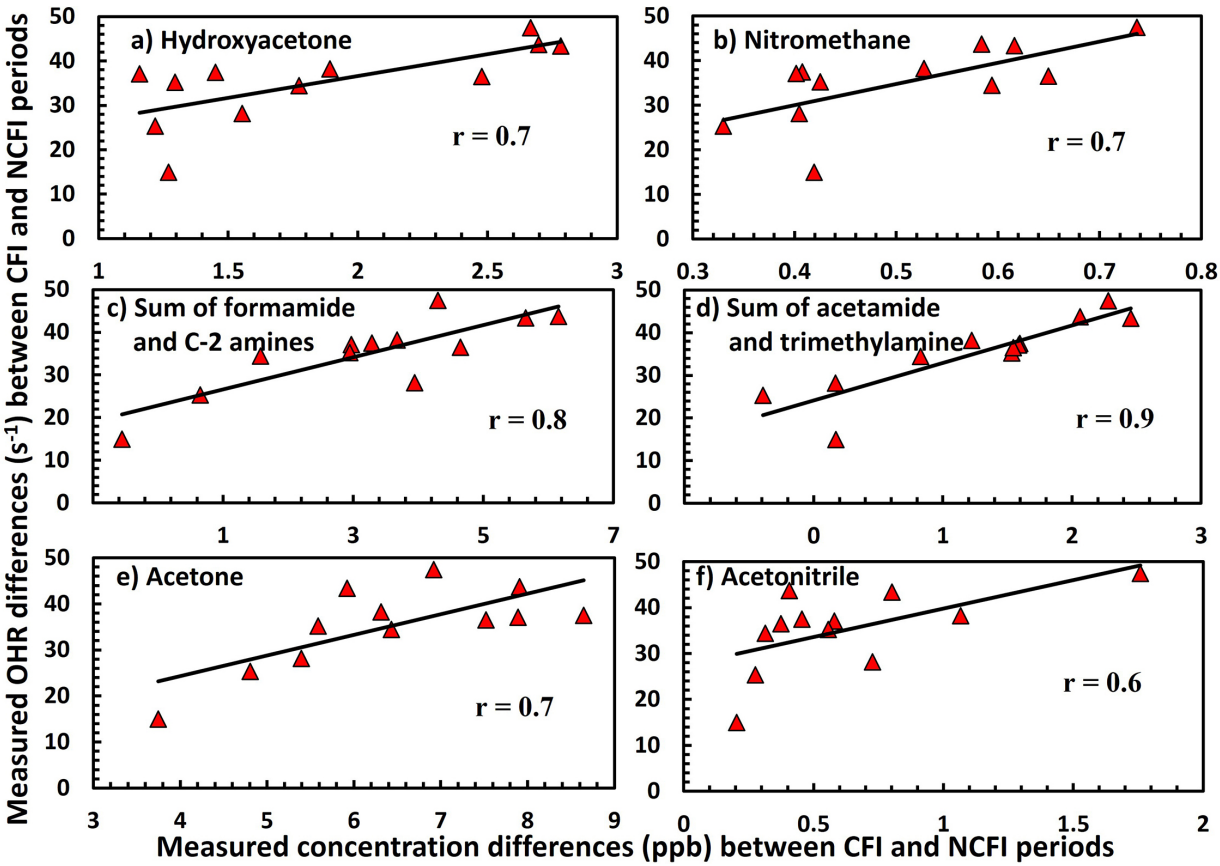

Figure 5.10: Linear regression lines showing correlation of the increased OH reactivity between CFI and NCFI periods with the absolute concentration increases between CFI and NCFI periods of a) hydroxyacetone, b) nitromethane, c) Sum of formamide and C-2 amines, d) Sum of acetamide and trimethylamine, e) acetone and f) acetonitrile (biomass burning tracer). The individual points in the different panels were obtained by calculating the differences between CFI and NCFI periods using the average diel profile data for measured OH reactivity shown in Fig. 5.6 and hydroxyacetone, nitromethane, acetone and acetonitrile shown in Fig. 5.8 and Sum of formamide and C-2 amines (m/z 46), Sum of acetamide and trimethylamine (m/z 60) shown in Fig. 5.9

radical which are of the same order of magnitude (10^{-11} $cm^3\,molecule^{-1}\,s^{-1}$; Table 5.4), and the observed diel profiles of m/z 46 and m/z 60 show values as high as 12 ppb and 3 ppb at night (m/z at which methylamine and ethylamine can contribute significantly at night), and the consideration that approximately 150 amines have been detected in ambient air (Ge et al., 2011) with smoke being a major source of amines, it is plausible that collectively amines could explain a major fraction of the missing OH reactivity in the crop residue fire impacted periods.

Grab sampling of wheat residue fires in a nearby agricultural field (30.652 °N, 76.709 °E, 305 m a.s.l.) under ambient smoldering (low modified combustion efficiency (MCE)) and flaming wheat straw fire stages yielded extremely high emission factors of several compounds during the smoldering stage of the fire (Table 5.5). Biomass combustion experiments conducted in laboratory studies (Stockwell et al., 2015) are based primarily on data from flaming stage fires. In the real world, such smoldering fires can persist for hours and the "poor" combustion conditions are rarely captured and characterized in laboratory studies. Considering that the temperatures are really high ($\sim$ 40 °C) during May in north-west IGP, in order to keep fires from spreading out of control, I noted that farmers do sprinkle water at the border of certain patches in their field. This practice could certainly contribute to smoldering fires characterized by low combustion efficiency at-least for several patches in a large agricultural field. Moreover the straws are less than 1 foot above the ground and root-bound at the time of fire, which can contribute to a lowering of the MCE. As the VOC emission factors of flaming stage fires are significantly lower than the smoldering stage, I believe my grab sampling experiment results support the contention that several compounds may be underestimated/unreported as emissions from biomass fires. Additionally, the high reactivity due to photochemically formed pollutants in the ambient atmospheric environments would escape notice in the laboratory studies focused on characterizing the primary emissions. The relevance of the reported emission factors for the smoldering stage fires in our study is that they demonstrate that several compounds with negligible emission factors in the flaming stage can have really high emission factors in the smoldering stage. As we could not sample statistically significant number of fires, it would be inappropriate to use them as representative values, but they are sufficient evidence for the primary point, that the reduced nitrogen compounds can be emitted in large quantities and this is the new insight of the emission factor data reported here.

Table 5.5: Emission factors (grams of VOC emitted per kg of dry fuel weight burnt) of different VOCs obtained from source sampling of emissions from open burning of wheat residue in the flaming and smoldering stages.

m/z	Major contributors	Emission factor (g/kg of fuel burnt) Flaming (MCE = 0.99)	Smoldering (MCE = 0.43)
33	Methanol*	0.2	41.3
45	Acetaldehyde$^{\gamma}$	0.2	23.3
97	2-Furaldehyde/ 2,5-Dimethylfuran$^{\gamma}$	0.1	16
75	Hydroxyacetone$^{\gamma}$	0.2	15.9
59	Acetone$^{\gamma}$	0.07	13.2
69	Isoprene/furan$^{\delta}$	0.09	11.5
87	Butane-2,3-dione$^{\gamma}$	0.2	10.7
61	Acetic acid$^{\delta}$	1.9	9.2
57	Acrolein/1-Butene$^{\gamma}$	0.1	7.8
73	MEK$^{\gamma}$	0.05	6.2
71	MVK + MACR$^{\gamma}$	0.04	5.2
42	Acetonitrile$^{\gamma}$	0.02	4.4
93	Toluene$^{\delta}$	0.03	2.8
79	Benzene$^{\delta}$	0.05	1.6
107	Sum of C-8 aromatics$^{\gamma}$	0.02	1.5
46	Formamide/Ethylamine /Dimethylamine$^{\delta}$	0.02	0.6
60	Acetamide/ Trimethylamine$^{\delta}$	< 0.01	0.6
121	Sum of C-9 aromatics$^{\delta}$	0.01	0.6
105	Styrene$^{\gamma}$	0.01	0.4
31	Formaldehyde$^{\delta}$	0.01	0.2
44	Isocyanic acid$^{\delta}$	0.03	0.2
63	Dimethylsufide$^{\epsilon}$	0.01	0.2
137	Monoterpenes$^{\gamma}$	0.002	0.2
47	Ethanol/Formic acid$^{\delta}$	0.01	0.1

Modified combustion efficiency (MCE)=$\Delta CO_2/(\Delta CO_2 + \Delta CO)$,*(Warneke et al., 2011) $^{\epsilon}$(Akagi et al., 2011),$^{\gamma}$(Stockwell et al., 2015), $^{\delta}$(Sarkar et al., 2016)

5.3.5 Implications for regional air quality and climate

Total OH reactivity provides a measure of all gaseous reactive pollutants that are directly emitted and formed by atmospheric oxidation of the emissions. The large missing OH reactivity during periods affected by agricultural fires has major implications for understanding the formation of tropospheric ozone and other secondary pollutants in biomass fire impacted atmospheric environments (Fig. 5.11). It reveals that in the biomass fire impacted periods almost half of the reactive atmospheric chemical composition is unknown and therefore their chemical feedbacks are not considered in typical models and field studies. For example, atmospheric oxidation of hydroxyacetone forms HO_2 radicals, which may be an important atmospheric pathway for reforming hydroxyl radicals and sustaining/enhancing oxidizing efficiency in a polluted environment (reactions [R28] - [R29]).

$$CH_3C(O)CH_2OH + OH \xrightarrow{91\,\%\,\text{yield}} CH_3C(O)CHOH + H_2O \qquad \text{[R28]}$$

$$CH_3C(O)CHOH + O_2 \longrightarrow CH_3C(O)CHO + HO_2 \qquad \text{[R29]}$$

It has previously been shown that the maximum number of exceedance events in the 8 h NAAQS for ozone in India (100 $\mu\,g\,m^{-3}$) occurred in the north-west Indo-Gangetic Plain during the month of May, which is strongly affected by the crop residue biomass fires. It was also observed in Chapter 2 that the ozone enhancement increased from 19 ppb to 28 ppb between pre-harvest and post-harvest summertime air of the north-west IGP for the air masses with high residence time over the burnt agricultural fields.
Several previous studies from the Indo-Gangetic plain region (for example Rajput et al. (2014) and Ram et al. (2010) have also reported direct emissions and secondary formation of carbonaceous aerosol particles such as elemental carbon and organic carbon including polycyclic aromatic hydrocarbons from the agricultural residue fires. Based on the estimates by Rajput et al. (2014) circa 26 % and $\sim$ 7 % of the $PM_{2.5}$ mass fraction is organic carbon and elemental carbon respectively in the wheat residue emissions from the IGP region. PM data from IISER Mohali atmospheric chemistry facility, during the period of this study show that between the NCFI and CFI periods, the average mass concentration of $PM_{2.5}$ increased from 57 $\mu\,g\,m^{-3}$ to 100 $\mu\,g\,m^{-3}$ whereas for PM_{10} it increased from 128 $\mu\,g\,m^{-3}$ to 213 $\mu\,g\,m^{-3}$. Wheat residue fires in the summertime have already been reported to increase the number of NAAQS exceedance events for both PM_{10} and $PM_{2.5}$ in the north-west IGP (Pawar et al., 2015). Garg et al. (2015) have previously also reported co-emission of black carbon in three wheat residue fire plumes in May 2013. Calculation of the Secondary Organic Aerosol (SOA) production potential due to measured

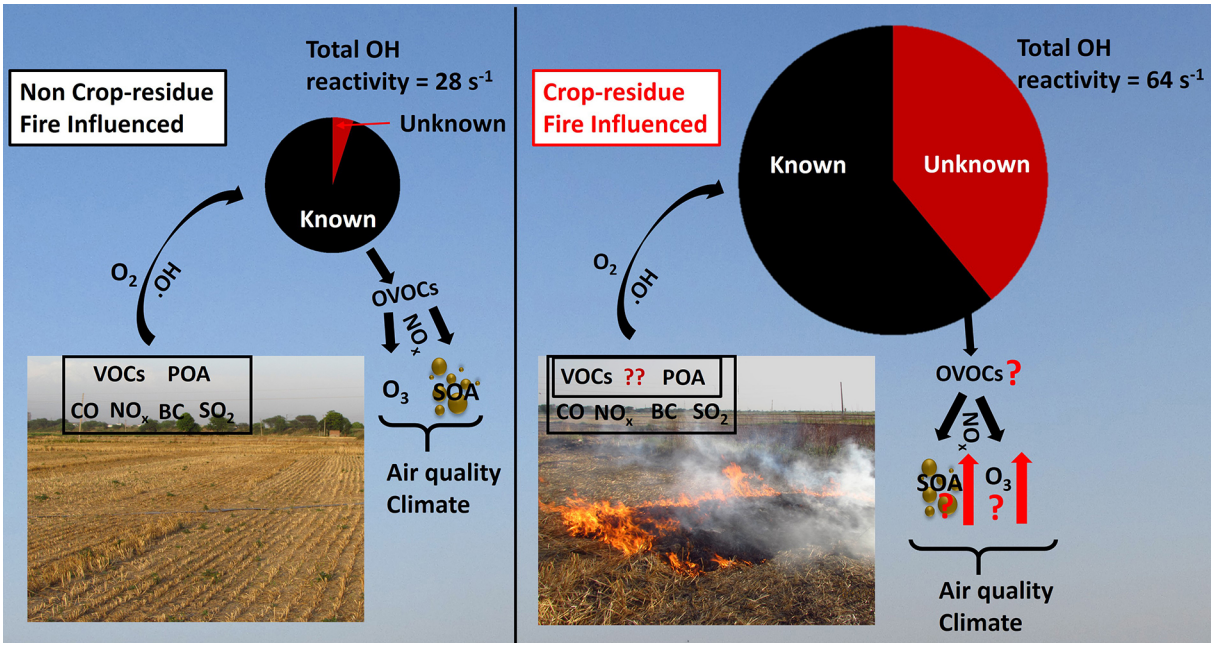

Figure 5.11: Diagram summarizing effects on air quality and climate relevant processes due to the large unknown suite of reactive compounds emitted directly and formed photochemically as a result of large scale agricultural crop-residue fires. The radius of the pie chart is scaled as per the observed total measured OH reactivities. SOA stands for secondary organic aerosol.

concentrations of toluene, benzene, xylene, isoprene and monoterpenes using the method used in Sarkar et al. (2016), showed a 40 % enhancement in SOA production potential due to these compounds between the NCFI (4.1 μ g m^{-3}) and CFI period (5.8 μ g m^{-3}). Detailed studies of SOA formation processes in similar biomass fire impacted atmospheric environments, also considering the role of amides and alkylamines which can participate in particle formation and growth processes (Tao et al., 2016) may be very important and will require further investigations.

Exposure to elevated concentrations of isocyanic acid has been documented to pose health risks (Roberts et al., 2011) and it is worth noting that the average hourly concentrations were always $>$ 1 ppb during the CFI periods. While alkylamines and amides can cause irritation in eye, skin and respiratory system upon high exposure, atmospheric oxidation of alkylamines in the presence of nitrogen oxides can also produce carcinogens like dimethylnitrosamine and dimethylnitramine ((Reactions [R30] - [R32]) (Ge et al., 2011)), which together with benzene, another known carcinogen emitted from the fires could pose enhanced health risks (Sarkar et al., 2013; Chandra and Sinha, 2016).

$$(CH_3)_2NH + OH \longrightarrow (CH_3)_2N + H_2O \qquad [R30]$$

$$(CH_3)_2N + NO_2 \longrightarrow (CH_3)_2N{-}NO_2 \quad \text{[R31]}$$

$$(CH_3)_2N + NO \longrightarrow (CH_3)_2N{-}NO \quad \text{[R32]}$$

Currently even the most detailed state-of-the art atmospheric chemistry models exclude formamide, acetamide, nitromethane and isocyanic acid and their highly reactive precursor alkyl-amines (e.g. methylamine, ethylamine, dimethylamine, trimethylamine). Thus, a larger suite of compounds and chemical reactions needs to be considered for air quality modeling of the resultant pollution haze. The large missing OH reactivity during periods affected by agricultural fires has major implications for understanding the formation of tropospheric ozone and other secondary pollutants in biomass fire impacted atmospheric environments (Figure 5.11).

5.4 Conclusion

This work reports the first ambient OH reactivity measurement in an atmospheric environment impacted by active fires from the under-studied north-west Indo-Gangetic plain. I have used the VOC-OHM technique for performing the measurement of ambient total OH reactivity and VOC concentrations. Crop residue fires in the summertime cause an enhancement in measured total OH reactivity from 28.0 s^{-1} to 64.1 s^{-1}. A corresponding increase was also observed in the calculated OH reactivity (due to measured OH reactants) from 15.0 s^{-1} to 21.0 s^{-1}. The measured OH reactants and their model calculated oxidation products were able to completely explain the total OH reactivity (missing OH reactivity was 5 % of the total which is well within the measurement uncertainty) in normal summertime condition while the same set of species could only explain 61 % of the total OH reactivity. Enhanced photochemical formation of several nitrogen containing oxygenated VOCs which are not included in current atmospheric chemistry models, was observed in the crop residue fire influenced period which confirms emission of their reactive precursors from the crop residue fires. The enhancement in their concentration from non crop residue fire influenced to crop residue fire influenced period correlated with the corresponding increase in the missing OH reactivity. As fire emissions are similar for same type of crop residue irrespective of their origin, to understand the impact of fires globally on atmospheric photochemical processes, it is necessary to focus attention on measurement of such compounds and and include them in the atmospheric chemistry models for accurate assessment of fire emission on the global atmospheric environment in

future studies. The concentrations of these VOCs are expected to increase in other areas of the world too, with their use in much-emphasized carbon capture and storage (Nielsen et al., 2012).

All the major compounds detected in the wheat stubble fires are also emitted from a large variety of biomass fuels burnt across various parts of world (Stockwell et al., 2015), including different types of crop residue, natural grasses and wood. However, the variation in the modified combustion efficiency and fuel type does change the emission factors of the VOCs. Emission factors during the flaming stage are not particularly high for wheat when compared to other fuel types. Thus while designing the ambient studies, it is important to take into account the major known emissions as highlighted in previous works (e.g. Stockwell et al. (2015) and Akagi et al. (2011)) and also discussed in this work. Emission factor recommendations for model predictions (Andreae and Merlet, 2001) typically use emission factors over the MCE range of 0.80 – 0.99. In order to accurately account for the emissions from the smoldering stages of biomass fires globally, emission factors at lower MCE, which can be significantly higher for some compounds should also be studied in detail in laboratory chamber studies of fires (if possible) and included in emission inventories used for model predictions.

As shown in this study incorporating direct OH reactivity measurements aids in accounting for the total gas phase reactivity and missing compounds. Future studies in the biomass burning affected regions including direct measurements of OH radicals and major OH radical production pathways in addition to the OH reactivity, could be very interesting also from the perspective of whether "shifts" in chemistry (Hofzumahaus et al., 2009; Lelieveld et al., 2008) occur and if so determining the net impact on the oxidation capacity of such perturbed atmospheric environments. As OH chemistry governs removal rate of climate active gases and formation of ozone and aerosol, these findings have major implications for understanding and predicting tropospheric chemistry and air-quality-climate feedbacks in fire-impacted atmospheric environments.

Chapter 6

Conclusions: Major findings and outlook

The Indo-Gangetic plain (IGP) which is home to more than one seventh of the world population faces serious environmental issues especially related to deteriorating air quality and consequent socio-economic and health impacts. This study reports the first two year-long (from August 2011 - September 2013) online in situ measurements of O_3, CO and NO_x at a regionally representative suburban site in the N.W. IGP. I have examined the ambient concentrations of O_3, CO and NO_x and the impact of season specific emissions (e.g. wheat residue fires in summer, paddy residue fires in post monsoon, biofuel combustion in winter) and meteorological conditions (e.g. availability of solar radiation, ambient temperature). The prevalence of agricultural crop residue fires in the summer and post monsoon seasons resulted in high $d[O_3]/dt$. In the summer season this caused $\sim$ 29 % enhancement in O_3, whereas, in the late post monsoon season, it caused an enhancement of $\sim$ 10 % in peak hourly O_3 concentrations despite lower radiation and temperatures compared to the early post monsoon. The enhancement in O_3 mixing ratios in the summertime was largest for air masses belonging to the local cluster, as they spent maximum contact time over the burning agricultural fields. The net rate of change of O_3 ($d[O_3]/dt$) from sunrise until attainment of peak daytime plateau region of diel profile was also observed to be the highest (9.2 ppb h^{-1}) during the fire influenced post monsoon seasons followed by 8.0 ppb h^{-1} during the clean post monsoon and fire influenced summer seasons. Exceedance of the 8h O_3 national ambient air quality standard (NAAQS) on 451 days during Aug 2011 - Sep 2013 ($\sim$ 62 %) suggests that regional surface O_3 pollution is serious and has been largely overlooked /unreported due to lack of in situ data from the region. Assessment of VOC specific O_3 production potentials using speciated VOC measurements will provide insights on VOCs responsible for high O_3 episodes and must be investigated on priority basis. Deployment of new instruments capable of directly measuring the in situ chemical

production of O_3 will improve apportionment of in situ chemical O_3 production and transported O_3 to ambient O_3 enhancements. Regulation of crop residue fires would certainly mitigate O_3 pollution and bring co-benefits for crop productivity, in particular for wheat, which is sown during winter in the N.W. IGP. The high summertime O_3 is not serious in terms of crop productivity as there are no standing crops at that time of the year, but impairs the regional air quality.

This work presents the first continuous long-term online measurement of a suite of 23 VOCs using a PTR-MS from the north-west Indo-Gangetic plain in Mohali for a period spanning from 01 March 2012 to 27 February 2013. In terms of their measured concentration, oxygenated VOCs are the most important among the measured VOCs with an annual average concentration of methanol, acetaldehyde, and acetone at 32.2, 5.9 and 5.6 ppb respectively. Despite being a suburban location, the annual average concentration of 1.6 ppb of isoprene is observed which is primarily due to biogenic emissions in the daytime and biomass burning emissions in the nighttime. Crop residue burning in the summer and post-monsoon seasons is found to cause approximately two-fold enhancements in evening and night time concentrations of acetonitrile, isoprene, aromatics and oxygenated VOCs. Very high seasonal average concentration of carcinogenic aromatic VOCs e.g. benzene and toluene at 1.5 and 2.5 ppb for the polluted summer and 2.4 and 3.5 ppb for polluted post monsoon respectively are observed. Favourable conditions for biogenic emissions e.g. soil moisture availability and uninterrupted sunlight in the clean post monsoon season results in maximum daytime observed concentrations of isoprene and acetaldehyde.

The average diel profile of OH reactivity due to measured species ranges between 8.1 s^{-1} and 40 s^{-1} in different seasons. Crop residue fires increase the night time VOC OH reactivity from 17.4 s^{-1} in the clean post monsoon to 34.8 s^{-1} and from 17.3 s^{-1} to 24.5 s^{-1} in the summertime. Isoprene and acetaldehyde are found to be the major contributor of reactive pollutant loading contributing to more than 38 % of the daytime VOC OH reactivity and ozone production potential in all the seasons. In terms of their OH reactivity contribution, among the different class of VOCs, oxygenated VOCs are the most important contributing to more than 37 % of the VOC OH reactivity and ozone production potential in all the seasons. The maximum VOC ozone production potential averaged for the peak daytime hours (11:00-14:00 L.T.) was observed to be 31.3 ppb h^{-1} in the clean post monsoon and the minimum was observed to be 10.2 ppb h^{-1} during winter. Crop residue fires in the summertime cause an increase of 7.5 ppb h^{-1} in the VOC ozone production potential from a baseline value of 15.3 ppb h^{-1}. The maximum calculated ozone production potential in the clean post monsoon does not correspond to the maximum observed ozone concentration. While the peak daytime ozone production is limited by the availability of NO_x in the clean post monsoon, both VOC and NO_x availability

strongly control the peak daytime ozone production in all other seasons. Future studies should include direct measurement of total OH reactivity and ozone production potential in all the seasons to accurately quantify the contribution of unmeasured VOCs towards the ozone production.

A new technique called VOC-OHM that enables rapid sequential measurements of ambient VOCs and total OH reactivity has been developed, validated and tested in the field with promising results. Whereas VOC-OHM is not a complete replacement for studies in which two PTR-MS systems can be deployed, as simultaneous measurements of both VOCs and OH reactivity are not possible with the system, its ability to measure both parameters with a gap of only few minutes ($\sim$ 13 minutes in this work) does open up new possibilities. VOC-OHM adds specificity to the PTR-MS equipped with a quadrupole mass analyser to distinguish the isobaric compounds by enabling direct measurement of their rate constants for reaction with OH radicals. There are several research groups and institutes in the world which possess only a single PTR-MS. This work provides a promising analytical technique to use the single PTR-MS for both total OH reactivity and ambient VOC measurements, and maximize the scientific outcome using available resources. This work also demonstrates a better and safer substitute for pressurized zero air bottles in the form of the gas calibration unit (GCU-A) which can be deploying for CRM OH reactivity field measurements. This system is a promising option for ground based air pollution and atmospheric chemistry studies, enabling instantaneous ozone production regimes (Sinha et al., 2012) and VOC speciation to be determined for policy makers. In addition to air pollution and atmospheric chemistry studies, the VOC-OHM system can also be applied for VOC headspace sampling studies in the food and flavour industry (Biasioli et al., 2011; Boscaini et al., 2004) and in chamber studies.

This work reports the first ambient OH reactivity measurement in an atmospheric environment impacted by active fires from the under-studied north-west Indo-Gangetic plain. I have used the VOC-OHM technique for performing the measurement of ambient total OH reactivity and VOC concentrations. Crop residue fires in the summertime cause an enhancement in measured total OH reactivity from 28.0 s^{-1} to 64.1 s^{-1}. A corresponding increase was also observed in the calculated OH reactivity (due to measured OH reactants) from 15.0 s^{-1} to 21.0 s^{-1}. The measured OH reactants and their model calculated oxidation products were able to completely explain the total OH reactivity (missing OH reactivity was 5 % of the total which is well within the measurement uncertainty) in normal summertime condition while the same set of species could only explain 61 % of the total OH reactivity. Enhanced photochemical formation of several nitrogen containing oxygenated VOCs which are not included in current atmospheric chemistry models, was observed in the crop residue fire influenced period which confirms emission of their

reactive precursors from the crop residue fires. The enhancement in their concentration from non-crop residue fire influenced to crop residue fire influenced period correlated with the corresponding increase in the missing OH reactivity. As fire emissions are similar for same type of crop residue irrespective of their origin, to understand the impact of fires globally on atmospheric photochemical processes, it is necessary to focus attention on measurement of such compounds and and include them in the atmospheric chemistry models for accurate assessment of fire emission on the global atmospheric environment in future studies. The concentrations of these VOCs are expected to increase in other areas of the world too, with their use in much-emphasized carbon capture and storage (Nielsen et al., 2012).

All the major compounds detected in the wheat stubble fires are also emitted from a large variety of biomass fuels burnt across various parts of world (Stockwell et al., 2015), including different types of crop residue, natural grasses and wood. However, the variation in the modified combustion efficiency and fuel type does change the emission factors of the VOCs. Emission factors during the flaming stage are not particularly high for wheat when compared to other fuel types. Thus while designing the ambient studies, it is important to take into account the major known emissions as highlighted in previous works (e.g. Stockwell et al. (2015) and Akagi et al. (2011)) and also discussed in this work. Emission factor recommendations for model predictions (Andreae and Merlet, 2001) typically use emission factors over the MCE range of 0.80 – 0.99. In order to accurately account for the emissions from the smoldering stages of biomass fires globally, emission factors at lower MCE, which can be significantly higher for some compounds should also be studied in detail in laboratory chamber studies of fires (if possible) and included in emission inventories used for model predictions.

As shown in this study incorporating direct OH reactivity measurements aids in accounting for the total gas phase reactivity and missing compounds. Future studies in the biomass burning affected regions including direct measurements of OH radicals and major OH radical production pathways in addition to the OH reactivity, could be very interesting also from the perspective of whether "shifts" in chemistry (Hofzumahaus et al., 2009; Lelieveld et al., 2008) occur and if so determining the net impact on the oxidation capacity of such perturbed atmospheric environments. As OH chemistry governs removal rate of climate active gases and formation of ozone and aerosol, these findings have major implications for understanding and predicting tropospheric chemistry and air-quality-climate feedbacks in fire-impacted atmospheric environments.

Thus, overall my thesis work and its findings represent major advancements in acquisition of new strategic knowledge necessary for detailed quantitative understanding of the impact of open fires on atmospheric composition and chemistry over the north-

west Indo-Gangetic Plain and the chemical speciation and reactivity perturbations that can be caused by large scale biomass fires, an emission activity that impacts the global atmosphere and occurs on varied temporal and spatial scales worldwide.

List of Figures

List of Tables

Bibliography

Aggarwal, P. K., Joshi, P. K., Ingram, J. S. I., and Gupta, R. K.: Adapting food systems of the Indo-Gangetic plains to global environmental change: key information needs to improve policy formulation, Environmental Science & Policy, 7, 487–498, doi:10.1016/j.envsci.2004.07.006, URL http://www.sciencedirect.com/science/article/pii/S1462901104000978, 2004.

Ahammed, Y. N., Reddy, R. R., Gopal, K. R., Narasimhulu, K., Basha, D. B., Reddy, L. S. S., and Rao, T. V. R.: Seasonal variation of the surface ozone and its precursor gases during 2001–2003, measured at Anantapur (14.62°N), a semi-arid site in India, Atmospheric Research, 80, 151–164, doi:10.1016/j.atmosres.2005.07.002, URL http://www.sciencedirect.com/science/article/pii/S0169809505001894, 2006.

Akagi, S. K., Yokelson, R. J., Wiedinmyer, C., Alvarado, M. J., Reid, J. S., Karl, T., Crounse, J. D., and Wennberg, P. O.: Emission factors for open and domestic biomass burning for use in atmospheric models, Atmos. Chem. Phys., 11, 4039–4072, doi:10.5194/acp-11-4039-2011, URL http://www.atmos-chem-phys.net/11/4039/2011/, 2011.

Ammann, C., Spirig, C., Neftel, A., Steinbacher, M., Komenda, M., and Schaub, A.: Application of PTR-MS for measurements of biogenic VOC in a deciduous forest, International Journal of Mass Spectrometry, 239, 87–101, doi:http://doi.org/10.1016/j.ijms.2004.08.012, URL http://www.sciencedirect.com/science/article/pii/S1387380604003884, 2004.

Ammann, C., Brunner, A., Spirig, C., and Neftel, A.: Technical note: Water vapour concentration and flux measurements with PTR-MS, Atmos. Chem. Phys., 6, 4643–4651, doi:10.5194/acp-6-4643-2006, URL http://www.atmos-chem-phys.net/6/4643/2006/, 2006.

Andreae, M. O. and Merlet, P.: Emission of trace gases and aerosols from biomass burning, Global Biogeochem. Cycles, 15, 955–966, doi:10.1029/2000gb001382, URL http://dx.doi.org/10.1029/2000GB001382, 2001.

Andreae, M. O., Rosenfeld, D., Artaxo, P., Costa, A. A., Frank, G. P., Longo, K. M., and Silva-Dias, M. A. F.: Smoking Rain Clouds over the Amazon, Science, 303, 1337–1342, doi:10.1126/science.1092779, 2004.

Andreae, M. O., Artaxo, P., Beck, V., Bela, M., Freitas, S., Gerbig, C., Longo, K., Munger, J. W., Wiedemann, K. T., and Wofsy, S. C.: Carbon monoxide and related trace gases and aerosols over the Amazon Basin during the wet and dry seasons, Atmos. Chem. Phys., 12, 6041–6065, doi:10.5194/acp-12-6041-2012, URL http://www.atmos-chem-phys.net/12/6041/2012/, 2012.

Ashworth, K., Wild, O., Eller, A. S. D., and Hewitt, C. N.: Impact of Biofuel Poplar Cultivation on Ground-Level Ozone and Premature Human Mortality Depends on Cultivar Selection and Planting Location, Environmental Science & Technology, 49, 8566–8575, doi:10.1021/acs.est.5b00266, URL http://dx.doi.org/10.1021/acs.est.5b00266, 2015.

Atkinson, R.: Kinetics and mechanisms of the gas-phase reactions of the hydroxyl radical with organic compounds under atmospheric conditions, Chemical Reviews, 86, 69–201, doi:10.1021/cr00071a004, URL http://dx.doi.org/10.1021/cr00071a004, 1986.

Atkinson, R.: Kinetics of the gas-phase reactions of OH radicals with alkanes and cycloalkanes, Atmos. Chem. Phys., 3, 2233–2307, doi:10.5194/acp-3-2233-2003, URL http://www.atmos-chem-phys.net/3/2233/2003/, 2003.

Atkinson, R. and Arey, J.: Atmospheric Degradation of Volatile Organic Compounds, Chemical Reviews, 103, 4605–4638, doi:10.1021/cr0206420, URL http://dx.doi.org/10.1021/cr0206420, 2003.

Atkinson, R. and Aschmann, S. M.: Rate constants for the reactions of O3 and OH radicals with a series of alkynes, International Journal of Chemical Kinetics, 16, 259–268, doi:10.1002/kin.550160308, URL http://dx.doi.org/10.1002/kin.550160308, 1984.

Atkinson, R. and Carter, W. P. L.: Kinetics and mechanisms of the gas-phase reactions of ozone with organic compounds under atmospheric conditions, Chemical Reviews, 84, 437–470, doi:10.1021/cr00063a002, URL http://pubs.acs.org/doi/abs/10.1021/cr00063a002, 1984.

Atkinson, R., Aschmann, S. M., and Carter, W. P. L.: Kinetics of the reactions of O3 and OH radicals with furan and thiophene at 298 ± 2 K, International Journal of Chemical

Kinetics, 15, 51–61, doi:10.1002/kin.550150106, URL http://dx.doi.org/10.1002/kin.550150106, 1983.

Atkinson, R., Aschmann, S. M., Winer, A. M., and Carter, W. P. L.: Rate constants for the gas phase reactions of OH radicals and O3 with pyrrole at 295 ± 1 K and atmospheric pressure, Atmospheric Environment (1967), 18, 2105–2107, doi:10.1016/0004-6981(84)90196-3, URL http://www.sciencedirect.com/science/article/pii/0004698184901963, 1984.

Atkinson, R., Baulch, D. L., Cox, R. A., Crowley, J. N., Hampson, R. F., Hynes, R. G., Jenkin, M. E., Rossi, M. J., and Troe, J.: Evaluated kinetic and photochemical data for atmospheric chemistry: Volume I - gas phase reactions of Ox, HOx, NOx and SOx species, Atmos. Chem. Phys., 4, 1461–1738, doi:10.5194/acp-4-1461-2004, URL http://www.atmos-chem-phys.net/4/1461/2004/, 2004.

Atkinson, R., Baulch, D. L., Cox, R. A., Crowley, J. N., Hampson, R. F., Hynes, R. G., Jenkin, M. E., Rossi, M. J., Troe, J., and Subcommittee, I.: Evaluated kinetic and photochemical data for atmospheric chemistry: Volume II - gas phase reactions of organic species, Atmos. Chem. Phys., 6, 3625–4055, doi:10.5194/acp-6-3625-2006, URL http://www.atmos-chem-phys.net/6/3625/2006/, 2006.

Badarinath, K. V. S., Chand, T. R. K., and Prasad, V. K.: Agriculture crop residue burning in the Indo-Gangetic Plains - A study using IRS-P6 AWiFS satellite data, Current Science, 91, 1085–1089, 2006.

Bahuguna, A.: Agricultural statistics at a glance 2014, Report, Ministry of Agriculture, URL eands.dacnet.nic.in/PDF/Agricultural-Statistics-At-Glance2014.pdf, 2015.

Bandow, H. and Washida, N.: Ring-cleavage Reactions of Aromatic Hydrocarbons Studied by FT–IR Spectroscopy. III. Photooxidation of 1,2,3-, 1,2,4-, and 1,3,5-Trimethylbenzenes in the NOx–Air System, Bulletin of the Chemical Society of Japan, 58, 2549–2555, doi:10.1246/bcsj.58.2549, URL http://dx.doi.org/10.1246/bcsj.58.2549, 1985.

Barletta, B., Meinardi, S., Simpson, I. J., Khwaja, H. A., Blake, D. R., and Rowland, F. S.: Mixing ratios of volatile organic compounds (VOCs) in the atmosphere of Karachi, Pakistan, Atmospheric Environment, 36, 3429–3443, doi:10.1016/S1352-2310(02)00302-3, URL http://www.sciencedirect.com/science/article/pii/S1352231002003023, 2002.

Bergamaschi, P., Hein, R., Brenninkmeijer, C. A. M., and Crutzen, P. J.: Inverse modeling of the global CO cycle: 2. Inversion of 13C/12C and 18O/16O isotope ratios, Journal of Geophysical Research: Atmospheres, 105, 1929–1945, doi:10.1029/1999JD900819, URL http://dx.doi.org/10.1029/1999JD900819, 2000.

Berndt, T., Richters, S., Jokinen, T., Hyttinen, N., Kurtén, T., Otkjær, R. V., Kjaergaard, H. G., Stratmann, F., Herrmann, H., Sipilä, M., Kulmala, M., and Ehn, M.: Hydroxyl radical-induced formation of highly oxidized organic compounds, Nature Communications, 7, 13 677, doi:10.1038/ncomms13677, URL http://dx.doi.org/10.1038/ncomms13677, 2016.

Biasioli, F., Gasperi, F., Yeretzian, C., and Märk, T. D.: PTR-MS monitoring of VOCs and BVOCs in food science and technology, TrAC Trends in Analytical Chemistry, 30, 968–977, doi:10.1016/j.trac.2011.03.009, URL http://www.sciencedirect.com/science/article/pii/S0165993611001233, 2011.

Blake, R. S., Monks, P. S., and Ellis, A. M.: Proton-Transfer Reaction Mass Spectrometry, Chemical Reviews, 109, 861–896, doi:10.1021/cr800364q, URL http://dx.doi.org/10.1021/cr800364q, 2009.

Boscaini, E., Mikoviny, T., Wisthaler, A., Hartungen, E. v., and Märk, T. D.: Characterization of wine with PTR-MS, International Journal of Mass Spectrometry, 239, 215–219, doi:10.1016/j.ijms.2004.07.023, URL http://www.sciencedirect.com/science/article/pii/S1387380604003537, 2004.

Bowman, D. M. J. S., Balch, J. K., Artaxo, P., Bond, W. J., Carlson, J. M., Cochrane, M. A., D'Antonio, C. M., DeFries, R. S., Doyle, J. C., Harrison, S. P., Johnston, F. H., Keeley, J. E., Krawchuk, M. A., Kull, C. A., Marston, J. B., Moritz, M. A., Prentice, I. C., Roos, C. I., Scott, A. C., Swetnam, T. W., van der Werf, G. R., and Pyne, S. J.: Fire in the Earth System, Science, 324, 481–484, doi:10.1126/science.1163886, URL http://www.sciencemag.org/content/324/5926/481.abstract, 2009.

Brain, C. K. and Sillent, A.: Evidence from the Swartkrans cave for the earliest use of fire, Nature, 336, 464–466, doi:10.1038/336464a0, URL http://dx.doi.org/10.1038/336464a0, 10.1038/336464a0, 1988.

Brune, W., Bloss, W., Shi, Z., Pope, F., Fuller, G., Monks, P. S., Tomlin, A., Karl, T., Hort, M., Mohr, C., MacKenzie, R., Vlachou, A., Tian, Z., Kramer, L. J., Heard, D., Purvis, R., Querol, X., Baltensperger, U., Dunmore, R., Harrison, R., Murrells, T., Jimenez, J. L., Cross, E., McFiggans, G., Kiendler-Scharr, A., Ho, T.-R., Charron,

A., Wallington, T., Krishna Kumar, N., Pieber, S., Geiger, F., Wahner, A., Mitchell, E., Prevot, A., Skouloudis, A., Kalberer, M., McDonald, B., Hewitt, C. N., Sioutas, C., Donahue, N. M., Lee, J., van Pinxteren, D., Moller, S., Minguillon, M. C., Shafer, M., Carslaw, D., Ehlers, C., and Pandis, S.: Urban case studies: general discussion, Faraday Discussions, 189, 473–514, doi:10.1039/C6FD90021F, URL http://dx.doi.org/10.1039/C6FD90021F, 2016.

Carlton, A. G., Wiedinmyer, C., and Kroll, J. H.: A review of Secondary Organic Aerosol (SOA) formation from isoprene, Atmos. Chem. Phys., 9, 4987–5005, doi:10.5194/acp-9-4987-2009, URL http://www.atmos-chem-phys.net/9/4987/2009/, 2009.

Carslaw, D. C. and Ropkins, K.: openair — An R package for air quality data analysis, Environmental Modelling & Software, 27–28, 52 – 61, doi:10.1016/j.envsoft.2011.09.008, URL http://www.sciencedirect.com/science/article/pii/S1364815211002064, 2012.

Carter, W. P. L.: Development of Ozone Reactivity Scales for Volatile Organic Compounds, Air & Waste, 44, 881–899, doi:10.1080/1073161X.1994.10467290, URL http://dx.doi.org/10.1080/1073161X.1994.10467290, 1994.

Cazorla, M. and Brune, W. H.: Measurement of Ozone Production Sensor, Atmos. Meas. Tech., 3, 545–555, doi:10.5194/amt-3-545-2010, URL http://www.atmos-meas-tech.net/3/545/2010/, 2010.

Chandra, B. P. and Sinha, V.: Contribution of post-harvest agricultural paddy residue fires in the N.W. Indo-Gangetic Plain to ambient carcinogenic benzenoids, toxic isocyanic acid and carbon monoxide, Environment International, 88, 187–197, doi:10.1016/j.envint.2015.12.025, URL http://www.sciencedirect.com/science/article/pii/S016041201530129X, 2016.

Chandra, B. P., Sinha, V., Hakkim, H., and Sinha, B.: Storage stability studies and field application of low cost glass flasks for analyses of thirteen ambient VOCs using proton transfer reaction mass spectrometry, Int. J. Mass Spectrom., In press, doi:10.1016/j.ijms.2017.05.008, 2017.

Chaney, L. W. and McClenny, W. A.: Unique ambient carbon monoxide monitor based on gas filter correlation: performance and application, Environmental Science & Technology, 11, 1186–1190, doi:10.1021/es60136a010, URL http://dx.doi.org/10.1021/es60136a010, 1977.

Charlson, R. J., Lovelock, J. E., Andreae, M. O., and Warren, S. G.: Oceanic phytoplankton, atmospheric sulphur, cloud albedo and climate, Nature, 326, 655–661, URL http://dx.doi.org/10.1038/326655a0, 10.1038/326655a0, 1987.

Christian, T. J., Kleiss, B., Yokelson, R. J., Holzinger, R., Crutzen, P. J., Hao, W. M., Saharjo, B. H., and Ward, D. E.: Comprehensive laboratory measurements of biomass-burning emissions: 1. Emissions from Indonesian, African, and other fuels, Journal of Geophysical Research: Atmospheres, 108, 4719, doi:10.1029/2003jd003704, URL http://dx.doi.org/10.1029/2003JD003704, 2003.

Crutzen, P., Williams, J., Pöschl, U., Hoor, P., Fischer, H., Warneke, C., Holzinger, R., Hansel, A., Lindinger, W., Scheeren, B., and Lelieveld, J.: High spatial and temporal resolution measurements of primary organics and their oxidation products over the tropical forests of Surinam, Atmospheric Environment, 34, 1161 – 1165, doi:http://dx.doi.org/10.1016/S1352-2310(99)00482-3, URL http://www.sciencedirect.com/science/article/pii/S1352231099004823, 2000.

Crutzen, P. J. and Andreae, M. O.: Biomass Burning in the Tropics: Impact on Atmospheric Chemistry and Biogeochemical Cycles, Science, 250, 1669–1678, doi:10.1126/science.250.4988.1669, 1990.

Curtis, A. R. and Sweetenham, W. P.: Facsimile/Chekmat Users Manual, AERE Report, R-12805, Her Majesty's Stationary Office England, URL https://books.google.co.in/books?id=doE4cgAACAAJ, 1988.

Davies, D. K., Ilavajhala, S., Wong, M. M., and Justice, C. O.: Fire Information for Resource Management System: Archiving and Distributing MODIS Active Fire Data, IEEE Transactions on Geoscience and Remote Sensing, 47, 72–79, doi:10.1109/TGRS.2008.2002076, 2009.

de Gouw, J. and Warneke, C.: Measurements of volatile organic compounds in the earth's atmosphere using proton-transfer-reaction mass spectrometry, Mass Spectrometry Reviews, 26, 223–257, doi:10.1002/mas.20119, URL http://dx.doi.org/10.1002/mas.20119, 2007.

de Gouw, J. A., Welsh-Bon, D., Warneke, C., Kuster, W. C., Alexander, L., Baker, A. K., Beyersdorf, A. J., Blake, D. R., Canagaratna, M., Celada, A. T., Huey, L. G., Junkermann, W., Onasch, T. B., Salcido, A., Sjostedt, S. J., Sullivan, A. P., Tanner, D. J., Vargas, O., Weber, R. J., Worsnop, D. R., Yu, X. Y., and Zaveri, R.: Emission and chemistry of organic carbon in the gas and aerosol phase at a sub-urban site near

Mexico City in March 2006 during the MILAGRO study, Atmos. Chem. Phys., 9, 3425–3442, doi:10.5194/acp-9-3425-2009, URL http://www.atmos-chem-phys.net/9/3425/2009/, 2009.

Derwent, R. G., Jenkin, M. E., and Saunders, S. M.: Photochemical ozone creation potentials for a large number of reactive hydrocarbons under European conditions, Atmospheric Environment, 30, 181–199, doi:10.1016/1352-2310(95)00303-G, URL http://www.sciencedirect.com/science/article/pii/135223109500303G, 1996.

Destaillats, H., Spaulding, R. S., and Charles, M. J.: Ambient Air Measurement of Acrolein and Other Carbonyls at the Oakland-San Francisco Bay Bridge Toll Plaza, Environmental Science & Technology, 36, 2227–2235, doi:10.1021/es011394c, URL http://dx.doi.org/10.1021/es011394c, 2002.

Di Carlo, P., Brune, W. H., Martinez, M., Harder, H., Lesher, R., Ren, X., Thornberry, T., Carroll, M. A., Young, V., Shepson, P. B., Riemer, D., Apel, E., and Campbell, C.: Missing OH Reactivity in a Forest: Evidence for Unknown Reactive Biogenic VOCs, Science, 304, 722–725, doi:10.1126/science.1094392, URL http://www.sciencemag.org/content/304/5671/722.abstract, 2004.

Dillon, T. J., Tucceri, M. E., Dulitz, K., Horowitz, A., Vereecken, L., and Crowley, J. N.: Reaction of Hydroxyl Radicals with C4H5N (Pyrrole): Temperature and Pressure Dependent Rate Coefficients, The Journal of Physical Chemistry A, 116, 6051–6058, doi:10.1021/jp211241x, URL http://dx.doi.org/10.1021/jp211241x, 2012.

Dolgorouky, C., Gros, V., Sarda-Esteve, R., Sinha, V., Williams, J., Marchand, N., Sauvage, S., Poulain, L., Sciare, J., and Bonsang, B.: Total OH reactivity measurements in Paris during the 2010 MEGAPOLI winter campaign, Atmos. Chem. Phys., 12, 9593–9612, doi:10.5194/acp-12-9593-2012, URL http://www.atmos-chem-phys.net/12/9593/2012/, 2012.

Dotan, I., Albritton, D. L., Lindinger, W., and Pahl, M.: Mobilities of CO2+, N2H+, H3O+, H3O+·H2O, and H3O+· (H2O)2 ions in N2, The Journal of Chemical Physics, 65, 5028–5030, doi:10.1063/1.432943, URL http://dx.doi.org/10.1063/1.432943http://aip.scitation.org/doi/10.1063/1.432943, 1976.

Dutta, C., Som, D., Chatterjee, A., Mukherjee, A. K., Jana, T. K., and Sen, S.: Mixing ratios of carbonyls and BTEX in ambient air of Kolkata, India and their associated health risk, Environmental Monitoring and Assessment, 148, 97–107, doi:10.1007/s10661-007-0142-0, URL https://doi.org/10.1007/s10661-007-0142-0, 2009.

Edwards, P. M., Evans, M. J., Furneaux, K. L., Hopkins, J., Ingham, T., Jones, C., Lee, J. D., Lewis, A. C., Moller, S. J., Stone, D., Whalley, L. K., and Heard, D. E.: OH reactivity in a South East Asian tropical rainforest during the Oxidant and Particle Photochemical Processes (OP3) project, Atmos. Chem. Phys., 13, 9497–9514, doi:10.5194/acp-13-9497-2013, URL http://www.atmos-chem-phys.net/13/9497/2013/, 2013.

Eerdekens, G., Yassaa, N., Sinha, V., Aalto, P. P., Aufmhoff, H., Arnold, F., Fiedler, V., Kulmala, M., and Williams, J.: VOC measurements within a boreal forest during spring 2005: on the occurrence of elevated monoterpene concentrations during night time intense particle concentration events, Atmos. Chem. Phys., 9, 8331–8350, doi:10.5194/acp-9-8331-2009, URL http://www.atmos-chem-phys.net/9/8331/2009/, 2009.

Elshorbany, Y. F., Kleffmann, J., Hofzumahaus, A., Kurtenbach, R., Wiesen, P., Brauers, T., Bohn, B., Dorn, H. P., Fuchs, H., Holland, F., Rohrer, F., Tillmann, R., Wegener, R., Wahner, A., Kanaya, Y., Yoshino, A., Nishida, S., Kajii, Y., Martinez, M., Kubistin, D., Harder, H., Lelieveld, J., Elste, T., Plass-Dülmer, C., Stange, G., Berresheim, H., and Schurath, U.: HOx budgets during HOxComp: A case study of HOx chemistry under NOx-limited conditions, Journal of Geophysical Research: Atmospheres, 117, D03 307, doi:10.1029/2011JD017008, URL http://dx.doi.org/10.1029/2011JD017008, 2012.

FAO: FAO Statistical Yearbook 2013: World Food and Agriculture, (Food and Agriculture Organization), FOOD & AGRICULTURE ORGN, URL https://books.google.co.in/books?id=ustmmgEACAAJ, 2013.

Feister, U. and Grewe, R.: SPECTRAL ALBEDO MEASUREMENTS IN THE UV and VISIBLE REGION OVER DIFFERENT TYPES OF SURFACES, Photochemistry and Photobiology, 62, 736–744, doi:10.1111/j.1751-1097.1995.tb08723.x, URL http://dx.doi.org/10.1111/j.1751-1097.1995.tb08723.x, 1995.

Finlayson-Pitts, B. J. and Jr., J. N. P.: {CHAPTER} 14 - Global Tropospheric Chemistry and Climate Change, in: Chemistry of the Upper and Lower Atmosphere, edited by Finlayson-Pitts, B. J. and Pitts, J. N., pp. 762 – 843, Academic Press, San Diego, doi:https://doi.org/10.1016/B978-012257060-5/50016-2, URL http://www.sciencedirect.com/science/article/pii/B9780122570605500162, 2000.

Fortner, E. C., Zheng, J., Zhang, R., Berk Knighton, W., Volkamer, R. M., Sheehy, P., Molina, L., and André, M.: Measurements of Volatile Organic Compounds Using Proton Transfer Reaction – Mass Spectrometry during the MILAGRO 2006 Cam-

paign, Atmos. Chem. Phys., 9, 467–481, doi:10.5194/acp-9-467-2009, URL http://www.atmos-chem-phys.net/9/467/2009/, 2009.

Fuchs, H., Novelli, A., Rolletter, M., Hofzumahaus, A., Pfannerstill, E. Y., Kessel, S., Edtbauer, A., Williams, J., Michoud, V., Dusanter, S., Locoge, N., Zannoni, N., Gros, V., Truong, F., Sarda-Esteve, R., Cryer, D. R., Brumby, C. A., Whalley, L. K., Stone, D., Seakins, P. W., Heard, D. E., Schoemaecker, C., Blocquet, M., Coudert, S., Batut, S., Fittschen, C., Thames, A. B., Brune, W. H., Ernest, C., Harder, H., Muller, J. B. A., Elste, T., Kubistin, D., Andres, S., Bohn, B., Hohaus, T., Holland, F., Li, X., Rohrer, F., Kiendler-Scharr, A., Tillmann, R., Wegener, R., Yu, Z., Zou, Q., and Wahner, A.: Comparison of OH reactivity measurements in the atmospheric simulation chamber SAPHIR, Atmospheric Measurement Techniques, 10, 4023–4053, doi:10.5194/amt-10-4023-2017, URL https://www.atmos-meas-tech.net/10/4023/2017/, 2017.

Garg, S., Chandra, B. P., Sinha, V., Sarda-Esteve, R., Gros, V., and Sinha, B.: Limitation of the Use of the Absorption Angstrom Exponent for Source Apportionment of Equivalent Black Carbon: a Case Study from the North West Indo-Gangetic Plain, Environmental Science & Technology, doi:10.1021/acs.est.5b03868, URL http://dx.doi.org/10.1021/acs.est.5b03868, 2015.

Gaur, A., Tripathi, S. N., Kanawade, V. P., Tare, V., and Shukla, S. P.: Four-year measurements of trace gases (SO2, NOx, CO, and O3) at an urban location, Kanpur, in Northern India, Journal of Atmospheric Chemistry, pp. 1–19, doi:10.1007/s10874-014-9295-8, URL http://dx.doi.org/10.1007/s10874-014-9295-8, 2014.

Gautam, R.: Challenges in Early Warning of the Persistent and Widespread Winter Fog over the Indo-Gangetic Plains: A Satellite Perspective, book section 3, pp. 51–61, Springer Netherlands, Dordrecht, doi:10.1007/978-94-017-8598-3_3, URL http://dx.doi.org/10.1007/978-94-017-8598-3_3, 2014.

Ge, X., Wexler, A. S., and Clegg, S. L.: Atmospheric amines – Part I. A review, Atmos. Environ., 45, 524–546, doi:10.1016/j.atmosenv.2010.10.012, URL www.sciencedirect.com/science/article/pii/S1352231010008745, 2011.

Gerosa, G., Ferretti, M., Bussotti, F., and Rocchini, D.: Estimates of ozone AOT40 from passive sampling in forest sites in South-Western Europe, Environmental Pollution, 145, 629–635, doi:10.1016/j.envpol.2006.02.030, URL http://www.sciencedirect.com/science/article/pii/S0269749106001941, 2007.

Ghude, S., Jain, S. L., Arya, B. C., Beig, G., Ahammed, Y. N., Kumar, A., and Tyagi, B.: Ozone in ambient air at a tropical megacity, Delhi: characteristics, trends and cumulative ozone exposure indices, Journal of Atmospheric Chemistry, 60, 237–252, doi: 10.1007/s10874-009-9119-4, URL http://dx.doi.org/10.1007/s10874-009-9119-4, 2008.

Giles, J.: Hikes in surface ozone could suffocate crops, Nature, 435, 7–7, doi:10.1038/435007a, URL http://dx.doi.org/10.1038/435007a, 10.1038/435007a, 2005.

Gilman, J. B., Lerner, B. M., Kuster, W. C., Goldan, P. D., Warneke, C., Veres, P. R., Roberts, J. M., de Gouw, J. A., Burling, I. R., and Yokelson, R. J.: Biomass burning emissions and potential air quality impacts of volatile organic compounds and other trace gases from fuels common in the US, Atmos. Chem. Phys., 15, 13 915–13 938, doi:10.5194/acp-15-13915-2015, URL http://www.atmos-chem-phys.net/15/13915/2015/, 2015.

Gligorovski, S., Strekowski, R., Barbati, S., and Vione, D.: Environmental Implications of Hydroxyl Radicals (•OH), Chemical Reviews, 115, 13 051–13 092, doi:10.1021/cr500310b, URL http://pubs.acs.org/doi/full/10.1021/cr500310b, 2015.

Goldstein, A. H. and Galbally, I. E.: Known and Unexplored Organic Constituents in the Earth's Atmosphere, Environmental Science & Technology, 41, 1514–1521, doi: 10.1021/es072476p, URL http://dx.doi.org/10.1021/es072476p, 2007.

Granier, C., Bessagnet, B., Bond, T., D'Angiola, A., Denier van der Gon, H., Frost, G. J., Heil, A., Kaiser, J. W., Kinne, S., Klimont, Z., Kloster, S., Lamarque, J.-F., Liousse, C., Masui, T., Meleux, F., Mieville, A., Ohara, T., Raut, J.-C., Riahi, K., Schultz, M. G., Smith, S. J., Thompson, A., van Aardenne, J., van der Werf, G. R., and van Vuuren, D. P.: Evolution of anthropogenic and biomass burning emissions of air pollutants at global and regional scales during the 1980–2010 period, Climatic Change, 109, 163, doi: 10.1007/s10584-011-0154-1, URL http://dx.doi.org/10.1007/s10584-011-0154-1, 2011.

Guenther, A., Karl, T., Harley, P., Wiedinmyer, C., Palmer, P. I., and Geron, C.: Estimates of global terrestrial isoprene emissions using MEGAN (Model of Emissions of Gases and Aerosols from Nature), Atmos. Chem. Phys., 6, 3181–3210, doi:10.5194/acp-6-3181-2006, URL http://www.atmos-chem-phys.net/6/3181/2006/, 2006.

Guenther, A. B., Monson, R. K., and Fall, R.: Isoprene and monoterpene emission rate variability: Observations with eucalyptus and emission rate algorithm de-

velopment, Journal of Geophysical Research: Atmospheres, 96, 10 799–10 808, doi:10.1029/91JD00960, URL http://dx.doi.org/10.1029/91JD00960, 1991.

Haagen-Smit, A. J.: Chemistry and Physiology of Los Angeles Smog, Industrial & Engineering Chemistry, 44, 1342–1346, doi:10.1021/ie50510a045, URL http://dx.doi.org/10.1021/ie50510a045, 1952.

Hansen, R. F., Griffith, S. M., Dusanter, S., Rickly, P. S., Stevens, P. S., Bertman, S. B., Carroll, M. A., Erickson, M. H., Flynn, J. H., Grossberg, N., Jobson, B. T., Lefer, B. L., and Wallace, H. W.: Measurements of total hydroxyl radical reactivity during CABINEX 2009 – Part 1: field measurements, Atmos. Chem. Phys., 14, 2923–2937, doi:10.5194/acp-14-2923-2014, URL http://www.atmos-chem-phys.net/14/2923/2014/, 2014.

Hansen, R. F., Blocquet, M., Schoemaecker, C., Léonardis, T., Locoge, N., Fittschen, C., Hanoune, B., Stevens, P. S., Sinha, V., and Dusanter, S.: Intercomparison of the comparative reactivity method (CRM) and pump–probe technique for measuring total OH reactivity in an urban environment, Atmos. Meas. Tech., 8, 4243–4264, doi:10.5194/amt-8-4243-2015, URL http://www.atmos-meas-tech.net/8/4243/2015/, 2015.

Harari, Y.: Sapiens: A Brief History of Humankind, HarperCollins, URL https://books.google.co.in/books?id=FmyBAwAAQBAJ, 2015.

Hatch, L. E., Yokelson, R. J., Stockwell, C. E., Veres, P. R., Simpson, I. J., Blake, D. R., Orlando, J. J., and Barsanti, K. C.: Multi-instrument comparison and compilation of non-methane organic gas emissions from biomass burning and implications for smoke-derived secondary organic aerosol precursors, Atmos. Chem. Phys., 17, 1471–1489, doi:10.5194/acp-17-1471-2017, URL https://www.atmos-chem-phys.net/17/1471/2017/, 2017.

Heard, D., ed.: Analytical techniques for atmospheric measurement, John Wiley & Sons, URL http://as.wiley.com/WileyCDA/WileyTitle/productCd-1405123575.html, 2008.

Heard, D. E. and Pilling, M. J.: Measurement of OH and HO2 in the Troposphere, Chemical Reviews, 103, 5163–5198, doi:10.1021/cr020522s, URL http://dx.doi.org/10.1021/cr020522s, 2003.

Hens, K., Novelli, A., Martinez, M., Auld, J., Axinte, R., Bohn, B., Fischer, H., Keronen, P., Kubistin, D., Nölscher, A. C., Oswald, R., Paasonen, P., Petäjä, T., Regelin, E., Sander, R., Sinha, V., Sipilä, M., Taraborrelli, D., Tatum Ernest, C., Williams, J.,

Lelieveld, J., and Harder, H.: Observation and modelling of HOx radicals in a boreal forest, Atmos. Chem. Phys., 14, 8723–8747, doi:10.5194/acp-14-8723-2014, URL http://www.atmos-chem-phys.net/14/8723/2014/, 2014.

Hewitt, C.: Reactive Hydrocarbons in the Atmosphere, Elsevier Science, URL https://books.google.co.in/books?id=Fn5368-Gv7AC, 1999.

Hewitt, C. and Jackson, A.: Handbook of Atmospheric Science: Principles and Applications, Wiley, URL http://books.google.co.in/books?id=fFKsjKoKmYAC, 2003.

Hexter, A. C. and Goldsmith, J. R.: Carbon Monoxide: Association of Community Air Pollution with Mortality, Science, 172, 265–267, doi:10.1126/science.172.3980.265, URL http://www.sciencemag.org/content/172/3980/265.abstract, 1971.

Hofzumahaus, A., Rohrer, F., Lu, K., Bohn, B., Brauers, T., Chang, C.-C., Fuchs, H., Holland, F., Kita, K., Kondo, Y., Li, X., Lou, S., Shao, M., Zeng, L., Wahner, A., and Zhang, Y.: Amplified Trace Gas Removal in the Troposphere, Science, 324, 1702–1704, doi:10.1126/science.1164566, URL http://science.sciencemag.org/content/sci/324/5935/1702.full.pdf, 2009.

Holzinger, R., Warneke, C., Hansel, A., Jordan, A., Lindinger, W., Scharffe, D. H., Schade, G., and Crutzen, P. J.: Biomass burning as a source of formaldehyde, acetaldehyde, methanol, acetone, acetonitrile, and hydrogen cyanide, Geophys. Res. Lett., 26, 1161–1164, doi:10.1029/1999gl900156, URL http://dx.doi.org/10.1029/1999GL900156, 1999.

Hoque, R. R., Khillare, P. S., Agarwal, T., Shridhar, V., and Balachandran, S.: Spatial and temporal variation of BTEX in the urban atmosphere of Delhi, India, Science of The Total Environment, 392, 30–40, doi:http://dx.doi.org/10.1016/j.scitotenv.2007.08.036, URL http://www.sciencedirect.com/science/article/pii/S0048969707009084, 2008.

Huntzicker, J. J. and Johnson, R. L.: Investigation of an ambient interference in the measurement of ozone by ultraviolet absorption photometry, Environmental Science & Technology, 13, 1414–1416, doi:10.1021/es60159a005, URL http://dx.doi.org/10.1021/es60159a005, 1979.

Ievgeniia, K., Konrad, S., Lukas, S., Bettina, B., Alexander, D., Alex, S., Karl, U., Günter, G., Patrik, p., David, S., and Anton, A.: Compounds enhanced in a mass spectrometric profile of smokers' exhaled breath versus non-smokers as determined in

a pilot study using PTR-MS, Journal of Breath Research, 2, 026 002, URL http://stacks.iop.org/1752-7163/2/i=2/a=026002, 2008.

Ingham, T., Goddard, A., Whalley, L. K., Furneaux, K. L., Edwards, P. M., Seal, C. P., Self, D. E., Johnson, G. P., Read, K. A., Lee, J. D., and Heard, D. E.: A flow-tube based laser-induced fluorescence instrument to measure OH reactivity in the troposphere, Atmos. Meas. Tech., 2, 465–477, doi:10.5194/amt-2-465-2009, URL http://www.atmos-meas-tech.net/2/465/2009/, 2009.

IPCC: Summary for policymakers, book section 1, pp. 1–18, Cambridge University Press,, Cambridge, United Kingdom and New York, NY, USA,, URL https://www.ipcc.ch/pdf/assessment-report/ar4/wg1/ar4-wg1-spm.pdf, 2007.

IPCC: Summary for Policymakers, book section SPM, p. 1–30, Cambridge University Press, Cambridge, United Kingdom and New York, NY, USA, doi:10.1017/CBO9781107415324.004, URL www.climatechange2013.org, 2013.

Irwine, A.: Black carbon:Tackling crop-residue burning in South Asia, Global Change, pp. 8–11, URL http://www.futureearth.org/blog/2015-feb-20/black-carbon-tackling-crop-residue-burning-south-asia, 2014.

Jacob, D.: Introduction to atmospheric chemistry, Princeton University Press, 1999.

Jacob, D. J., Field, B. D., Li, Q., Blake, D. R., de Gouw, J., Warneke, C., Hansel, A., Wisthaler, A., Singh, H. B., and Guenther, A.: Global budget of methanol: Constraints from atmospheric observations, Journal of Geophysical Research: Atmospheres, 110, n/a–n/a, doi:10.1029/2004JD005172, URL http://dx.doi.org/10.1029/2004JD005172, d08303, 2005.

Jenkin, M. E., Saunders, S. M., and Pilling, M. J.: The tropospheric degradation of volatile organic compounds: a protocol for mechanism development, Atmospheric Environment, 31, 81–104, doi:10.1016/S1352-2310(96)00105-7, URL http://www.sciencedirect.com/science/article/pii/S1352231096001057, 1997.

Jenkin, M. E., Young, J. C., and Rickard, A. R.: The MCM v3.3.1 degradation scheme for isoprene, Atmos. Chem. Phys., 15, 11 433–11 459, doi:10.5194/acp-15-11433-2015, URL http://www.atmos-chem-phys.net/15/11433/2015/, 2015.

Jerrett, M., Burnett, R. T., Pope, C. A., Ito, K., Thurston, G., Krewski, D., Shi, Y., Calle, E., and Thun, M.: Long-Term Ozone Exposure and Mortality, New England Journal of Medicine, 360, 1085–1095, doi:10.1056/NEJMoa0803894, URL http://www.nejm.org/doi/full/10.1056/NEJMoa0803894, 2009.

Kaiser, J., Skog, K. M., Baumann, K., Bertman, S. B., Brown, S. B., Brune, W. H., Crounse, J. D., de Gouw, J. A., Edgerton, E. S., Feiner, P. A., Goldstein, A. H., Koss, A., Misztal, P. K., Nguyen, T. B., Olson, K. F., St. Clair, J. M., Teng, A. P., Toma, S., Wennberg, P. O., Wild, R. J., Zhang, L., and Keutsch, F. N.: Speciation of OH reactivity above the canopy of an isoprene-dominated forest, Atmos. Chem. Phys., 16, 9349–9359, doi:10.5194/acp-16-9349-2016, URL http://www.atmos-chem-phys.net/16/9349/2016/, 2016.

Karl, T., Apel, E., Hodzic, A., Riemer, D. D., Blake, D. R., and Wiedinmyer, C.: Emissions of volatile organic compounds inferred from airborne flux measurements over a megacity, Atmos. Chem. Phys., 9, 271–285, doi:10.5194/acp-9-271-2009, URL http://www.atmos-chem-phys.net/9/271/2009/, 2009a.

Karl, T., Guenther, A., Turnipseed, A., Tyndall, G., Artaxo, P., and Martin, S.: Rapid formation of isoprene photo-oxidation products observed in Amazonia, Atmos. Chem. Phys., 9, 7753–7767, doi:10.5194/acp-9-7753-2009, URL http://www.atmos-chem-phys.net/9/7753/2009/, 2009b.

Karl, T., Harley, P., Emmons, L., Thornton, B., Guenther, A., Basu, C., Turnipseed, A., and Jardine, K.: Efficient Atmospheric Cleansing of Oxidized Organic Trace Gases by Vegetation, Science, 330, 816–819, doi:10.1126/science.1192534, URL http://science.sciencemag.org/content/sci/330/6005/816.full.pdf, 2010.

Kaskaoutis, D. G., Kumar, S., Sharma, D., Singh, R. P., Kharol, S. K., Sharma, M., Singh, A. K., Singh, S., Singh, A., and Singh, D.: Effects of crop residue burning on aerosol properties, plume characteristics, and long-range transport over northern India, Journal of Geophysical Research: Atmospheres, 119, 2013JD021 357, doi:10.1002/2013JD021357, URL http://dx.doi.org/10.1002/2013JD021357, 2014.

Kato, S., Sato, T., and Kajii, Y.: "A method to estimate the contribution of unidentified VOCs to OH reactivity", Atmospheric Environment, 45, 5531–5539, doi:10.1016/j.atmosenv.2011.05.074, URL http://www.sciencedirect.com/science/article/pii/S1352231011005917, 2011.

Kesselmeier, J. and Staudt, M.: Biogenic Volatile Organic Compounds (VOC): An Overview on Emission, Physiology and Ecology, Journal of Atmospheric Chemistry, 33, 23–88, doi:10.1023/a:1006127516791, URL http://dx.doi.org/10.1023/A:1006127516791, 1999.

Khillare, P. S., Hoque, R. R., Shridhar, V., Agarwal, T., and Balachandran, S.: Temporal variability of benzene concentration in the ambient air of Delhi: A com-

parative assessment of pre- and post-CNG periods, Journal of Hazardous Materials, 154, 1013–1018, doi:http://dx.doi.org/10.1016/j.jhazmat.2007.11.006, URL http://www.sciencedirect.com/science/article/pii/S0304389407016081, 2008.

Kirchner, F., Jeanneret, F., Clappier, A., Krüger, B., van den Bergh, H., and Calpini, B.: Total VOC reactivity in the planetary boundary layer: 2. A new indicator for determining the sensitivity of the ozone production to VOC and NO x, Journal of Geophysical Research: Atmospheres, 106, 3095–3110, doi:10.1029/2000jd900603, URL http://dx.doi.org/10.1029/2000JD900603, 2001.

Kleinman, L. I., Daum, P. H., Imre, D., Lee, Y. N., Nunnermacker, L. J., Springston, S. R., Weinstein-Lloyd, J., and Rudolph, J.: Ozone production rate and hydrocarbon reactivity in 5 urban areas: A cause of high ozone concentration in Houston, Geophysical Research Letters, 29, 105–1–105–4, doi:10.1029/2001GL014569, URL http://dx.doi.org/10.1029/2001GL014569, 2002.

Koppmann, R.: Volatile Organic Compounds in the Atmosphere, Blackwell, doi:10.1002/9780470988657, URL http://books.google.co.in/books?id=Q3KigVJvjaMC, 2007.

Kovacs, T. and Brune, W.: Total OH Loss Rate Measurement, Journal of Atmospheric Chemistry, 39, 105–122, doi:10.1023/a:1010614113786, URL http://dx.doi.org/10.1023/A%3A1010614113786, 2001.

Kovacs, T. A., Brune, W. H., Harder, H., Martinez, M., Simpas, J. B., Frost, G. J., Williams, E., Jobson, T., Stroud, C., Young, V., Fried, A., and Wert, B.: Direct measurements of urban OH reactivity during Nashville SOS in summer 1999, Journal of Environmental Monitoring, 5, 68–74, doi:10.1039/b204339d, URL http://dx.doi.org/10.1039/B204339D, 2003.

Kubistin, D., Harder, H., Martinez, M., Rudolf, M., Sander, R., Bozem, H., Eerdekens, G., Fischer, H., Gurk, C., Klüpfel, T., Königstedt, R., Parchatka, U., Schiller, C. L., Stickler, A., Taraborrelli, D., Williams, J., and Lelieveld, J.: Hydroxyl radicals in the tropical troposphere over the Suriname rainforest: comparison of measurements with the box model MECCA, Atmos. Chem. Phys., 10, 9705–9728, doi:10.5194/acp-10-9705-2010, URL http://www.atmos-chem-phys.net/10/9705/2010/, 2010.

Kumar, V. and Sinha, V.: VOC–OHM: A new technique for rapid measurements of ambient total OH reactivity and volatile organic compounds using a single proton transfer reaction mass spectrometer, International Journal of Mass Spectrometry, 374, 55–63, doi:10.1016/j.ijms.2014.10.012, URL http://www.sciencedirect.com/science/article/pii/S1387380614004266, 2014.

Kumar, V., Sarkar, C., and Sinha, V.: Influence of post-harvest crop residue fires on surface ozone mixing ratios in the N.W. IGP analyzed using 2 years of continuous in situ trace gas measurements, Journal of Geophysical Research: Atmospheres, 121, 2015JD024 308, doi:10.1002/2015JD024308, URL http://dx.doi.org/10.1002/2015JD024308, 2016.

Kurokawa, J., Ohara, T., Morikawa, T., Hanayama, S., Janssens-Maenhout, G., Fukui, T., Kawashima, K., and Akimoto, H.: Emissions of air pollutants and greenhouse gases over Asian regions during 2000–2008: Regional Emission inventory in ASia (REAS) version 2, Atmos. Chem. Phys., 13, 11 019–11 058, doi:10.5194/acp-13-11019-2013, URL http://www.atmos-chem-phys.net/13/11019/2013/, 2013.

Lal, D. M., Ghude, S. D., Patil, S. D., Kulkarni, S. H., Jena, C., Tiwari, S., and Srivastava, M. K.: Tropospheric ozone and aerosol long-term trends over the Indo-Gangetic Plain (IGP), India, Atmospheric Research, 116, 82–92, doi:10.1016/j.atmosres.2012.02.014, URL http://www.sciencedirect.com/science/article/pii/S0169809512000543, 2012.

Lal, R.: World crop residues production and implications of its use as a biofuel, Environ. Int., 31, 575–584, doi:https://doi.org/10.1016/j.envint.2004.09.005, URL http://www.sciencedirect.com/science/article/pii/S0160412004001564, 2005.

Lal, S. and Patil, R. S.: Monitoring of Atmospheric Behaviour of NOx from Vehicular Traffic, Environmental Monitoring and Assessment, 68, 37–50, doi:10.1023/a:1010730821844, URL http://dx.doi.org/10.1023/A%3A1010730821844, 2001.

Lal, S., Naja, M., and Subbaraya, B. H.: Seasonal variations in surface ozone and its precursors over an urban site in India, Atmospheric Environment, 34, 2713–2724, doi:10.1016/S1352-2310(99)00510-5, URL http://www.sciencedirect.com/science/article/pii/S1352231099005105, 2000.

Langford, B., Nemitz, E., House, E., Phillips, G. J., Famulari, D., Davison, B., Hopkins, J. R., Lewis, A. C., and Hewitt, C. N.: Fluxes and concentrations of volatile organic compounds above central London, UK, Atmos. Chem. Phys., 10, 627–645, doi:10.5194/acp-10-627-2010, URL http://www.atmos-chem-phys.net/10/627/2010/, 2010.

Lee, J. D., Young, J. C., Read, K. A., Hamilton, J. F., Hopkins, J. R., Lewis, A. C., Bandy, B. J., Davey, J., Edwards, P., Ingham, T., Self, D. E., Smith, S. C., Pilling, M. J., and Heard, D. E.: Measurement and calculation of OH reactivity at

a United Kingdom coastal site, Journal of Atmospheric Chemistry, 64, 53–76, doi: 10.1007/s10874-010-9171-0, URL http://dx.doi.org/10.1007/s10874-010-9171-0, 2009.

Leighton, P.: Photochemistry of Air Pollution, Academic Press, 1961.

Lelieveld, J., Dentener, F. J., Peters, W., and Krol, M. C.: On the role of hydroxyl radicals in the self-cleansing capacity of the troposphere, Atmos. Chem. Phys., 4, 2337–2344, doi:10.5194/acp-4-2337-2004, URL http://www.atmos-chem-phys.net/4/2337/2004/, 2004.

Lelieveld, J., Butler, T. M., Crowley, J. N., Dillon, T. J., Fischer, H., Ganzeveld, L., Harder, H., Lawrence, M. G., Martinez, M., Taraborrelli, D., and Williams, J.: Atmospheric oxidation capacity sustained by a tropical forest, Nature, 452, 737–740, doi: 10.1038/nature06870, URL http://www.nature.com/nature/journal/v452/n7188/abs/nature06870.html, 2008.

Lelieveld, J., Gromov, S., Pozzer, A., and Taraborrelli, D.: Global tropospheric hydroxyl distribution, budget and reactivity, Atmospheric Chemistry and Physics, 16, 12 477–12 493, doi:10.5194/acp-16-12477-2016, URL http://www.atmos-chem-phys.net/16/12477/2016/, 2016.

Levy, H.: Normal Atmosphere: Large Radical and Formaldehyde Concentrations Predicted, Science, 173, 141–143, doi:10.1126/science.173.3992.141, URL http://www.sciencemag.org/content/173/3992/141.abstract, 1971.

Lewis, A. C., Carslaw, N., Marriott, P. J., Kinghorn, R. M., Morrison, P., Lee, A. L., Bartle, K. D., and Pilling, M. J.: A larger pool of ozone-forming carbon compounds in urban atmospheres, Nature, 405, 778–781, doi:10.1038/35015540, URL http://dx.doi.org/10.1038/35015540, 10.1038/35015540, 2000.

Lindinger, W., Hansel, A., and Jordan, A.: On-line monitoring of volatile organic compounds at pptv levels by means of proton-transfer-reaction mass spectrometry (PTR-MS) medical applications, food control and environmental research, International Journal of Mass Spectrometry and Ion Processes, 173, 191–241, doi:10.1016/s0168-1176(97)00281-4, URL http://www.sciencedirect.com/science/article/pii/S0168117697002814, 1998.

Lou, S., Holland, F., Rohrer, F., Lu, K., Bohn, B., Brauers, T., Chang, C. C., Fuchs, H., Häseler, R., Kita, K., Kondo, Y., Li, X., Shao, M., Zeng, L., Wahner, A., Zhang, Y., Wang, W., and Hofzumahaus, A.: Atmospheric OH reactivities in the Pearl River Delta

– China in summer 2006: measurement and model results, Atmos. Chem. Phys., 10, 11 243–11 260, doi:10.5194/acp-10-11243-2010, URL http://www.atmos-chem-phys.net/10/11243/2010/, 2010.

Lu, K. D., Hofzumahaus, A., Holland, F., Bohn, B., Brauers, T., Fuchs, H., Hu, M., Häseler, R., Kita, K., Kondo, Y., Li, X., Lou, S. R., Oebel, A., Shao, M., Zeng, L. M., Wahner, A., Zhu, T., Zhang, Y. H., and Rohrer, F.: Missing OH source in a suburban environment near Beijing: observed and modelled OH and HO¡sub¿2¡/sub¿ concentrations in summer 2006, Atmos. Chem. Phys., 13, 1057–1080, doi:10.5194/acp-13-1057-2013, URL http://www.atmos-chem-phys.net/13/1057/2013/, 2013.

Luke, W. T.: Evaluation of a commercial pulsed fluorescence detector for the measurement of low-level SO2 concentrations during the Gas-Phase Sulfur Intercomparison Experiment, Journal of Geophysical Research: Atmospheres, 102, 16 255–16 265, doi:10.1029/96jd03347, URL http://dx.doi.org/10.1029/96JD03347, 1997.

Madronich, S. and Flocke, S.: The Role of Solar Radiation in Atmospheric Chemistry, pp. 1–26, Springer Berlin Heidelberg, Berlin, Heidelberg, doi:10.1007/978-3-540-69044-3_1, URL http://dx.doi.org/10.1007/978-3-540-69044-3_1, 1999.

Mallik, C. and Lal, S.: Seasonal characteristics of SO2, NO2, and CO emissions in and around the Indo-Gangetic Plain, Environmental Monitoring and Assessment, 186, 1295–1310, doi:10.1007/s10661-013-3458-y, URL http://dx.doi.org/10.1007/s10661-013-3458-y, 2014.

Mallik, C., Ghosh, D., Ghosh, D., Sarkar, U., Lal, S., and Venkataramani, S.: Variability of SO2, CO, and light hydrocarbons over a megacity in Eastern India: effects of emissions and transport, Environmental Science and Pollution Research, 21, 8692–8706, doi:10.1007/s11356-014-2795-x, URL http://dx.doi.org/10.1007/s11356-014-2795-x, 2014.

Manion, J. A., Huie, R. E., Levin, R. D., Jr, D. R. B., Orkin, V. L., Tsang, W., McGivern, W. S., Hudgens, J. W., Knyazev, V. D., Atkinson, D. B., Chai, E., Tereza, A. M., Lin, C.-Y., Allison, T. C., Mallard, W. G., Westley, F., Herron, J. T., Hampson, R. F., and Frizzell, D. H.: NIST Chemical Kinetics Database, URL http://kinetics.nist.gov/, 2015.

Mao, J., Ren, X., Brune, W. H., Olson, J. R., Crawford, J. H., Fried, A., Huey, L. G., Cohen, R. C., Heikes, B., Singh, H. B., Blake, D. R., Sachse, G. W., Diskin, G. S., Hall,

S. R., and Shetter, R. E.: Airborne measurement of OH reactivity during INTEX-B, Atmos. Chem. Phys., 9, 163–173, doi:10.5194/acp-9-163-2009, URL http://www.atmos-chem-phys.net/9/163/2009/, 2009.

Mao, J., Ren, X., Chen, S., Brune, W. H., Chen, Z., Martinez, M., Harder, H., Lefer, B., Rappenglück, B., Flynn, J., and Leuchner, M.: Atmospheric oxidation capacity in the summer of Houston 2006: Comparison with summer measurements in other metropolitan studies, Atmospheric Environment, 44, 4107 – 4115, doi:10.1016/j.atmosenv.2009.01.013, URL http://www.sciencedirect.com/science/article/pii/S1352231009000351, 2010.

Mao, J., Ren, X., Zhang, L., Van Duin, D. M., Cohen, R. C., Park, J. H., Goldstein, A. H., Paulot, F., Beaver, M. R., Crounse, J. D., Wennberg, P. O., DiGangi, J. P., Henry, S. B., Keutsch, F. N., Park, C., Schade, G. W., Wolfe, G. M., Thornton, J. A., and Brune, W. H.: Insights into hydroxyl measurements and atmospheric oxidation in a California forest, Atmos. Chem. Phys., 12, 8009–8020, doi:10.5194/acp-12-8009-2012, URL http://www.atmos-chem-phys.net/12/8009/2012/, 2012.

Michoud, V., Hansen, R. F., Locoge, N., Stevens, P. S., and Dusanter, S.: Detailed characterizations of the new Mines Douai comparative reactivity method instrument via laboratory experiments and modeling, Atmos. Meas. Tech., 8, 3537–3553, doi:10.5194/amt-8-3537-2015, URL http://www.atmos-meas-tech.net/8/3537/2015/, 2015.

Millet, D. B., Guenther, A., Siegel, D. A., Nelson, N. B., Singh, H. B., de Gouw, J. A., Warneke, C., Williams, J., Eerdekens, G., Sinha, V., Karl, T., Flocke, F., Apel, E., Riemer, D. D., Palmer, P. I., and Barkley, M.: Global atmospheric budget of acetaldehyde: 3-D model analysis and constraints from in-situ and satellite observations, Atmos. Chem. Phys., 10, 3405–3425, doi:10.5194/acp-10-3405-2010, URL http://www.atmos-chem-phys.net/10/3405/2010/, 2010.

Miyazaki, K., Eskes, H. J., and Sudo, K.: Global NOx emission estimates derived from an assimilation of OMI tropospheric NO2 columns, Atmos. Chem. Phys., 12, 2263–2288, doi:10.5194/acp-12-2263-2012, URL http://www.atmos-chem-phys.net/12/2263/2012/, 2012.

Murali, S., Shrivastava, R., and Saxena, M.: Green house gas emissions from open field burning of agricultural residues in India, J Environ Sci Eng, 52, 277–284, 2010.

Naja, M. and Lal, S.: Surface ozone and precursor gases at Gadanki (13.5°N, 79.2°E), a tropical rural site in India, Journal of Geophysical Research: Atmospheres, 107,

ACH 8–1–ACH 8–13, doi:10.1029/2001jd000357, URL http://dx.doi.org/10.1029/2001JD000357, 2002.

Nakashima, Y., Kato, S., Greenberg, J., Harley, P., Karl, T., Turnipseed, A., Apel, E., Guenther, A., Smith, J., and Kajii, Y.: Total OH reactivity measurements in ambient air in a southern Rocky mountain ponderosa pine forest during BEACHON-SRM08 summer campaign, Atmospheric Environment, 85, 1–8, doi:10.1016/j.atmosenv.2013.11.042, URL http://www.sciencedirect.com/science/article/pii/S1352231013008844, 2014.

Nielsen, C. J., Herrmann, H., and Weller, C.: Atmospheric chemistry and environmental impact of the use of amines in carbon capture and storage (CCS), Chem. Soc. Rev., 41, 6684–6704, doi:10.1039/C2CS35059A, URL http://dx.doi.org/10.1039/C2CS35059A, 2012.

Nölscher, A. C., Sinha, V., Bockisch, S., Klüpfel, T., and Williams, J.: Total OH reactivity measurements using a new fast Gas Chromatographic Photo-Ionization Detector (GC-PID), Atmos. Meas. Tech., 5, 2981–2992, doi:10.5194/amt-5-2981-2012, URL http://www.atmos-meas-tech.net/5/2981/2012/, 2012a.

Nölscher, A. C., Williams, J., Sinha, V., Custer, T., Song, W., Johnson, A. M., Axinte, R., Bozem, H., Fischer, H., Pouvesle, N., Phillips, G., Crowley, J. N., Rantala, P., Rinne, J., Kulmala, M., Gonzales, D., Valverde-Canossa, J., Vogel, A., Hoffmann, T., Ouwersloot, H. G., Vilá-Guerau de Arellano, J., and Lelieveld, J.: Summertime total OH reactivity measurements from boreal forest during HUMPPA-COPEC 2010, Atmos. Chem. Phys., 12, 8257–8270, doi:10.5194/acp-12-8257-2012, URL http://www.atmos-chem-phys.net/12/8257/2012/, 2012b.

Nölscher, A. C., Butler, T., Auld, J., Veres, P., Muñoz, A., Taraborrelli, D., Vereecken, L., Lelieveld, J., and Williams, J.: Using total OH reactivity to assess isoprene photooxidation via measurement and model, Atmospheric Environment, doi:10.1016/j.atmosenv.2014.02.024, URL http://www.sciencedirect.com/science/article/pii/S1352231014001204, 2014.

Nölscher, A. C., Yanez-Serrano, A. M., Wolff, S., de Araujo, A. C., Lavric, J. V., Kesselmeier, J., and Williams, J.: Unexpected seasonality in quantity and composition of Amazon rainforest air reactivity, Nat Commun, 7, doi:10.1038/ncomms10383, URL http://dx.doi.org/10.1038/ncomms10383, 2016.

Ojha, N., Naja, M., Singh, K. P., Sarangi, T., Kumar, R., Lal, S., Lawrence, M. G., Butler, T. M., and Chandola, H. C.: Variabilities in ozone at a semi-urban site in the Indo-

Gangetic Plain region: Association with the meteorology and regional processes, Journal of Geophysical Research: Atmospheres, 117, D20 301, doi:10.1029/2012jd017716, URL http://dx.doi.org/10.1029/2012JD017716, 2012.

Okabe, H., Splitstone, P. L., and Ball, J. J.: Ambient and Source SO2 Detector Based on a Fluorescence Method, Journal of the Air Pollution Control Association, 23, 514–516, doi:10.1080/00022470.1973.10469797, URL http://dx.doi.org/10.1080/00022470.1973.10469797, 1973.

Omenetto, N., Boutilier, G. D., Weeks, S. J., Smith, B. W., and Winefordner, J. D.: Pulsed vs. continuous wave atomic fluorescence spectrometry, Analytical Chemistry, 49, 1076–1078, doi:10.1021/ac50015a051, URL http://dx.doi.org/10.1021/ac50015a051, 1977.

Ortega, A. M., Day, D. A., Cubison, M. J., Brune, W. H., Bon, D., de Gouw, J. A., and Jimenez, J. L.: Secondary organic aerosol formation and primary organic aerosol oxidation from biomass-burning smoke in a flow reactor during FLAME-3, Atmos. Chem. Phys., 13, 11 551–11 571, doi:10.5194/acp-13-11551-2013, URL https://www.atmos-chem-phys.net/13/11551/2013/, 2013.

Pandey, J. and Agrawal, M.: Ozone: Concentration variabilities in a seasonally dry tropical climate, Environment International, 18, 515–520, doi:10.1016/0160-4120(92)90270-E, URL http://www.sciencedirect.com/science/article/pii/016041209290270E, 1992.

Parry, M., Canziani, O., Palutikof, J., van der Linden, P., and Hanson, Eds, C.: Climate Change 2007: Impacts, Adaptation and Vulnerability : Contribution of Working Group II to the Fourth Assessment Report of the Intergovernmental Panel on Climate Change, Cambridge University Press, URL http://books.google.co.in/books?id=TNo-SeGpn7wC, 2007.

Pawar, H., Garg, S., Kumar, V., Sachan, H., Arya, R., Sarkar, C., Chandra, B. P., and Sinha, B.: Quantifying the contribution of long-range transport to particulate matter (PM) mass loadings at a suburban site in the north-western Indo-Gangetic Plain (NW-IGP), Atmos. Chem. Phys., 15, 9501–9520, doi:10.5194/acp-15-9501-2015, URL http://www.atmos-chem-phys.net/15/9501/2015/, 2015.

Piccot, S. D., Watson, J. J., and Jones, J. W.: A global inventory of volatile organic compound emissions from anthropogenic sources, Journal of Geophysical Research: Atmospheres, 97, 9897–9912, doi:10.1029/92JD00682, URL http://dx.doi.org/10.1029/92JD00682, 1992.

Pitts, J. N., Grosjean, D., Van Cauwenberghe, K., Schmid, J. P., and Fitz, D. R.: Photooxidation of aliphatic amines under simulated atmospheric conditions: formation of nitrosamines, nitramines, amides, and photochemical oxidant, Environ. Sci. Technol., 12, 946–953, doi:10.1021/es60144a009, URL http://dx.doi.org/10.1021/es60144a009, 1978.

Prasad, R.: Panchtatva, Agriculture, and Sustainability of Life on Earth., Asian Agri-History, 20, 141–154, URL http://asianagrihistory.org/volume-20/rajendra-prasad.pdf, 2016.

Prockop, L. D. and Chichkova, R. I.: Carbon monoxide intoxication: An updated review, Journal of the Neurological Sciences, 262, 122–130, doi:10.1016/j.jns.2007.06.037, URL http://www.sciencedirect.com/science/article/pii/S0022510X0700456X, 2007.

Rajput, P., Sarin, M., Sharma, D., and Singh, D.: Characteristics and emission budget of carbonaceous species from post-harvest agricultural-waste burning in source region of the Indo-Gangetic Plain, Tellus B: Chemical and Physical Meteorology, 66, 21 026, doi:10.3402/tellusb.v66.21026, URL http://dx.doi.org/10.3402/tellusb.v66.21026, 2014.

Ram, K., Sarin, M. M., and Tripathi, S. N.: A 1 year record of carbonaceous aerosols from an urban site in the Indo-Gangetic Plain: Characterization, sources, and temporal variability, Journal of Geophysical Research: Atmospheres, 115, doi:10.1029/2010JD014188, URL http://dx.doi.org/10.1029/2010JD014188, 2010.

Rao, A. M., Pandit, G. G., Sain, P., Sharma, S., Krishnamoorthy, T. M., and Nambi, K. S. V.: Non-methane hydrocarbons in industrial locations of Bombay, Atmospheric Environment, 31, 1077–1085, doi:http://dx.doi.org/10.1016/S1352-2310(96)00266-X, URL http://www.sciencedirect.com/science/article/pii/S135223109600266X, 1997.

Rasmussen, R. A. and Khalil, M. A. K.: Atmospheric benzene and toluene, Geophysical Research Letters, 10, 1096–1099, doi:10.1029/GL010i011p01096, URL http://dx.doi.org/10.1029/GL010i011p01096, 1983.

Ravishankara, A. R., Hancock, G., Kawasaki, M., and Matsumi, Y.: Photochemistry of Ozone: Surprises and Recent Lessons, Science, 280, 60–61, doi:10.1126/science.280.5360.60, URL http://science.sciencemag.org/content/280/5360/60, 1998.

Ren, X., Harder, H., Martinez, M., Lesher, R. L., Oliger, A., Shirley, T., Adams, J., Simpas, J. B., and Brune, W. H.: HOx concentrations and OH reactivity observations in New York City during PMTACS-NY2001, Atmospheric Environment, 37,

3627–3637, doi:10.1016/S1352-2310(03)00460-6, URL http://www.sciencedirect.com/science/article/pii/S1352231003004606, 2003.

Ren, X., Brune, W. H., Cantrell, C. A., Edwards, G. D., Shirley, T., Metcalf, A. R., and Lesher, R. L.: Hydroxyl and Peroxy Radical Chemistry in a Rural Area of Central Pennsylvania: Observations and Model Comparisons, Journal of Atmospheric Chemistry, 52, 231–257, doi:10.1007/s10874-005-3651-7, URL http://dx.doi.org/10.1007/s10874-005-3651-7, 2005.

Ren, X., Brune, W. H., Oliger, A., Metcalf, A. R., Simpas, J. B., Shirley, T., Schwab, J. J., Bai, C., Roychowdhury, U., Li, Y., Cai, C., Demerjian, K. L., He, Y., Zhou, X., Gao, H., and Hou, J.: OH, HO2, and OH reactivity during the PMTACS–NY Whiteface Mountain 2002 campaign: Observations and model comparison, Journal of Geophysical Research: Atmospheres, 111, D10S03, doi:10.1029/2005jd006126, URL http://dx.doi.org/10.1029/2005JD006126, 2006.

Ren, X., Olson, J. R., Crawford, J. H., Brune, W. H., Mao, J., Long, R. B., Chen, Z., Chen, G., Avery, M. A., Sachse, G. W., Barrick, J. D., Diskin, G. S., Huey, L. G., Fried, A., Cohen, R. C., Heikes, B., Wennberg, P. O., Singh, H. B., Blake, D. R., and Shetter, R. E.: HOx chemistry during INTEX-A 2004: Observation, model calculation, and comparison with previous studies, Journal of Geophysical Research: Atmospheres, 113, doi:10.1029/2007JD009166, URL http://dx.doi.org/10.1029/2007JD009166, 2008.

Roberts, J. M., Veres, P. R., Cochran, A. K., Warneke, C., Burling, I. R., Yokelson, R. J., Lerner, B., Gilman, J. B., Kuster, W. C., Fall, R., and de Gouw, J.: Isocyanic acid in the atmosphere and its possible link to smoke-related health effects, Proc. Natl. Acad. Sci., 108, 8966–8971, doi:10.1073/pnas.1103352108, URL http://www.pnas.org/content/108/22/8966.abstract, 2011.

Roberts, J. M., Veres, P. R., VandenBoer, T. C., Warneke, C., Graus, M., Williams, E. J., Lefer, B., Brock, C. A., Bahreini, R., Öztürk, F., Middlebrook, A. M., Wagner, N. L., Dubé, W. P., and de Gouw, J. A.: New insights into atmospheric sources and sinks of isocyanic acid, HNCO, from recent urban and regional observations, J. Geophys. Res., 119, 1060–1072, doi:10.1002/2013JD019931, URL http://dx.doi.org/10.1002/2013JD019931, 2014.

Rohrer, F. and Berresheim, H.: Strong correlation between levels of tropospheric hydroxyl radicals and solar ultraviolet radiation, Nature, 442, 184–187, doi:10.1038/nature04924, URL http://dx.doi.org/10.1038/nature04924, 2006.

Rosenfeld, D., Lohmann, U., Raga, G. B., O'Dowd, C. D., Kulmala, M., Fuzzi, S., Reissell, A., and Andreae, M. O.: Flood or Drought: How Do Aerosols Affect Precipitation?, Science, 321, 1309–1313, doi:10.1126/science.1160606, URL http://www.sciencemag.org/content/321/5894/1309.abstract, 2008.

Sadanaga, Y., Yoshino, A., Kato, S., Yoshioka, A., Watanabe, K., Miyakawa, Y., Hayashi, I., Ichikawa, M., Matsumoto, J., Nishiyama, A., Akiyama, N., Kanaya, Y., and Kajii, Y.: The importance of NO2 and volatile organic compounds in the urban air from the viewpoint of the OH reactivity, Geophysical Research Letters, 31, L08 102, doi: 10.1029/2004GL019661, URL http://dx.doi.org/10.1029/2004GL019661, 2004a.

Sadanaga, Y., Yoshino, A., Watanabe, K., Yoshioka, A., Wakazono, Y., Kanaya, Y., and Kajii, Y.: Development of a measurement system of OH reactivity in the atmosphere by using a laser-induced pump and probe technique, Review of Scientific Instruments, 75, 2648–2655, doi:10.1063/1.1775311, URL http://scitation.aip.org/content/aip/journal/rsi/75/8/10.1063/1.1775311, 2004b.

Sahai, S., Sharma, C., Singh, D. P., Dixit, C. K., Singh, N., Sharma, P., Singh, K., Bhatt, S., Ghude, S., Gupta, V., Gupta, R. K., Tiwari, M. K., Garg, S. C., Mitra, A. P., and Gupta, P. K.: A study for development of emission factors for trace gases and carbonaceous particulate species from in situ burning of wheat straw in agricultural fields in india, Atmospheric Environment, 41, 9173–9186, doi:10.1016/j.atmosenv.2007.07.054, URL http://www.sciencedirect.com/science/article/pii/S1352231007006814, 2007.

Sahu, L. K. and Lal, S.: Characterization of C2−C4 NMHCs distributions at a high altitude tropical site in India, Journal of Atmospheric Chemistry, 54, 161–175, doi: 10.1007/s10874-006-9023-0, URL http://dx.doi.org/10.1007/s10874-006-9023-0, 2006a.

Sahu, L. K. and Lal, S.: Distributions of C2–C5 NMHCs and related trace gases at a tropical urban site in India, Atmospheric Environment, 40, 880–891, doi:http://dx.doi.org/10.1016/j.atmosenv.2005.10.021, URL http://www.sciencedirect.com/science/article/pii/S1352231005009970, 2006b.

Sahu, L. K. and Saxena, P.: High time and mass resolved PTR-TOF-MS measurements of VOCs at an urban site of India during winter: Role of anthropogenic, biomass burning, biogenic and photochemical sources, Atmospheric Research, 164–165, 84–94, doi:http://dx.doi.org/10.1016/j.atmosres.2015.04.021, URL http://www.sciencedirect.com/science/article/pii/S0169809515001386, 2015.

Sahu, L. K., Yadav, R., and Pal, D.: Source identification of VOCs at an urban site of western India: Effect of marathon events and anthropogenic emissions, Journal of Geophysical Research: Atmospheres, 121, 2416–2433, doi:10.1002/2015JD024454, URL http://dx.doi.org/10.1002/2015JD024454, 2016.

Sander, R.: Compilation of Henry's law constants (version 4.0) for water as solvent, Atmos. Chem. Phys., 15, 4399–4981, doi:10.5194/acp-15-4399-2015, URL http://www.atmos-chem-phys.net/15/4399/2015/, 2015.

Sarkar, C., Kumar, V., and Sinha, V.: Massive emissions of carcinogenic benzenoids from paddy residue burning in North India, Current Science, 104, 1703–1706, URL http://www.currentscience.ac.in/Volumes/104/12/1703.pdf, 2013.

Sarkar, C., Sinha, V., Kumar, V., Rupakheti, M., Panday, A., Mahata, K. S., Rupakheti, D., Kathayat, B., and Lawrence, M. G.: Overview of VOC emissions and chemistry from PTR-TOF-MS measurements during the SusKat-ABC campaign: high acetaldehyde, isoprene and isocyanic acid in wintertime air of the Kathmandu Valley, Atmos. Chem. Phys., 16, 3979–4003, doi:10.5194/acp-16-3979-2016, URL http://www.atmos-chem-phys.net/16/3979/2016/, 2016.

Saunders, S. M., Jenkin, M. E., Derwent, R. G., and Pilling, M. J.: World wide web site of a master chemical mechanism (MCM) for use in tropospheric chemistry models, Atmospheric Environment, 31, 1249, doi:10.1016/S1352-2310(97)85197-7, URL http://www.sciencedirect.com/science/article/pii/S1352231097851977, 1997.

Saunders, S. M., Jenkin, M. E., Derwent, R. G., and Pilling, M. J.: Protocol for the development of the Master Chemical Mechanism, MCM v3 (Part A): tropospheric degradation of non-aromatic volatile organic compounds, Atmos. Chem. Phys., 3, 161–180, doi:10.5194/acp-3-161-2003, URL http://www.atmos-chem-phys.net/3/161/2003/, 2003.

Schmale, J., Shindell, D. T., Schneidemesser, v. E., Chabay, I., and Lawrence, M.: Air pollution: Clean up our skies, Nature, 515, 335–337, doi:10.1038/515335a, 2014.

Shetter, R. E., Davidson, J. A., Cantrell, C. A., Burzynski, N. J., and Calvert, J. G.: Temperature dependence of the atmospheric photolysis rate coefficient for NO2, Journal of Geophysical Research: Atmospheres, 93, 7113–7118, doi:10.1029/JD093iD06p07113, URL http://dx.doi.org/10.1029/JD093iD06p07113, 1988.

Shirley, T. R., Brune, W. H., Ren, X., Mao, J., Lesher, R., Cardenas, B., Volkamer, R., Molina, L. T., Molina, M. J., Lamb, B., Velasco, E., Jobson, T., and Alexander,

M.: Atmospheric oxidation in the Mexico City Metropolitan Area (MCMA) during April 2003, Atmos. Chem. Phys., 6, 2753–2765, doi:10.5194/acp-6-2753-2006, URL http://www.atmos-chem-phys.net/6/2753/2006/, 2006.

Singh, A., Sarin, S. M., Shanmugam, P., Sharma, N., Attri, A. K., and Jain, V. K.: Ozone distribution in the urban environment of Delhi during winter months, Atmospheric Environment, 31, 3421–3427, doi:10.1016/S1352-2310(97)00138-6, URL http://www.sciencedirect.com/science/article/pii/S1352231097001386, 1997.

Singla, V., Satsangi, A., Pachauri, T., Lakhani, A., and Kumari, K. M.: Ozone formation and destruction at a sub-urban site in North Central region of India, Atmospheric Research, 101, 373–385, doi:10.1016/j.atmosres.2011.03.011, URL http://www.sciencedirect.com/science/article/pii/S0169809511000949, 2011.

Sinha, B., Singh Sangwan, K., Maurya, Y., Kumar, V., Sarkar, C., Chandra, B. P., and Sinha, V.: Assessment of crop yield losses in Punjab and Haryana using 2 years of continuous in situ ozone measurements, Atmos. Chem. Phys., 15, 9555–9576, doi:10.5194/acp-15-9555-2015, URL http://www.atmos-chem-phys.net/15/9555/2015/, 2015.

Sinha, V., Williams, J., Meyerhöfer, M., Riebesell, U., Paulino, A. I., and Larsen, A.: Air-sea fluxes of methanol, acetone, acetaldehyde, isoprene and DMS from a Norwegian fjord following a phytoplankton bloom in a mesocosm experiment, Atmos. Chem. Phys., 7, 739–755, doi:10.5194/acp-7-739-2007, URL http://www.atmos-chem-phys.net/7/739/2007/, 2007.

Sinha, V., Williams, J., Crowley, J. N., and Lelieveld, J.: The Comparative Reactivity Method – a new tool to measure total OH Reactivity in ambient air, Atmos. Chem. Phys, p. 2213–2227, URL www.atmos-chem-phys.net/8/2213/2008/, 2008.

Sinha, V., Custer, T. G., Klüpfel, T., and Williams, J.: The effect of relative humidity on the detection of pyrrole by PTR-MS for OH reactivity measurements, International Journal of Mass Spectrometry, 282, 108–111, doi:10.1016/j.ijms.2009.02.019, URL http://www.sciencedirect.com/science/article/pii/S1387380609000700, 2009.

Sinha, V., Williams, J., Lelieveld, J., Ruuskanen, T. M., Kajos, M. K., Patokoski, J., Hellen, H., Hakola, H., Mogensen, D., Boy, M., Rinne, J., and Kulmala, M.: OH Reactivity Measurements within a Boreal Forest: Evidence for Unknown Reactive Emissions, Environmental Science & Technology, 44, 6614–6620, doi:10.1021/es101780b, URL http://dx.doi.org/10.1021/es101780b, 2010.

Sinha, V., Williams, J., Diesch, J. M., Drewnick, F., Martinez, M., Harder, H., Regelin, E., Kubistin, D., Bozem, H., Hosaynali-Beygi, Z., Fischer, H., André s Herná ndez, M. D., Kartal, D., Adame, J. A., and Lelieveld, J.: Constraints on instantaneous ozone production rates and regimes during DOMINO derived using in-situ OH reactivity measurements, Atmos. Chem. Phys., 12, 7269–7283, doi:10.5194/acp-12-7269-2012, URL http://www.atmos-chem-phys.net/12/7269/2012/, 2012.

Sinha, V., Kumar, V., and Sarkar, C.: Chemical composition of pre-monsoon air in the Indo-Gangetic Plain measured using a new air quality facility and PTR-MS: high surface ozone and strong influence of biomass burning, Atmos. Chem. Phys., 14, 5921–5941, doi:10.5194/acp-14-5921-2014, URL http://www.atmos-chem-phys.net/14/5921/2014/, 2014.

Srivastava, A., Joseph, A. E., Patil, S., More, A., Dixit, R. C., and Prakash, M.: Air toxics in ambient air of Delhi, Atmospheric Environment, 39, 59–71, doi:http://dx.doi.org/10.1016/j.atmosenv.2004.09.053, URL http://www.sciencedirect.com/science/article/pii/S1352231004009422, 2005.

Srivastava, A., Joseph, A. E., and Devotta, S.: Volatile organic compounds in ambient air of Mumbai—India, Atmospheric Environment, 40, 892–903, doi:http://dx.doi.org/10.1016/j.atmosenv.2005.10.045, URL http://www.sciencedirect.com/science/article/pii/S1352231005009982, 2006.

Stockwell, C. E., Veres, P. R., Williams, J., and Yokelson, R. J.: Characterization of biomass burning emissions from cooking fires, peat, crop residue, and other fuels with high-resolution proton-transfer-reaction time-of-flight mass spectrometry, Atmos. Chem. Phys., 15, 845–865, doi:10.5194/acp-15-845-2015, URL http://www.atmos-chem-phys.net/15/845/2015/, 2015.

Stone, D., Whalley, L. K., and Heard, D. E.: Tropospheric OH and HO2 radicals: field measurements and model comparisons, Chem. Soc. Rev., 41, 6348–6404, doi:10.1039/C2CS35140D, URL http://dx.doi.org/10.1039/C2CS35140D, 2012.

Stroud, C. A., Morneau, G., Makar, P. A., Moran, M. D., Gong, W., Pabla, B., Zhang, J., Bouchet, V. S., Fox, D., Venkatesh, S., Wang, D., and Dann, T.: OH-reactivity of volatile organic compounds at urban and rural sites across Canada: Evaluation of air quality model predictions using speciated VOC measurements, Atmospheric Environment, 42, 7746–7756, doi:10.1016/j.atmosenv.2008.05.054, URL http://www.sciencedirect.com/science/article/pii/S1352231008005104, 2008.

Stull, R.: An Introduction to Boundary Layer Meteorology, Springer Netherlands, URL http://books.google.co.in/books?id=eRRz9RNvNOkC, 1988.

Swamy, Y. V., Venkanna, R., Nikhil, G. N., Chitanya, D. N. S. K., Sinha, P. R., Ramakrishna, M., and Rao, A. G.: Impact of Nitrogen Oxides, Volatile Organic Compounds and Black Carbon on Atmospheric Ozone Levels at a Semi Arid Urban Site in Hyderabad, Aerosol and Air Quality Research, 12, 662–671, doi:10.4209/aaqr.2012.01.0019, URL https://doi.org/10.4209/aaqr.2012.01.0019, 2012.

Tani, A., Hayward, S., Hansel, A., and Hewitt, C. N.: Effect of water vapour pressure on monoterpene measurements using proton transfer reaction-mass spectrometry (PTR-MS), International Journal of Mass Spectrometry, 239, 161–169, doi:10.1016/j.ijms.2004.07.020, URL http://www.sciencedirect.com/science/article/pii/S1387380604003495, 2004.

Tao, Y., Ye, X., Jiang, S., Yang, X., Chen, J., Xie, Y., and Wang, R.: Effects of amines on particle growth observed in new particle formation events, Journal of Geophysical Research: Atmospheres, 121, 324–335, doi:10.1002/2015JD024245, URL http://dx.doi.org/10.1002/2015JD024245, 2016.

Trebs, I., Bohn, B., Ammann, C., Rummel, U., Blumthaler, M., Königstedt, R., Meixner, F. X., Fan, S., and Andreae, M. O.: Relationship between the NO2 photolysis frequency and the solar global irradiance, Atmos. Meas. Tech., 2, 725–739, doi:10.5194/amt-2-725-2009, URL http://www.atmos-meas-tech.net/2/725/2009/, 2009.

U.S.EPA: Clean Air Act Amendments 1990, United States Environmental Protection Agency, Office of Air and Radiation, Pennsylvania Ave., Washington, D. C., URL https://www.epa.gov/clean-air-act-overview/1990-clean-air-act-amendment-summary, 1990.

U.S.EPA: GUIDELINE ON DATA HANDLING CONVENTIONS FOR THE 8-HOUR OZONE NAAQS, United States Environmental Protection Agency, 1998.

U.S.EPA: Risk and Exposure Assessment to Support the Review of the NO2 Primary National Ambient Air Quality Standard, Report, U.S. Environmental Protection Agency, URL http://www.epa.gov/ttn/naaqs/standards/nox/data/20081121_NO2_REA_final.pdf, 2008.

Varshney, C. K. and Aggarwal, M.: Ozone pollution in the urban atmosphere of Delhi, Atmospheric Environment. Part B. Urban Atmosphere, 26, 291–294,

doi:10.1016/0957-1272(92)90004-C, URL http://www.sciencedirect.com/science/article/pii/095712729290004C, 1992.

Venkataraman, C., Habib, G., Kadamba, D., Shrivastava, M., Leon, J. F., Crouzille, B., Boucher, O., and Streets, D. G.: Emissions from open biomass burning in India: Integrating the inventory approach with high-resolution Moderate Resolution Imaging Spectroradiometer (MODIS) active-fire and land cover data, Global Biogeochemical Cycles, 20, doi:10.1029/2005GB002547, URL http://dx.doi.org/10.1029/2005GB002547, 2006.

Wang, T., Cheung, T. F., Li, Y. S., Yu, X. M., and Blake, D. R.: Emission characteristics of CO, NOx, SO2 and indications of biomass burning observed at a rural site in eastern China, Journal of Geophysical Research: Atmospheres, 107, ACH 9–1–ACH 9–10, doi:10.1029/2001jd000724, URL http://dx.doi.org/10.1029/2001JD000724, 2002.

Warneke, C., Roberts, J. M., Veres, P., Gilman, J., Kuster, W. C., Burling, I., Yokelson, R., and de Gouw, J. A.: VOC identification and inter-comparison from laboratory biomass burning using PTR-MS and PIT-MS, International Journal of Mass Spectrometry, 303, 6–14, doi:10.1016/j.ijms.2010.12.002, URL http://www.sciencedirect.com/science/article/pii/S1387380610004628, 2011.

Wennberg, P. O.: Atmospheric chemistry: Radicals follow the Sun, Nature, 442, 145–146, doi:10.1038/442145a, URL http://dx.doi.org/10.1038/442145a, 10.1038/442145a, 2006.

Whalley, L. K., Stone, D., Bandy, B., Dunmore, R., Hamilton, J. F., Hopkins, J., Lee, J. D., Lewis, A. C., and Heard, D. E.: Atmospheric OH reactivity in central London: observations, model predictions and estimates of in situ ozone production, Atmos. Chem. Phys., 16, 2109–2122, doi:10.5194/acp-16-2109-2016, URL https://www.atmos-chem-phys.net/16/2109/2016/, 2016.

WHO: WHO Air quality guidelines for particulate matter, ozone, nitrogen dioxide and sulfur dioxide : Summary of risk assessment, techreport, World Health Organization, URL http://www.who.int/phe/health_topics/outdoorair/outdoorair_aqg/en/, 2005.

Williams, J. and Brune, W.: A roadmap for OH reactivity research, Atmospheric Environment, 106, 371–372, doi:10.1016/j.atmosenv.2015.02.017, URL http://www.sciencedirect.com/science/article/pii/S1352231015001363, 2015.

Williams, J., Pöschl, U., Crutzen, P. J., Hansel, A., Holzinger, R., Warneke, C., Lindinger, W., and Lelieveld, J.: An Atmospheric Chemistry Interpretation of Mass Scans Ob-

tained from a Proton Transfer Mass Spectrometer Flown over the Tropical Rainforest of Surinam, Journal of Atmospheric Chemistry, 38, 133–166, doi:10.1023/A:1006322701523, URL http://dx.doi.org/10.1023/A:1006322701523, 2001.

Williams, J., Keßel, S. U., Nölscher, A. C., Yang, Y., Lee, Y., Yáñez-Serrano, A. M., Wolff, S., Kesselmeier, J., Klüpfel, T., Lelieveld, J., and Shao, M.: Opposite OH reactivity and ozone cycles in the Amazon rainforest and megacity Beijing: Subversion of biospheric oxidant control by anthropogenic emissions, Atmospheric Environment, 125, Part A, 112–118, doi:10.1016/j.atmosenv.2015.11.007, URL http://www.sciencedirect.com/science/article/pii/S1352231015305161, 2016.

Wolfe, G. M., Marvin, M. R., Roberts, S. J., Travis, K. R., and Liao, J.: The Framework for 0-D Atmospheric Modeling (F0AM) v3.1, Geosci. Model Dev., 9, 3309–3319, doi:10.5194/gmd-9-3309-2016, URL http://www.geosci-model-dev.net/9/3309/2016/, gMD, 2016.

Yáñez-Serrano, A. M., Nölscher, A. C., Williams, J., Wolff, S., Alves, E., Martins, G. A., Bourtsoukidis, E., Brito, J., Jardine, K., Artaxo, P., and Kesselmeier, J.: Diel and seasonal changes of biogenic volatile organic compounds within and above an Amazonian rainforest, Atmos. Chem. Phys., 15, 3359–3378, doi:10.5194/acp-15-3359-2015, URL http://www.atmos-chem-phys.net/15/3359/2015/, 2015.

Yang, Y., Shao, M., Wang, X., Nölscher, A. C., Kessel, S., Guenther, A., and Williams, J.: Towards a quantitative understanding of total OH reactivity: A review, Atmos. Environ., 134, 147–161, doi:10.1016/j.atmosenv.2016.03.010, URL http://www.sciencedirect.com/science/article/pii/S1352231016301819, 2016.

Yevich, R. and Logan, J. A.: An assessment of biofuel use and burning of agricultural waste in the developing world, Global Biogeochem. Cycles, 17, doi:10.1029/2002GB001952, URL http://dx.doi.org/10.1029/2002GB001952, 2003.

Yokelson, R. J., Burling, I. R., Gilman, J. B., Warneke, C., Stockwell, C. E., de Gouw, J., Akagi, S. K., Urbanski, S. P., Veres, P., Roberts, J. M., Kuster, W. C., Reardon, J., Griffith, D. W. T., Johnson, T. J., Hosseini, S., Miller, J. W., Cocker Iii, D. R., Jung, H., and Weise, D. R.: Coupling field and laboratory measurements to estimate the emission factors of identified and unidentified trace gases for prescribed fires, Atmos. Chem. Phys., 13, 89–116, doi:10.5194/acp-13-89-2013, URL http://www.atmos-chem-phys.net/13/89/2013/, 2013.

Yoshino, A., Nakashima, Y., Miyazaki, K., Kato, S., Suthawaree, J., Shimo, N., Matsunaga, S., Chatani, S., Apel, E., Greenberg, J., Guenther, A., Ueno, H., Sasaki, H.,

Hoshi, J.-y., Yokota, H., Ishii, K., and Kajii, Y.: Air quality diagnosis from comprehensive observations of total OH reactivity and reactive trace species in urban central Tokyo, Atmos. Environ., 49, 51–59, doi:10.1016/j.atmosenv.2011.12.029, URL http://www.sciencedirect.com/science/article/pii/S1352231011013021, 2012.

Yuan, B., Koss, A. R., Warneke, C., Coggon, M., Sekimoto, K., and de Gouw, J. A.: Proton-Transfer-Reaction Mass Spectrometry: Applications in Atmospheric Sciences, Chemical Reviews, doi:10.1021/acs.chemrev.7b00325, URL http://dx.doi.org/10.1021/acs.chemrev.7b00325, 2017.

Zannoni, N., Gros, V., Lanza, M., Sarda, R., Bonsang, B., Kalogridis, C., Preunkert, S., Legrand, M., Jambert, C., Boissard, C., and Lathiere, J.: OH reactivity and concentrations of biogenic volatile organic compounds in a Mediterranean forest of downy oak trees, Atmos. Chem. Phys., 16, 1619–1636, doi:10.5194/acp-16-1619-2016, URL http://www.atmos-chem-phys.net/16/1619/2016/, 2016.

Zhang, Q., Streets, D. G., Carmichael, G. R., He, K. B., Huo, H., Kannari, A., Klimont, Z., Park, I. S., Reddy, S., Fu, J. S., Chen, D., Duan, L., Lei, Y., Wang, L. T., and Yao, Z. L.: Asian emissions in 2006 for the NASA INTEX-B mission, Atmos. Chem. Phys., 9, 5131–5153, doi:10.5194/acp-9-5131-2009, URL http://www.atmos-chem-phys.net/9/5131/2009/, 2009.

Zhao, D. F., Kaminski, M., Schlag, P., Fuchs, H., Acir, I. H., Bohn, B., Häseler, R., Kiendler-Scharr, A., Rohrer, F., Tillmann, R., Wang, M. J., Wegener, R., Wildt, J., Wahner, A., and Mentel, T. F.: Secondary organic aerosol formation from hydroxyl radical oxidation and ozonolysis of monoterpenes, Atmos. Chem. Phys., 15, 991–1012, doi:10.5194/acp-15-991-2015, URL http://www.atmos-chem-phys.net/15/991/2015/, 2015.

Zhao, J. and Zhang, R.: Proton transfer reaction rate constants between hydronium ion (H3O+) and volatile organic compounds, Atmospheric Environment, 38, 2177 – 2185, doi:http://doi.org/10.1016/j.atmosenv.2004.01.019, URL http://www.sciencedirect.com/science/article/pii/S1352231004000895, 2004.

Zhou, X., Civerolo, K., Dai, H., Huang, G., Schwab, J., and Demerjian, K.: Summertime nitrous acid chemistry in the atmospheric boundary layer at a rural site in New York State, Journal of Geophysical Research: Atmospheres, 107, ACH 13–1–ACH 13–11, doi:10.1029/2001JD001539, URL http://dx.doi.org/10.1029/2001JD001539, 4590, 2002.